

Assessment of enhanced silicate rock weathering feasibility as a soil ameliorant and its influence on other terrestrial negative emission technologies

Dissertation

zur Erlangung des Doktorgrades der Naturwissenschaften
an der Fakultät für Mathematik, Informatik und Naturwissenschaften
Fachbereich Geowissenschaften
der Universität Hamburg

vorgelegt von

Wagner de Oliveira Garcia

aus

Iúna, Brasilien

Hamburg, 2020

Als Dissertation angenommen am Fachbereich Geowissenschaften

Tag des Vollzugs der Promotion:

17.09.2020

Gutachter:

Prof. Dr. Jens Hartmann

Prof. Dr. Jörn Peckmann

Vorsitzender des Fachpromotionsausschusses
Geowissenschaften:

Prof. Dr. Dirk Gajewski

Dekan der Fakultät MIN:

Prof. Dr. Heinrich Graener

Table of Contents

Summary	v
Zusammenfassung	vii
List of publications	x
1. Introduction	1
1.1. Terrestrial NETs	2
1.1.1. Bioenergy with carbon capture and storage (BECCS) and Afforestation, Reforestation and natural growing forests (AR)	2
1.1.2. Biochar	3
1.1.3. Enhanced silicate rock Weathering (EW)	4
1.2. Potential synergies of co-deployment of EW with AR and BECCS	5
1.3. Objectives	5
1.3.1. Specific objectives	6
2. Forest nutrient budget in wood export regions	7
2.1. Abstract	7
2.2. Introduction	7
2.3. Methods	8
2.3.1. Timberland wood composition and nutrient loss	8
2.3.2. Nutrient supply	9
2.3.3. Nutrient budget	10
2.4. Results and Discussion	10
2.5. Conclusions	13
3. Impacts of enhanced silicate rock weathering on biomass production for negative emission technologies and soil hydrology	15
3.1. Abstract	15
3.2. Introduction	15
3.3. Methods	17
3.3.1. Global land-system model output	19
3.3.1.1. Afforestation and reforestation	19
3.3.1.2. Biomass production from bioenergy grass	20
3.3.2. Nutrient demand	20
3.3.2.1. Afforestation and reforestation	20
3.3.2.2. Biomass production from bioenergy grass	23
3.3.3. Geogenic P supply for AR	23
3.3.4. Estimating geogenic P gap; related C-fixation reduction; and balanced Mg, Ca, and K supply for AR	24
3.3.5. Enhanced silicate rock weathering Mg, K, Ca, and P potential supply	25
3.3.6. Related impacts on soil hydrology from enhanced silicate rock weathering deployment	26
3.4. Results	28
3.4.1. Afforestation and reforestation P gaps and enhanced silicate rock weathering as nutrient source	28
3.4.2. Enhanced silicate rock weathering coupled to biomass production from bioenergy grass	33

3.4.3.	Impacts on soil hydrology	33
3.5.	Discussion and implications	35
3.5.1.	Enhanced silicate rock weathering coupled to afforestation and reforestation	35
3.5.2.	Enhanced silicate rock weathering coupled to bioenergy grass production	37
3.5.3.	Impacts on soil hydrology	38
3.5.4.	Challenges of rock powder deployment.....	39
3.6.	Conclusions	40
4.	Systematic Review: Effects of biochar and terrestrial enhanced silicate rock weathering on soil and plant properties	42
4.1.	Abstract	42
4.2.	Introduction	42
4.3.	Methods	44
4.3.1.	Data compilation, categorization, and treatment	44
4.3.2.	Meta-analysis	46
4.4.	Results	48
4.4.1.	Biochar effects on soil properties and plant biomass	48
4.4.2.	EW effects on soil properties and plant biomass	52
4.5.	Discussion	56
4.5.1.	Biochar effects on soil properties and plant biomass	57
4.5.2.	EW effects on soil properties and plant biomass	59
4.5.3.	Potential benefits for biochar and EW coapplication.....	60
4.5.4.	Guidelines for biochar and EW experiments	62
4.6.	Conclusions	62
5.	Synthesis	64
6.	Bibliography.....	67
Appendix.....		83
A.	Personal contribution to listed publications.....	83
B.	Timberland wood composition and nutrient loss	84
C.	Nutrient Supply	94
D.	Nutrient budget	108
E.	EW coupled with AR	113
i.	AR N-limited.....	113
ii.	AR N-unlimited	115
F.	EW coupled to bioenergy grass production	121
G.	Impacts on soil hydrology	121
H.	Systematic-review	122
Acknowledgements		132
Eidesstattliche Versicherung.....		133

Summary

To sustainably counterbalance some unavoidable greenhouse gas sources, active carbon dioxide removal (CDR) from the atmosphere demands a portfolio of negative emission technologies (NETs) that not only remove carbon dioxide but also offer additional co-benefits to the ecosystem. Bioenergy with carbon capture and storage (BECCS), afforestation, reforestation and natural growing forests (AR), enhanced silicate rock weathering (EW), and biochar are some of the current NETs that share the same deployment medium and can be applied as a portfolio. Additionally to the atmospheric carbon sequestration potential, EW and biochar can establish chemical and physical properties of soils by positively affecting their nutrient pools. EW can remineralize soils, supply macro- (e.g., Mg, Ca, K, P, and S) and micronutrients (e.g., B, Mo, Cu, Fe, Mn, Zn, Ni), and establish soil pH once weathering of pristine minerals start. Thus, the potential coapplication of EW to nutrient-demanding technologies like AR or bioenergy plantations for BECCs needs to be studied. Therefore, the aim of this thesis is to expand the analysis of CDR assessing the potential synergies between different NETs.

In the first part of this thesis, the geogenic nutrients' ability to replenish nutrients exported by biomass harvesting for bioenergy production was studied based on spatially explicit information for U.S. timberland forests. The tree species within timberland areas were derived from the U.S. forest type distribution map. Thus, the chemistry of the identified tree species for each tree compartment were used in projections of Mg, Ca, K, and P export for spatially explicit harvest rates. The nutrients supplied by weathering and atmospheric deposition (i.e., the geogenic supply) within the timberland areas were used to check at which extent the projected nutrients exported by harvest can be replenished. Therefore, for an U.S. timberland area of 33,570 km² a negative budget occurs in 50, 57, 45, and 96 % of the total area for Ca, K, Mg, and P, respectively for an intensive harvest scenario.

Projections on nutrient export for intensive harvest rates, triggered by bioenergy generation as an attempt to decrease net CO₂ emissions, and the potential geogenic nutrient supply of different lithological classes were considered for a more general nutrient budget. For an average geogenic supply, the nutrient export by intensive harvest rates cannot be replenished. Therefore, to keep up with intensive harvest rates, an external source of nutrients (e.g., rock powder) or sustainable forest management is necessary.

Later on, the capability of geogenic P supply for an N-stock-based P demand for a simulated global AR scenario occurring from 2006 – 2099 was investigated. The AR scenario accounted for natural N supply (N-limited) and N supply by fertilization (N-unlimited). The additional AR P demand was approximated by stoichiometric P:N ratios, derived from databases of hard- and softwood, and foliar biome-specific nutrient content for mean and range (5th and 95th percentiles) concentrations. The inferred P demand was compared to geogenic P supply, and the effects of potential P undersupply on carbon (C) storage in biomass was investigated. If P demand is neglected, the potential global C sequestration from the AR models is 190 Gt C and 224 Gt C for the N-limited and N-unlimited scenarios respectively. However, if a mean P demand by AR and a low geogenic P supply scenario is assumed, the global C sequestration from the AR models would fall to 119 Gt C (N-limited) and 136 Gt C (N-unlimited), due to a negative P budget (i.e., areas in which AR P demand is higher than the geogenic P supply). Thus, geogenic P supply can limit projected C sequestration from climate models. Therefore, to reach the projected C sequestration, P should be supplied in areas having negative P budget. Rhyolite, dacite, andesite, and basalt powder, deployed as means of EW within the areas of negative P budgets may remineralize soils and supply P after congruent and complete dissolution of rock powder. Additionally to a P supply, balanced Mg, Ca, and K supply is also expected. However, due to faster weathering fluxes and a higher P content, basalt has a greater potential to replace or decrease the use of industrial fertilizers in regions of negative P budgets. Thus, for a period

from 2006 – 2099, approximately 150 Gt basalt and 200 Gt basalt would be necessary to supply P for negative P budget areas from the N-limited and from the N-unlimited scenario respectively. The use of basalt powder as means of EW could sequester, on average, ~12 and ~16 Gt C until 2099.

Furthermore, the effects of large scale basalt powder deployment may affect soil hydraulic properties, which influence soil water behavior and may affect plant growth. Thus, changes in soil hydraulic properties were estimated for deploying basalt powder within the projected negative P budget areas and for a range of upper limits of basalt powder deployment. The soil hydraulic conductivity and plant-available water were the considered hydraulic properties, and their changes for different soils were estimated by the use of pedotransfer functions. The impacts of basalt powder application on soil hydraulic conductivity and plant-available water, to cover the projected negative P budget areas, would depend on the basalt and soil texture, but in general, they are marginal. Later on, the efficiency of EW as a nutrient source for bioenergy grass plantations for BECCS was investigated. Thus, from the output from an agricultural production model, the minimum and maximum exported N proportional to harvest rates for a period from 1995 – 2090 were obtained. The harvest exported P and K were estimated based on P:N and K:N stoichiometric ratios from the literature and used to estimate the necessary mass of basalt powder to replenish the harvest exported nutrients from the fields. Deploying 8 kg basalt m⁻² a⁻¹ may, on average, replenish the exported K and P by intensive harvest rates.

A further part of this thesis comprises a systematic review on the potential effects, interactions, and synergies on soil properties and plant response after deploying EW or biochar to the soil. Therefore, a database created from selected peer-reviewed articles was used to perform a random-effects model meta-analysis to assess the potential effects. The complexity of mechanisms governing the effects of biochar or EW on soil and plant properties could be demonstrated. Different variables (e.g., grain size, deployment rate, pyrolysis temperature, etc.) control the responses of soil and plant properties, with some having significant positive results. Thus, a general deployment setup to optimize plant response and soil for any scale and location is unlikely to exist, as indicated by the system complexity. However, these variables can be adapted to meet the nutritional needs of local soil and specific plant species. Generally, positive effects on soil and plant properties are likely to happen after biochar or EW deployment, but the probability of a negative effect cannot be neglected. Higher yields of plants, greater positive effects on soil pH, and available P occur after deploying EW than after deploying biochar. However, biochar deployment resulted in greater positive effects for dry plant and Dry shoot mass, main stem diameter, plant height, cation exchange capacity, and soil exchangeable K.

This thesis demonstrates that geogenic nutrient supply cannot replenish the exported nutrients by intensive harvest rates of forest biomass and that sustainable forest management and external source of nutrients will be necessary. EW has the potential to act as a nutrient source and it can be coapplied to nutrient-demanding NETs (AR or bioenergy grass for BECCS). Additionally, EW application could improve plant-available water capacity depending on deployed amounts of rock powder. The systematic review showed that plant and soil properties response were enhanced after biochar or EW were deployed, but negative effects may occur. Coapplication of biochar and EW may magnify the plant and soil properties but more research to check this hypothesis is necessary.

Zusammenfassung

Um einige unvermeidbare Treibhausgasquellen nachhaltig auszugleichen, erfordert die Aktiv Kohlendioxid-Entnahme (CDR) aus der Atmosphäre eine Kombination von Technologien für negative Emissionen (NET), die nicht nur Kohlendioxid entnimmt, sondern auch zusätzliche Vorteile für das Ökosystem bietet. Bioenergie mit Kohlenstoffabscheidung und -speicherung (BECCS), Aufforstung, Wiederaufforstung und natürlich wachsende Wälder (AR), Beschleunigte Verwitterung (EW) und Erzeugung von Pflanzenkohle (Biochar) sind einige der aktuellen NETs, die im selben Medium, nämlich dem Boden, eingesetzt und in Kombination verwendet werden können. Zusätzlich zur atmosphärischen Kohlendioxid-Entnahme können EW und Biochar chemische und physikalische Eigenschaften von Böden mitbestimmen, indem sie ihre Nährstoffspeicher positiv beeinflussen. EW kann Böden remineralisieren, Makro- (z. B. Mg, Ca, K, P und S) und Mikronährstoffe (z. B. B, Mo, Cu, Fe, Mn, Zn, Ni) liefern und den pH-Wert des Bodens bestimmen, sobald die Verwitterung von ursprünglichen Mineralien beginnt. Deshalb sollte die mögliche gemeinsame Anwendung von EW mit nährstoffintensiven Technologien wie AR oder Bioenergieplantagen für BECCs untersucht werden. Ziel dieser Arbeit ist es daher, die Analyse der CDR zu erweitern und die potenziellen Synergien zwischen verschiedenen NETs zu bewerten.

Im ersten Teil dieser Arbeit wurde die Fähigkeit geogener Nährstoffe untersucht, Nährstoffe wieder aufzufüllen, die durch die Ernte von Biomasse für Bioenergieproduktion exportiert wurden. Die Baumarten in den Waldgebieten wurden aus der US-amerikanischen Waldtypverteilungskarte abgeleitet. Es wurde die chemische Zusammensetzung der identifizierten Baumarten für jeden Baumabschnitt benutzt, um Projektionen des Mg-, Ca-, K- und P-Exports für die Ernte in den bestimmten Gebieten zu erstellen. Die Nährstoffversorgung durch Verwitterung und atmosphärischen Eintrag innerhalb der Waldgebiete wurde verwendet, um zu überprüfen, inwieweit die Nährstoffe, die durch die Ernte exportiert werden, wieder aufgefüllt werden können. Für ein US-amerikanisches Waldgebiet von 33.570 km² ergibt sich somit ein negatives Budget in 50, 57, 45 und 96 % der Gesamtfläche für Ca, K, Mg und P für ein intensives Ernteszenario.

Die Erzeugung von Bioenergie, um Netto-CO₂-Emissionen zu senken, benötigt enorme Erntemengen. Projektionen zum Nährstoffexport letzterer und zur potentiellen geogenen Nährstoffversorgung durch verschiedene lithologische Klassen wurden für ein allgemeineres Nährstoffbudget berücksichtigt. Bei einer durchschnittlichen geogenen Versorgung kann der Nährstoffexport durch intensive Erntemengen nicht wieder aufgefüllt werden. Um mit diesen Mengen Schritt zu halten, ist daher eine externe Nährstoffquelle (z. B. Gesteinspulver) oder eine nachhaltige Waldbewirtschaftung erforderlich.

Im Anschluss wurde die Fähigkeit des geogenen P-Angebots untersucht, eine vom N-Vorrat abhängige P-Nachfrage für ein simuliertes globales AR-Szenario zu erfüllen. Das AR-Szenario berücksichtigte die natürliche N-Versorgung (N-limitiert) und die N-Versorgung durch Düngung (N-unlimitiert). Der zusätzliche AR P-Bedarf wurde durch stöchiometrische P:N-Verhältnisse angenähert, die aus Datenbanken des Biom-spezifischen Hart-, Weichholz- und Blatt-Nährstoffgehalts für mittlere Konzentrationen und Konzentrationen im 5. und 95. Perzentil abgeleitet wurden. Der abgeleitete P-Bedarf wurde mit dem geogenen P-Angebot verglichen und die Auswirkungen einer möglichen P-Unterversorgung auf die Speicherung von Kohlenstoff (C) in Biomasse untersucht. Wenn der P-Bedarf vernachlässigt wird, beträgt die potenzielle globale C-Bindung aus den AR-Modellen 190 Gt C und 224 Gt C für das N-limitierte- bzw. Das N-unlimitierte-Szenario. Wenn jedoch ein Szenario mit mittlerer P-Nachfrage von AR und niedrigem geogenen P-Angebot angenommen wird, fällt die globale C-Bindung in den AR-Modellierungen auf 119 Gt C (N-limitiert) und 136 Gt C (N-unlimitiert). Dies

geschieht aufgrund eines negativen P-Budgets in Gebieten, in denen die P-Nachfrage von AR höher ist als das geogene P-Angebot. Somit kann die geogene P-Versorgung die prognostizierte C-Entnahme aus Klimamodellen begrenzen. Um diese aber zu erreichen, sollte P daher in Gebieten mit negativem P-Budget zugeführt werden. Rhyolith-, Dacit-, Andesit- und Basaltpulver können im Rahmen von EW in Gebieten mit negativem P-Budget eingesetzt werden, um die Böden zu remineralisieren und um, nachdem es gleichmäßig und vollständig aufgelöst wurde, P zu liefern. Zusätzlich zu einer P-Versorgung kann hierdurch eine ausgeglichene Mg-, Ca- und K-Versorgung erfolgen. Aufgrund schnellerer Verwitterungsflüsse und eines höheren P-Gehalts hat Basalt jedoch ein größeres Potenzial, den Einsatz von Industriedünger in Regionen mit negativem P-Budget zu ersetzen oder zu verringern. Für den Zeitraum 2006 bis 2099 wären für das N-limitierte-Szenario ungefähr 150 Gt Basalt und für das N-unlimitierte-Szenario 200 Gt Basalt erforderlich, um P für Gebiete mit negativem P-Budget zu liefern. Die Verwendung von Basaltpulver für EW könnte bis 2099 durchschnittlich ~12 und ~16 Gt C binden.

Darüber hinaus können die Auswirkungen des Einsatzes von Basaltpulver in großem Maßstab die hydraulischen Eigenschaften des Bodens beeinflussen, welche Auswirkungen auf das Bodenwasser und somit auf das Pflanzenwachstum haben kann. Unter Verwendung von Pedotransferfunktionen wurden daher die hydraulische Leitfähigkeit des Bodens und das verfügbare Pflanzenwasser in Böden in den prognostizierten Gebieten mit negativem P-Budget bei einem Einsatz von verschiedenen Mengen an Basaltpulver geschätzt. Die Auswirkungen der Anwendung von Basaltpulver auf die hydraulische Leitfähigkeit des Bodens und das verfügbare Pflanzenwasser zur Abdeckung der prognostizierten negativen P-Budget-Gebiete hängen von der Basalt- und Bodentextur ab, sind aber im Allgemeinen gering.

Im weiteren Teil wurde die Effizienz von EW als Nährstoffquelle für Bioenergie-Grasplantagen für BECCS untersucht. So wurden aus den Ergebnissen eines Modells zur landwirtschaftlichen Produktion dieser Plantagen die minimalen und maximalen exportierten Mengen an N proportional zu den Erntemengen für einen Zeitraum von 1995 bis 2090 erhalten. Die exportierten Mengen an P und K wurden basierend auf den stöchiometrischen Verhältnissen P:N und K:N der Literatur entnommen und zur Schätzung der erforderlichen Menge an Basaltpulver, welches benötigt ist um die durch intensive Ernte hervorgerufenen P- und K-Defizite wieder auszugleichen, verwendet. Im Durchschnitt ist dies durch den Einsatz von 8 kg Basalt m⁻² a⁻¹ möglich.

Ein weiterer Teil dieser Arbeit umfasst eine systematische Überprüfung der möglichen Auswirkungen, Wechselwirkungen und Synergien auf die Bodeneigenschaften und die Reaktionen der Pflanzen nach dem Einsatz von EW oder Biochar im Boden. Daher wurde eine Datenbank, die aus ausgewählten, von Experten begutachteten Artikeln erstellt wurde, zur Durchführung einer Metaanalyse mit einem "random-effects-model" verwendet, um die potenziellen Auswirkungen zu bewerten. Die Komplexität der Mechanismen, die die Auswirkungen von Biochar oder EW auf die Boden- und Pflanzeigenschaften steuern, konnte demonstriert werden. Verschiedene Variablen (z. B. Korngröße, Verwendungsrate und Pyrolysetemperatur usw.) steuern die Reaktionen der Boden- und Pflanzeigenschaften, wobei einige signifikant positive Ergebnisse aufweisen. Daher ist eine allgemeine Empfehlung zum Einsatz von Biochar oder EW, um die Boden- und Pflanzeigenschaften zu verbessern, nicht möglich, wie dies durch die Systemkomplexität gezeigt wird. Diese Variablen können jedoch verändert werden, um den Bedürfnissen des Bodens und bestimmter Pflanzenarten gerecht zu werden. Eine allgemeinere Analyse zeigt, dass positive Auswirkungen auf die Boden- und Pflanzeigenschaften nach dem Einsatz von Biochar oder EW wahrscheinlich sind, die Möglichkeit eines negativen Effekts jedoch nicht vernachlässigt werden darf. Nach dem Einsatz von EW treten höhere Erträge und größere positive Auswirkungen auf den pH-Wert des Bodens und auf verfügbares P auf als nach dem Einsatz von Biochar. Letzterer führte jedoch zu größeren positiven Effekten

für das Trockengewicht von Pflanzen und Trieben, den Hauptstammdurchmesser, die Pflanzenhöhe, die Kationenaustauschkapazität und das austauschbare Kalium im Boden.

Diese Arbeit zeigt, dass die geogene Nährstoffversorgung die durch intensive Erntemengen von Waldbiomasse exportierten Nährstoffe nicht auffüllen kann und dass eine nachhaltige Waldbewirtschaftung und eine externe Nährstoffquelle erforderlich sind. EW hat das Potenzial, als eine solche zu fungieren, und kann gleichzeitig für nährstoffintensive NETs (AR oder Bioenergiegras für BECCS) angewendet werden. Darüber hinaus könnte der EW-Einsatz die verfügbare Wasserkapazität in Abhängigkeit von den eingesetzten Mengen an Gesteinspulver verbessern. Die systematische Überprüfung ergab, dass die Pflanzen- und Bodeneigenschaften nach dem Einsatz von Biochar oder EW verbessert wurden, jedoch negative Auswirkungen auftreten können. Für die Hypothese, dass der gleichzeitige Einsatz der beiden Methoden die Pflanzen- und Bodeneigenschaften verbessern kann, ist jedoch noch weitere Forschung erforderlich.

List of publications

Chapter 2 of this thesis was published in Nature Scientific Reports, while chapter 3 was published in Biogeosciences and chapter 4 was prepared to be submitted. The author has also contributed in other publications during his doctoral studies. The publications are listed below and the author's individual contribution to the publications are described in Appendix A.

Published manuscripts

Garcia, W. de O., Amann, T., and Hartmann, J.: Increasing biomass demand enlarges negative forest nutrient budget areas in wood export regions, *Scientific Reports*, 8, 5280, 10.1038/s41598-018-22728-5, 2018. (Chapter 2 of this thesis)

Minx, J. C., Lamb, W. F., Callaghan, M. W., Fuss, S., Hilaire, J., Creutzig, F., Amann, T., Beringer, T., **Garcia, W. de O.**, and Hartmann, J.: Negative emissions—Part 1: Research landscape and synthesis, *Environmental Research Letters*, 13, 063001, 2018.

Fuss, S., Minx, J. C., Lamb, W. F., Callaghan, M. W., Hilaire, J., Creutzig, F., Amann, T., Beringer, T., **Garcia, W. de O.**, Hartmann, J., Khanna, T., Luderer, G., Nemet F, G., Rogelj, J., Smith, P., Vicente Vicente, J. L., Wilcox, J., and del Mar Zamora Dominguez, M.: Negative emissions—Part 2: Costs, potentials and side effects, *Environmental Research Letters*, 13, 063001, 2018.

Amann, T., Hartmann, J., Struyf, E., **Garcia, W. de O.**, Fischer, E. K., Janssens, I., Meire, P., and Schoelynck, J.: Enhanced Weathering and related element fluxes – a cropland mesocosm approach, *Biogeosciences*, 17, 103-119, 10.5194/bg-17-103-2020, 2020.

Garcia, W. de O., Amann, T., Hartmann, J., Karstens, K., Popp, A., Boysen, L. R., Smith, P., and Goll, D.: Impacts of enhanced weathering on biomass production for negative emission technologies and soil hydrology, *Biogeosciences*, 17, 2107-2133, 10.5194/bg-17-2107-2020, 2020. (Chapter 3 of this thesis)

Manuscripts in preparation

Garcia, W. de O., Amann, T., and Hartmann, J., Romero-Mujalli, G., Schmidt, H.-P., Hagemann, N.: Systematic Review: Effects of biochar and terrestrial enhanced silicate rock weathering on soil and plant properties. (Chapter 4 of this thesis)

1. Introduction

The carbon cycle controls the carbon exchange between different Earth's compartments through biogeochemical interactions. Over geological Earth's history, the atmospheric carbon dioxide concentrations presented high variability (Berner, 1997; Royer et al., 2004). Estimations based on geochemical models reveal that atmospheric carbon dioxide went from 20 times higher than preindustrial levels in 500 million years ago to approximately 400 ppm in 358.9 million years ago (Berner, 1997; Royer et al., 2004). The estimated decrease in atmospheric carbon dioxide levels during the Devonian period (419.2 to 358.9 million years ago) is related to the appearance of rooted plants that boosted weathering of rocks and consumed atmospheric carbon dioxide (Berner, 1997). Later on, these plants were stored in geological reservoirs as fossil fuels. In the recent history, atmospheric carbon dioxide increased from ~280 ppm (preindustrial levels) to over ~400 ppm in 2019 (Earth System Research Laboratory, 2019) due to anthropogenic activities (mainly by fossil fuels combustion). As a consequence of high levels of atmospheric carbon dioxide, it is expected a long-term rise in the average temperature of the Earth's climate system (National Research Council, 2010), which may affect hydrologic cycles worldwide increasing extreme rainfalls and making droughts and flood events more frequent (Lorenz et al., 2007; Sillmann et al., 2013). Changes in hydrologic cycles may affect biomass production since plants are sensitive to water availability (Ehlers and Goss, 2016). Thus, human responses to climate change are necessary and they include mitigation or adaptation strategies (Minx et al., 2018). Mitigation of current climate change account either for reducing the sources or enhancing the sinks (e.g., weathering, biomass growth) of greenhouse gases (Edenhofer, 2015; Houghton et al., 2001; Metz et al., 2007). Adaptation considers any human intervention in the environmental system to countermeasure the effects of climate change (Edenhofer, 2015; Houghton et al., 2001; Metz et al., 2007).

Research on negative emission technologies (NETs) for active carbon dioxide removal (CDR) as a mean of mitigation are necessary. As well as research on adaptation strategies such as solar radiation management (SRM) or on new water-saving techniques, etc. The large-scale human intervention in the Earth's climate system to mitigate the diverse effects of global warming is known as climate engineering or geoengineering (Intergovernmental Panel on Climate Change, 2014).

Limiting the average temperature increase to “well below 2°C above preindustrial levels” according to the Paris agreement at the end of the 21st century is expected to decrease some effects of climate change, but it demands early deployment of different NETs to ensure safe and sustainable CDR (Obersteiner et al., 2018). Enhanced silicate rock weathering (EW), ocean alkalization, biochar, bioenergy with carbon capture and storage (BECCS), afforestation, reforestation and naturally growing forests (AR), wetland restoration, ocean fertilization, direct air capture and storage, soil carbon sequestration (Fuss et al., 2018; Smith et al., 2019) and the expansion, plantation, or protection of vegetated coastal ecosystems including seagrass meadows (blue carbon; Johannessen and Macdonald, 2016) are the current available NETs for CDR. Techniques to remove from the atmosphere non-carbon dioxide greenhouse gases like methane and nitrous oxides also exist (de Richter et al., 2017; Ming et al., 2016; Stolaroff et al., 2012). However, the radiative forcing (i.e., the difference between absorbed insolation by Earth and energy radiated back to space) of carbon dioxide is the highest when compared to methane, nitrous dioxide, and other greenhouse gases (Myhre et al., 2013).

Different scenarios for future anthropogenic greenhouse gas emissions and its consequences to climate exist. Starting a late atmospheric carbon dioxide removal might imply in higher efforts to mitigate climate change since soil and ocean carbon dioxide reservoirs would outgas and become a source (Cao and Caldeira, 2010; Vichi et al., 2013). Integrated assessment models (IAMs) consider a large-scale deployment of NETs (Smith et al., 2016) to

mitigate climate change, which may cause considerable impacts on energy demand, water and land use, nutrient cycles, albedo, and economy (Smith et al., 2016). This will result in significant social and environmental consequences (Dooley et al., 2018).

Currently, no NETs are available to be implemented to meet the Paris agreement targets and it is necessary to reduce greenhouse gas emissions rather than solely relying on NETs to mitigate climate change (Smith et al., 2016). Nevertheless, there are some sources of greenhouse gases that cannot be avoided and the removal from atmospheric carbon dioxide through technical means is going to be needed (Anderson and Peters, 2016). Thus, if NETs are not deployed or the removal potential of atmospheric carbon dioxide from these NETs is unsatisfactory, society will be forced to follow a high-temperature pathway (Anderson and Peters, 2016). Therefore, research to expand the analysis of CDR for potential synergies between these different NETs to reach long-term sustainable CDR is necessary. BECCS, AR, biochar, and EW are the terrestrial NETs studied in this thesis and are detailed described in the following chapter.

1.1. Terrestrial NETs

1.1.1. Bioenergy with carbon capture and storage (BECCS) and Afforestation, Reforestation and natural growing forests (AR)

Producing energy from biomass and the subsequent capture and storage of carbon is the aim of BECCS. In the first step, the carbon dioxide removal occurs by photosynthesis, which is a process involving the conversion of radiant energy into more stable chemical energy (Minagawa, 2009). Photosynthesis occurs in different organisms from bacteria to vascular plants, including algae (Pierce and Curtis, 2012). Therefore, different energy-rich organic compounds can be used as raw material for bioenergy production, they are: (i) crop and forestry residues (Smith, 2012; Smith et al., 2012; Tokimatsu et al., 2017); (ii) dedicated bioenergy grasses plantations (Humpenöder et al., 2014; Smith, 2012; Smith et al., 2012); or (iii) short rotation woody biomass from forestry (Cornelissen et al., 2012; Smeets and Faaij, 2007). The energy-rich organic compounds are converted into bioenergy by combustion, fermentation, or other conversion method (Olsson and Hillring, 2012). During this energy conversion process, carbon dioxide is emitted and sequestered at the energy production facility. Later on, the sequestered carbon dioxide may be injected into secure geological reservoirs, where chemical reactions with the hosting rock minerals may occur (Gaus, 2010; Krevor et al., 2015). Thus, the injected carbon dioxide is immobilized from decades to millennia (Krevor et al., 2015). Another use for the sequestered carbon dioxide at the energy production facility may be the production of different types of chemicals and fuels (Ampelli et al., 2015).

AR consists of planting trees in abandoned lands (afforestation), or restoring the tree cover of deforested areas (reforestation) by actively planting or letting the trees to naturally regrowth (Fuss et al., 2018; Smith et al., 2019). The additional tree growth from AR results in atmospheric carbon dioxide sequestration (Hall et al., 2012; Schroeder, 1992). Appropriate AR deployment and management result in positive impacts on biodiversity and ecosystem services (Kraxner et al., 2017), which may not occur on landscapes reforested with monoculture plantations (Hall et al., 2012) affecting biodiversity conservation.

Tropical regions are more suitable for AR than high-latitude regions (Betts et al., 2007). At the tropics, a doubled cooling effect by AR is expected due to increase in cloud formation and in evaporation (Betts et al., 2007) while in high-latitudes AR would decrease the albedo consequently warming these regions and increasing climate change impacts (Betts, 2000; Betts et al., 2007).

Large-scale AR and bioenergy plantation for BECCS will change landscape configuration (Boysen et al., 2017a; Humpenöder et al., 2014; Kracher, 2017; Popp et al., 2017), increase water demand (Bonsch et al., 2016; Boysen et al., 2017b), and affect future food prices (Popp et al., 2017). Fertilizers will be necessary to increase or maintain elevated yields of bioenergy plantations or elevated growth rates of AR potentially reducing the CDR efficiency due to related emissions of N₂O (Creutzig, 2016; Popp et al., 2011). However, agroforestry may be a solution for AR or for bioenergy plantations for BECCS (Smith et al., 2019) that can improve food and nutritional security, mitigate environmental degradation, and contribute to biodiversity (Mbow et al., 2014; Nair, 2007) either at countries under development or developed ones.

1.1.2. Biochar

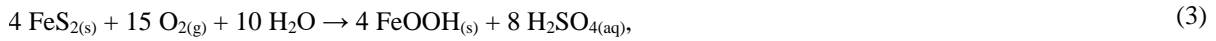
Biochar is the solid product of pyrolysis, the burning of biomass under oxygen-limiting conditions at atmospheric pressure and any sort of material can be used as biochar feedstock (Schmidt et al., 2018; Smith et al., 2019). Biomass decay of buried organic carbon in soils, either in the form of woody parts or crop residues, is faster than the decay of buried biochar (Lehmann et al., 2006; Schmidt et al., 2018), which has a mean residence time of 556 years (Wang et al., 2016a). Therefore, the use of biochar to increase soil carbon sequestration is attractive (Schmidt et al., 2018). Its production can be easily implemented by smallholder farmers (Glaser et al., 2002) by low tech solutions like the flame-curtain pyrolysis in the “Kon-Tiki” (Cornelissen et al., 2016; Schmidt et al., 2014) or by other industrial technologies (Boateng et al., 2015).

Additionally to carbon sequestration, biochar deployment in soils may increase nutrient availability to plants, establish soil pH, and increase electrical conductivity (Chan et al., 2007; Chan et al., 2008; Glaser et al., 2002; Kizito et al., 2019; Schmidt et al., 2017). Thus, positive effects on plant yield may occur depending on the plant species (Backer et al., 2016; Boersma et al., 2017). Once biochar is applied into soil, bioturbation increases as well (Abujabhah et al., 2016), consequently enhancing the transport of particles through different soil layers (Fishkis et al., 2010) and boost biochar concentration into deeper soil horizons (Ameloot et al., 2013). In addition, biochar may positively influence the symbiosis between plant and mycorrhizal fungi (LeCroy et al., 2013; Vanek and Lehmann, 2015). However, in cases of high nutrient availability conditions, the need for symbionts is reduced and abundance of mycorrhizal fungi decreases (Lehmann et al., 2011). Furthermore, it is necessary to enhance and combine biochar with nutrients before deployment occurs; otherwise, it may compete with plants for soil nutrients and reduce plant growth (Joseph et al., 2018; Kammann et al., 2015).

Besides returning a solid phase (biochar), the pyrolysis of organic matter also results in a liquid (bio-oil) and a gaseous phase (Schmidt et al., 2018). The bio-oil may be rich in polycyclic aromatic hydrocarbons (PAHs; Fagernäs et al., 2012), which may have toxic, mutagenic, and carcinogenic properties (Abdel-Shafy and Mansour, 2016). Kuśmierz and Oleszczuk (2014) found that the sum of the content of 16 PAHs in soil samples collected nearby a traditional biochar-producing plant in Poland exceeded the norms permitted in many European countries. Therefore, used as soil amendment, the PAHs concentration in biochar should be below threshold values (Fagernäs et al., 2012). Another side effect may be a decrease in the surface albedo of agricultural soils (Genesio et al., 2012). After deploying 30 – 60 t biochar ha⁻¹, the surface albedo decreased in up to 80% compared to control due to biochar’s dark colour (Genesio et al., 2012), which resulted in higher soil temperatures potentially affecting soil organic matter. However, the soil temperature decreased after two years (Genesio et al., 2012).

1.1.3. Enhanced silicate rock Weathering (EW)

Mineral weathering is a natural process responsible for supplying nutrients (e.g., Mg, Ca, K, P, etc.) to the soil and controlling atmospheric carbon dioxide over geological timescales (Berner et al., 1983; Kempe, 1979; Lenton and Britton, 2006; Walker et al., 1981; Yasunari, 2020). Weathering of primary minerals from silicate rocks (e.g., K-feldspars Eq. (1), Pyroxenes Eq. (2), and Pyrites Eq. (3)) may result in genesis of secondary minerals like Kaolinite Eq. (1), and Goethite Eq. (2) and Eq. (3).



Secondary mineral formation will depend on availability of ions (K^+ , Mg^{+2} , Ca^{+2} , etc.) and leaching conditions of the soil profile. In general, common secondary minerals from silicate rock weathering are clay minerals (illite, montmorillonite, kaolinite, etc.), and iron and aluminum hydrous-oxides (Wilson, 2004). Sorption of organic matter onto the surfaces of formed secondary minerals can contribute to soil organic matter stabilization (Saidy et al., 2012; Wiseman and Püttmann, 2006).

According to Lasaga et al. (1994), the change in concentration of a chemical element 'i' over time ($\frac{dC_i}{dt}$) happening at the mineral surface, as described by equations (1), (2), and (3), can be represented by the following general reaction rate equation Eq. (4):

$$\frac{dC_i}{dt} = k_i A_{min.} (1 - SI), \quad (4)$$

with:

$$k_i = k_0 e^{\frac{-E_a}{RT}}, \quad (5)$$

where SI is the saturation index of the mineral, which is influenced by the activity of H^+ ions in aqueous solution (i.e., by changes in soil pH) and by the activities of other aqueous ions (K^+ , Mg^{+2} , Ca^{+2} , etc.). k_i is the rate constant dependent on a pre-exponential factor k_0 , on the apparent activation energy E_a of the mineral-fluid reaction, the gas constant R , and on the temperature T in Kelvin. $A_{min.}$ is the reactive surface area of the mineral.

Therefore, the aim of EW is to speed up the weathering rates of minerals by directly changing some parameters from Eq. (4) to favor CDR in form of alkalinity or precipitation of carbonate minerals (Beerling et al., 2018; Hartmann et al., 2013). Additionally, EW can supply macro- (e.g., Mg, Ca, K, P, and S), and micronutrients (e.g., B, Mo, Cu, Fe, Mn, Zn, and Ni) to the soil (Anda et al., 2015; Beerling et al., 2018; Hartmann et al., 2013; Leonardos et al., 1987; Nkouathio et al., 2008).

Weathering rates of minerals can be enhanced by the following mechanisms: (a) direct increase of reactive surface area of minerals by grinding different rocks, in general mafic and ultramafic rocks (i.e., Basalt, Dunite, Peridotite, etc.). (b) Changes in the saturation index of a mineral triggered by biological activity of plants and microorganisms. At the rhizosphere, saturation index of minerals is influenced by the changes in the soil pH and soil solution composition triggered by plant nutritional needs (Arcand and Schneider, 2006; Harley and Gilkes, 2000). At soil profile, saturation index of minerals is influenced by colonization of mineral surfaces, especially pores and cracks, by plants, lichens, fungi, and bacteria (Uroz et al., 2009), which will increase the weathering rates of minerals

according to nutrient requirements of the soil microbiota (Bennett et al., 2001) that use organic ligands to dissolve the silicate surfaces to access the needed nutrient (Rogers and Bennett, 2004). (c) Soil redox conditions, which may enhance weathering rates of silicate minerals bearing Fe^{2+} Eq. (2) and (3) or Mn^{2+} in their crystallographic structure. (d) Temperature (Hayes et al., 2020; Lasaga et al., 1994).

Some additional side-effects of EW are related to the potential oxidation of different metal sulfide minerals, which may be constituents of various igneous, metamorphic, or sedimentary rocks. Metal sulfide minerals can trigger acid rock drainage (ARD) by formation of the strong acid $\text{H}_2\text{SO}_{4(\text{aq})}$ as explained by Eq. (3) if a rock with e.g. 1% or 2% of pyrite (Earle, 2018) is deployed at considerable amounts. The percolating acidic water from the ARD would favor the leaching of nutrients (Haynes and Swift, 1986) and heavy metals (Hesterberg, 1993) from the soil profile. Some silicate rocks can release considerable amounts of Na^+ during weathering (Von Wilpert and Lukes, 2003), which can gradually replace divalent cations on exchange surfaces of clay minerals contributing to soil salinization (Vengosh, 2003). Therefore, before EW deployment occurs, it is necessary to consider the cumulative effects of rock powder application. Additionally it is important to perform petrographical, mineralogical, and geochemical characterization of the selected rock, which needs to be adjusted to local soil, climate, and nutrient requirement of crops, trees, and soils to anticipate the potential side-effects.

1.2. Potential synergies of co-deployment of EW with AR and BECCS

Plant growth is largely dependent on soil nutrient and water availability. Mineral weathering and atmospheric nutrient deposition are the medium- to long-term geogenic nutrient sources (Ranger and Turpault, 1999) while the short-term is divided in above ground (nutrients in plants) and soil nutrients (Ranger and Turpault, 1999; Vangansbeke et al., 2015). However, to increase or maintain elevated yields of agricultural bioenergy crops or elevated growth rates of forests, external sources of nutrients will be necessary (Garcia et al., 2018; Garcia et al., 2020). Thus, deploying EW in soils is supposed to remineralize them and reload their nutrient pools, which may directly influence AR or plantations for BECCS production, especially if some nutrient is limiting it.

Additionally, intensification of dry conditions due to climate change may directly affect terrestrial negative emission technologies like EW, BECCS, and AR since plant growth may be limited by water availability (Ehlers and Goss, 2016) as well as weathering of pristine minerals (Beerling et al., 2018; Hartmann et al., 2013). Therefore, strategies to enhance water infiltration through soil profile and water availability to plants are necessary to countermeasure drought effects (Sullivan, 2000). Increasing the plant-available water at the depth of the root system may mitigate drought effects on crops (Rossato et al., 2017) and EW may contribute to increase plant-available water.

1.3. Objectives

The sustainable deployment of a portfolio of NETs that not only remove carbon from the atmosphere but also offer co-benefits to the ecosystem are necessary. Therefore, this study extensively investigates the potential effects of geogenic nutrient limitation on growth of forests and yield of bioenergy crops and the use of Enhanced silicate rock Weathering (EW) as alternative long-term nutrient source for these areas, based on different databases and numerical model outputs. Poor plant nutrition reduces carbon dioxide sequestration and EW represents a sustainable method for the portfolio of terrestrial NETs (Biochar, AR, BECCS) that can restore degraded soils and positively affect the water use of plants. Therefore, the main objective of this thesis is to identify at which extent

plant growth and yield can be limited by poor nutrition and check EW feasibility as a soil ameliorant and its influence on other terrestrial NETs. In order to fulfill this objective the following tasks were defined:

1.3.1. Specific objectives

1. To evaluate if geogenic nutrient supply is able to meet nutrient export occasioned by high harvest rates for an increased bioenergy demand scenario.
2. To assess if applications of rock mineral based P sources could close eventual nutritional gaps in an environment with natural or fertilized N supply, based on a global afforestation scenario.
3. To investigate the effects of coupling nutrient-supplying (EW) to nutrient-demanding (AR and BG) land-based NETs by focusing on the efficiency of different upper limits of basalt powder deployment to supply nutrients.
4. To determine threshold values for impacts on soil hydraulic conductivity, and plant-available water due to EW deployment.
5. To determine and compare the effects of EW or biochar on plant and soil properties before implementing EW or biochar as NET.
6. Provide future recommendations for studies on EW and Biochar for CDR.

2. Forest nutrient budget in wood export regions

This chapter has been published as: Garcia, W. de O., Amann, T., and Hartmann, J.: Increasing biomass demand enlarges negative forest nutrient budget areas in wood export regions, Scientific Reports, 8, 5280, 10.1038/s41598-018-22728-5, 2018.

2.1. Abstract

Energy production from biomass is one of the adopted strategies in different European countries to limit global warming to within the 1.5 – 2 ° targets after the 2015 UN climate agreement. This will motivate enhanced forest harvest rates and whole tree harvest to supply the increasing biomass demand. Negative nutrient budgets for certain timberland areas where geogenic nutrient supply cannot cope with harvesting rates will be one consequence. A spatially explicit analysis for a U.S. timberland area of 33,570 km² reveals that for a minimum nutrient loss and supply scenario, negative nutrient budgets occur in 17, 20, 16, and almost 94 % of the studied areas for Ca, K, Mg, and P, respectively. For a maximum nutrient loss (considering intensive harvesting) and supply assumptions, the affected areas increase to 50, 57, 45 and 96 % for Ca, K, Mg, and P, respectively. In general, atmospheric nutrient deposition is of minor importance for the high weathering supply cases. Increasing global woody biomass demand may cause additional pressure on forested ecosystems, enlarging negative nutrient budget areas. If woody biomass demand rises, strategies to counterbalance nutrient gaps might be needed, for example, by preparing harvested areas with rock products, designed to replenish growth limiting nutrients, and or implementing forest management strategies to minimize nutrient export.

2.2. Introduction

Global woody biomass use for energy is expected to increase by 2050 (Lauri et al., 2014), driven by the biomass co-firing in conventional coal power plants and household fuelwood (Lauri et al., 2014) as attempt to decrease net carbon dioxide emissions (Delattin et al., 2006; Kazagic et al., 2016). Biomass co-firing might be beneficial in the long run only if the harvested land regrowth reaches the pre-harvest biomass levels, and if the biomass is maintained there (John et al., 2018). Some authors point out the controversial climate impacts of replacing coal by biomass as an energy source (John et al., 2018). However, choosing woody biomass for energy production is mainly influenced by its low CO₂ mitigation costs and its negative financial gap to coal from -0.03 to 0.04 € kWh_{el}⁻¹ or -8.3×10^{-9} to 11×10^{-9} € J⁻¹ (Ehrig and Behrendt, 2013). EU-27 plus Norway and Switzerland reported a CO₂ emission reduction by 12.6×10^6 t using wood pellets as an alternative energy source in 2008 (Sikkema et al., 2010). Globally retrofitting coal power plants and firing them with 1 – 10 % of biomass is expected to reduce CO₂ emissions by $45 - 450 \times 10^6$ t a⁻¹ by 2035 (Lempp, 2013).

In 2014, wood and agglomerated wood products; i.e., pellets and briquettes, provided almost half (45 %) of EU-28's total inland energy production by renewables (Eurostat, 2016). Current European renewable energy policy will boost woody biomass demand (Mantau et al., 2010) and, considering 2015 as baseline, the global woody biomass demand is expected to be 23×10^6 t a⁻¹ in 2024 representing a 70 % increase (RISI, 2015). For 2050 (Lauri et al., 2014), global woody biomass use for energy is expected to increase by 1.6×10^{10} t a⁻¹ (obtained from 2.3×10^{10} m³ a⁻¹ by assuming 0.7 t m⁻³ as average woody biomass bulk density) representing a potential energy production ranging from $2.7 - 3 \times 10^{20}$ J a⁻¹ (for a $1.7 - 1.9 \times 10^{10}$ J t⁻¹ biomass' energy output (DIN, 1996; Sherman, 2012)). By the late 21st century, the biomass energy production is expected to be $2.4 - 8.5 \times 10^{20}$ J a⁻¹

(Hoogwijk et al., 2005), which is approximately two orders of magnitude higher than the 2016 biomass energy production of $1.8 \times 10^{18} \text{ J a}^{-1}$ (Ren21, 2017).

The increasing European demand of forest related biomass requires imports from other areas in the world (Sikkema et al., 2011). Frequent logging residue removal can impact long-term nutrient cycling (Smolander et al., 2010). Since practices like whole-tree harvest are adopted, the wood and increasingly its “remains” are permanently detracted from the local nutrient cycle. High rates of nutrient export can negatively impact the nutrient budgets in low geogenic nutrient supply areas (Smolander et al., 2010).

Already, soil nutrient deficiency is observed for forests with intensive harvest practices in Germany (Knust et al., 2016) and in Belgium (Vangansbeke et al., 2015). Considering tree harvest, negative budgets were reported for North America (Crowley et al., 2012; Duchesne and Houle, 2008; Keys et al., 2016; Vadeboncoeur et al., 2014). Deficiency in nutrients causes elevated tree mortality and lower resistance to pests (Duchesne and Houle, 2008) as well a decrease in biomass productivity (Jonard et al., 2015; Vangansbeke et al., 2015) and soil fertility (Vangansbeke et al., 2015). Low tree mineral nutrition is already limiting the biomass yield in European forests (Jonard et al., 2015).

Natural nutrient pools are divided in short- and medium- to long-term stocks. The short-term nutrient stock in trees, forest floor, and soil has a larger nutrient contribution to tree growth than the long-term stock. The former can be divided in above ground (nutrients in trees and forest floor) and soil nutrients (Ranger and Turpault, 1999; Vangansbeke et al., 2015). Soil nutrients are expected to be most abundant in the upper 50 cm, while nutrient concentrations decrease with increasing depths (Jobbágy and Jackson, 2001; Phillips and Watmough, 2012; Vangansbeke et al., 2015). The medium- to long-term pool is represented by geogenic supply of nutrients from weathering and from atmospheric deposition (Ranger and Turpault, 1999). In some cases, slow weathering nutrient allocation may limit the biomass yield (Keys et al., 2016).

Lateral and partly trans-continental woody biomass exports potentially lead to significant nutrient loss in local ecosystems, which cannot be compensated by geogenic resupply, being itself controlled by local lithology and climatic conditions. This imbalance between harvest nutrient export and geogenic nutrient supply would lead to forest nutritional gaps. However, an evaluation of the potential gap between projected removal rates and the capacity of a system to replenish the geogenic nutrients is necessary. Therefore, exemplary quantification of potential continental United States nutritional gaps is done by quantifying the wood harvesting geogenic nutrient removal and subsequent export for different applied harvesting intensities. The obtained nutrient export is compared to quantified in-situ weathering and atmospheric deposition resupply rates. Such a comparison, in principle, enables the local pools potential nutrient depletion prediction for different harvesting rates and reforestation scenarios. Predicting potential nutrient depletion may help to guide future forest management practices (Ranger and Turpault, 1999). The objective here is to evaluate if geogenic nutrient supply is able to meet forest nutrient demand under high harvest rates for an increasing bioenergy demand in the future.

2.3. Methods

2.3.1. Timberland wood composition and nutrient loss.

Different variables control the nutrient concentration within biomass compartments, resulting in high nutrient variability in trees (Paré et al., 2013), which only enables first order large scale estimates. Based on the U.S. forest

type distribution map (USDA Forest Service and U.S. Geological Survey, 2000) and a tree chemistry database (Pardo et al., 2005), the lateral exports for Mg, Ca, K, and P nutrients by wood harvest were quantified.

Considering future bioenergy demand increase, a complete dead wood, stem, bole, branch, twig, and foliage harvest is assumed (Olsson et al., 2017; Vangansbeke et al., 2015), making it possible to neglect the nutrient contribution by in-situ biomass decay. In addition, a scenario is provided assuming twigs and leaves remaining in the ecosystem. Wood harvest area distribution and harvest intensities (Appendix B), ranging from ≤ 140 to $\geq 1574 \text{ m}^3 \text{ km}^{-2}$ (Appendix B Fig. S 1), were taken from the U.S. Forest Service (2016). Mg, Ca, K and P loss rate of ecosystems based on these harvest rate intensities were calculated by Eq. (6):

$$\text{Nutrient loss } (N_i) = M_i C_w, \quad (6)$$

with

$$\text{Wood yield } (M_i) = \text{Class}_i \rho_{\text{wood}} V_b, \quad (7)$$

where N_i represents the nutrient loss [$\text{kg km}^{-2} \text{ a}^{-1}$] calculated for 25th or 75th exported nutrient quartiles, M_i is the area normalized wood harvested mass [$\text{kg km}^{-2} \text{ a}^{-1}$], C_w [-] is the 25th or 75th quartile fraction of each nutrient ‘w’ within Timberland wood (Appendix B Table S 1), Class_i [$\text{m}^3 \text{ km}^{-2}$] represents the minimum or maximum harvest rate per harvest class provided by the U.S Forest Service (2016), ρ_{wood} [kg m^{-3}] is the wood density (Forest Products Laboratory, 2010; Appendix B Table S1), V_b is a correction factor for bundled wood volume, depending on material properties such as tortuosity, homogeneity, diameter and log length, assumed to be 0.7 [-] according to Hahn et al. (2014).

2.3.2. Nutrient supply.

Nutrients are sourced from weathering and atmospheric deposition. They consider spatially explicit and averaged data. Geogenic nutrient supply is the sum of weathering nutrient fluxes and atmospheric nutrient precipitation. Total (wet + dry) atmospheric nutrient precipitation rates from atmospheric deposition maps (National Atmospheric Deposition Program, 2016) were used for obtaining the applied 25th and 75th quartiles, and median deposition rates for Mg, Ca, and K for 2000 until 2015 (Appendix C, Fig. S 3 to Fig. S 5). The phosphorus atmospheric deposition rate was obtained from a global model (Mahowald et al., 2008) with a coarser resolution than for the other elements (Appendix C Fig. S 5).

Nutrient supply from chemical weathering for twelve aggregated lithological classes (Appendix C section C3) are estimated assuming complete mass dissolution, based on spatially explicitly modeled weathering rates from literature (Appendix C section C2). To assess the probable long-term nutrient release range, the 25th and 75th quartiles, and median geochemical compositions for each lithological class were derived from geochemical databases (Appendix C Table S 4). The overall nutrient release rate (Appendix C section C4) is then calculated assuming a nutrient release rate proportional to the nutrient content in the lithological class relative to the sum of base cations released (Mg, K, Ca, Na, and Si) by Eq. (8):

$$Nf_{\text{calc}} = WR_{\text{calc}} \frac{C_e}{\sum_i^n C_i}, \quad (8)$$

where Nf_{calc} is the total nutrient release rate via weathering to the soil-ecosystem for element ‘e’ [$\text{kg km}^{-2} \text{ a}^{-1}$], which is Mg, K, Ca, or P. WR_{calc} (Appendix C section C2) is the weathering rate [$\text{kg km}^{-2} \text{ a}^{-1}$] taken from the model output after Hartmann et al. (2014b). C_e is the element ‘e’ (Mg, K, Ca, or P) concentration. C_i is the sum of base cations and silicon released via weathering concentration [weight - %]. For each considered element within

a lithological class, the 25th and 75th percentiles were used as minimum and maximum boundary scenarios (Appendix C section C3 Table S 4). Spatially explicit weathering nutrient release from each lithological class were used for quantifying the 25th and 75th quartiles, and median weathering nutrient fluxes (Appendix C section C4), which were added to the atmospheric precipitation rates to quantify the total geogenic nutrient fluxes (Appendix C section C5).

The averaged geochemical nutrient fluxes were compared to river hydrochemical fluxes from U.S. watersheds covered with at least 95 % of forests. The comparison should provide an estimate of the considered geogenic nutrients leaching (Appendix C section C5 Fig. S 8). As dissolved compounds' leaching is in general lower than calculated geogenic supply, the deficit calculations presented are interpreted as being conservative.

2.3.3. Nutrient budget.

The spatially explicit nutrient budget for geogenic nutrient supply and nutrient export was done to evaluate the actual system's nutrient situation. The spatially explicit nutrient budget considers geogenic nutrient supply and nutrient loss by practiced harvest rates derived from spatially explicit information. The procedures for obtaining the spatially explicit information for geogenic nutrient supply and harvest loss is described in Appendix D. The resulting maps for each element are presented in Appendix D (Fig. S 18 to Fig. S 25).

Diagrams to predict nutrient supply efficiency for different harvest nutrient loss scenarios considered eight differentiated scenarios (Appendix D Fig. S 17). Special attention is given to scenarios 1 and 8, as they represent the overall 25th and 75th percentiles for nutrient supply and nutrient harvest losses. For harvest loss, scenarios 1 and 8 are represented by the inferior and superior horizontal limits of the grey boxes in Fig. 1 and Fig. 2. The scenarios 2 to 7 correspond to the filled grey boxes. For the studied timberland area weathering supply only (Fig. 1) and total geogenic supply, including atmospheric deposition (Fig. 2), the vertical lines' lower and upper limits correspond to the 25th and 75th nutrient supply percentiles, while the filled circles represents the median values. The diagrams allow for a general discussion and provide an easy to understand tool to rapidly identify the potential weathering (Fig. 1) or geogenic (Fig. 2) general nutrient balance for a specific harvest rate. The detailed spatially explicit nutrient budgets calculations are shown in Appendix D for each element.

2.4. Results and Discussion

Nutrient supplies and losses for the total studied area, considering either supply by weathering, or weathering plus atmospheric deposition, are presented distinguishing supply scenarios for the given lithological classes (Fig. 1 and Fig. 2). Differences in weathering supply rates can be related to the following variables: (i) spatial correlation between the lithological geochemical composition; (ii) climate; (iii) weatherability of the lithological class. Thus, the lithology plays a major role for the calculated budgets provided in the Appendix D. For the presented data Fig. 1 and Fig. 2, the harvest rate related nutrient loss is constant, while the nutrient supply rates are variable.

Averaged nutrient loss and given weathering supply scenarios (Fig. 1) suggest that, in general, the phosphorus supply from all lithological classes cannot support the highest reported harvest rate of 3150 m³ km⁻² a⁻¹. For other nutrients, the highest losses can only be countered by certain lithological classes, depending on the element. However, in a spatially explicit case and considering maximum reported harvest rates, this might be different depending on the locality, as discussed below. For the lowest considered harvest rate of 70 m³ km⁻² a⁻¹, which is unlikely to occur in an intensive bioenergy demand scenario, averaged nutrient export potentially does not exceed the weathering supply for all investigated nutrients and for all lithological classes, with exception of one case (Fig.

1). If additional atmospheric nutrient deposition is taken into account, differences between nutrient supply and loss would decrease, depending on the harvest rate (Fig. 2).

Comparing the geogenic nutrient supply values from Fig. 2 to the measured averaged weathering/leaching rates, based on stream water samples of U.S. catchments covered with at least 95% forests, suggests overestimation for Mg, Ca, K, and P by two orders of magnitude or more (Appendix C section C5 Fig. S 8). However, physical erosion is another relevant nutrient loss term that is not considered here. Further evaluation for forested areas to address nutrient sinks caused by erosion is necessary. Nutrient export by erosion remains a critical sink term to be investigated for timberland area, which would show elevated physical erosion compared to natural forests (Croke et al., 1999; Mohr et al., 2013; Mohr et al., 2014).

Atmospheric Ca, K, Mg, and P deposition can be locally important for nutrient supply if weathering nutrient supply is low, like in dry areas. To highlight this, maps plotting the difference by subtracting the weathering supply from the atmospheric deposition supply were calculated for different supply scenarios (Appendix C section C5 Fig. S 9 to Fig. S 16). In general, the atmospheric deposition plays a minor role for the considered timberland areas, but can locally be relevant (cf., Appendix C section C5).

Local forest management would need regional data to reliably adjust the nutrient resupply to losses. Spatially explicit results for the studied 33,570 km² U.S. timberland area suggest that harvest nutrient loss exceeds geogenic nutrient supply for a significant proportion of that area, given the continental scale analysis approach. Considering a conservative scenario with minimum harvest nutrient loss and geogenic nutrient supply, negative budgets exist for Ca, K, Mg, and P in 17, 20, 16, and 94 % of the timberland area, respectively (Appendix D and Fig. S 18 to Fig. S 21). For a maximum harvest nutrient loss and geogenic nutrient supply, the affected areas with a negative budget increase to 50, 57, 45, and 96 % for Ca, K, Mg, and P, respectively (Appendix D and Fig. S 22 to Fig. S 25).

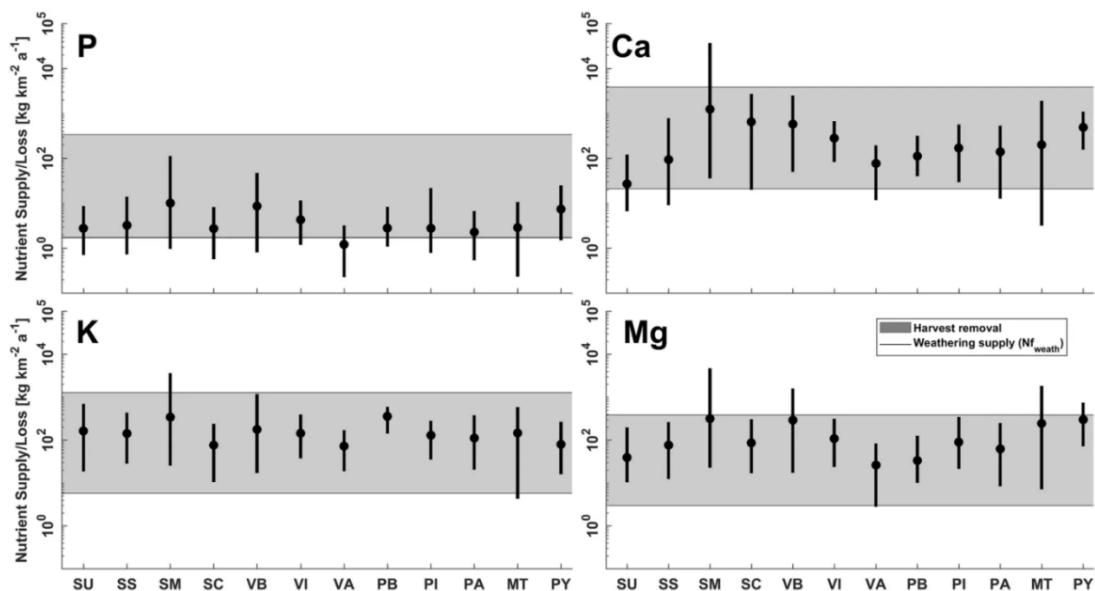


Fig. 1: Weathering nutrient supply averaged for all spatially explicitly studied areas, considering median (filled circles), minima, and maxima (whiskers) nutrient supply, compared to the potential nutrient loss by clear-cut scenarios (horizontal grey filled boxes). Harvest rates ranging between 70 m³ km⁻² a⁻¹ (Scenario 1 from Appendix D Fig. S 17) and 3150 m³ km⁻² a⁻¹ (Scenario 8 from Appendix D Fig. S 17) correspond to the shaded areas. Abbreviations: Unconsolidated sediments (SU), siliciclastic sedimentary rocks (SS), mixed sedimentary rocks (SM) and carbonate sedimentary rocks (SC) representing the group of sedimentary rocks. Basic volcanic rocks (VB), intermediate volcanic rocks (VI) and acid volcanic rocks (VA), represent the volcanic rock group. Basic plutonic rocks (PB), intermediate plutonic rocks (PI) and acid plutonic rocks (PA), constitute the plutonic rock group. Metamorphic rocks (MT) and pyroclastic rocks (PY). The number of samples used for rock class composition statistics (n values) are presented in Appendix C section C3 Table S 4.

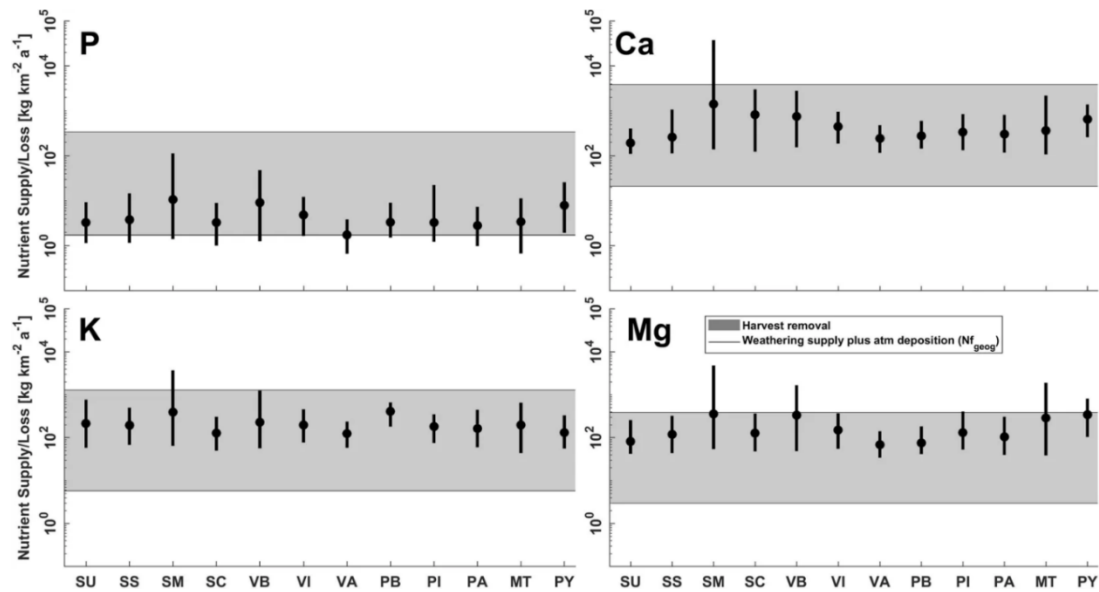


Fig. 2: Total assumed geogenic supply by weathering and atmospheric deposition averaged for all spatially explicitly studied areas, considering median (filled circles), minima, and maxima (whiskers) nutrient supply, compared to the potential nutrient loss by clear-cut scenarios (horizontal grey filled boxes). Harvest rates ranging between $70 \text{ m}^3 \text{ km}^{-2} \text{ a}^{-1}$ (Scenario 1 from Appendix D Fig. S 17) and $3150 \text{ m}^3 \text{ km}^{-2} \text{ a}^{-1}$ (Scenario 8 from Appendix D Fig. S 17). Nutrient loss for scenarios 2 to 7 from Appendix D Fig. S 17 correspond to the shaded areas. For abbreviations refer to Fig. 1.

Higher harvest rotation frequencies are expected to meet an increasing biomass demand for energy production (Hoogwijk et al., 2005; Lauri et al., 2014; RISI, 2015). Rotations and tree clear-cut intensification will widen the areas with a negative nutrient budget. To manage these gaps between nutrient supply and loss, and to avoid growth limitations, a sustainable forest management will rely on external nutrient sources to provide a long-term balanced system. However, to assess when a system becomes growth limited by shortage of one or more of the nutrients discussed is still a matter of debate (Jonard et al., 2015; Vangansbeke et al., 2015).

Aside from negative nutrient budget issues, the wood harvest intensification may increase soil nutrient leaching (Grand et al., 2014; Huber et al., 2010; Lewandowski et al., 2016), runoff and soil erosion rates (Croke et al., 1999; Mohr et al., 2013; Mohr et al., 2014), and the organic carbon loss from soils if no countermeasures are taken (Achat et al., 2015; Christophel et al., 2013; Dean et al., 2017; Foote et al., 2015; Ortiz et al., 2014).

Whole-tree or clear-cut harvests magnify nutrient losses due to biomass export. From the analysis, harvest rates and nutrient export are proportionally related. Implementing lower harvest rates would diminish nutrient export, decrease nutritional gaps and, in some cases, even avoid them or lead to a positive nutrient budget. Logging residue removal can negatively impact the long-term nutrient balance (Smolander et al., 2010), especially in low geogenic nutrient resupply regions. An alternative practice to keep the long-term nutrient balance is to leave the logging residues (branches and tops) on the harvested site due to their high nutrients concentration relative to other tree compartments (Thiffault et al., 2011).

For the spatially explicit data, if harvest remains are left in the field, calculated negative budget areas decrease only slightly to 16, 17, 15, and 93 % of the total area for Ca, K, Mg, and P respectively, for a conservative scenario with minimum harvest nutrient loss and geogenic nutrient supply. For a maximum harvest nutrient loss and geogenic nutrient supply, the negative budget areas would decrease to 46, 51, 42, and 95 % of the total area for Ca, K, Mg, and P respectively. Therefore, this practice to restore a balanced nutrient budget does not seem to be suitable for all locations.

Suitable rock products as slow-release nutrient sources (on decennial timescales) are an alternative that might be used to artificially replenish the system (Hartmann et al., 2013) for harvest rotations in a centennial time span.

Mafic or carbonate rock sources may be suitable for Ca and Mg supply, while more felsic plutonic rock sources (Manning, 2010) might be needed to supply K. Excess cation release, not taken up by plants, has the potential to sequester atmospheric CO₂ (Hartmann et al., 2013; Strefler et al., 2018; Taylor et al., 2015). Coupling the application of rock products with other soil amendment strategies, such as biochar, may increase the plant nutrient availability by increasing soil's cation exchange capacity, especially from highly weathered soils of low fertility (Glaser et al., 2001).

Some of the exported nutrients can potentially be returned to the catchment by the application of ash residues from bioenergy production (Freire et al., 2015), and probably mitigate nutrient loss. This practice can also supply nutrients like Ca, Mg, K (Freire et al., 2015; Trivedi et al., 2016), and P (Brannvall et al., 2015; Cruz-Paredes et al., 2017), without extra N input (Knust et al., 2016) at the same time, therefore, creating a reuse of ash remnants from biomass burning (evaluating the nutrient cycle of the considered element). However, in this case, issues of solubility speed and nutrient release from ash must be addressed (Freire et al., 2015) to prevent early loss from the system via lateral water transfer to river systems. In 2014, European countries imported 20.5×10^6 t of wood pellets (FAO, 2015) representing an inlet of 3.7, 24.6, 12.1 and 1.8×10^3 t of Mg, Ca, K, and P, respectively. For K and P, it represents 0.5 and 0.3% of 2014 western and central Europe fertilizer consumption (IFA, 2017).

2.5. Conclusions

Tree nutrient removal by high harvest rates, within studied timberland areas, can often not be compensated by atmospheric deposition and weathering nutrient supply. Increasing future woody biomass demand will likely lead to intensified forest harvesting. Growing rates for reaching the demand may be restrained by negative nutrient budgets due to limiting kinetics in nutrient resupply by weathering (Hartmann et al., 2014b). Additionally, high harvest rates will trigger enhanced soil nutrient leaching (Grand et al., 2014; Huber et al., 2010; Lewandowski et al., 2016), runoff, and soil erosion rates (Croke et al., 1999; Mohr et al., 2013; Mohr et al., 2014), decreasing the nutrient stocks. It has been experimentally shown that an expected fertilization effect of increasing atmospheric CO₂ can be potentially prevented by limited nutrient stocks (Oren et al., 2001). However, the numbers of studies focusing on this effect or nutrient limitations in biomass production for future bioenergy demands are lacking. Therefore, the additional biomass amount, which can be produced by closing the supply-demand gap, is until now not known. Compilations of studies, which provide the needed parameters to optimize forest biomass production for a given climate, lithological underground, soil and atmospheric deposition would guide and assist future large or global scale forest management strategies.

Negative nutrient budgets can be avoided by decreasing harvest intensities, recycling harvest remains (Thiffault et al., 2011; Wall and Hytönen, 2011) and or by providing an external nutrient input, either by industrial agrochemicals or natural rock products of specifically tailored geochemical character (Hartmann et al., 2013; Straaten, 2007; Strefler et al., 2018). However, proper knowledge on spatially explicit limitations on forest biomass growth rates is still missing, yet would be needed to assess a realistic global forest bioenergy potential and to close local geogenic nutrient gaps by appropriate measures (Huber et al., 2010; Jonard et al., 2015; Knust et al., 2016; Vangansbeke et al., 2015).

Through the export of wood products, nutrients are transported across continents; e.g., nutrients taken from North America are exported to Europe. Remains from biomass combustion represent a yet mostly untapped source of nutrients which could partly buffer increasing nutrient deficiencies, if they re-enter the local scale nutrient cycles, and if early flushing out of the system can be avoided (Freire et al., 2015).

This study presents an overview for timberland nutrient budgets, considering increasing bioenergy demand. Empirical data is necessary to assess and verify global effects of projected increasing harvest rates. Therefore, a multitude of tailored local scale studies and compilations of past studies might be necessary. The development of proper weathering models to calculate nutrient budgets for local forest management is also necessary. Details on nutrient requirements and geogenic nutrient supply would allow location-specific cataloguing of the geogenic nutrient demand for reforestation procedures based on lithologic, climatic and soil properties. As geogenic supply will probably not be able to cope with increasing biomass demands, forest management alternatives for long-term nutrient resupply are needed.

3. Impacts of enhanced silicate rock weathering on biomass production for negative emission technologies and soil hydrology

This chapter has been published as: Garcia, W. de O., Amann, T., Hartmann, J., Karstens, K., Popp, A., Boysen, L. R., Smith, P., and Goll, D.: Impacts of enhanced weathering on biomass production for negative emission technologies and soil hydrology, Biogeosciences, 17, 2107-2133, 10.5194/bg-17-2107-2020, 2020.

3.1. Abstract.

Limiting global mean temperature changes to well below 2°C likely requires a rapid and large-scale deployment of negative emission technologies (NETs). Assessments so far have shown a high potential of biomass-based terrestrial NETs, but only a few assessments have included effects of the commonly found nutrient-deficient soils on biomass production. Here, we investigate the deployment of enhanced silicate rock weathering (EW) to supply nutrients to areas of afforestation-reforestation and naturally growing forests (AR) and bioenergy grasses (BG) that are deficient in phosphorus (P), besides the impacts on soil hydrology. Using stoichiometric ratios and biomass estimates from two established vegetation models, we calculated the nutrient demand of AR and BG. Insufficient geogenic P supply limits C storage in biomass. For a mean P demand by AR and a low-geogenic-P-supply scenario, AR would sequester 119 Gt C in biomass; for a high-geogenic-P-supply and low-AR-P-demand scenario, 187 Gt C would be sequestered in biomass; and for a low geogenic P supply and high AR P demand, only 92 Gt C would be accumulated by biomass. An average amount of ~150 Gt basalt powder applied for EW would be needed to close global P gaps and completely sequester projected amounts of 190 Gt C during the years 2006 – 2099 for the mean AR P demand scenario (2 – 362 Gt basalt powder for the low-AR-P-demand and for the high-AR-P-demand scenarios would be necessary, respectively). The average potential of carbon sequestration by EW until 2099 is ~12 Gt C (~0.2 – ~27 Gt C) for the specified scenarios. For BG, 8 kg basalt m⁻² a⁻¹ might, on average, replenish the exported potassium (K) and P by harvest. Using pedotransfer functions, we show that the impacts of basalt powder application on soil hydraulic conductivity and plant-available water, to close predicted P gaps, would depend on basalt and soil texture, but in general the impacts are marginal. We show that EW could potentially close the projected P gaps of an AR scenario, and nutrients exported by BG harvest, which would decrease or replace the use of industrial fertilizers. Besides that, EW ameliorates the soil's capacity to retain nutrients and soil pH and replenish soil nutrient pools. Lastly, EW application could improve plant-available-water capacity depending on deployed amounts of rock powder - adding a new dimension to the coupling of land-based biomass NETs with EW.

3.2. Introduction

To limit temperature increase due to climate change to well below 2°C compared to preindustrial levels by the end of the century, research efforts on negative emission technologies (NETs; i.e., ways to actively remove CO₂ from the atmosphere) intensify. Terrestrial NETs comprises, bioenergy with carbon capture and storage (BECCS); afforestation, reforestation and naturally growing forests (AR); enhanced silicate rock weathering (EW); biochar; restoration of wetlands; and soil carbon sequestration. From these land-based NET options, BECCS, AR, biochar, and EW can potentially be combined to increase atmospheric carbon dioxide removal (CDR) according to different authors (Amann and Hartmann, 2019; Beerling et al., 2018; Smith et al., 2016).

BECCS combines energy production from biomass and carbon capture at the power plant with subsequent storage. Sources for biomass-based energy production are crop and forestry residues (Smith, 2012; Smith et al., 2012;

Tokimatsu et al., 2017), dedicated bioenergy grass (BG) plantations (Smith, 2012; Smith et al., 2012), or short-rotation woody biomass from forestry (Cornelissen et al., 2012; Smeets and Faaij, 2007). Large-scale AR, as well as bioenergy plantations, requires extensive landscape modifications for growing forests or natural regrowth of trees in deforested areas to increase terrestrial CDR (Boysen et al., 2017a; Humpeöder et al., 2014; Kracher, 2017; Popp et al., 2017), and huge quantities of irrigation water (Bonsch et al., 2016; Boysen et al., 2017b). The biomass yields of AR and agricultural bioenergy crops directly correlate with fertilizer application, which in turn could reduce CDR efficiency due to related emissions of N₂O (Creutzig, 2016; Popp et al., 2011) and initiate unwanted side effects like acidification of soils (Rockström et al., 2009; Vitousek et al., 1997), streams and rivers, and lakes (Vitousek et al., 1997).

Under intensive growth scenarios, nutrient supply is a critical factor (Garcia et al., 2018). According to Liebig's law of the minimum, supplying high amounts of nitrogen (N) might shift growth limitation to other nutrients (von Liebig and Playfair, 1843). Some U.S. forests are already showing changes in line with moving from an N-limited to a phosphorus-limited (P-limited) system caused by increases in N atmospheric deposition (Crowley et al., 2012) along with magnesium (Mg), potassium (K) and calcium (Ca) deficiencies (Garcia et al., 2018; Jonard et al., 2012). Poor nutrient supply, related to deficient mineral nutrition, may reduce tree growth (Augusto et al., 2017). Impacts on biomass production due to poor tree nutrition has been observed in European forests (Jonard et al., 2015; Knust et al., 2016), decreasing the carbon sequestration of forest ecosystems (Oren et al., 2001) – a factor rarely included in climate models, leading to overestimated CDR potential.

Specifically, global simulations with an N-enabled land surface model (Kracher, 2017) suggest that insufficient soil nitrogen availability for a representative greenhouse concentration pathway 4.5 (RCP4.5) AR scenario (Thomson et al., 2011) could lead to a reduction in the cumulative forest carbon sequestration between the years 2006 and 2099 by 15%. Goll et al. (2012) showed that carbon sequestration during the 21st century in the JSBACH land surface model was 25% lower when N and P effects were considered.

Mineral weathering is a natural and primary source of geogenic nutrients (e.g., Mg, Ca, K, and P; Hopkins and Hüner, 2008; Landeweert et al., 2001; Singh and Schulze, 2015; Waldbauer and Chamberlain, 2005) and controls atmospheric CO₂ concentrations over geological timescales (Berner et al., 1983; Lenton and Britton, 2006; Waldbauer and Chamberlain, 2005; Walker et al., 1981; Yasunari, 2020). Chemical dissolution of silicate minerals increases alkalinity fluxes (Gaillardet et al., 1999; Hartmann et al., 2009; Kempe, 1979), and natural weathering sequestration can range from 0.1 to 0.3 Gt C a⁻¹ (Gaillardet et al., 1999; Hartmann et al., 2009; Moon et al., 2014). To sequester significant amounts of CO₂ within decades, EW aims to speed up weathering processes by increasing the mineral reactive surfaces through rock comminution (Hartmann and Kempe, 2008; Hartmann et al., 2013; Schuiling and Krijgsman, 2006). Mineral–soil–microorganism interactions (e.g., by mycorrhizal fungi; Kantola et al., 2017; Landeweert et al., 2001; Taylor et al., 2009) increase the volume of soil that plant roots can extract nutrients from (Clarkson and Hanson, 1980; Hopkins and Hüner, 2008), which might enhance the weathering activity in addition to the reaction with dissolved CO₂. EW further increases soil pH by alkalinity fluxes, and could be a long-term source of macronutrients (e.g., Mg, Ca, K, P, and S) and micronutrients (e.g., B, Mo, Cu, Fe, Mn, Zn, and Ni; Anda et al., 2015; Beerling et al., 2018; Hartmann et al., 2013; Leonardos et al., 1987; Nkouathio et al., 2008), rejuvenating the nutrient pools of soils.

P is a rather immobile soil nutrient, and only a small fraction of soil P is readily available for plant uptake, limiting plant growth in a wide range of ecosystems (Elser et al., 2007; Shen et al., 2011). P content in soils is a result of a process controlled by the interactions of parent material (primary rocks) with climate, tectonic uplift, and erosion

history through geological time (Porder and Hilley, 2011). The processes of P transfer between biologically available and recalcitrant P pools influence at most P availability (Porder and Hilley, 2011). Orthophosphate (H_2PO_4^- or HPO_4^{2-}) is the chemical species adsorbed by plants (Shen et al., 2011) and its solubility is controlled by soil pH as deprotonation occurs when pH increases. Ideal pH conditions for orthophosphate availability are from 5 to 8 (Holtan et al., 1988), with soil moisture influencing soil P availability for different crops (He et al., 2005; He et al., 2002; Shen et al., 2011), and natural ecosystems (Goll et al., 2018).

The inclusion of soil hydraulic properties in the evaluation of EW effects is important as the soil water content has a strong influence on average crop yield. Practices that increase the plant-available water (PAW) are thought to mitigate drought effects on crops (Rossato et al., 2017). The water content of soils also seems to influence soil erosion rates and surface runoff (Bissonnais and Singer, 1992). In addition, soil water content influences soil pCO_2 production, which is a relevant agent for mineral dissolution (Romero-Mujalli et al., 2018).

Deploying land-based NETs would imply large changes in a local landscape nutrient and water cycle. At least 65% of worldwide soils (6.8×10^9 ha of land) have unfavorable soil conditions for agricultural production (Fischer et al., 2001). Therefore, we assess if applications of rock mineral-based P sources could close eventual nutritional gaps in an environment with natural N supply (N-limited) and with N fertilization (N-unlimited), using a global afforestation scenario. In addition, we investigate the effects of coupling nutrient-supplying (EW) to nutrient-demanding (AR and BG) land-based NETs by focusing on the efficiency of different upper limits of basalt powder to supply nutrients. We hypothesize that large-scale EW deployment potentially changes soil texture. Therefore, threshold values for impacts on soil hydraulic conductivity and plant-available water will be determined.

3.3. Methods

Since phosphorus (P) is a limiting nutrient in a wide range of ecosystems (Elser et al., 2007), we performed a P budget for an N-stock-based P demand from an AR scenario considering natural N supply (hereafter N-limited) and N fertilization (hereafter N-unlimited). We selected two N supply scenarios since the related P demand is proportional to biomass N stock, but in the main text we discuss only the N-limited AR scenario. We estimated the balanced supply of Mg, Ca, and K for each supplied P-based on ideal Mg, Ca, and K demand of AR derived from databases of biomass nutrient content. Balanced nutrient supply is necessary to avoid shift of growth limitation to other nutrients, which can occur according to Liebig's law (von Liebig and Playfair, 1843). Shift of growth limitation to other nutrients is observed for some U.S. forests that changed from an N-limited to a P-limited system after an increase in atmospheric N deposition (Crowley et al., 2012). Based on minimum and maximum harvest rates of bioenergy grass (BG), we estimated the related P and K export by harvest from the fields. We decided on these nutrients for BG since crops require large amounts of K and P, once N demand is covered. The amount of rock powder required for enhanced silicate rock weathering (EW) to cover projected P gaps and to replenish exported nutrients was estimated. The projected impacts on soil hydrology due to EW deployment were carried out by pedotransfer functions since they are used to estimate soil hydraulic properties (Schaap et al., 2001; Whitfield and Reid, 2013; Wösten et al., 2001) and such approximations have proven to be a suitable approach (Vienken and Dietrich, 2011).

The additional AR P demand, obtained for the 21st century for a N-unlimited and N-limited AR scenario (Kracher, 2017), was approximated by stoichiometric P:N ratios for mean and range (5th and 95th percentiles), which is a similar approach to that of Sun et al. (2017). The ratios were derived from databases of hardwood and softwood (Pardo et al., 2005) and foliar biome-specific nutrient content (Vergutz et al., 2012). We then compared the inferred

P demand to geogenic P supply given by observation-based estimates of soil inorganic labile P and organic P (Yang et al., 2014a); observation-based estimates of P release (Hartmann et al., 2014b) from weathering corrected to future temperature increases, since the uncertainty in the future hydrological cycle is too high (Goll et al., 2014); and estimated atmospheric P depositions from Wang et al. (2017) to derive the potential geogenic P deficits (i.e., the P gap) during the 21st century. Since the geogenic P supply cannot cope with N-stock-based P demand from the different AR scenarios within P gapped areas, the biomass production and biomass C sequestration, predicted by the AR scenarios, will be lower. Based on the amount of missing P, we estimated the C-stock reduction within P gapped areas by using stoichiometric C:P ratios. The C:P ratios were derived from simulated C-stock content (Kracher, 2017) and inferred N-stock-based P demand.

Necessary Mg, Ca, and K supply for balanced tree nutrition based on P supply was derived from N-stock-based Mg, Ca, and K additional demand normalized to the N-stock-based additional P demand (Fig. 3). The nutrient demand of bioenergy grass was estimated based on stoichiometric P:N and K:N ratios, used in Bodirsky et al. (2012), for minimum and maximum exported N proportional to harvest rates of the 1995 – 2090 period obtained from the agricultural production model MAGPIE (Fig. 3). Later on, the necessary amount of rock to cover the P gaps of the AR scenario and to resupply the nutrients exported by BG harvest was estimated (Fig. 3). In addition, the potential impact of deploying rock powder into the topsoil hydrology was modeled.

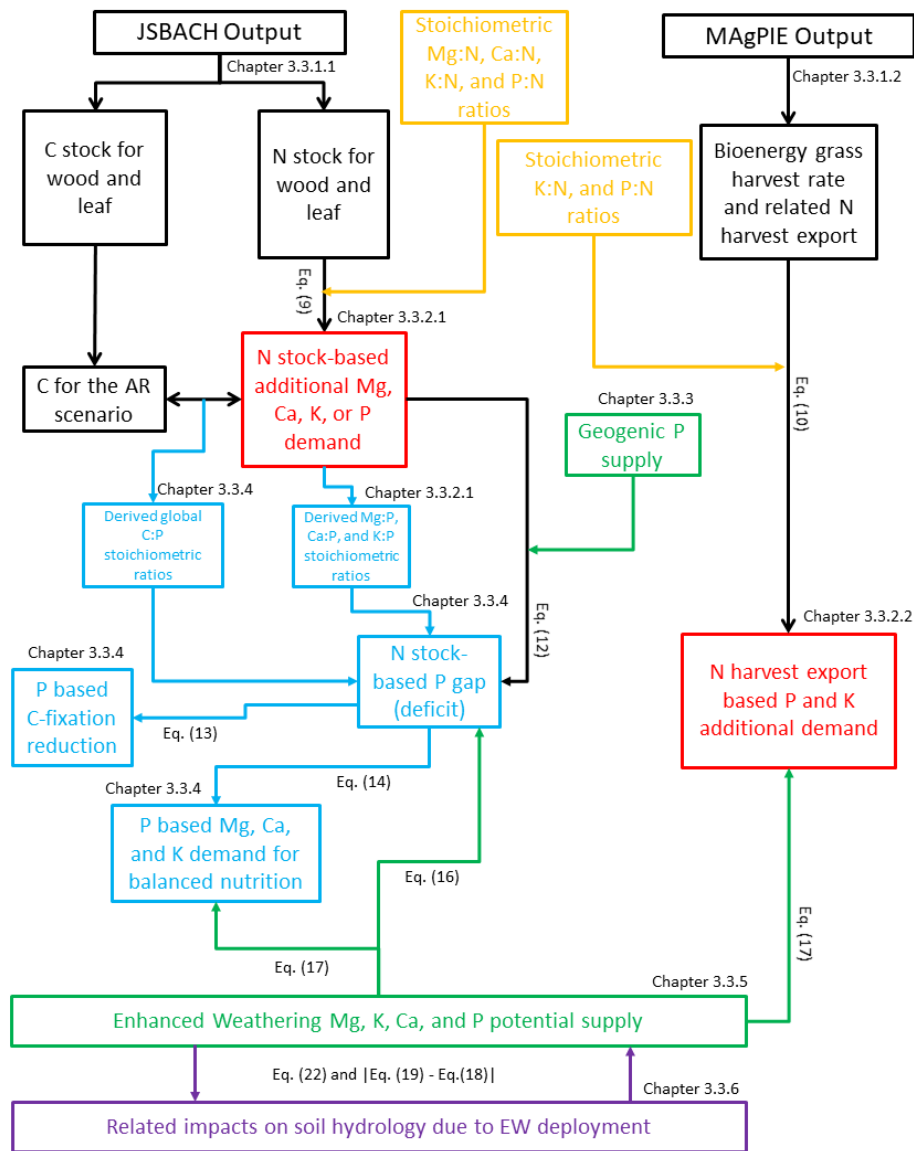


Fig. 3: Schematic steps and datasets used to derive geogenic nutrient demand from simulated biomass changes; P gaps; reduced C sequestration; and Ca, K, and Mg supply for balanced tree nutrition. Black colors: outputs from land surface model JSBACH and agricultural production model MAgPIE. Yellow colors: stoichiometric Mg:N, Ca:N, K:N, and P:N ratios used to obtain the N-stock-based nutrient demand. Red colors: N-stock-based P, Mg, Ca, and K demand for wood and leaf (AR) or N harvest export-based P and K demand (BG). Green colors: nutrient supply from geogenic sources (atmospheric P deposition and different soil P pools) or from enhanced silicate rock weathering. Blue colors: derived P gap for AR; derived stoichiometric C:P, Mg:P, Ca:P, and K:P ratios; P-based C-fixation reduction; and P-based Mg, Ca, and K supply for balanced tree nutrition. Purple colors: related EW deployment impacts on soil hydrology estimated by pedotransfer functions. AR: afforestation-reforestation, BG: bioenergy grass.

3.3.1. Global land-system model output

3.3.1.1. Afforestation and reforestation

The idealized simulations for the AR system from Kracher (2017) performed by the land surface model JSBACH (Reick et al., 2013) for RCP4.5 were used (Thomson et al., 2011). The RCP4.5 scenario assumes that the emissions peak is around 2040 and considers that forest lands expand from their present-day extent (Thomson et al., 2011). The coupled terrestrial nitrogen-carbon cycle model assumes N-unlimited and N-limited conditions and considers harvest rates and transitions between different anthropogenic and natural land cover types (Hurt et al., 2011) for a Gaussian grid of approximately $2^{\circ} \times 2^{\circ}$ resolution. Accounting for the N cycle reduces the uncertainty in atmospheric carbon sequestration prediction by AR models (Zaehle and Dalmonech, 2011). In JSBACH, the N

supply for plants is controlled by competition between plants and decomposing microbes, while other numerical models prioritize immobilization or plant growth (Achat et al., 2016).

The net primary productivity (NPP) calculation was based on atmospheric CO₂ concentrations, stomatal conductance, and water availability. JSBACH considers mass conservation, a supply–demand ansatz, and fixed C:N ratios (Goll et al., 2012). The coupled terrestrial nitrogen–carbon cycle model was selected since it (i) considered forest regrowth on abandoned croplands (which in the long-term become acidic and consequently favor leaching of nutrients and heavy metals; Hesterberg, 1993), (ii) considered natural shift in natural vegetation, (iii) considered a natural N supply scenario (N-limited) and an N-fertilized scenario (N-unlimited), (iv) considered future CO₂ increase leading to CO₂ fertilization, and (v) explicitly considered large-scale afforestation.

We retrieved the annual changes in N and C content of different pools, i.e., wood (above and below ground, also including litter) and foliar (above and below ground, also including litter) for temperate, cold, tropical, and subtropical plant functional types climate growing forests and shrubs for the years 2006 – 2099 and annual model output.

3.3.1.2. Biomass production from bioenergy grass

Simulations of BG nutritional needs from the agricultural production model MAgPIE, a framework for modeling global land systems (Dietrich et al., 2018; Lotze-Campen et al., 2008; Popp et al., 2010), were used. The objective of MAgPIE is to minimize total costs of production for a given amount of regional food, bioenergy demand and a given climate target (here RCP4.5, to correspond to the AR simulations). In its biophysical core, the yields in the model are based on LPJmL (Beringer et al., 2011; Bondeau et al., 2007; Müller and Robertson, 2013), a dynamic global vegetation model, which is designed to simulate vegetation composition and distribution for both natural and agricultural ecosystems.

At the starting point of the simulation, the LPJmL bioenergy grass yields have been scaled using agricultural land use intensity levels (Dietrich et al., 2012) for different world regions accounting for the yield gap between potential and observed yields for the period 1995 – 2005. For the future yields (2005 – 2090), the development is then driven by investments into yield-increasing technologies (Dietrich et al., 2014) based on the socioeconomic boundary conditions of the system.

The MAgPIE output had a frequency of 10 a, and the global minimum and maximum of each output year were taken to obtain the potential bioenergy grass minimum (0.7 kg m⁻² a⁻¹) and maximum (3.6 kg m⁻² a⁻¹) harvest rate for the simulation period for the areas with bioenergy plantations.

3.3.2. Nutrient demand

3.3.2.1. Afforestation and reforestation

The P, Mg, Ca, and K additional demand is defined as the amount of P, Mg, Ca, and K needed to realize the state of ecosystem N variables in each grid cell and year according to JSBACH output (Fig. 3). It was estimated from the spatially explicit information on average forest N content of each stock and plant functional type for a N-unlimited, and an N-limited AR scenario from Kracher (2017). Since P limits forest growth in a wide range of ecosystems (Elser et al., 2007), we performed a P budget for each AR scenario. The ideal P, Mg, Ca, and K biomass additional demands were based on the difference in the simulated change in N pools at that time with respect to the simulation year of 2006 multiplied by their corresponding Mg:N, Ca:N, K:N, or P:N ratios (r_{ij}) and were calculated following Eq. (9):

$$\Delta M_{pool,i} = \sum_{j=1}^n \Delta N_{ij} \times r_{ij}, \quad (9)$$

where $\Delta M_{pool,i}$ [$\text{kg m}^{-2} \text{a}^{-1}$] is the average N-stock-based Mg, Ca, K, or P demand for a given time in the future simulation time range (2007 – 2099) within a cell for biome i . ΔN_{ij} [$\text{kg m}^{-2} \text{a}^{-1}$] is the average N-stock change in pool j . The number of N pools is n . The N pools considered are: wood (above and below ground, including litter) and foliar (above and below ground, including litter).

The P, Mg, Ca, K, and N content of leaves obtained from a global leaf chemistry database (Vergutz et al., 2012) was used to derive the Mg:N, Ca:N, K:N, or P:N ratios (Table 1), which were already biome classified. For wood, the tree chemical composition database of US forests (Pardo et al., 2005) was used in order to derive the global ratios, which were assumed to represent the chemical composition of all biomes (Table 1).

The AR C content (Fig. 4) from Kracher (2017) and the resulting N-stock-based Mg, Ca, and K demand were normalized by the N-stock-based P demand to estimate the mean and range of the C:P, Mg:P, Ca:P, and K:P ratios of each grid cell. The stoichiometric C:P, Mg:P, Ca:P, and K:P ratios were used to derive the C-fixation reduction due to P deficiencies and the necessary Mg, Ca, and K supply for a balanced biomass nutrition based on supplied P (Fig. 3).

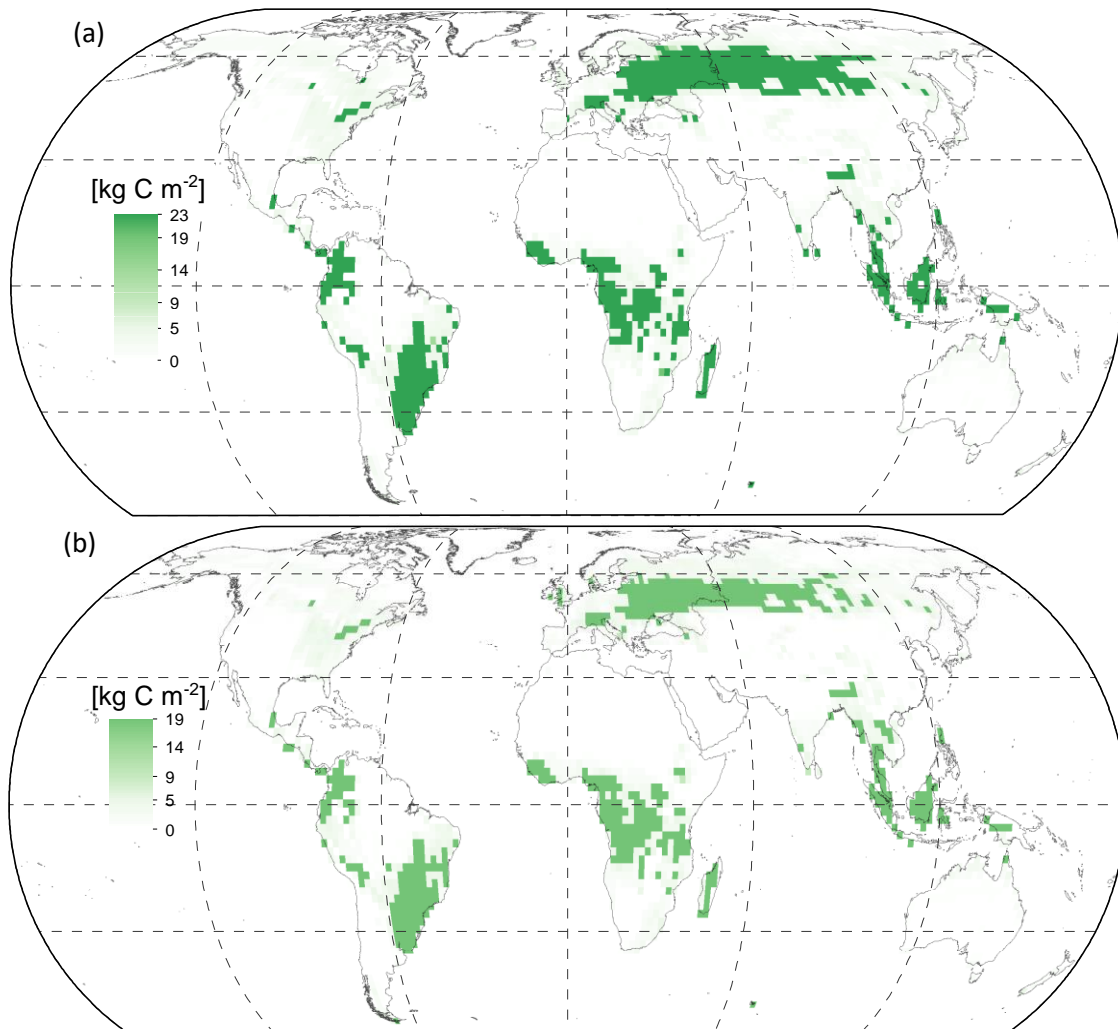


Fig. 4: Carbon sequestered in different afforestation-reforestation scenarios for the 21st century period (2006 – 2099) for an RCP4.5 scenario, according to Kracher (2017). a) For a N-unlimited AR scenario the global C sequestration is 224 Gt C. b) For an N-limited AR scenario the global C sequestration is 190 Gt C. Map generated with ESRI ArcGIS ver. 10.6 (<http://www.esri.com>).

Table 1: Stoichiometric parameters for different pools and biomes used in this study.

Biome	Tropical evergreen					Tropical deciduous					Temperate evergreen					
	Leaf ^a	mean	Std	n	5 th	95 th	mean	Std	n	5 th	95 th	mean	Std	n	5 th	95 th
C:N		29.7	15	4	16.3	46.5	27*	10.5*	171*	14.5*	46.7*	49.1	12.1	8	33.5	65.7
P:N		0.06	0.02	59	0.04	0.1	0.07	0.03	43	0.04	0.1	0.09	0.03	23	0.05	0.1
K:N	[-]	0.97	0.80	2	0.5	1.5	1.3	0.9	22	0.2	2.45	0.5	0.09	12	0.33	0.6
Ca:N		2.7	3.44	2	0.5	4.9	1.5	0.8	22	0.5	2.9	0.7*	0.7*	150*	0.16*	1.9*
Mg:N		0.40	0.52	2	0.07	0.7	0.4	0.3	22	0.1	0.8	0.2*	0.2*	115*	0.05*	0.7*
Wood ^b		mean	Std	n	5 th	95 th	mean	Std	n	5 th	95 th	mean	Std	n	5 th	95 th
C:N		235	244	9	56	610	235	244	9	56	610	235	244	9	56	610
P:N		0.1	0.2	684	0.04	0.3	0.15	0.2	684	0.04	0.3	0.1	0.2	684	0.04	0.3
K:N	[-]	0.6	0.4	700	0.2	1.2	0.6	0.4	700	0.2	1.2	0.6	0.4	700	0.2	1.2
Ca:N		1.8	1.3	705	0.4	4.3	1.8	1.3	705	0.4	4.3	1.8	1.3	705	0.4	4.3
Mg:N		0.2	0.1	681	0.1	0.4	0.2	0.1	681	0.1	0.4	0.2	0.1	681	0.1	0.4

Biome	Temperate deciduous					Shrubs raingreen					Shrubs deciduous					
	Leaf ^a	mean	Std	n	5 th	95 th	mean	Std	n	5 th	95 th	mean	Std	n	5 th	95 th
C:N		55.3	12	2	47.6	62.9	26.3	6.8	2	22	30.6	27*	10.5*	171*	14.5*	46.7*
P:N		0.08	0.03	32	0.04	0.1	0.07	0.01	2	0.06	0.08	0.08*	0.05*	662*	0.04*	0.2*
K:N	[-]	0.4	0.1	23	0.2	0.6	0.4	0.02	2	0.4	0.39	0.6*	0.4*	207*	0.2*	1.5*
Ca:N		0.7*	0.7*	150*	0.2*	1.9*	0.4	0.08	2	0.4	0.50	0.7*	0.7*	150*	0.2*	1.9*
Mg:N		0.2*	0.2*	115*	0.05*	0.7*	0.09	0.04	2	0.06	0.12	0.2*	0.2*	115*	0.05*	0.7*
Wood ^b		mean	Std	n	5 th	95 th	mean	Std	n	5 th	95 th	mean	Std	n	5 th	95 th
C:N		235	244	9	56	610	235	244	9	56	610	235	244	9	56	610
P:N		0.15	0.2	684	0.04	0.3	0.1	0.2	684	0.04	0.3	0.1	0.2	684	0.04	0.3
K:N	[-]	0.6	0.4	700	0.2	1.2	0.6	0.4	700	0.2	1.2	0.6	0.4	700	0.2	1.2
Ca:N		1.8	1.3	705	0.4	4.3	1.8	1.3	705	0.4	4.3	1.8	1.3	705	0.4	4.3
Mg:N		0.2	0.1	681	0.1	0.4	0.2	0.1	681	0.1	0.4	0.2	0.1	681	0.1	0.4

*Values obtained from all biomes. ^a Stoichiometric ratios derived from a global leaf chemistry database (Vergutz et al., 2012). ^b Stoichiometric ratios derived from a US soft- and hardwood database (Pardo et al., 2005).

3.3.2.2. Biomass production from bioenergy grass

The BG yield was obtained by the spatially explicit harvest rates within a grid cell for an output frequency of 10 a and a period of 95 a (1995 – 2090). The minimum $0.7 \text{ kg m}^{-2} \text{ a}^{-1}$ and maximum $3.6 \text{ kg m}^{-2} \text{ a}^{-1}$ harvest rates were used. With the information on exported N by each harvest rate, the exported K or P from cultivation fields (Eq. 2) was estimated based on the P:N, and K:N stoichiometric ratios used in Bodirsky et al. (2012). We have chosen these nutrients since crops require large amounts of K and P, once N demand is covered.

The simulated forests from the AR scenario are perennial, unlike bioenergy grasses which are completely harvested regularly due to their use as biomass feedstock for BECCS. Thus, the natural system's nutrient supply is insufficient for maintaining successive and constant yields, and the nutrients exported by harvest need to be replenished (Cadoux et al., 2012) to maintain high yields. The exported nutrients were calculated following Eq. (10):

$$Bio_x = r_x \times N_{harvest}, \quad (10)$$

where Bio_x corresponds to the exported nutrient P or K [$\text{kg m}^{-2} \text{ a}^{-1}$] by harvest. The P:N or K:N stoichiometric ratio used in Bodirsky et al. (2012) is r_x . $N_{harvest}$ is the exported N for a minimum $0.7 \text{ kg m}^{-2} \text{ a}^{-1}$ or a maximum $3.6 \text{ kg m}^{-2} \text{ a}^{-1}$ harvest rate. The harvest rate value was based on the MAGPIE output for each grid cell, representing the minimum and maximum projected global harvest rate for a period of 95 a.

3.3.3. Geogenic P supply for AR

The geogenic P source databases have different spatial resolutions (Table 2); we resampled each of them to a coarser $2^\circ \times 2^\circ$ spatial resolution field by nearest-neighbor interpolation to minimize distortions of location (Pontius, 2000). The nearest-neighbor interpolation method reliably retains the overall proportions of an original fine-resolution map (Christman and Rogan, 2012). As the uncertainty in which P pool is available for long-term plant nutrition is high (Johnson et al., 2003), two scenarios for soil P supply were investigated: scenario one, considering P from weathering and atmospheric P deposition, and scenario two, the same as scenario one plus inorganic labile P and organic P (Yang et al., 2014a).

The atmospheric dry and wet P deposition rates were taken from simulation outputs for the 2006 – 2013 period and for the years 2030, 2050, and 2099 for an RCP4.5 scenario for a grid cell size of 1° (Wang et al., 2017). The simulations were based on P emissions of sea salt, dust, biogenic aerosol particles, and P emitted by combustion processes, and performed by the global aerosol chemistry-climate model LMDz-INCA (see Wang et al. (2017), for a detailed description of model and model assumptions). The simulation gaps were closed by linear regression and the cumulative atmospheric P deposition was calculated by summing up the deposition rate of each cell for the 2006 – 2099 period according to Eq. (11):

$$P_{tot} = \sum_{i=2006}^{2099} P_i, \quad (11)$$

where P_{tot} [kg m^{-2}] is the cumulative atmospheric P deposition of the 2006 – 2099 period (Fig. 5a). P [$\text{kg m}^{-2} \text{ a}^{-1}$] is the atmospheric P deposition of each year i within a grid cell.

The total soil P map from Yang et al. (2014a) was used to estimate the projected long-term available P in the soil system (Fig. 5b). The total P supply by weathering for the 21st century (2006 – 2099) was based on Hartmann et al. (2014b) maps (Fig. 5c) that depict the chemical weathering as a function of runoff and lithology, corrected for temperature and soil thickness (Hartmann et al., 2014b) and calibrated on 381 catchments in Japan (Hartmann et al., 2009). A relationship between air temperature and weathering rate was used, which was derived from reconstructed weathering rates and different climate change scenarios for the recent past (1860-2005) using the

weathering model applied here. The relationship in which P weathering increases by 9% per 1°C increase (Goll et al., 2014) implicitly accounts for changes in soil hydrology, without accounting for P concentration changes in primary and secondary P minerals. Due to the large uncertainties in projected changes in soil hydrology we omitted a more detailed representation of hydrological effects on weathering.

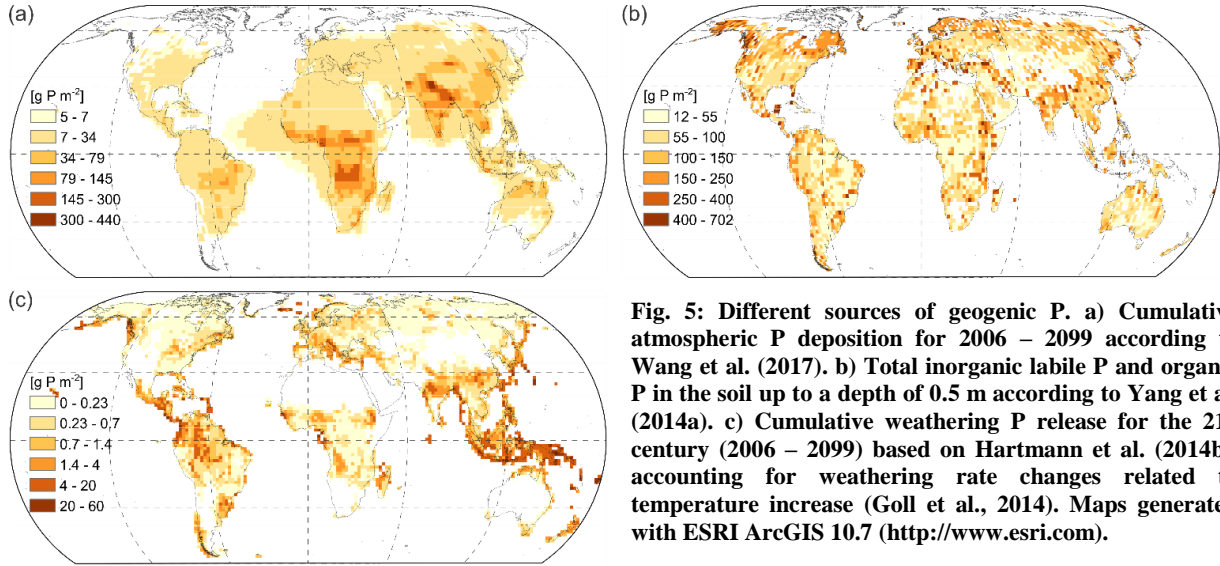


Fig. 5: Different sources of geogenic P. a) Cumulative atmospheric P deposition for 2006 – 2009 according to Wang et al. (2017). b) Total inorganic labile P and organic P in the soil up to a depth of 0.5 m according to Yang et al. (2014a). c) Cumulative weathering P release for the 21st century (2006 – 2009) based on Hartmann et al. (2014b), accounting for weathering rate changes related to temperature increase (Goll et al., 2014). Maps generated with ESRI ArcGIS 10.7 (<http://www.esri.com>).

Table 2: Geogenic P sources used for each geogenic P supply scenario.

P source	Resolution	Geogenic P supply scenario one	Geogenic P supply scenario two	Reference
Soil organic P and inorganic labile P	0.5°		X	(Yang et al., 2014a)
Atmospheric P deposition	1°	X	X	(Wang et al., 2017)
Geogenic P release rates	1 km ²	X	X	(Hartmann et al., 2014b)

3.3.4. Estimating geogenic P gap; related C-fixation reduction; and balanced Mg, Ca, and K supply for AR

The potential P gap (P_{gap} [kg m⁻²]) was estimated as the difference between the mean and range (95th and 5th percentiles) of additional P demand estimated from the N stock for the two different AR scenarios (see section 3.3.2.1), and the geogenic P supply from the different supply scenarios (P_{sup} [kg m⁻²]) within the cover fraction for a grid cell of biome i (f_i [-]), for the 21st century (2006 – 2009) according to Eq. (12):

$$P_{gap} = P_{sup} \times f_i - \Delta P_{pool,i} \quad (12)$$

The plant C-fixation reduction was estimated based on the P gap and calculated following Eq. (13):

$$C = r_C \times P_{gap} \quad (13)$$

where C [kg m⁻²] is the plant reduced plant C fixation due to the projected P gap. The used stoichiometric C:P ratio based on the mean and range (5th and 95th percentiles) chemistry for wood and leaves derived from the N-limited and N-unlimited AR scenario N stock as described in section 3.3.2.1 is r_C .

The Mg, Ca, and K necessary supply for balanced biomass nutrition (M_x [kg m⁻²]) should be proportional to the supplied P (P_{EW} [kg m⁻²]) and was calculated following Eq. (14):

$$M_x = r_x \times P_{EW}, \quad (14)$$

with P_{EW} being equal to the projected P_{gap} since it is covered by P from enhanced silicate rock weathering according to Eq. (15):

$$P_{EW} = P_{gap}, \quad (15)$$

where r_x is the used stoichiometric ratio Mg:P, Ca:P, or K:P obtained by normalizing the N-stock-based additional Mg, Ca, and K demand to the N-stock-based additional P demand.

3.3.5. Enhanced silicate rock weathering Mg, K, Ca, and P potential supply

To cover the potential of different igneous rocks for EW strategies, rhyolite and dacite (acidic rocks), andesite (intermediate rock), and basalt (basic rock) were selected to project necessary amounts to cover P gaps from the AR scenarios. Data on macronutrient concentrations (Mg, Ca, K, and P) in weight percent within these rocks were downloaded from the EarthChem web portal (Fig. 6; <http://www.earthchem.org>, last access: 14 July 2017). The data were selected for rocks categorized as rhyolite, dacite, andesite, and basalt, neglecting intermediate compositions between different lithotypes (i.e., a trachybasalt that has its chemical composition lying between trachyte and basalt). Rocks that were under any metamorphism grade (e.g., metabasalt) were neglected because metamorphism can change rock mineralogy. We neglected rocks known to have a high content of minerals rich in trace elements (e.g., an alkali basalt can have a P concentration >3000 ppm (Porder and Ramachandran, 2013), but it is rich in olivine (Irvine and Baragar, 1971; Winter, 2001), which contains elevated concentrations of nickel and chromium (Edwards et al., 2017)). Nickel and chromium are trace elements problematic for agriculture (Edwards et al., 2017). Thus, following the classification criteria, the numbers of selected data to calculate descriptive statistics for Mg, Ca, K, and P content within rocks were 2985 chemical analyses for rhyolite, 3008 chemical analyses for dacite, 11099 chemical analyses for andesite, and 23816 chemical analysis for basalt.

The nutrient supply was estimated assuming complete rock powder dissolution in the system considering the median and range (5th or 95th percentile) of chemical composition. The duration of complete rock powder dissolution varies depending on the grain size (i.e., 1 a for grain sizes between 0.6 and 90 μm for basalt; Strefler et al., 2018). The results and discussion will focus on basalt rock powder considering median P values (500 ppm) and range (5th (157 ppm) and 95th (1833 ppm) percentiles), as basalt is abundant worldwide (Amiotte Suchet et al., 2003; Börker et al., 2019) and has a high P content compared to acidic and intermediate rocks (Porder and Ramachandran, 2013). Median P concentration can be >3000 ppm for alkali basalts, but for a broader basalt classification that considered 97895 samples, it can be 916 ppm (Porder and Ramachandran, 2013). The necessary mass of rock powder to supply macronutrients (Mg, Ca, K, or P) was calculated following Eq. (16):

$$R_d = \frac{M_{ex}}{f_{nut}}, \quad (16)$$

where R_d [kg rock m^{-2} or $\text{kg rock m}^{-2} \text{a}^{-1}$] represents the mass of a rock type to cover AR or BG nutritional needs, M_{ex} [kg m^{-2} or $\text{kg m}^{-2} \text{a}^{-1}$] is the mass of required nutrient for AR or BG (e.g., P to cover a P_{gap} obtained by Eq. (12)), and f_{nut} [-] is the median and range (5th or 95th percentile) fractions of interest nutrient within the selected rock.

However, the potential nutrient supply by EW for different amounts of rock powder being deployed was also estimated following Eq. (17):

$$Nut_{in} = M_{rock} \times f_{nut}, \quad (17)$$

where Nut_{in} [kg m^{-2} or $\text{kg m}^{-2} \text{a}^{-1}$] represents the macronutrient input by dissolving a chosen rock. M_{rock} [kg rock m^{-2} or $\text{kg rock m}^{-2} \text{a}^{-1}$] is the mass of rock added to the natural system.

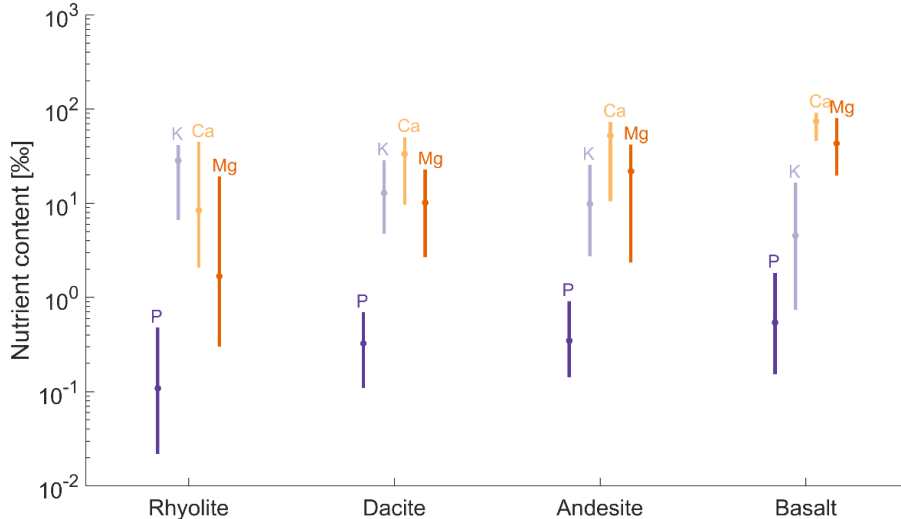


Fig. 6: Statistical data of major element concentration in rocks with median values (filled circles) and range (5th and 95th percentiles; whiskers). Values from EarthChem webportal (<http://www.earthchem.org>, last access: 14 July 2017). The numbers of chemical analyses used to calculate the descriptive statistics were 2985 chemical analyses for rhyolite, 3008 chemical analyses for dacite, 11099 chemical analyses for andesite, and 23816 chemical analyses for basalt.

3.3.6. Related impacts on soil hydrology from enhanced silicate rock weathering deployment

Large-scale deployment of rock powder on soils is expected to influence its texture. The deployed amount and texture of rock powder will somehow affect hydraulic conductivity, water retention capacity, and specific soil surface area. Pedotransfer functions (PTFs) are used to estimate soil hydraulic properties (Schaap et al., 2001; Whitfield and Reid, 2013; Wösten et al., 2001), and such approximations have proven to be a suitable approach (Vienken and Dietrich, 2011). PTFs make use of statistical analysis (Saxton and Rawls, 2006; Wösten et al., 2001), artificial neural networks, and other methods applied to large soil databases of measured data (Wösten et al., 2001). The equations from Saxton et al. (1986) performed the best estimations of soil hydraulic properties (Gijssman et al., 2002). Later on, Saxton and Rawls (2006) improved Saxton et al. (1986) PTFs, and they are used to estimate the effects on soil hydraulic properties due to deployment of basalt powder (Eqs. (18) – (26)).

The potential changes in soil hydraulic properties, due to the application of a fine basalt texture (15.6 % clay, 83.8 % silt, and 0.6 % fine sand) or a coarse basalt texture (15.6 % clay, 53.8 % silt, and 30.6 % fine sand), were estimated as a function of rock powder deployment for soils corresponding to P gap areas from the N-unlimited AR scenario. According to the international organization for standardization, the synthetic materials can be classified according to their grain sizes; therefore, here the clay comprises grain diameters $\leq 2 \mu\text{m}$, silt comprises grain diameters $2 - 63 \mu\text{m}$, and fine sand comprises grain diameters $63 - 200 \mu\text{m}$ (ISO 14688-1:2002), but since full dissolution is assumed, the ground basalt fine sand encompasses grain sizes of diameter $63 - 90 \mu\text{m}$ remaining within the ISO 14688-1:2002 classification. The N-unlimited AR scenario was selected since it would have the highest P deficiencies requiring more rock powder to cover the P gaps (i.e., it represents the maximum effect). The estimations are for a homogeneous mixture of rock powder and topsoil depth of 0.3 m. Downward transport of fine-grained material is neglected for simplification. The considered values represent upper limits of rock powder application. The impacts on plant-available water (PAW) is given by the difference between water content at a

pressure head of -33 kPa (Eq. (19)) and -1500 kPa (Eq. (18)), while the impact on soil hydraulic conductivity is given by Eq. (22) (Saxton and Rawls, 2006):

$$\theta_{1500} = \theta_{1500t} + (0.14 \times \theta_{1500t} - 0.02), \quad (18)$$

$$\theta_{33} = \theta_{33t} + (1.283 \times (\theta_{33t})^2 - 0.374 \times (\theta_{33t}) - 0.015), \quad (19)$$

$$\theta_{(S-33)} = \theta_{(S-33)t} + (0.636 \times \theta_{(S-33)t} - 0.107), \quad (20)$$

$$\theta_S = \theta_{33} + \theta_{(S-33)} - 0.097 \times S + 0.043, \quad (21)$$

$$K_S = 1930 \times (\theta_S - \theta_{33})^{(3-\lambda)}, \quad (22)$$

with:

$$\theta_{1500t} = -0.024 \times S + 0.487 \times C + 0.006 \times OM + 0.005 \times (S \times OM) - 0.013(C \times OM) + 0.068(S \times C) + 0.031, \quad (23)$$

$$\theta_{33t} = -0.251 \times S + 0.195 \times C + 0.011 \times OM + 0.006 \times (S \times OM) - 0.027 \times (C \times OM) + 0.452(S \times C) + 0.299, \quad (24)$$

$$\theta_{(S-33)t} = 0.278 \times S + 0.034 \times C + 0.022 \times OM - 0.018 \times (S \times OM) - 0.027 \times (C \times OM) - 0.584 \times (S \times C) + 0.078, \quad (25)$$

$$\lambda = \left[\frac{\ln(1500) - \ln(33)}{\ln(\theta_{33}) - \ln(\theta_{1500})} \right]^{-1}, \quad (26)$$

where S and C , respectively, represent the soil texture corresponding to sand and clay diameters [wt %]; OM is the soil organic matter [wt %]; and the moisture [wt %] is estimated by θ_{1500} and θ_{33} , respectively, representing the soil moisture for a pressure head of -1500 kPa ($R^2 = 0.86$) and -33 kPa ($R^2 = 0.63$). $\theta_{(S-33)}$ and θ_S , respectively, correspond to the 0 kPa to -33 kPa moisture ($R^2 = 0.36$), and to the saturated (0 kPa) moisture ($R^2 < 0.25$). K_S [mm h^{-1}] represents the saturated soil hydraulic conductivity, and λ is the slope of the logarithmic tension-moisture curve. The numbers in front of each described variable are regression coefficients (Saxton and Rawls, 2006).

The initial hydrologic properties of topsoil were estimated for a depth of 0.3 m, as it is the average depth at which usual machinery can homogeneously mix topsoil (Fageria and Baligar, 2008). Greater depths can be reached but under higher energy and labor costs (Fageria and Baligar, 2008). The global dataset of derived soil properties (Batjes, 2005), which had textural information (sand, silt, and clay content) for shallow soil depths (0.3 m), was used. The raster had a resolution of 0.5 °, and the soil properties for the interest areas of biomass growth limitation (the same as the areas displayed in Appendix E section ii Fig. S 32a) were included by a spatial join (using Esri ArcMap 10.8). The nutrient-deficient areas encompass soils of different textures and organic matter content, which had their initial K_S estimated separately based on Eq. (22). The sum of clay, silt, and sand fractions within each cell should always be a unity and were corrected when necessary by Eq. (27):

$$G_{cor} = \frac{(G_{ini} \times M_{soil_cell})}{\sum(G_{ini} \times M_{soil_cell})}, \quad (27)$$

with:

$$M_{soil_cell} = V_{cell} \times \rho_{bulk_cell}, \quad (28)$$

where G_{ini} represents the initial topsoil texture (sand, silt, and clay content) of a specific raster cell [-]. V_{cell} [km^3] is the raster cell volume obtained by multiplying the area [km^2] to the soil depth of 0.3×10^{-3} km. ρ_{bulk_cell} [kg km^{-3}] is the raster cell topsoil bulk density. M_{soil_cell} [kg] is the total soil mass of a raster cell. G_{cor} [-] is the corrected soil texture (sand, silt, and clay content).

The necessary rock powder mass was estimated by Eq. (16) to close the P_{gap} obtained by Eq. (12). The effect of basalt powder application in soil K_s and PAW was estimated by assuming a homogeneous mixture between applied basalt powder and topsoil. The changes in initial soil organic matter (SOM) concentration within a raster grid cell were obtained by normalizing the SOM to the sum of applied basalt mass, mass of soil, and initial SOM mass by Eq. (29). This was necessary since the SOM concentration at the moment of basalt deployment would have a relative decrease compared to initial SOM concentration:

$$OM_c = \frac{OM_{cell}}{M_{b_cell} + M_{soil_cell} + OM_{cell}} \times 100, \quad (29)$$

with

$$OM_{cell} = OM_{wt\%} \times M_{soil_cell}, \quad (30)$$

where OM_c [wt %] is the corrected soil organic matter content, OM_{cell} [kg] is the organic matter mass within the raster cell. M_{b_cell} and M_{soil_cell} , both in kilograms, are the mass of basalt and mass of soil for a specific raster cell. The impacts on soil texture by rock powder application considered the textures of applied basalt mass added to the initial soil mass by Eq. (31). A content of 15.6 % clay, 83.8 % silt, and 0.6 % fine sand for fine basalt powder and 15.6 % clay, 53.8 % silt, and 30.6 % fine sand for a coarse basalt powder was assumed.

$$G_{bs} = \frac{(G_{ini} \times M_{sed_cell} + M_{b_cell} \times G_{basalt})}{\Sigma(G_{ini} \times M_{sed_cell} + M_{b_cell} \times G_{basalt})}, \quad (31)$$

where G_{basalt} corresponds to the texture fractions of the fine or coarse basalt powder. G_{bs} corresponds to the texture fractions of the resulting mixture of basalt plus soil. Thus, the texture fractions of resulting mixture of basalt plus soil obtained by Eq. (31) were replaced within Eqs. (23) to Eq. (25) to estimate the impacts on soil hydraulic conductivity by Eq. (22) and PAW by subtracting the outcome from Eq. (19) to the outcome from Eq. (18), with clay size (grains $> 1 \mu\text{m}$ and $< 3.9 \mu\text{m}$) being the finest grain size we can consider.

Besides texture and organic matter, intrinsic grain properties (e.g., the shape of grains and pores, tortuosity, specific surface area, and porosity) should be considered (Bear, 1972). The equations from Beyer (1964) are based on the nonuniformity of grain size distribution and density of the grain packing to estimate soil properties. Carrier (2003) uses information on the particle grain size distribution, the particle shape, and the void ratio in his equations to estimate soil properties. However, such detailed information on a global scale is missing, making Beyer (1964) and Carrier (2003) equations not applicable to our analysis.

3.4. Results

3.4.1. Afforestation and reforestation P gaps and enhanced silicate rock weathering as nutrient source

The global C sequestration for the N-limited AR scenario is 190 Gt C, while for the N-unlimited AR scenario it is 34 Gt C higher. The AR model from Kracher (2017) shows an increase in biomass production in tropical and temperate zones (Fig. 4). The results only focus on the N-limited scenario since it considered natural N supply, but

the results for the N-unlimited scenario are presented in the appendix (Appendix E ii). The calculated P budgets according to Eq. (12) for the AR time of 2006 – 2099 (Fig. 8) considered different geogenic supply scenarios (scenario one – P from weathering and atmospheric P deposition; scenario two – the same as scenario one plus inorganic labile P and organic P) and the average and range N-stock-based P demand (calculated following Eq. (9)) for the AR simulation from Kracher (2017).

The ideal P biomass additional demand (calculated from Eq. (9)) to sequester 190 Gt C (N-limited AR scenario) amounts to 200 Mt P on a global scale for a mean wood and leaves P content; for the 5th and 95th percentile, the estimated P demand would be 71 and 345 Mt P, respectively. The P budget (estimated from Eq. (12)) for geogenic P supply scenario one suggests that P deficiency areas are distributed around the world but with more frequent occurrences in the Northern Hemisphere (Fig. 8a) and the P gaps can potentially reach up to $\sim 17 \text{ g P m}^{-2}$ ($\sim 4 - \sim 30 \text{ g P m}^{-2}$ for the 5th and 95th percentiles of wood and leaves chemistry; Table 3) or a global P gap of $\sim 77 \text{ Mt P}$ ($\sim 9 - 181 \text{ Mt P}^2$ for the 5th and 95th percentiles of wood and leaves chemistry; Table 3). However, for geogenic P supply scenario two, the P deficiency areas are predominantly located in the Southern Hemisphere (Fig. 8c) and the P gaps can potentially reach up to $\sim 7 \text{ g P m}^{-2}$ ($\sim 2 - \sim 12 \text{ g P m}^{-2}$ for the 5th and 95th percentiles of wood and leaves chemistry; Table 3) or a global P gap of $\sim 10 \text{ Mt P}$ ($1 - \sim 35 \text{ Mt P}^2$ for the 5th and 95th percentiles of wood and leaves chemistry; Table 3).

The P and N limitations cause an average C reduction of 47% for the geogenic P supply scenario one and 19% for the geogenic P supply scenario two (obtained by accounting for the C reduction from N limitation, which is 34 Gt C plus the C reduction from Table 3, and then normalizing by the global sequestration for the N-unlimited scenario of 224 Gt C) or ~ -1.1 and $\sim -0.5 \text{ Gt C a}^{-1}$, respectively. In some areas, the C sequestration can be reduced by up to 100% compared to the predicted C sequestration of the AR models (Fig. 7). Accounting for N and P limitation on AR suggests that the biomass production will be affected, consequently decreasing the C sequestration potential of AR strategies (Table 3 and Fig. 7). Therefore, supplying the demanded P would positively contribute to biomass reaching the predicted growth of the specific AR scenario.

Besides removing carbon from the atmosphere, EW can also amend soils by supplying nutrients and increasing alkalinity fluxes (Anda et al., 2015; Beerling et al., 2018; Hartmann et al., 2013; Leonardos et al., 1987; Nkouathio et al., 2008). Since basalt has higher P content compared to acidic and intermediate rocks (Porder and Ramachandran, 2013), it could be used as raw material for EW to cover the estimated P gaps of Fig. 8a and c. For a median basalt P content of 500 ppm (cf., subchapter 2.5), it would be necessary to apply ~ 33 and $\sim 13 \text{ kg basalt m}^{-2}$ (Fig. 8b and d) in areas of high P deficiency (~ 17 and $\sim 7 \text{ g P m}^{-2}$; Fig. 8a and c, respectively), considering the AR time span, the deployment rates would be less than $1 \text{ kg basalt m}^{-2} \text{ a}^{-1}$ if complete congruent dissolution occurs as assumed for further given scenarios.

The total amount of basalt powder to close the estimated P gaps seen in Fig. 8 would depend on the assumed geogenic P supply scenario and chemical composition of wood and leaves, but for a mean P chemical composition, at least $\sim 153 \text{ Gt basalt}$ would be necessary for geogenic P supply scenario one and $\sim 20 \text{ Gt basalt}$ for geogenic P supply scenario two. Basalt has a carbon capture potential of $\sim 0.3 \text{ t CO}_2 \text{ t}^{-1} \text{ basalt}$ (Renforth, 2012), resulting in $\sim 46 \text{ Gt CO}_2$ ($\sim 12.4 \text{ Gt C}$) and 6 Gt CO_2 (1.6 Gt C) capture by closing the P gaps from Fig. 8a and Fig. 8c, respectively. If wood and leaves P concentration corresponds to 5th percentiles (Table 1), $\sim 2 \text{ Gt basalt}$ would be needed for closing the P gaps from a geogenic P supply scenario two (Appendix E subsection i Fig. S 26), which would potentially sequester $\sim 0.6 \text{ Gt CO}_2$ ($\sim 0.2 \text{ Gt C}$) due to weathering. If wood and leaves P concentration corresponds to 95th percentiles (Table 1) $\sim 362 \text{ Gt basalt}$ for closing the P gaps from a geogenic P supply scenario

one (Appendix E subsection i Fig. S 28) would be necessary, which would potentially sequester ~98 Gt CO₂ (~27 Gt C) due to weathering. The amount of basalt needed was estimated for a P content of 500 ppm, and an increase in basalt P concentrations would represent a decrease in the necessary amounts of basalt powder. The incongruent dissolution of basalt might occur, consequently increasing the necessary amounts of deployed basalt to cover the estimated P gaps.

Basalt deployment can also guarantee a balanced supply of Mg, Ca, and K for different deployment rates (Fig. 9), potentially preventing the shift of growth limitation to some of these nutrients within the P gapped areas (Fig. 8). Rhyolite, dacite, or andesite could be used as alternatives to basalt as a source of P, but these rocks generally have lower P content (Fig. 6). As a consequence, the necessary amounts of rhyolite, dacite, or andesite would be higher than that of basalt. Even though, for a median rock nutrient content, if these rocks are used to close the projected P gaps, they can potentially supply the necessary amount of Ca, Mg, and K for balanced tree nutrition (Fig. 10).

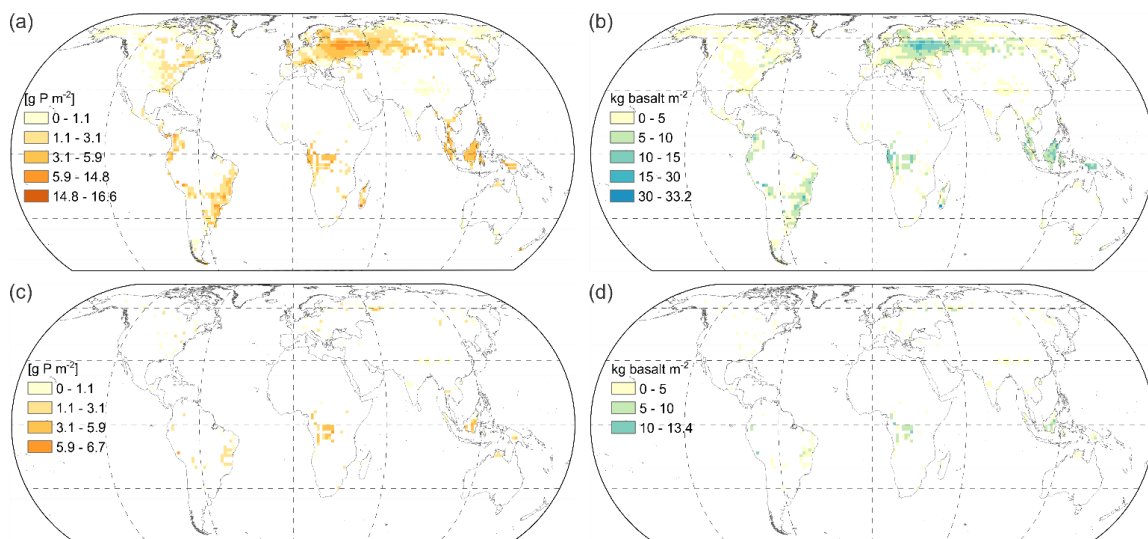


Fig. 8: Areas with potential P gap for the nutrient budget of the N-limited AR scenario (after 94 a of simulation), assuming P concentrations within foliar and wood material corresponding to mean values (Table 1). a) Geogenic P supply scenario one (geogenic P from weathering plus atmospheric P deposition as source of P). b) Basalt deployment necessary to close P gaps from P budget scenario of Fig. 8a. c) Geogenic P supply scenario two (geogenic P from soil inorganic labile P and organic P pools plus atmospheric P deposition and P from weathering as source of P). d) Basalt deployment necessary to close P gaps from P budget scenario of Fig. 8c. Map generated with ESRI ArcGIS 10.7 (<http://www.esri.com>).

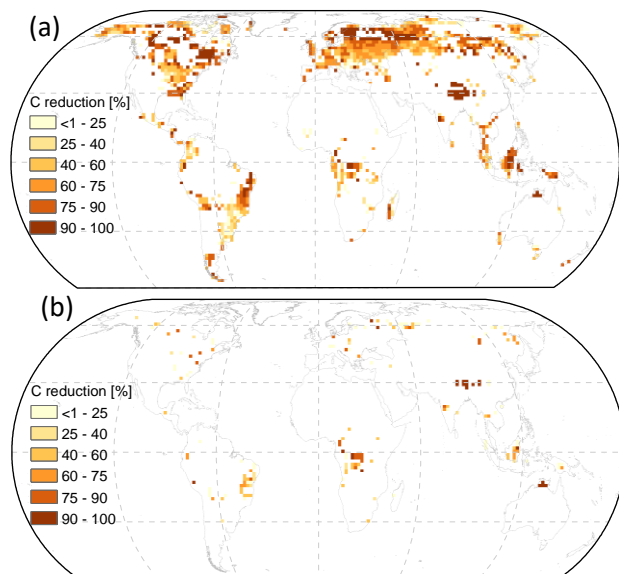


Fig. 7: Reduction of forest C sequestration due to geogenic P limitation. C reduction estimated from stoichiometric C:P ratios for the N-limited AR scenario assuming P concentrations within foliar and wood material corresponding to mean values (Table 1). In Fig. 4b we present the C sequestration potential if geogenic P supply is not limiting biomass growth. a) C reduction based on P gaps in Fig. 8a, obtained for geogenic P supply scenario one (geogenic P from weathering plus atmospheric P deposition as source of P). b) C reduction based on P gaps of Fig. 8c, obtained for geogenic P supply scenario two (geogenic P from soil inorganic labile P and organic P pools plus atmospheric P deposition and P from weathering as source of P). For resulting global C reduction check Table 3. Map generated with ESRI ArcGIS 10.7 (<http://www.esri.com>).

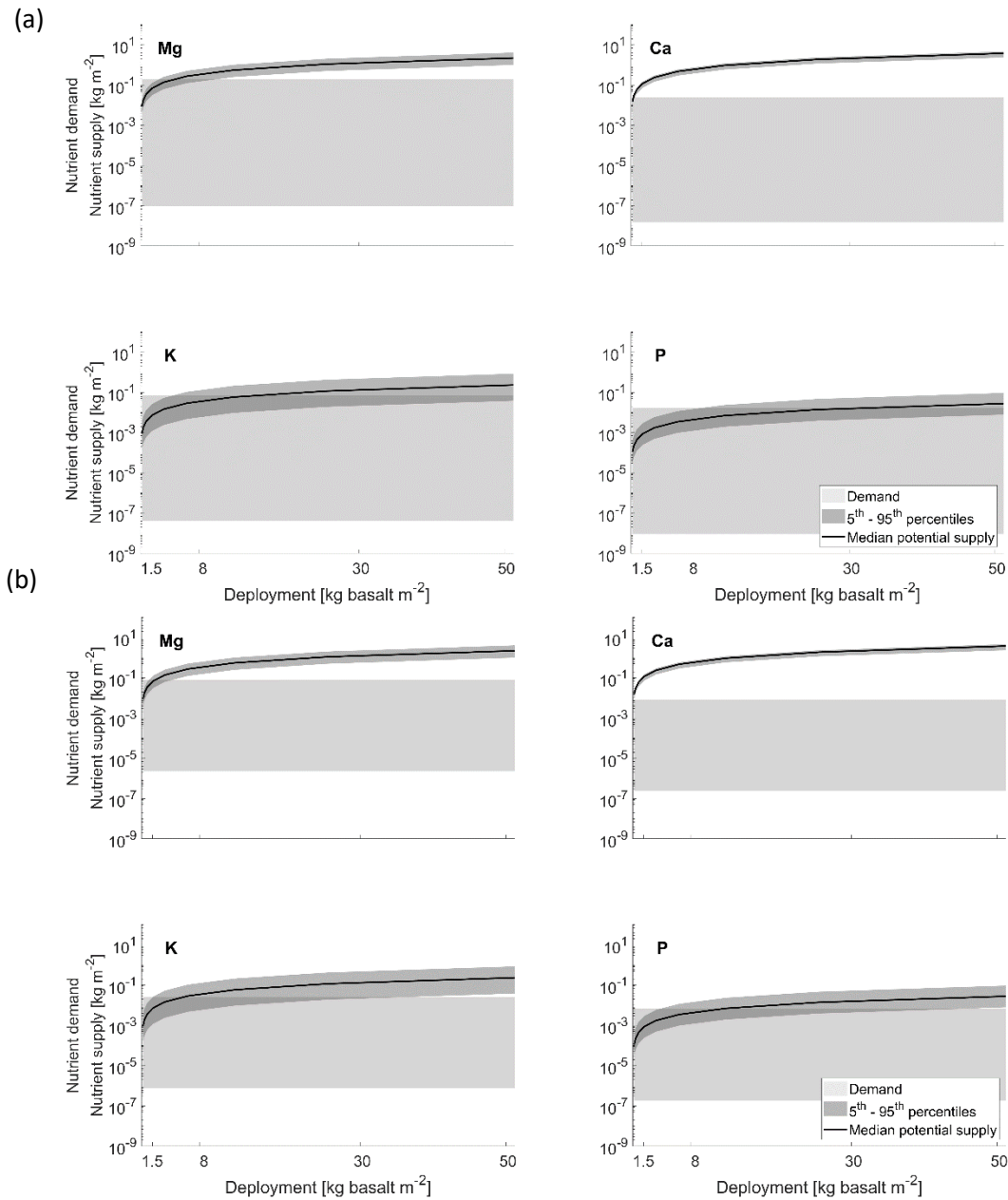


Fig. 9: Mg, Ca, K, and P supply by basalt dissolution (logarithmic curve) given as medians and ranges (5th and 95th percentiles; dark grey areas). Horizontal filled boxes indicate the nutrient demand for the maximum (17.1 g P m⁻²) and minimum (<<1 g P m⁻²) gap of each geogenic P supply scenario for P and derived Mg, Ca, and K demand for balanced tree nutrition assuming mean foliar and wood material chemistry (Table 1). a) Based on minimum and maximum P gap values of <1 g P m⁻² and 16.6 g P m⁻², which were obtained for a geogenic P supply scenario one (geogenic P from weathering plus atmospheric P deposition as source of P). b) Based on minimum and maximum P gap values of <1 g P m⁻² and 6.7 g P m⁻², which were obtained for a geogenic P supply scenario two (geogenic P from soil inorganic labile P and organic P pools plus atmospheric P deposition and P from weathering as source of P).

Table 3: Global P gap, maximum estimated P gap, maximum C sequestration reduction, and global C reduction for the natural N supply (N-limited) AR scenario (projected C sequestration of 190 Gt C).

N supply	Geogenic P supply	Maximum estimated P gap [g P m ⁻²]			Global P gap [Mt P]			Maximum C sequestration reduction [kg C m ⁻²]			Global C reduction [Gt C]		
		5 th percentile	Mean	95 th percentile	5 th percentile	Mean	95 th percentile	Wood and leaves P content			5 th percentile	mean	95 th percentile
								5 th percentile	mean	95 th percentile			
Limited	Scenario one	4.1	16.6	30.2	9.2	76.6	181.0	9.7	14.5	15.6	23.0	71.0	98.0
	Scenario two	1.6	6.7	12.2	1.0	9.9	34.7	4.7	6.2	6.5	3.0	9.5	19.0

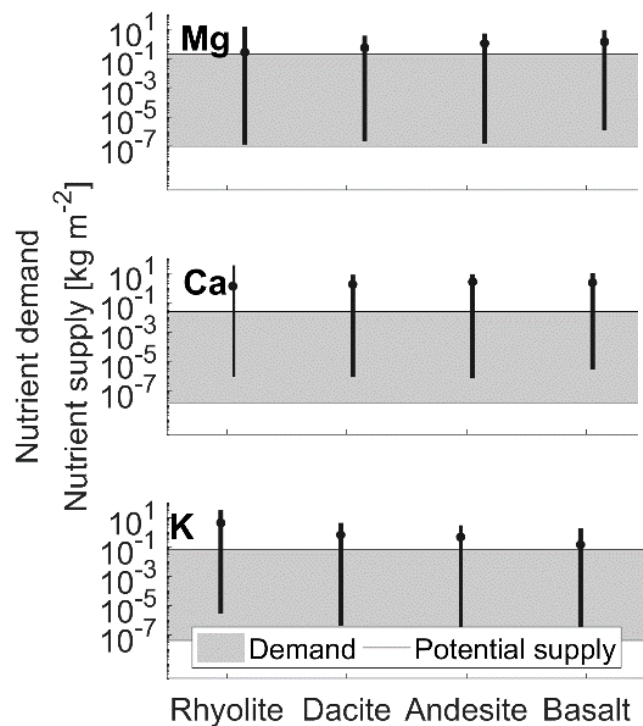


Fig. 10: Potential macronutrient (Mg, Ca, and K) supply of different rocks for closing projected P gaps of <<1 to 17.1 g P m⁻². Medians and ranges (5th and 95th percentiles) of potential supply based on rock chemistry.

3.4.2. Enhanced silicate rock weathering coupled to biomass production from bioenergy grass

For the simulation time span of 1995 – 2090 the minimum and maximum biomass growth yields amount to 0.7 and 3.6 kg m⁻² a⁻¹, which represent a K export of 4.2 – 22 g m⁻² and a P export of 0.7 – 3.6 g m⁻² according to Eq. (2). To guarantee maximum bioenergy grass yield, the exported nutrients should be replaced. For a high nutrient content (95th percentile) deploying up to 1.5 kg basalt m⁻² a⁻¹ could meet the K needs of bioenergy grass (Fig. 11) and would be able to replenish up to 75% of the exported P if the maximum bioenergy grass yield is considered (Fig. 11). Industrial fertilizer coapplication would be indicated to completely replenish exported P, reducing industrial fertilizer dependency. Deploying 8 kg basalt m⁻² a⁻¹ would be enough to replenish exported K and P by harvest assuming median nutrient content of basalt powder, and congruent and complete dissolution (Fig. 11).

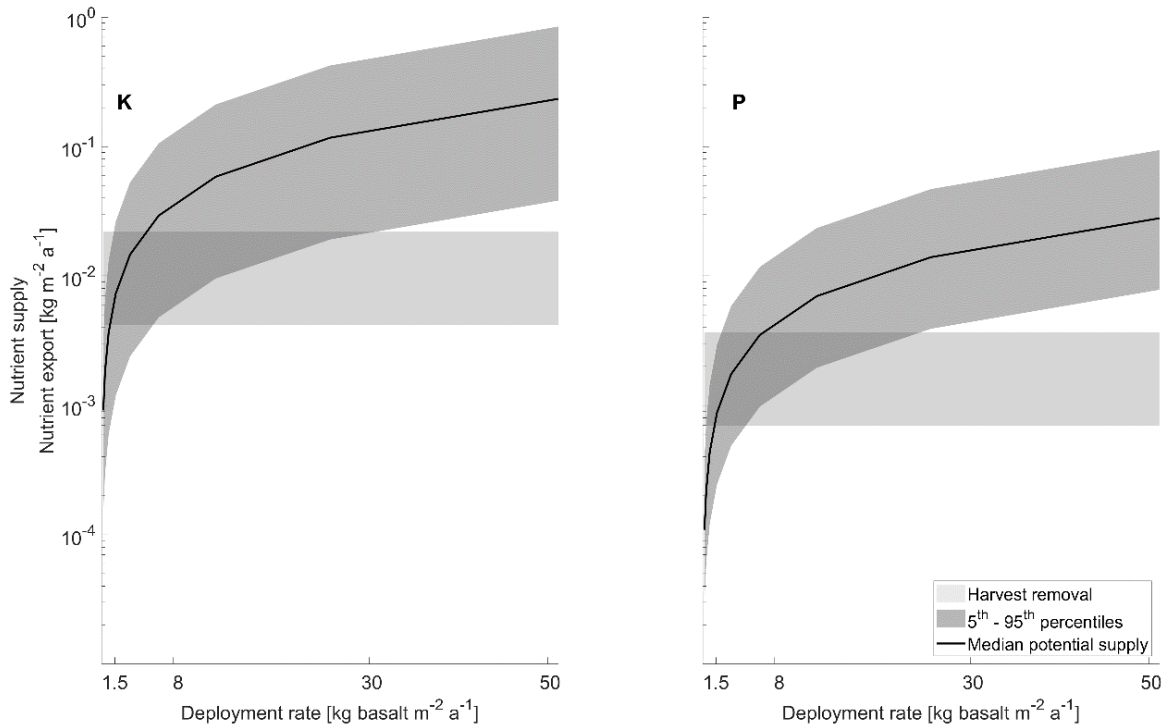


Fig. 11: Projected K and P supply (logarithmic curve) by basalt dissolution given as median ranges (5th and 95th percentiles) for bioenergy grasses K and P demand (horizontal filled boxes) based on global minimum 0.7 kg m⁻² a⁻¹ and maximum 3.6 kg m⁻² a⁻¹ harvest rates for simulation years of 1995 – 2090. The number of exported nutrients by several harvest rates higher than the minimum and lower than the maximum harvest rates are represented by the horizontal filled boxes.

3.4.3. Impacts on soil hydrology

The baseline hydraulic properties for soils within the P gap areas from the N-unlimited AR scenario, since this scenario represents the maximum effect, were estimated by Eq. (18), and they show high variability. The projected hydraulic conductivity (K_S) of topsoils for areas corresponding to those of the P budget from geogenic P supply scenario one (Appendix E subsection ii Fig. S 32a), for the N-unlimited AR scenario, encompasses values ranging from 1.5×10^{-7} to 7.8×10^{-5} m s⁻¹ and with PAW of 4% and 32% (Table 4). Neglecting the topography, soils having low K_S , (e.g., values of 1.5×10^{-7} m s⁻¹) would experience the lowest water infiltration rate under saturated conditions. The impacts of deploying a fine basalt texture (15.6% clay, 83.8% silt, and 0.6% fine sand) or a coarse basalt texture (15.6% clay, 53.8% silt, and 30.6% fine sand), which are in the range of commercial powders (Nunes et al., 2014), on soil hydrology were estimated by Eq. (10) for different application upper limits.

The effects of rock powder deployment could be neglected, on average, for upper limits of 50 and 205 kg basalt m⁻² for a fine- and coarse-textured rock powder, respectively. However, deviations from what is expected for the

mean might occur (Fig. 12 and Fig. 13). The average values of PAW increase together with the increase in the upper limits of rock powder application, but for a coarse basalt powder some areas might experience a decrease in PAW (Fig. 12 and Fig. 13).

Closing the observed P gap areas in the N-unlimited AR scenario would require a maximum deployment of 34 kg basalt m⁻² if geogenic P supply scenario one is assumed and 13 kg basalt m⁻² if geogenic P supply scenario two is assumed (Appendix E subsection ii Fig. S 32). Filling the P gaps from scenario two by a coarse or fine basalt powder (given the complete dissolution of P-bearing minerals), the related changes in soil hydrology would remain below $\pm 10\%$ for most of the areas (Appendix G Fig. S 37). If the geogenic P supply from scenario one, for the N-unlimited AR scenario (Appendix E subsection ii Fig. S 32a), is assumed and a fine basalt powder is applied, the changes in hydraulic conductivity range between 58 % and -11 % (Fig. 14a). A decrease in PAW could be neglected for most of the deployment areas, but some would have an increase of up to 31 % (from 13.8 % to 18.2 %; Fig. 14c). A coarse basalt powder would, in general, cause fewer impacts to soil hydraulic properties (Fig. 14b and d).

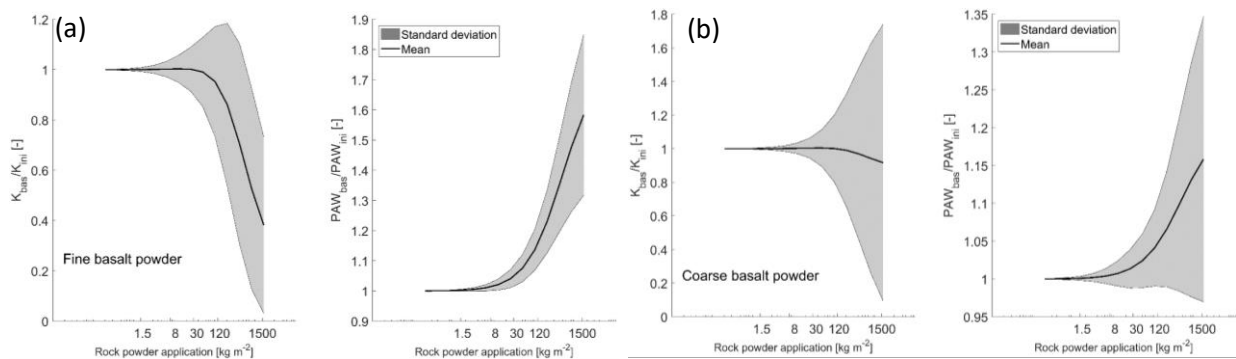


Fig. 12: Relative impacts on soil saturated hydraulic conductivity (K_S) and plant-available water (PAW). K_{bas} and PAW_{bas} , respectively, represent the estimated soil K_S and PAW after basalt application. K_{ini} is the estimated initial soil K_S , and PAW_{ini} is the estimated initial PAW of different soils. a) Application of a fine basalt texture (15.6% clay, 83.8% silt, and 0.6% fine sand). b) Application of a coarse basalt texture (15.6% clay, 53.8% silt, and 30.6% fine sand) for areas corresponding to P gaps of geogenic P supply scenario one, for the N-unlimited AR scenario (Appendix E subsection ii Fig. S 32a). Mean and standard deviations for $n=15318$ grid cells. See Appendix G for impacts of initial K_S and PAW of fine or coarse basalt powder texture on soils of P gap areas from Appendix E subsection ii Fig. S 32c.

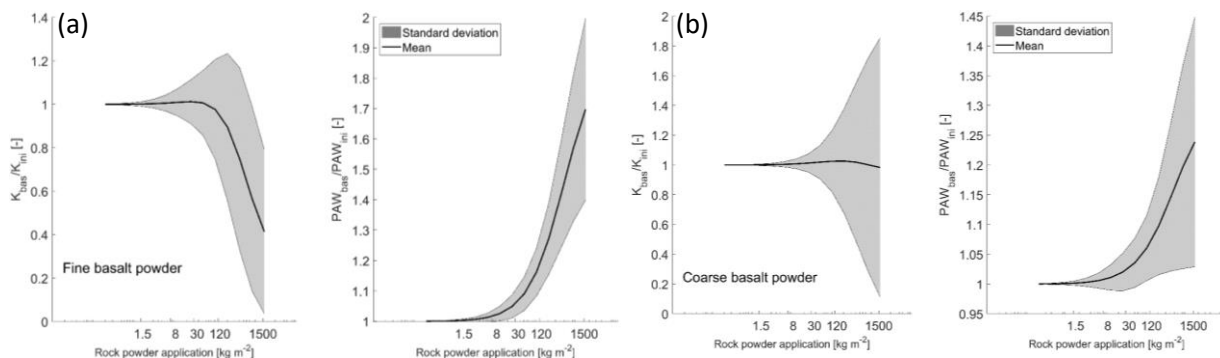


Fig. 13: Relative impacts on soil saturated hydraulic conductivity (K_S) and plant-available water (PAW). K_{bas} and PAW_{bas} respectively, represent the estimated soil K_S and PAW after basalt application. K_{ini} is the estimated initial soil K_S and PAW_{ini} is the estimated initial PAW of different soils. a) Application of a fine basalt texture (15.6% clay, 83.8% silt, and 0.6% fine sand). b) Application of a coarse basalt texture (15.6% clay, 53.8% silt, and 30.6% fine sand) for areas corresponding to P budget scenario two, for the N-unlimited AR scenario (Appendix E subsection ii Fig. S 32c). Mean and standard deviations for $n=2525$ grid cells.

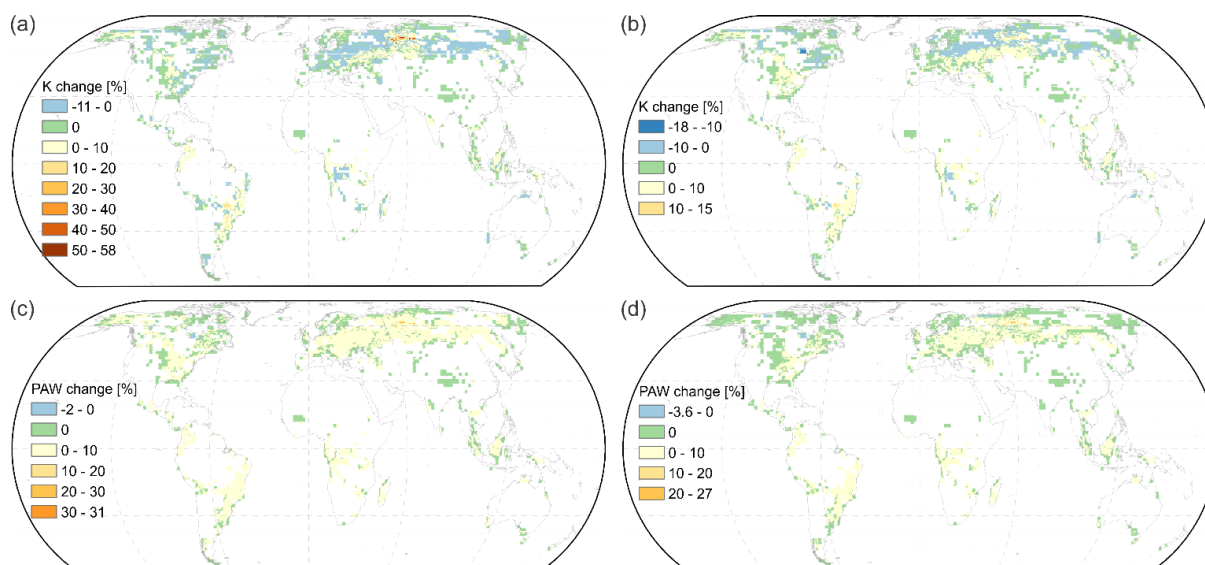


Fig. 14: Impacts on soil hydrology estimated according to the equations of Saxton and Rawls (2006) for basalt deployment mass coincident with areas with potential P gaps for the nutrient budget of the N-unlimited AR scenario assuming P concentrations within foliar and wood material corresponding to mean values (Appendix E subsection ii Fig. S 32a). a) Hydraulic conductivity (K) changes relative to initial soil values for a fine basalt texture (15.6% clay, 83.8% silt, and 0.6% sand) being deployed. b) Hydraulic conductivity (K) changes relative to initial soil values for a coarse basalt texture (15.6% clay, 53.8% silt, and 30.6% fine sand) being deployed. c) Plant-available water (PAW) changes relative to initial soil values for a fine basalt texture (15.6% clay, 83.8% silt, and 0.6% sand) being deployed. d) Plant-available water (PAW) changes relative to initial soil values for a coarse basalt texture (15.6% clay, 53.8% silt, and 30.6% fine sand) being deployed. Map generated with ESRI ArcGIS 10.7 (<http://www.esri.com>).

Table 4: Minimum and maximum soil hydraulic conductivity for areas coincident with the P gap areas of each geogenic P supply scenario, for the N-unlimited AR scenario (Appendix E subsection ii Fig. S 32a).

	Geogenic P supply scenario one	Geogenic P supply scenario two
Hydraulic conductivity (K) [m s^{-1}]		
Min	1.5×10^{-7}	2.7×10^{-7}
Max	1.7×10^{-4}	7.8×10^{-5}
Plant available water (PAW) [%]		
Min	4	6
Max	32	28

3.5. Discussion and implications

3.5.1. Enhanced silicate rock weathering coupled to afforestation and reforestation

Phosphorus (P) is a limiting nutrient in a wide range of ecosystems (Elser et al., 2007) and in temperate and tropical climate zones (Du et al., 2020). P deficiency might affect biomass growth of tropical (Herbert and Fownes, 1995; Tanner et al., 1998; Wright et al., 2011) and northern forests (Goswami et al., 2018; Menge et al., 2012) with mineral P already limiting biomass production in European forests (Jonard et al., 2015) and in forests in the USA (Garcia et al., 2018), as well as in agricultural areas (Kvakić et al., 2018; Ringeval et al., 2019). The uncertainty in which the P pool is available for long-term plant nutrition is high (Johnson et al., 2003; Sun et al., 2017), and we tackled this uncertainty assuming two potential geogenic P supply scenarios. Geogenic supply scenario two, assuming P from weathering and atmospheric deposition plus inorganic labile P and organic P, is a very optimistic assumption that may not correspond to reality based on the already-observed P limitation on different ecosystems

(Elser et al., 2007). However, we cannot rule out that gradual shifts in soil organic P fractions occur, which make comparable amounts of P to that available in scenario two over time.

The numerical simulations of Kracher (2017) predicted biomass growth for the 21st century (Fig. 4) considering natural water supply, CO₂ fertilization, and N-unlimited and N-limited scenarios for an RCP4.5 greenhouse gas concentration trajectory and land use transitions. The predicted C sequestration by the N-limited AR scenarios from Kracher (2017) is ~2 Gt C a⁻¹. Different authors have reported the potential C sequestration by afforestation or reforestation being of 0.3 – 3.3 Gt C a⁻¹ for the end of 2099 (National Research Council, 2015; Lenton, 2010; Lenton, 2014; Smith et al., 2015 apud Fuss et al., 2018). However, the predicted sequestration potential estimated by Kracher (2017) can drop to ~1.3 Gt C a⁻¹ if geogenic P supply scenario one for mean P content within wood and leaves is selected. If geogenic P supply scenario two for mean P content within wood and leaves is selected, it drops to ~1.9 Gt C a⁻¹.

More than 60,000 tree species are recorded worldwide (Beech et al., 2017), and a precise estimation regarding tree chemistry, which we attempted to represent by the considered ranges of wood and leaves chemistry from the databases, represents a challenge. However, different pathways and mechanisms control soil P availability to the plant (Vitousek et al., 2010), and they are not considered in our estimations, leading to conservative predictions. Adding soil P dynamics to models would allow for the reliable quantification of the C sequestration potential of AR (e.g., using P-enabled land surface models; Goll et al., 2012; Goll et al., 2017; Sun et al., 2017; Wang et al., 2017; Wang et al., 2010; Yang et al., 2014b).

Kracher (2017) has shown that N can limit biomass production and consequently C sequestration. To achieve the projected C sequestration of 190 Gt C for the N-limited scenario, the estimated P gaps must be closed. Potential P sources are industrial fertilizers, like diammonium phosphate (DAP) or rock powder (e.g., basalt). However, DAP potentially represents an extra input of ammonium to the groundwater, and it is expected, in the long term, that DAP deployment will acidify the soil (Fertilizer Technology Research Centre, 2016).

Most of the world's soils are acidic, with some being strongly acidic (IGBP-DIS, 1998), which generally favors the sorption of orthophosphate onto Fe- and Al-(hydro)oxide surfaces and clay minerals, essentially demobilizing P (Shen et al., 2011). Besides that, the long AR time span can undermine the effectiveness of DAP to supply P to forests due to the high soil acidification potential of DAP. Therefore, rock powder application can be an alternative as nutrients are slowly released and an increase in alkalinity fluxes is expected (Dietzen et al., 2018), which can raise and stabilize the pH of soils.

Re-establishing soil pH to (near-)neutral conditions, generally between 6.6 and 7, will provide new nutrient-holding sites at Fe- and Al-(hydro)oxide surfaces and in soil organic matter, which makes the sorbed orthophosphate plant available. An application of 8 kg m⁻² basalt powder can increase the cation exchange capacity (CEC) of Oxisols by 150 – 300% (Anda et al., 2015; Anda et al., 2009) and improve the C and N mineralization (Mersi et al., 1992); for Ultisols, the CEC increases by 44% after deploying ~7 kg m⁻² basalt powder (Noordin et al., 2017).

To avoid shifts of nutrient limitation, the supply of macronutrients like Mg, Ca, and K must be proportional to P supply since Mg is required as an essential element in chlorophyll, Ca has a structural role, and K is responsible for water and ionic balance (Hopkins and Hüner, 2008). Rock powder can be used as a source of these nutrients, as suggested by different authors (Beerling et al., 2018; Hartmann et al., 2013; Straaten, 2007) and according to our results seen in Fig. 9 and Fig. 10. However, the potential of basalt powder to supply K, based on chemical composition, is lower than for other analyzed rocks. For median values, rhyolite has the highest content of K;

however, if occurring in K-feldspars it will not be plant available. Blending these rocks in different proportions could result in a more balanced macronutrient supply (Leonardos et al., 1987).

The RCP8.5 scenario predicts that global agricultural areas (crop land and pastures) are going to increase in the course of the 21st century due to a decrease in forested area (Sonntag et al., 2016). Assuming a future scenario of high atmospheric CO₂ levels (RCP8.5) but using the land use transitions and wood harvest rates from an RCP4.5 scenario (Sonntag et al., 2016), a similar forest cover fraction to the one presented in Fig. 4 is expected (see Figure 1 in Sonntag et al. (2016)), and geogenic P supply would also limit the predicted biomass growth. Similar areas of forest growth were observed in the study from Yousefpour et al. (2019) by comparing Figure 2c presented in that study and Fig. 4 in our study. Though using only one model induces uncertainty, it would not change the general message of our work.

3.5.2. Enhanced silicate rock weathering coupled to bioenergy grass production

Generally, natural soil P content is inadequate for the long-term cultivation of agricultural plants. To overcome this issue, P is supplied by fertilizers to reach or maintain optimum levels of crop productivity (Sharpley, 2000) after several harvest rotations. In order to keep a positive CO₂ balance, an alternative to industrial fertilizers might be used to replenish the nutrients exported by harvest. The chemical composition of rocks is highly variable (Fig. 6), and different rock types can be used for EW. Ideal rock types need to be chosen in order to resolve a specific plant nutrient deficiency and enhance the nutrient reservoir of a target soil, besides increasing the soil pH and the CEC (Anda et al., 2015; Anda et al., 2009) and improving the C and N mineralization (Mersi et al., 1992), the soil organic carbon (Doetterl et al., 2018), and the supply of Si (Beerling et al., 2018; Hartmann et al., 2013). In the case of Oxisols, which are also found over about 8% of the glacier-free land surface and common in tropical and subtropical agricultural regions, application of 8 kg m⁻² basalt powder can increase the CEC by 150 – 300% (Anda et al., 2015; Anda et al., 2009). For Ultisols, which are found over about 8% of the glacier-free land surface, application of ~7 kg m⁻² basalt powder can increase the CEC by 44% (Noordin et al., 2017).

Overall, rock application has the potential to resupply the harvest-exported nutrients and partially or totally close the short- and long-term nutrient gaps in soil. Individual rock types, from basic (Mg, Ca) to acidic (K, Na), contain varying amounts of target nutrients and mixing them might increase the overall nutrient supply capacity (Leonardos et al., 1987). Intrinsic mineralogical and or petrographic structures can influence the release of nutrients (Ciceri et al., 2017), which makes them plant unavailable in some cases. K can also limit plant growth; it occurs in K-feldspars as a plant-unavailable form, in the case of acidic rocks, but becomes accessible after hydrothermal treatment (Liu et al., 2015; Ma et al., 2016a; Ma et al., 2016b). However, research on release processes of other macro- and micronutrients and on nutrient release optimization (e.g., by hydrothermal decomposition) is necessary to be able to parameterize this effect in the soil environment.

Harvest rates control the nutrient export from bioenergy grass fields. Therefore, an increase in harvest rate represents an increase in nutrient export and vice versa. Thus, to keep a sustainable nutritional balance of soils, the exported nutrients must be replenished; otherwise maintaining the high harvest rates becomes unsustainable. Accounting for other simulation setups or a numerical model different from MAgPIE might change the harvest rates of this study. If we assume that the maximum harvest rate of 3.6 kg m⁻² a⁻¹ hypothetically increases by 1 order of magnitude, the maximum exported nutrients would be ~0.2 kg K m⁻² a⁻¹ and ~0.04 kg P m⁻² a⁻¹, which would demand a basalt deployment rate of ~13 kg m⁻² a⁻¹ and ~20 kg m⁻² a⁻¹, respectively (considering 95th percentiles of the chemical composition of basalt), to replenish the exported nutrients. If median K and P concentrations in basalt powder are assumed, the basalt deployment rate increases to ~48 kg m⁻² a⁻¹ and 73 kg m⁻² a⁻¹, respectively, to

replenish the exported nutrients (Appendix F Fig. S 36). However, such an increase in harvest rates might not correspond to reality. Harvest rates lower than $0.7 \text{ kg m}^{-2} \text{ a}^{-1}$ (the minimum) represent less nutrient export, decreasing the basalt powder deployment rates necessary to replenish the nutrients exported by harvest.

3.5.3. Impacts on soil hydrology

AR and BECCS demand huge quantities of irrigation water (Bonsch et al., 2016; Boysen et al., 2017b), and it is projected that climate change will affect the water balance, and consequently influence crop yields (Kang et al., 2009). Soils with higher water-holding capacity will tolerate the impacts of drought better (Kang et al., 2009). Therefore, practices that improve water availability to plants at the root system are used as strategies to mitigate drought effects (Rossato et al., 2017). We investigated whether deployment of rock powder can change the topsoil hydraulic conductivity and plant-available water (PAW) for different application ranges.

Concrete effects of EW on biomass productivity would depend on whether the changes in the initial PAW values in topsoils reached PAW threshold values to trigger biomass productivity (Sadras and Milroy, 1996). In general, the average changes in topsoil PAW related to basalt powder application would not be enough to trigger biomass growth. Therefore, areas showing PAW changes from 14% to 21% would not trigger leaf and stem expansion of maize, wheat, or soybean (Sadras and Milroy, 1996) but could increase leaf and stem expansion of pearl millet (Sadras and Milroy, 1996) after deploying $50 \text{ kg basalt m}^{-2}$ with a fine texture. A deployment of $50 \text{ kg basalt m}^{-2}$ of coarse powder changes PAW by 19% consequently not triggering biomass productivity.

The finest grain size able to be considered in the equations of Saxton and Rawls (2006) is the clay fraction (grain diameter $>1 \text{ }\mu\text{m}$ and $<3.9 \text{ }\mu\text{m}$). Fine grain sizes influence the exposed reactive surface area of rock powder, which affect the weathering rates. The fine basalt would have the grain sizes ranging between 0.6 and $90 \text{ }\mu\text{m}$ which might be enough to completely dissolve the deployed rock powder after 1 a (Stefler et al., 2018). For the coarse basalt powder, $\sim 70\%$ of its granulometry falls into the $0.6 - 90 \text{ }\mu\text{m}$ range, and from the other 30%, about 20% might be dissolved in 1 a (Stefler et al., 2018). Based on the used pedotransfer functions, if a basalt powder contained only grains of the clay size fraction, the effects on soil hydraulic conductivity would decrease by 37% for a deployment amount of $30 \text{ kg basalt m}^{-2}$ (for the fine rock powder used in our work, the hydraulic conductivity would decrease by only 2%). The finer the grain becomes the higher the energy input for grinding is, which can drastically affect the costs of EW (it can reach up to $500\text{\$ tCO}_2^{-1}$ sequestered; Stefler et al., 2018). Since grains of different diameters need different times for complete dissolution, a rock powder with different grain sizes would act as a constant source of nutrients to soil.

During the weathering of rock powder, clay mineral genesis can occur and potentially increase the water-holding capacity of soils (Gaiser et al., 2000), which can subsequently change the estimated PAW. The added fresh silicate minerals to the soil by EW will have high reactivity releasing a significant number of nutrients, which increases soil nutrient pools. The increased nutrient availability will increase the potential of soils to stabilize carbon (Doetterl et al., 2018), and a positive effect on PAW is expected to occur based on Eqs. (23) to (25) and according to Olness and Archer (2005). The suitable amounts of rock powder applied depend on the target changes in the chosen soil, and on the soil's intrinsic grain size distribution and organic matter content. Intrinsic grain properties like the shape of grains and pores, tortuosity, specific surface area, and porosity should be considered (Bear, 1972) for the evaluation of changes in soil hydraulic properties by pedotransfer functions and their consequences for dissolution kinetics. A large set of data from field and laboratory experiments covering different soil types, climatic regions, and plant species would enable a qualitatively and quantitatively reliable assessment of not only soil hydrology impacts but also dissolution rates and changes in the soils' mineralogy. The effects on soil

microorganisms should be taken into account in order to correct the limits of rock powder deployment. The potential of rock powder to trigger plant suffocation, if gas exchange is prevented by water saturation of pores (Sairam, 2011), should also be considered before deployment.

3.5.4. Challenges of rock powder deployment

Average tillage depth is 0.3 m, and greater depths can be reached with higher energy and labor costs (Fageria and Baligar, 2008). Since annual crops have an effective rooting depth typically in the range of 0.4 – 0.7 m (Aslyng, 1976; Madsen, 1985; Munkholm et al., 2003; Olsen, 1958), a deployment depth of 0.3 m seems to be reasonable. Since tillage can trigger soil carbon loss (La Scala et al., 2006; Reicosky, 1997), deploying rock powder at soil surface might be a solution. At the soil surface, the long-term water percolation and/or bioturbation (Fishkis et al., 2010; Taylor et al., 2015) can transport and mix fine-grained material to deeper regions within the soil profile, which potentially can change the K_s and PAW at crop rooting zones. Groundwater recharge rates might change if clogging of pores at deeper regions of the soil profile occurs or if the changes in soil hydraulic properties due to rock deployment can significantly influence the initial soil hydraulic conditions for a constant water precipitation. Taylor et al. (2015) argue that downward transport of a silt-textured powder deployed at a soil surface would easily reach the rooting zone of trees, which is in the majority of cases at a depth of up to 0.4 m. The authors suggest that in tropical regions greater depths might be reached due to intensive rain and bioturbation.

Detailed field studies to better comprehend downward transport of grained material through the soil profile, changes in soil water residence time, PAW, mineralogy, nutrient pools, CEC (Anda et al., 2013; Anda et al., 2015), and bioavailability of released trace metals (Renforth et al., 2015) are necessary. This would provide management recommendations for the diverse existing settings for EW application. In the present study, estimates for different basalt powder application upper limits are made for changes in soil hydraulic properties without accounting for downward transport of fine particles through the soil profile.

Besides avoiding clogging of pores of the topsoil by rock powder application to a certain extent, downward transport of rock powder can contribute freshly ground material that comes into contact with roots of trees or crops, which can enhance the weathering rates and create new sites to retain nutrients (Anda et al., 2015; Kantola et al., 2017).

Once the freshly ground material is in contact with the soil, different factors control the nutrient supply efficiency of rock powder. The nutrients from fresh material are initially inert, protected within the crystallographic structures of the minerals, and would become plant available only in solution or when associated with mineral surfaces (Appelo and Postma, 2005). The release of nutrients by weathering is controlled by film and intraparticle diffusion-limited mass transfer influenced by pH and ionic strength of the soil aqueous solution (Grathwohl, 2014), both being controlled by rooting exudates in the rhizosphere and the chemical composition of infiltrating waters.

Full dissolution is a simplification based on modeled scenarios (Strefler et al., 2018; Taylor et al., 2015). Under field conditions, soil water could rapidly reach near-equilibrium concentrations (Grathwohl, 2014), which would decrease weathering rates. The opposite would occur if near-equilibrium conditions could be disturbed by a sink of nutrients by nutrient root uptake (Stefánsson et al., 2001) or by percolation of water unequilibrated with soil porous water (Calabrese et al., 2017).

The nutrient (Mg, Ca, K, P, etc.) content of rocks can vary significantly. Besides that, deploying rock powders with grain sizes $> 90 \mu\text{m}$ would decrease the reactive surface area of deployed rock powder decreasing the weathering fluxes (Goddéris et al., 2006). The median and the range (5th or 95th percentile) values for Mg, Ca, K, and P content obtained from the EarthChem database considered chemical analysis of 2985 rhyolites, 3008 dacites,

11099 andesites, and 23816 basalts. Broadening the classification criteria for these rocks would change the median and the ranges (5th or 95th percentile) for chemical composition; however, the selected median and the ranges of this study are conservative estimates. As an illustration, Porder and Ramachandran (2013) adopted another selection criterion, for the same database, which resulted in a total of 97895 samples and estimated a median P content of basalt of 916 ppm. Additionally, the selected rock chemistry database influences the descriptive statistics results. Recently published values of P content within basalt considering the GEOROC database are 1309 ppm for median content, 428 ppm for 10th percentile, and 3186 ppm for the 90th percentile (Amann and Hartmann, 2019). Thus, before deploying EW to supply nutrients, the chemical composition of rock powder should be known to properly estimate the necessary amount of rock for supplying the demanded nutrients of a specific plant. This would allow for the easy estimation of the impacts on soil hydrology by the pedotransfer functions of this study or by specific laboratory experiments.

Besides the potential to be used to rejuvenate soil nutrient pools (Leonardos et al., 1987), silicate rock powder can be used to reduce the risk of nitrate mobilization and is indicated for regions in which special care regarding water preservation is needed. However, extra input of sodium (Na) to the system, if the rock is rich in this element, could disturb this amelioration effect (Von Wilpert and Lukes, 2003). Besides decreasing nitrate mobilization, coapplication of rock powder with other fertilizers can increase the biomass production of crops (Anda et al., 2013; Leonardos et al., 1987; Theodoro et al., 2013).

An additional challenge of the application of rock products will be the assessment of the fate of weathering products, which might be transported eventually into river systems and alter geochemical baselines as evidenced by past land use changes in some large rivers (Hartmann et al., 2007; Raymond and Hamilton, 2018).

3.6. Conclusions

Our results illustrate the potential of enhanced silicate rock weathering (EW) to act as a nutrient source for nutrient-demanding AR and BG. This is an important, yet often overlooked, aspect of EW besides CO₂ sequestration. The investigated scenarios show that areas with undersupply of P exist, and a C-stock reduction is expected to occur if P is the only limiting nutrient. Considering N and P deficiency together for a low geogenic P supply and high biomass P demand, the C-stock reduction will be up to 59 % of the projected total global C sequestration potential of 224 Gt C from the N-unlimited AR scenario. Potential P deficiencies were here based on the soil P availability and P demand scenarios, indicating that the inclusion of P cycles in AR models is necessary to accurately project the C sequestration of forests. Industrial fertilizers can be used to alleviate the P deficiency but the extra input of ammonium along with it can undermine the carbon budget and acidify the soils. Furthermore, acidic soil conditions generally favor the sorption of orthophosphate onto Fe- and Al-(hydro)oxides surfaces and clay minerals, essentially demobilizing P (Shen et al., 2011).

Besides the high chemical P content and relatively fast weathering rates, the equilibrated supply of Ca, K, and Mg puts the use of basalt powder one step ahead of other rocks as a potential alternative to industrial fertilizers. Regrowth of forests on abandoned agricultural land is a passive landscape restoration method (Bowen et al., 2007). In most of the cases soils become acidic on abandoned agricultural land in the long term (Hesterberg, 1993), which favors the leaching of nutrients (Haynes and Swift, 1986) and heavy metals (Hesterberg, 1993). As a consequence, the regrowth rate of forests might be limited in acidic soils. The use of basalt powder will keep a positive carbon budget; increase the soil pH (Anda et al., 2015; Anda et al., 2009), as basalt powder would act as a buffer maintaining soil pH under neutral to slight alkaline conditions; and close nutritional needs of AR and BG, and rock

powder can be used to reduce the risk of nitrate mobilization (Von Wilpert and Lukes, 2003). However, to be able to assess the global potential of the combination of land-based biomass NETs with EW, it is necessary to explore related physicochemical changes in soil influenced by varying EW deployment rates, based on already-available data, and then develop improved EW models. They should be tested with field-based approaches. For example, tracking added elements through the ecosystem's soil and plant reservoirs probably needs test sites that use advanced methods of nutrient balance and isotope studies, as recently developed (Uhlig et al., 2017; Uhlig and von Blanckenburg, 2019).

In addition to the use for replenishing soil nutrient content, our research suggests that deployment of rock powder on the topsoil can enhance plant-available water (PAW) for different upper limits. Apart from controlling the nutrient release rates, the texture of deployed rock powder would influence the impacts on soil hydrology together with the initial soil texture. In general, EW appears to have considerable potential for water retention management of topsoils. This is an important characteristic that has not been explored before, since under a future scenario of climate change, EW can potentially mitigate or alleviate drought effects to a certain extent within areas used for AR and BG plantation. Field and laboratory experiments are needed to quantify soil hydraulic changes under a natural and controlled environment. Besides that, investigation of potential changes in coupling EW with other terrestrial NETs such as biochar is necessary, since biochar and EW can increase the amount of soil organic matter, a variable also responsible for increasing the water retention of soils.

We show that EW can be an important part of the solution to the problem of nutrient limitation that AR and BG might suffer from. Specifically, its potential for hydrological management of soils was shown, and it could be used in areas where seasonality and droughts might affect the biomass growth. The use of enhanced silicate rock weathering for hydrological management coupled to land-based NETs is worth investigating. Global management of carbon pools will need a full-ecosystem understanding, addressing nutrient fluxes and related soil mineralogy changes, soil hydrology, impacts on soil microorganisms, and responses of plants to the diverse array of soil types and climates. Applied ecosystem engineering is likely to be a future nexus discipline which needs to link local ecosystem processes with a global perspective on carbon pools within a universal effort to manage the carbon cycle.

4. Systematic Review: Effects of biochar and terrestrial enhanced silicate rock weathering on soil and plant properties

4.1. Abstract

A portfolio of negative emission technologies (NETs) for carbon dioxide removal (CDR) is necessary to sustainably reach the 1.5 °C target. Here, we systematically reviewed the potential effects, interactions and synergies on soil properties and plant response after applying enhanced silicate rock weathering (EW) or biochar for a range of edaphoclimatic conditions. A database created from selected peer-reviewed articles was used to perform a random-effects model meta-analysis to assess the potential effects. After EW is applied, cation exchange capacity (CEC), soil pH, exchangeable K, available P, and biomass yield increased, on average, by 3 %, 6 %, 10 %, 11 %, and 15 % respectively for application rates < 10 t rock ha⁻¹. For biochar, the average increment was 9 %, 3 %, 9 %, and 17 % for CEC, soil pH, available P, and yield for application rates < 10 t biochar ha⁻¹, respectively, but the exchangeable K reduced by -13 % compared to the control. In general, rising the dosages of EW and biochar raise the CEC, soil pH, exchangeable K, available P, and yield. The observed positive effects on the exchangeable K and available P after biochar and EW application indicates that both NETs can improve soil fertility, which can reduce the use of industrial fertilizers. To avoid plant growth inhibition, it is necessary to enhance biochar with nutrients before using it as soil amendment. Only fewer authors used EW as nutrient source for enhancing biochar. This may be a solution for overcoming, in some cases, the relative low nutrient release rates of EW but further research is necessary. Coapplication of EW and biochar can potentially promote the stabilization of soil organic matter, which will enhance the carbon storage in soils. Both amendments can influence soil bulk density, porosity, water retention capacity, water infiltration rate, and aggregate stability. However, studies lasting to one to two years compose 90 % of our database emphasizing the need for long-term studies for EW and biochar. In general, this study highlights the multitude of variables controlling the effects of EW and biochar soil application on biomass productivity and soil properties, differentiated by environmental and management factors and underline the need to investigate the effects of biochar and EW coapplication on soil ecology, nutrient availability, plant-available water, and biomass growth and yield. For the first time, the effects on soil and plant properties after biochar or EW application were compared and the average effects for specific variables or more generalized configuration either for EW or for biochar is available.

4.2. Introduction

To sustainably reach the 1.5 °C target from the Paris Climate Agreement, a portfolio of negative emission technologies (NET) should be considered that not just provide carbon dioxide removal (CDR) but also offer co-benefits. Aside from carbon forestry and soil carbon enhancement by traditional methods, enhanced silicate rock weathering (EW), and biochar are some of the current available land-management options for CDR (Fuss et al., 2018; Smith et al., 2019), which have a high potential of being combined, as both provide the co-benefit of improving soil fertility (Amann and Hartmann, 2019; Beerling et al., 2018). Thus, future research and development is going to investigate the synergies and trade-offs between the variety of CDR options (Amann and Hartmann, 2019; Smith et al., 2019).

The use of rock powder for plant nutrition was triggered by empirical studies during the early 19th century as described by Hensel (1894) with more research following soon (De Turk, 1919; Honcamp, 1910; Sachse, 1927;

Swanback, 1950). Rock powder use for soil remineralization on highly weathered soils successfully raised crop productivity (Anda et al., 2015; Kronberg, 1977; Leonardos et al., 1976; Leonardos et al., 1982) by adding depleted macro- (e.g., Mg, Ca, K, P, and S), and micronutrients (e.g., B, Mo, Cu, Fe, Mn, Zn, and Ni; Anda et al., 2015; Beerling et al., 2018; Hartmann et al., 2013; Leonardos et al., 1987; Nkouathio et al., 2008) and by establishing soil pH to neutral or near neutral conditions due to dissolution of silicate minerals (Anda et al., 2015; Anda et al., 2009; Kronberg, 1977). During the weathering process, clay minerals (illite, montmorillonite, kaolinite), and iron and or aluminum (hydr)oxides are formed (Kronberg, 1977; Wilson, 2004), which can contribute to stabilization of soil organic matter by sorption onto these minerals (Saidy et al., 2012). Industrial fertilizers are easily leached in highly weathered soils with low levels of soil organic matter due to the low capacity of nutrient retention of quartz, gibbsite, kaolinite, goethite, and hematite, which are common minerals of highly weathered soils (Ciceri et al., 2017; Kronberg, 1977; Leonardos et al., 1987). Therefore, rock powder showed to be a viable alternative for plant nutrition in tropical areas (Van Straaten, 2006) due to its relatively low nutrient release rates (Chesworth et al., 1989; Ciceri et al., 2017; Coroneos et al., 1996; Gillman, 1980; Hinsinger et al., 1996; Leonardos et al., 1987; Sanz Scovino and Rowell, 1988; Von Wilpert and Lukes, 2003; Weerasuriya et al., 1993). However, depending on the rock powder added, $\text{Na}^+_{(\text{aq})}$ can be released and impact the long-term ameliorative effects (Von Wilpert and Lukes, 2003). Weathering also controls atmospheric CO_2 concentrations over geological time scales (Berner et al., 1983; Kempe, 1979; Lenton and Britton, 2006; Walker et al., 1981; Yasunari, 2020) and Schuiling and Krijgsman (2006) proposed the use of ground silicate rocks to actively sequester atmospheric CO_2 , creating the term enhanced weathering in context of geoengineering.

Chemical weathering rates of minerals are controlled by the following parameters: (i) soil pH (Arshad et al., 1972; Grathwohl, 2014; Lasaga et al., 1994), with the highest weathering rates occurring under highly acidic or highly basic soil conditions (Casey and Bunker, 1990); (ii) redox conditions for the dissolution of Fe and Mn minerals (Cánovas et al., 2019; Gilkes et al., 1973; Hering and Stum, 1990); (iii) soil solution composition (Grathwohl, 2014; Hayes et al., 2020; Lasaga et al., 1994); (iv) temperature (Hayes et al., 2020; Lasaga et al., 1994; Velbel et al., 1990); and (v) grain size/density of exposed structural defects on mineral surfaces (Arshad et al., 1972; Cánovas et al., 2019; Holdren Jr and Speyer, 1985; Lasaga et al., 1994). Physical and chemical conditions of soils are strongly influenced by biological activity of plants and microorganisms, especially in the rhizosphere (Arcand and Schneider, 2006; Harley and Gilkes, 2000) where mycorrhizal fungi increase the volume of soil that roots can extract nutrients from (Clarkson and Hanson, 1980; Hopkins and Hüner, 2008; Taylor et al., 2009), making plant nutrient uptake more efficient (Arcand and Schneider, 2006). Additionally, at the rhizosphere, soil pH and soil solution composition varies according to plant nutritional needs and their production of root exudates, which might boost the weathering rates of pristine minerals from fine ground rocks (Arcand and Schneider, 2006; Harley and Gilkes, 2000).

Biochar is the solid product of biomass pyrolysis, the thermal conversion under oxygen-limited conditions at ambient pressure. Its residence time in soil is longer than that of fresh organic matter (Lehmann et al., 2006; Schmidt et al., 2018). Based on a meta-analysis that considered 116 observations, the mean residence time of biochar in soils was estimated to be 556 years (Wang et al., 2016a). Biochar can be produced from any type of biomass. This may include, but is not restricted to woody materials (Agegnehu et al., 2015a; Agegnehu et al., 2016b; Arif et al., 2017; Boersma et al., 2017; Bruun et al., 2014; De Tender et al., 2016); crop residues (Amoakwah et al., 2017; Li et al., 2018; Pratiwi and Shinogi, 2016; Wang et al., 2016a); manure (Hossain et al., 2015; Inal et al., 2015; Kammann et al., 2015; Macdonald et al., 2014; Park et al., 2011) or marine biomass (Bird

et al., 2011; Roberts et al., 2015). Biochar is traditionally used for various purposes in agriculture, including animal feed amendment, bedding material and composting additive (Allen, 1846; Hagemann et al., 2018; Schmidt et al., 2019). With any of these applications, biochar eventually is deployed to the soil and thus provides benefits at multiple levels (e.g. improved animal health, odor control, soil improvement) within a single life cycle, which today is called the “cascading use of biochar” (O’Toole et al., 2016). In the soil, biochar improves the nutrients retention in a plant-available form, establishing soil pH and soil moisture (McHenry, 2011; Wu et al., 2017) besides stimulating soil microbial biomass growth (Irfan et al., 2019; Lehmann et al., 2011; Wang and Li, 2018). However, positive response of crops to biochar amendment is so far mainly described for the tropics, where most soils are highly weathered (Crane-Droesch et al., 2013). To obtain positive effects on biomass production also in temperate climate and in rather fertile soils, biochar should be enhanced and combined with nutrients, e.g. by composting or mixing with compost or nutrient rich solutions (Hagemann et al., 2017a; Hagemann et al., 2017b; Schmidt et al., 2017). Otherwise, biochar competes with plants for soil nutrients (Joseph et al., 2018; Kammann et al., 2015). Biochar can be produced at any scale, including low-tech solutions for smallholder farmers like the flame-curtain pyrolysis in the “Kon-Tiki” (Cornelissen et al., 2016; Schmidt et al., 2014) and numerous industrial biochar production technologies (Boateng et al., 2015).

Either EW or biochar can be used for CDR and as soil conditioners; both have the potential to improve soil fertility. At least 6.8 billion hectares of land have unfavorable conditions for agricultural production (Fischer et al., 2001). This shows the high potential for the use of both terrestrial NETs as soil conditioner. They can enable degraded soils to produce food or biomass for afforestation or reforestation (AR) and for perennial grasses for bioenergy with carbon capture and storage (BECCS) or agroforestry systems (Abbas et al., 2017) that could be combined with further biochar production (Schmidt et al., 2018; Werner et al., 2018).

Poor nutrient conditions will limit plant growth (Garcia et al., 2018; Oren et al., 2001) and thus food and biomass production subsequently suppressing the CDR potentials as observed by empirical data (Oren et al., 2001) and predicted by AR numerical models (Garcia et al., 2020; Goll et al., 2012; Kracher, 2017). Before implementing EW and biochar as NET, the manifold drivers of EW and biochar application and the many sources of heterogeneity between experiments (application rates, soil types, climatic conditions, different crops, different biochar feedstocks and production parameters, different rock powder chemistry and granulometry, etc.) should be addressed by a systematic review of peer-reviewed publications. The review aims to: (i) Determine and compare the effects of rock powder and biochar on plant and soil properties; and (ii) provide recommendations for future studies on EW and biochar as CDR.

4.3. Methods

4.3.1. Data compilation, categorization, and treatment

Peer-reviewed articles evaluating the effects of biochar and rock powder application on soil properties (CEC, pH, available P, or exchangeable K) and plant response (dry plant and dry shoot mass, main stem diameter, plant height, or yield) were identified by searching the Google Scholar (<https://scholar.google.com/>, last access: 21 September 2018) and the Web of Science (<https://webofknowledge.com>, last access: 21 September 2018) using the keywords biochar, char, black carbon, and charcoal for biochar and the keywords enhanced weathering, rock powder, stonemeal, basalt powder, “rochagem”, “pó de rocha”, “polvo de roca”, “Gesteinsmehl”, “Gesteinspulver”, and “Steinmehl” for enhanced silicate rock weathering (EW), with no restriction on the publication year for search queries of both technologies.

With regard to soil properties, we focused on cation exchange capacity (CEC), soil pH, K, and P (either as exchangeable or available forms). Soil pH influences the CEC of soils and consequently the nutrient availability. P and K are the most required nutrients for crops, besides N. For this review, N was neglected since its supply by EW is negligible and none of the peer-reviewed articles focused on it. The dry total plant mass is the dry mass of above and below ground parts of the plant.

To guarantee reproducibility of the results and to allow the application of a random-effects model meta-analysis (cf., sub-chapter 4.3.2), the following criteria were applied to the selected publications on biochar or EW: (i) the changes between treatment and control groups must be compared and the treatment and control groups must have the same initial aspects; e.g., the same geographical location, the same initial soil properties (pH, CEC), the same plant species, etc., with exception for application rates; (ii) the standard deviation (SD) and the number of replicates (n) for each experiment must be given. Where standard error (SE) was given, SD was calculated after Eq. (32) or from other given statistical indicator like *p-tests* (p) by Eq. (33) according to Higgins and Green (2011); (iii) the culture medium was soil; and (iv) information on application rates must be given. These selection criteria resulted in 26 published studies for EW, and 63 published studies for biochar (Appendix H Table S7 and Table S8, Fig. S 38 to Fig. S 41).

$$SD = SE\sqrt{n}, \quad (32)$$

$$SD = \frac{n-1}{t_{inv}(p,n-1)}\sqrt{n}, \quad (33)$$

If multiple sampling campaigns were described in the same primary study, the last sampling campaign was selected to ensure statistical independence (i.e., the selected data does not affect the likelihood that a positive or a negative plant or soil response will take place after EW or biochar application during the experiment) among each observation, which is necessary to perform meta-analysis (Borenstein et al., 2010; Borenstein et al., 2011; Hedges et al., 1999). Different application rates, experimental environment, experiment duration, and soil textures were considered as individual variables for control conditions and treatment for biochar and EW. For EW, extra individual variables for control conditions and treatment, like the grain size of rock powder and the different igneous rocks; i.e., acid, intermediate, and basic rocks were needed. For biochar, the pyrolysis temperature, and feedstock group were the extra-considered individual variables for control conditions and treatment. Therefore, several effect sizes were often obtained in a single primary study.

The data were collected from tables presented in the peer-reviewed articles and data in figures were extracted using Engauge Digitizer (Mitchell et al., 2018). If the biochar or the EW application rates were presented in mass percentage, they were converted to mass per area assuming a soil bulk density of 1.4 t m^{-3} , a soil depth of 0.3 m, and an application area of 1 ha unless otherwise provided. If the converted application rate was significantly higher than common application rate values used in the agronomy literature, the study was neglected in accordance with criteria (iv). The soil pH(CaCl₂) values were transformed to pH(H₂O) according to Augusto et al. (2008) by Eq. (34):

$$pH_{H_2O} = 1.65 + (0.86 \times pH_{CaCl_2}), \quad (34)$$

The considered individual variables for control conditions and treatment were categorized into different experimental factors, which affect the level of biomass production and changes in soil properties, into the following groups: (i) experimental type (studies under field or laboratory conditions); (ii) rock type chemistry grouped

according to the silica content as: acid (Gneiss, Orthoclase, Charnokite, Granodiorite, Granite, Migmatite, Dacite, Zinwaldite, and Waste mica), and basic (Phonolite, Basalt, Steatite, and Olivine/Dunite) rocks, mixed rocks were included within the acid and basic rocks group and in the intermediate rock group; (iii) soil texture class was grouped according to USDA Soil Classification System as fine (Clay, Clay Loam, Silty Clay Loam, and Silty Clay), medium (Loam, Silt Loam, and Silt), and coarse (Sandy Loam, Sandy Clay Loam, Loamy Sand, and Sand); (iv) application rate, classified according to its distribution ($< 10 \text{ t ha}^{-1}$, $10 - 40 \text{ t ha}^{-1}$, and $\geq 40 \text{ t ha}^{-1}$ for EW and $\leq 10 \text{ t ha}^{-1}$, $10 - 30 \text{ t ha}^{-1}$, $30 - 80 \text{ t ha}^{-1}$ and $> 80 \text{ t ha}^{-1}$ for biochar); (v) biochar feedstocks, grouped as wood (multifarious wood, and unidentified wood mixtures) and crop (straw of different cereals; i.e., wheat, maize, etc; grasses, and crop residues); (vi) biochar pyrolysis temperature ($\leq 350 \text{ }^\circ\text{C}$, $350 - 500 \text{ }^\circ\text{C}$, and $> 500 \text{ }^\circ\text{C}$); and (vii) grain size of rock powder classified according to the majority amount of powder passing through sieves of different meshes as: $< 0.053 \text{ mm}$, $0.053 - 0.1 \text{ mm}$, $0.1 - 0.2 \text{ mm}$, and $0.2 - 2 \text{ mm}$; (viii) lasting time of experiment (≤ 3 months, $3 - 6$ months, $6 - 9$ months, $9 - 12$ months, $12 - 24$ months, and $24 - 40$ months), and (ix) a summary condition for the input data without classification. As moderators (i.e., the property of interest), the single biomass production indicators (dry plant and dry shoot mass, main stem diameter, plant height, or yield) or soil property (CEC, pH, available P, or exchangeable K) were selected. The selected studies covered a range of climatic zones, from temperate to tropical and subtropical environments. The Pearson and the Spearman Rank correlation analysis showed the correlation between the specified moderators and application rates of biochar or EW.

4.3.2. Meta-analysis

The generated database was categorized into the moderators and experimental factors groups described in section 4.3.1 and analyzed by employing a meta-analysis. We have applied a random-effects model meta-analysis because: (i) the collected studies were realized independently; and (ii) the selected studies have enough in common to be synthesized, but they are unlikely to share exactly the same population mean (Borenstein et al., 2010; Borenstein et al., 2011; Hedges et al., 1999). The meta-analysis allowed for the comparison of results of experiments from different studies after standardization, contributing to obtain a bigger picture of the potential impact of EW or biochar to a selected moderator considering different experimental groups. To implement the meta-analysis, we assumed that the data approximately follow a normal distribution. Therefore, the mean and standard deviations from the selected studies approximately represent the central tendency of the normal distribution and its variability respectively. The paired mean values of the control and of different application rates for biochar or EW were recorded from individual studies, standardized, and used to estimate the natural logarithm of the response ratio (L_i) according to Borenstein et al. (2011) and Hedges et al. (1999) by Eq. (35):

$$L_i = \ln(\overline{X_{ei}}) - \ln(\overline{X_{ci}}), \quad (35)$$

where $\overline{X_{ei}}$ and $\overline{X_{ci}}$ are the means of the experiment (e.g., for each biochar or EW application rate) and control from the i^{th} study. In this case, a negative value of L_i means that the treatment negatively influenced the considered moderator (e.g., a hypothetical application of 10 t ha^{-1} of biochar or EW hypothetically decreased the CEC of a determined soil). According to Hedges et al. (1999) the natural logarithm of the response ratio is advantageous since it follows more a normal distribution in small samples than the simple use of a response ratio (obtained by $\left(\frac{\overline{X_{ei}}}{\overline{X_{ci}}}\right)$, which is skewed).

The standard deviations and the number of replicates of control and experiments were needed for estimating the variance v_i of each obtained L_i according to Hedges et al. (1999) by Eq. (36):

$$v_i = \frac{SD_{ei}^2}{n_{ei} \bar{X}_{ei}^2} + \frac{SD_{ci}^2}{n_{ci} \bar{X}_{ci}^2}, \quad (36)$$

where SD_{ei} and SD_{ci} represent the standard deviations of experiment and control, respectively. n_{ei} and n_{ci} are the number of experiment and control replicates, respectively from the i^{th} study.

An approximate $100(1-\alpha)$ % confidence interval for the individual natural logarithm response ratio L_i is given by Eq. (37) according to Borenstein et al. (2011):

$$L_i - t_{df}^{\alpha/2} \sqrt{v_i} \leq L_i \leq L_i + t_{df}^{\alpha/2} \sqrt{v_i}, \quad (37)$$

where $t_{df}^{\alpha/2}$ is the t-value corresponding to the $100(1-\alpha)$ % confidence interval, in our case for an $\alpha = 0.05$, to the $df = n_i - 1$ degrees of freedom and n_i corresponding to the number of replicates within the selected i^{th} study.

Once the natural logarithm of the response ratio, the variance, and the confidence intervals for $\alpha = 0.05$ were calculated for each biochar and EW application rate, the individual effect sizes (i.e., L_i and 95 % confidence intervals) were used to estimate a summary effect (the weighted arithmetic mean of the natural logarithm response ratios (\bar{L}^*) and the confidence interval ($CI_{\bar{L}^*}$) of each considered experimental factor group for a moderator; the selected experimental factor groups and moderators are described in section 4.3.1. Therefore, the between-experiment variance is obtained by Eq. (38) based on different authors (Borenstein et al., 2010; Borenstein et al., 2011; Hedges et al., 1999):

$$T^2 = \frac{Q-df}{\sum_{i=1}^k w_i - \frac{\sum_{i=1}^k w_i^2}{\sum_{i=1}^k w_i}} \quad (38)$$

with:

$$Q = \sum_{i=1}^k w_i L_i^2 - \frac{(\sum_{i=1}^k w_i L_i)^2}{\sum_{i=1}^k w_i}, \quad (39)$$

where df is the degree of freedom obtained by the total number of experiments for the summary effect calculation – 1. w_i is a weighting factor for the i^{th} experiment being the same as the inverse of estimated variance of the i^{th} experiment Eq. (36).

The weighted arithmetic mean of the natural logarithm response ratios was estimated for each experimental factor of a selected moderator according to Eq. (40) based on different authors (Borenstein et al., 2010; Borenstein et al., 2011; Hedges et al., 1999):

$$\bar{L}^* = \frac{\sum_{i=1}^k w_i^* L_i}{\sum_{i=1}^k w_i^*}, \quad (40)$$

with $w_i^* = (v_i + T^2)^{-1}$

The confidence interval for the weighted arithmetic mean of the natural logarithm response ratios, for a considered experimental factor as described in section 4.3.1 (e.g., application rates $< 10 \text{ t ha}^{-1}$ of biochar or EW) were calculated by Eq. (41) for degrees of freedom df being obtained by the total number of experiments for the summary effect calculation – 2 (Borenstein et al., 2011):

$$CI_{\bar{L}^*} = \bar{L}^* \pm t_{df}^{\alpha/2} SE(\bar{L}^*), \quad (41)$$

In the cases that the number of selected experiments were smaller than 50, the standard error was estimated by Eq. (42) after Hedges et al. (1999) otherwise it was estimated by Eq. (43) based on different authors (Borenstein et al., 2010; Borenstein et al., 2011; Hedges et al., 1999):

$$SE(\bar{L}^*) = \sqrt{\left[\sum_{i=1}^k w_i^{*-1} \right] \left\{ 1 + 4 \sum_{i=1}^k (n_{ie} + n_{ic} - 2)^{-1} \left(\frac{w_i^*}{w_i} \right)^2 \frac{w_i^* [(\sum_{i=1}^k w_i^*) - w_i^*]}{\sum_{i=1}^k w_i^{*2}} \right\} + T^2}, \quad (42)$$

$$SE(\bar{L}^*) = \sqrt{\sum_{i=1}^k (w_i^*)^{-1} + T^2}, \quad (43)$$

The calculated weighted arithmetic mean of the natural logarithm response ratios (\bar{L}^*) and the confidence interval ($CI_{\bar{L}^*}$) for the weighted mean of the natural logarithm response ratios were converted to mean percent changes (MPC) by Eq. (44):

$$MPC = [\exp(\bar{L}^* \text{ or } CI_{\bar{L}^*}) - 1] \times 100, \quad (44)$$

If the confidence intervals did not overlap zero, the effect of the experimental factor group on a moderator was considered significant (Borenstein et al., 2011), meaning that the considered effect represents the characteristic of the whole population and the null hypothesis (e.g., decrease in soil pH) can be neglected. The random-effects model meta-analysis results are directly linked to the input data (Borenstein et al., 2010; Borenstein et al., 2011). Thus, if some of the selected studies are biased (i.e., the included analysis systematically differ from the other selected studies), the results may be influenced by it (Borenstein et al., 2011). The sources of variation in the random-effects model meta-analysis are: (i) within-study error variance (Eq. (36)); and (ii) the between-studies variance (Eq. (38)). Therefore, to decrease wide confidence intervals, and consequently increase the statistical power of the meta-analysis, the number of used studies need to increase if the between-studies variance is large. If the within-study error variance is large, it is necessary to increase the sample size of each study (Borenstein et al., 2010).

4.4. Results

Part of the selected works treated EW or biochar with some sort of nutrients (Appendix H Table S7 and Table S8) before its use. The descriptive statistics of the input data is shown in the Appendix H Fig. S 38 to Fig. S 41. The estimated natural logarithm of the response ratios and the confidence intervals are approximately following a normal distribution since the upper and lower limits of the confidence intervals are symmetrically spaced from the estimated mean values (Fig. 15 to Fig. 18).

4.4.1. Biochar effects on soil properties and plant biomass

The biochar application effects on plant (dry plant and dry shoot mass, main stem diameter, plant height, and yield, Fig. 15) and soil properties (CEC, pH, exchangeable K, and Available P, Fig. 16) for field and laboratory studies are positive for most of the experimental factors of the moderators. Compared to the control, dry shoot mass increase was ~53 % and had the highest response after biochar addition in laboratory studies (Appendix H Table S9); while for field studies, dry shoot mass rose by ~6 %. The dry shoot mass gain at laboratory studies was substantially greater than that observed for dry total plant mass, main stem diameter, plant height, and yield. However, biochar application could significantly increase the dry total plant mass and yield at laboratory trials (Fig. 15). For field studies, significant effects were not observed. However, the dry total plant mass had a raise of ~42 % (Appendix H Table S9). The exchangeable K had the highest gain of ~93 % for laboratory experiments but

for field conditions, it remained by ~41 % (Appendix H Table S10). Either for plant (dry shoot mass, main stem diameter, plant height, and yield, Fig. 15) or soil properties (CEC, pH, exchangeable K, and Available P, Fig. 16), the positive effects of biochar application decreases with time except dry total plant mass that had a significant positive effect after 12 – 24 months of ~35 % (confidence intervals (CI) of 20 % to 53 %).

Rising the pyrolysis temperature of biochar decreased the plant response in some cases but positive effects can still occur. The highest effect was for dry shoot mass (~106 % increase) followed by plant height (~20 % gain) for biochar with pyrolysis temperatures > 500 °C, which also had significant positive effects for dry total plant mass (Fig. 15, Appendix H Table S9). The soil response was higher with rising the pyrolysis temperature of deployed biochar except the CEC (increase of ~55 %) that had a wide confidence interval (~-100 % to >> 100 %) for low pyrolysis temperature biochar (≤ 350 °C) and had a slight reduction of ~-0.2 % in soil pH (Fig. 16; Appendix H Table S10).

The use of wood feedstock for biochar production positively impacted all the investigated soil and plant properties (for lab and field experiments combined) except yield that drop by -4 % (Appendix H Table S9). Compared with control groups, CEC raised by ~24 % with wide confidence intervals (~-18 % to ~86 %) for applying wood biochar (Fig. 16). Exchangeable K raise by ~63 % for crop residue biochar, and the wide confidence intervals (~-100 % to >> 100 %) expose its great uncertainty (Fig. 16; Appendix H Table S10). For the plant properties, the greatest response was for dry total plant mass that grew by ~17 % with wide confidence intervals (~-71 % to ~380 %). The use of crop residues as feedstocks for biochar production boosted all the investigated plant and soil properties, the highest gain was ~20 % for main stem diameter and ~63 % for exchangeable K (Fig. 16), while the available P increase by 0.1 % (Appendix H Table S10).

The effects of biochar application rates positively influence the investigated plant properties with the highest increase of ~86 % for dry shoot mass for applying 30 – 80 t biochar ha⁻¹ (Fig. 15; Appendix H Table S9). Application rates between 10 – 30 t biochar ha⁻¹ and 30 – 80 t biochar ha⁻¹ could significantly increase the dry total plant mass (Fig. 16). The investigated soil properties were positively influenced by biochar application except for exchangeable K (Fig. 16), which decreased by ~-13 % for ≤ 10 t biochar ha⁻¹ (Appendix H Table S10).

The response of investigated plant properties varied with soil texture, however, were positive for a fine, medium, as well as coarse soil texture (Appendix H Table S10). The highest observed increase was ~46 % for dry shoot mass for a fine textured soil (Fig. 15; Appendix H Table S9). The positive impacts tend to be smaller for coarse textured soils (Fig. 16).

In summary, applying biochar on soil positively affected all the plant properties with the dry total plant mass significantly increasing by 29 % (CI of 15 % to 44 %; Fig. 15, Appendix H Table S9). Biochar application in soil positively affected all the investigated soil properties, with the exchangeable K having the highest gain of ~54% (CI of ~-46 % to >> 100 %). However, the different experimental factors, in general, reveal that the values of investigated soil properties raise with rising pyrolysis temperature and application rate of biochar. Woody feedstock is more effective for increasing the CEC and available P, while crop residues are more efficient for increasing soil pH and exchangeable K (Fig. 16). The effects of biochar application were most pronounced to fine textured soils for all investigated soil properties. Apparently, pyrolysis temperatures in the range of 350 °C – 500 °C resulted in the highest positive impacts for all investigated plant properties except dry shoot mass and plant height. Biochar produced from crop residues feedstock had the highest responses on plant properties except dry total plant mass. Application rates in the range of 30 t ha⁻¹ – 80 t ha⁻¹ resulted in the highest positive changes to all plant properties. Increasing the application rates of biochar negatively influenced the available P for

Pearson's correlation and dry total plant mass for Pearson's and Spearman's Rank correlation. The other investigated plant and soil properties are positively correlated to biochar application rates (Table 5).

Table 5: Pearson's and Spearman's Rank correlation for moderators and biochar application rates. 'n' is the number of used data, R is the Pearson's or Spearman's Rank correlation coefficient.

Moderators	R	p-test	SE	R*	p-test*	n
CEC	0.4	5.0×10^{-3}	0.04	0.5	2.0×10^{-4}	61
pH	0.6	5.0×10^{-15}	0.006	0.5	5.0×10^{-13}	163
Dry shoot mass	0.6	1.0×10^{-5}	0.1	0.4	8.0×10^{-3}	54
Plant height	0.4	5×10^{-4}	0.3	0.4	1.0×10^{-3}	65
Yield	0.2	0.08	0.2	0.2	0.2	71
Dry total plant mass	-0.1	0.3	0.09	-0.04	0.8	67
Available P	-0.1	0.3	0.4	0.03	0.8	74
Exchangeable K	0.6	4.0×10^{-4}	0.4	0.7	6.0×10^{-5}	26
Main stem diameter	0.8	7.0×10^{-3}	0.07	0.8	3.0×10^{-3}	11

*Spearman's Rank correlation

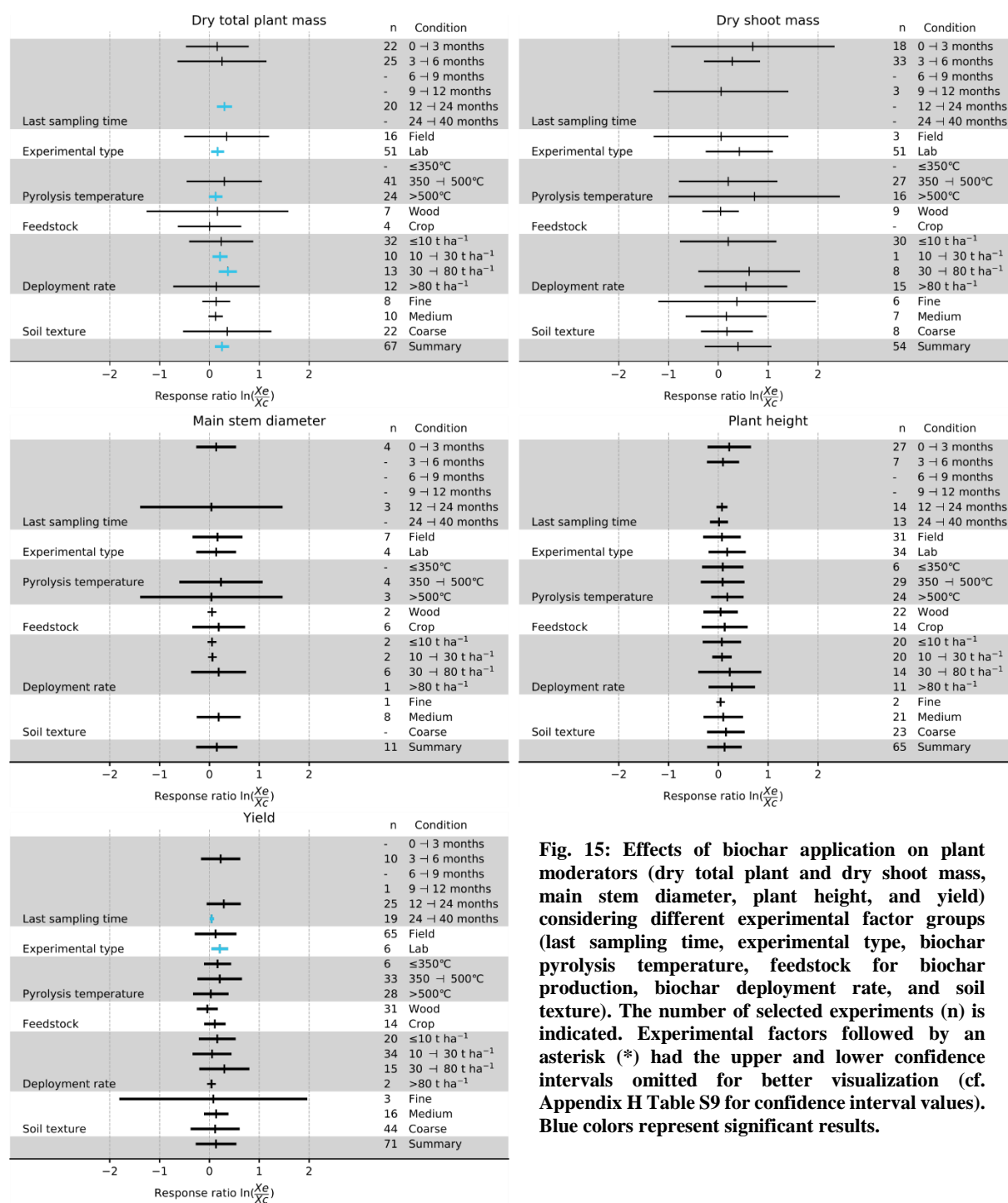


Fig. 15: Effects of biochar application on plant moderators (dry total plant and dry shoot mass, main stem diameter, plant height, and yield) considering different experimental factor groups (last sampling time, experimental type, biochar pyrolysis temperature, feedstock for biochar production, biochar deployment rate, and soil texture). The number of selected experiments (n) is indicated. Experimental factors followed by an asterisk (*) had the upper and lower confidence intervals omitted for better visualization (cf. Appendix H Table S9 for confidence interval values). Blue colors represent significant results.

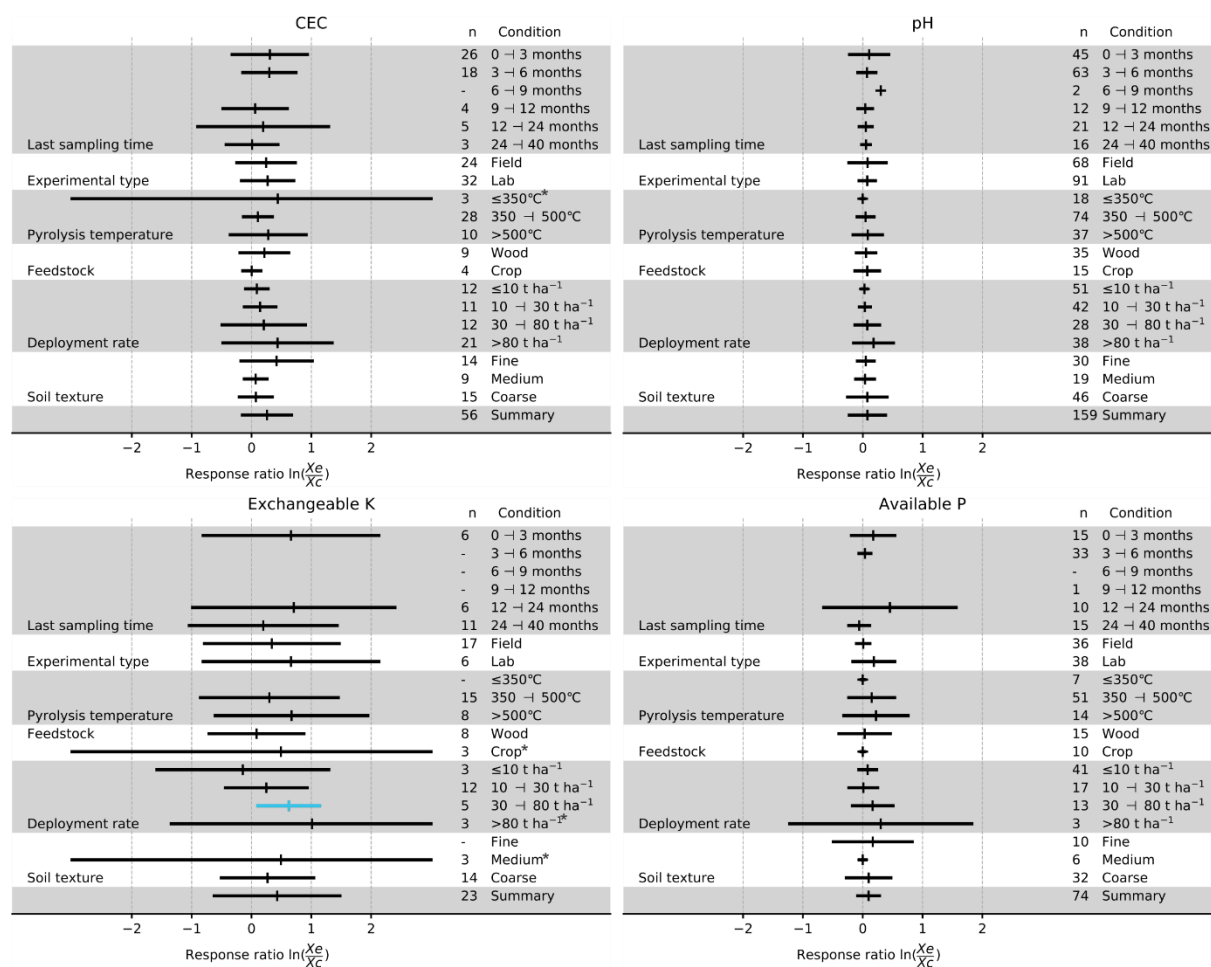


Fig. 16: Effects of biochar application on soil moderators (CEC, pH, exchangeable K, and Available P) considering different experimental factor groups (last sampling time, experimental type, biochar pyrolysis temperature, feedstock for biochar production, biochar application rate, and soil texture). The number of selected experiments (n) is indicated. Experimental factors followed by an asterisk (*) had the upper and lower confidence intervals omitted for better visualization (cf. Appendix H Table S10 for confidence interval values). Blue colors represent significant results.

4.4.2. EW effects on soil properties and plant biomass

Experiments (for lab and field combined) performed in a time from three to six months after rock powder application increased dry shoot mass (~27 %) and yield (~69 %) but resulted in negative responses of all other properties investigated. In general, the positive effects on yield, after applying EW, increased with time (Fig. 17, Appendix H Table S11). The effects on exchangeable K and available P after EW application increase with time while the effects on soil pH and CEC after EW application do not (Fig. 18, Appendix H Table S12). However, for soil and plant effects, the confidence intervals are wide and the statistical power of the analysis still need to be enhanced.

Applying rock powder (for lab and field combined) with the major amount of grains passing through meshes < 0.053 mm reduced the dry total plant mass by ~-15 %, and by -1 %, for size 0.2 – 2 mm (Fig. 17, Appendix H Table S11). For grain size < 0.053 mm yield gain was ~69 % but for grain sizes between 0.2 – 2 mm, it diminished by ~-22 % (Fig. 17, Appendix H Table S11). For grain sizes between 0.053 – 0.1 mm, the plant height decreased by ~-11 % (Fig. 17). High response occurred for soil CEC (~63 % rise) and exchangeable K (~31 % increase) after applying rock powder with grain size < 0.053 mm (Fig. 18, Appendix H Table S12) but CEC had wide confidence intervals (~-100 % to >> 100 %; Appendix H Table S12). High response occurred for available P (212 % increment) and for exchangeable K (~43 % rise) after applying rock powder with grain sizes between 0.053 – 0.1 mm (Fig. 18, Appendix H Table S12).

In field experiments, yield of plants increased by ~10 % after rock powder application (Appendix H Table S11, Fig. 17) and showed positive impacts for all investigated soil properties (Fig. 18), with available P increasing by ~111 % and exchangeable K showing significant positive effects (~81 % growth; Appendix H Table S12). Laboratory trials resulted in reduction of ~36 % for available K, of ~15 % for dry total plant mass, of -19 % for main stem diameter, and of ~24 % for plant height (Appendix H Table S12).

The use of basic rock powder boosted the investigated soil properties (Fig. 18, Appendix H Table S12) but decreased the investigated plant properties except yield (~17 % increase; Appendix H Table S11, Fig. 17). Applying basic rocks resulted in significant positive effects on soil pH (~14 % increase). Applying acid rocks caused positive effects on the investigated soil properties except available P, which fell by ~12 % (Appendix H Table S12) and augmented the dry plant (40 %) and dry shoot mass (~56 %). Additionally, acid rock powder showed significantly positive effects on yield (~35 %; Appendix H Table S11).

For application rates ≥ 40 t rock ha⁻¹, rock powder positively affected the investigated soil properties with exchangeable K (~232 %) and soil pH (~18 %) showing significant positive effects. Available P also had positive effect (~43 % increase) for a wide confidence interval (~100 % to $\gg 100$ %; Appendix H Table S12, Fig. 18). For the same application rate, dry plant and dry shoot mass grew by ~9 % and by ~56 % respectively but plant height shrank by ~11 % (Fig. 17, Appendix H Table S11). The statistical significance for exchangeable K for rock powder application rates < 10 t rock ha⁻¹ and for 10 – 40 t rock ha⁻¹ is low, but the impacts of rock powder application are still positive for exchangeable K and available P. On the one hand, application rates of 10 – 40 t rock ha⁻¹ reduced all investigated plant properties (Appendix H Table S11), on the other hand, application rates of < 10 t rock ha⁻¹ boosted all investigated plant properties except plant height that fell by ~6 % (Fig. 17; Appendix H Table S11).

Applying rock powder on coarsely textured soils resulted in positive effects for all plant properties while on finely textured soils, the responses of dry total plant and dry shoot mass, main stem diameter, and plant height reduced by ~14 %, ~7 %, -19 %, and ~18 %, respectively (Fig. 17, Appendix H Table S11). The yield grew for the investigated soil textures showing significant results, but it went from ~71 % in fine to ~34 % in coarse textured soils. Rock powder application positively impacted all the investigated soil properties except for the exchangeable K for fine textured soils (Fig. 18; ~5% decrease; Appendix H Table S12).

In summary, applying EW in soil positively affected the dry total plant mass (~11 %), dry shoot mass (~27 %), and yield (~23 %) and negatively affected the other plant properties (stem diameter, and plant height, Fig. 17, Appendix H Table S11). EW application in soil positively affected all the investigated soil properties, with the exchangeable K having the highest gain of ~30 % (confidence interval of ~67 % to 421 %). However, for the different experimental factors, in general, rock powder grain sizes < 0.053 mm have the highest positive impacts on CEC and soil pH, while grain sizes in the range of 0.053 – 0.1 mm effectively rose available P and exchangeable K. Acid rocks efficiently raised the CEC and exchangeable K while basic rocks could efficiently increase the soil pH and the available P. The effects on fine soils were greater for soil pH than the effects on coarse soils after applying EW. However, for coarse soils, the exchangeable K and available P response were greater compared to fine soils. The available data on plant response after rock powder application was scarce; however, the grain sizes in the range of 0.053–0.1 mm showed the highest impacts on dry total plant mass; besides that, the application rates < 10 t ha⁻¹, the use of acid rocks, and applying EW onto coarse textured soils also had the highest effects on dry total plant mass. Nevertheless, grain sizes < 0.053 mm, application rates > 40 t ha⁻¹, and fine textured soils show the highest response for yield. The investigated soil properties are positively correlated to rock powder

application rates but increasing the application rates of rock powder negatively influence the plant height, dry total plant mass, and main stem diameter (Table 6).

Table 6: Pearson's and Spearman's Rank correlation for moderators and rock powder application rates. 'n' is the number of used data, R is the Pearson's or Spearman's Rank correlation coefficient.

Moderators	R	p-test	SE	R*	p-test*	n
CEC	0.9	2.0×10^{-4}	0.2	1	2.0×10^{-5}	9
pH	0.2	0.03	0.03	0.3	4.0×10^{-3}	71
Dry shoot mass	0.7	0.02	0.3	0.8	2.0×10^{-03}	10
Plant height	-0.1	0.6	0.05	-0.1	0.7	11
Yield	0.4	0.08	0.4	0.4	5.0×10^{-2}	23
Dry total plant mass	-0.2	0.2	0.2	-0.2	0.2	32
Available P	0.3	0.1	0.7	0.09	0.7	24
Exchangeable K	0.5	1.0×10^{-5}	0.9	0.4	4.0×10^{-3}	57
Main stem diameter	-0.5	0.4	1.2	-0.4	0.5	5

*Spearman's Rank correlation

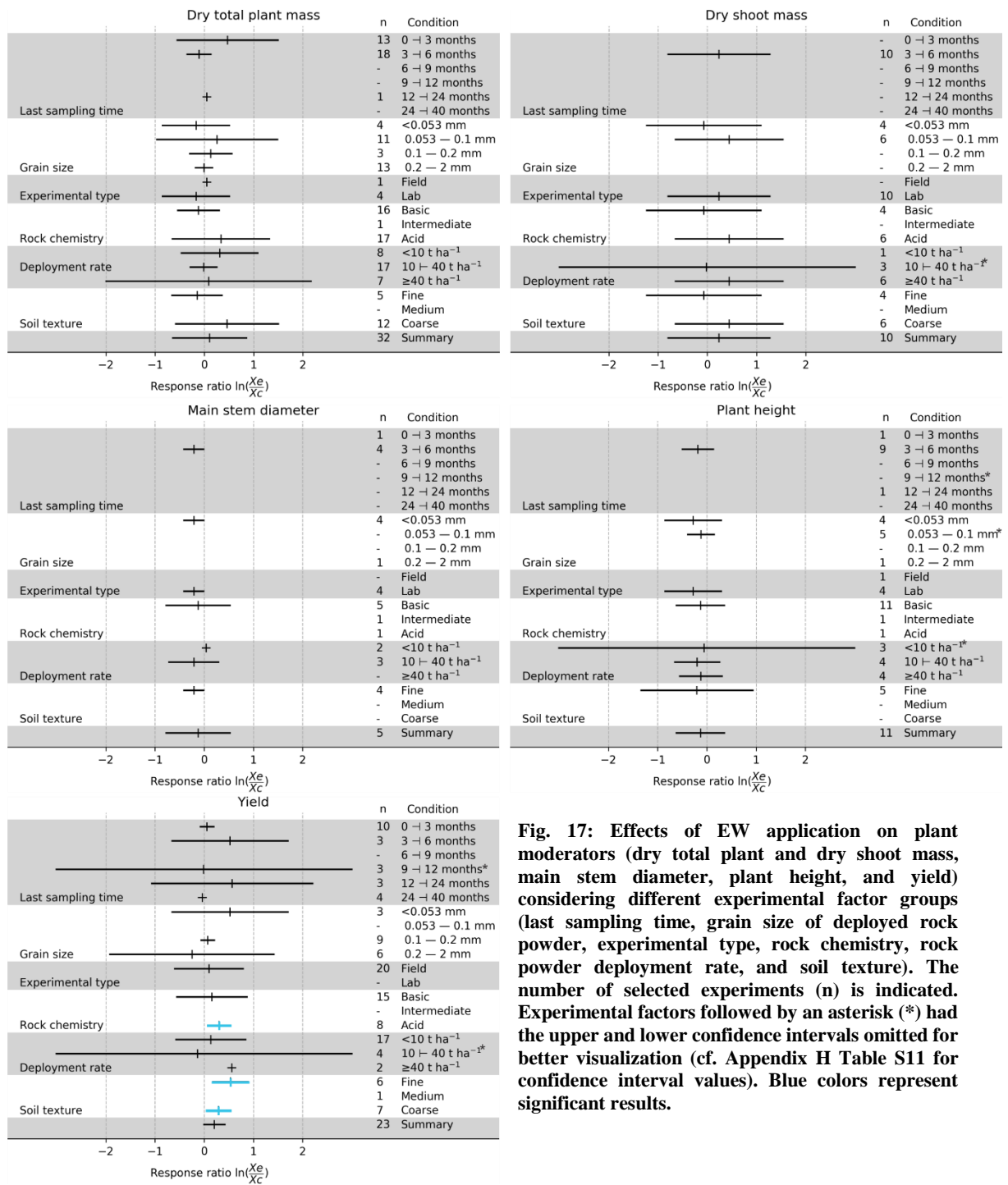


Fig. 17: Effects of EW application on plant moderators (dry total plant and dry shoot mass, main stem diameter, plant height, and yield) considering different experimental factor groups (last sampling time, grain size of deployed rock powder, experimental type, rock chemistry, rock powder deployment rate, and soil texture). The number of selected experiments (n) is indicated. Experimental factors followed by an asterisk (*) had the upper and lower confidence intervals omitted for better visualization (cf. Appendix H Table S11 for confidence interval values). Blue colors represent significant results.

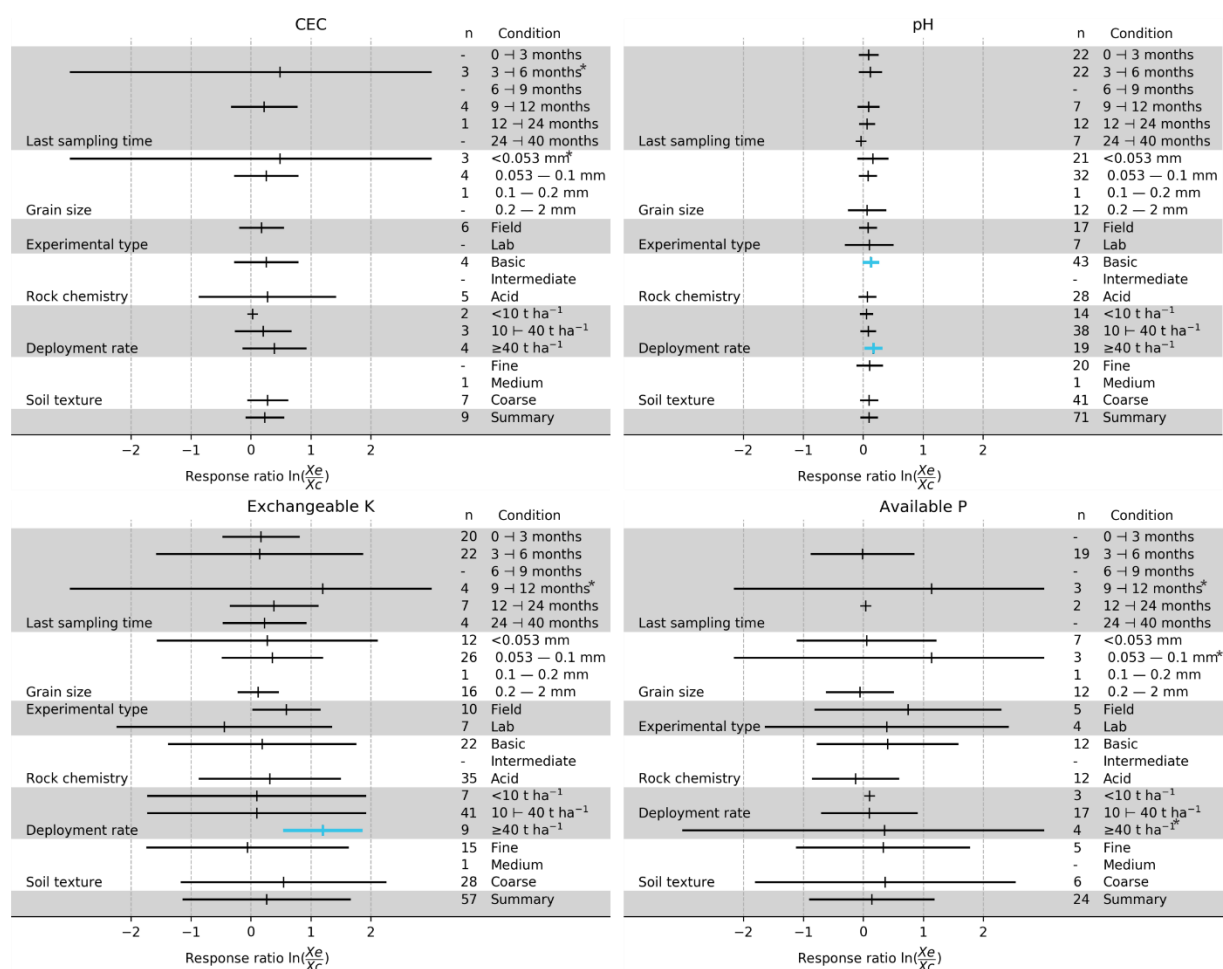


Fig. 18: Effects of EW application on soil moderators (CEC, pH, exchangeable K, and Available P) considering different experimental factor groups (last sampling time, grain size of deployed rock powder, experimental type, rock chemistry, rock powder application rate, and soil texture). The number of selected experiments (n) is indicated. Experimental factors followed by an asterisk (*) had the upper and lower confidence intervals omitted for better visualization (cf. Appendix H Table S12 for confidence interval values). Blue colors represent significant results.

4.5. Discussion

For this systematic review, 63 studies were available for biochar and 26 studies were available for enhanced silicate rock weathering. Some experimental factors like application rate < 10 t ha⁻¹ for CEC and main stem diameter for EW or plant height for fine textured soils for biochar merely had two paired experiments, which were combined to calculate the effect sizes and respective weighted means of the natural logarithm response ratios. In cases that only one paired experiment existed, the data was excluded, e.g. medium soil texture for CEC, pH, exchangeable K, and available P for EW or available P and yield for experiment running time of 9 – 12 months for biochar. The number of experiments (n) indicated in Fig. 15 to Fig. 18 shows where scarcity of data exists and further research can focus to overcome it and enhance the statistical power of this systematic review. The selected studies range from 1 to 40 months for biochar and from 1 to 60 months for EW. Either for biochar or EW, more than 60 % of the selected studies in this analysis showed results for experiments running only up to 12 months, and 90 % to up to 24 months. Only one study performed measurements for 40 (biochar) and 60 months (EW). Therefore, long-term studies on the effects of biochar and EW application to soil on plant and soil properties are still necessary. Long-term studies are necessary to anticipate side-effects since application at any scale of EW and biochar as NET is going to occur to sustainably reach the 1.5 °C target from the Paris Climate Agreement (Amann and Hartmann, 2019; Minx et al., 2018).

For biochar, the field experiments were done in its majority in temperate (~76 %), followed by tropical (~21 %) and subtropical (3 %) climate zones, while for EW, field experiments were placed in its majority in tropical (75 %) and temperate (25 %) climate zones.

The response of a selected experimental factor from the peer-reviewed articles was, in some cases, being influenced by other experimental factors (e.g., basic rocks experimental factor was often falling into different grain size class, or application rate, or experiment running time, etc.). Therefore, at this moment, performing a more detailed classification of the data for the meta-analysis would compromise its statistical power. However, it would be possible in successive systematic reviews if more data is available. To increase the statistical power with the current data, we estimated the summary result for each moderator without accounting for a specific experimental factor. The summary results allowed to test a more general null hypothesis (i.e., applying EW or biochar to soil will decrease CEC), assuming that the contribution from the different experimental factors are the same. This more general analysis indicated that positive effects on soil and plant properties are likely to occur after biochar or EW application, but the probability that a negative effect will occur cannot be neglected. Thus, before application at any location and scale, it is necessary to properly understand the ecosystem characteristics to select the appropriate configuration of biochar or EW by adapting their characteristics (e.g., grain size, pyrolysis temperature, etc.).

Each selected experimental factor influenced differently each of the soil or plant moderator after biochar or EW application, with some showing significant positive results. This indicates the complexity of mechanisms governing a selected moderator response and highlight the importance to understand how the soil physico-chemical processes are governing the biological response after biochar or EW application. This is necessary before application of these NET for greenhouse gas removal occurs at any given location and scale. In general, the potential of rock powder to ameliorate soil pH, and available P is higher than that of biochar while biochar can increase CEC and soil exchangeable K more than EW (cp. summary results from Fig. 16 with Fig. 18 and the summary values from Appendix H Table S10 with Table S12). Biochar potential to ameliorate plant properties is generally higher than that of EW except for plant yield (cp. summary from Fig. 15 with Fig. 17 and the values from Appendix H Table S9 with Table S11). However, this picture might change as research on EW increases since the number of peer-reviewed papers for biochar is almost three times higher than that for EW.

4.5.1. Biochar effects on soil properties and plant biomass

Using biochar to sequester atmospheric carbon dioxide is attractive due to its recalcitrant nature, its high potential to enhance soil organic carbon, soil fertility, soil water retention, and other ecosystem properties (Fuss et al., 2018; Glaser et al., 2002; LeCroy et al., 2013; Schmidt et al., 2018; Vanek and Lehmann, 2015). Rising biochar pyrolysis temperature boost its CEC (Lehmann, 2007), and applying biochar with pyrolysis temperatures > 500 °C can promote soil CEC gain (Fig. 16), because the point of net zero charge of biochar of high pyrolysis temperature is higher than that of soil (Lehmann, 2007). Increasing nutrient retention capacity of soils directly contributes to the efficient use of commercial fertilizers (Ding et al., 2016; Kizito et al., 2019). High pyrolysis temperature biochar can also lead to greater suppression of N₂O emissions than low pyrolysis temperature biochar (Nelissen et al., 2014; Wang et al., 2020). However, the decrease in N₂O emissions is influenced by a set of factors like effects of biochar on soil pH, microbial N immobilization, non-electrostatic sorption of NH₄⁺ and NO₃⁻ (Borchard et al., 2019; Nelissen et al., 2014), with soil microbes exerting strong influence (Harter et al., 2016; Ji et al., 2020).

The observed soil pH drop (~-0.2 %) after applying low pyrolysis temperature biochar (≤ 350 °C) is probably due its oxidation process (Cheng et al., 2006; Inal et al., 2015; Liu and Zhang, 2012) that release acidic functional groups (Inal et al., 2015; Liu and Zhang, 2012). Nevertheless, a positive effect on soil pH occurs for most of the

investigated experimental factors after biochar application being positive for summary result (Fig. 16). Thus, biochar has the potential to establish soil pH, which can reduce N₂O emissions (Borchard et al., 2019; Nelissen et al., 2014). In cases where soil pH can be re-established to (near) neutral conditions macro- (e.g., Mg, Ca, K, P, and S), and micronutrients (e.g., B, Mo, Cu, Fe, Mn, Zn, Ni), if present at an amended soil, would be available for plant nutrition (Brady, 1984).

The positive effects on soil properties after biochar application (Fig. 16) might explain the observed gains in the investigated plant properties since a more efficient use of nutrients by plants can occur if soil CEC and pH increase (Cornelissen et al., 2013). Besides the improvement of the investigated soil properties, biochar addition may also increase plant-available water, which can positively affect the investigated plant properties (Cornelissen et al., 2013; Omondi et al., 2016).

Most of selected works in our database enhanced the biochar with nutrients (NPK) before its application. However, the available P and exchangeable K content in the soil declined for some experimental factors probably due to a competition for P between biochar and ferrihydrite (Jones et al., 2012; Liang et al., 2014) and to a natural shrinkage in biochar K content with time due to K desorption (Jones et al., 2012). Alternatively, the observed decline in available P and exchangeable K may be also associated to analytical methods, which cannot extract all adsorbed P and K from biochar pores (Kammann et al., 2015). To keep the levels of K and P and to avoid nutrient depletion, a constant input of nutrients is important to guarantee high biomass growth and yield (Garcia et al., 2020).

A positive impact on biomass yield for all the experimental factors is expected except for wood biochar (Fig. 15), which shows a slight tendency to negative effects but the statistical power of this analysis is low. Different authors reported a yield suppression after wood biochar application (Backer et al., 2016; Boersma et al., 2017; Haider et al., 2017), while others reported positive effects (Agbna et al., 2017; Agegnehu et al., 2016a; Agegnehu et al., 2015a; Arif et al., 2017; Chen et al., 2010; Li et al., 2018). This highlights the complexity of biochar reactions with soil and its consequences to the biomass, especially as biochar may play different roles as according to Jeffery et al. (2017) that in their meta-analysis differentiated between “structure” (wood and crop residues) and “nutrient” (biosolids and manure) biochars. A structure biochar may increase nutrient availability by reducing leaching, while nutrient biochars may additionally release nutrients. Our study did not include nutrient biochars. However, considering our focus on P and K, crop residue biochars may have stronger nutrient effect (i.e., fertilizing effect) with regard to K and P, unlike wood biochars (Glaser and Lehr, 2019; Yuan et al., 2011).

Apparently, the soil nutrient pool may influence the effects of added biochar on plants since biochar amended to soils under nutrient stress boosted plant response (biochar might stimulate microbial activity and thus nutrient release e.g. by mineralization), while it diminished the plant response in nutrient rich soils due to sorption of nutrients (Boersma et al., 2017; De Tender et al., 2016). However, some works also reported positive effects on yield after biochar application on moderate nutrient rich soils (Rajkovich et al., 2012) and highly fertile soils (Schmidt et al., 2017). The contrasting results may be related to which treatment biochar undergoes prior to soil application. Complete biochar enhancement with nutrients is necessary before applying it to soils, otherwise the added biochar may compete for soil nutrients with the growing biomass, which would reduce the biomass growth and yield rates (Joseph et al., 2018). Also any pre-treatment of biochar to add nutrients, such as composting, will alter biochar’s properties through interaction with microorganism and dissolved organic matter (Hagemann et al., 2017a). Additionally, the plant response after biochar amendment to soil would also depend on the selected plant species (Backer et al., 2016; Boersma et al., 2017).

4.5.2. EW effects on soil properties and plant biomass

EW is another terrestrial negative emission technology (Fuss et al., 2018) that can be used as soil conditioner due to its potential to enhance the soil fertility, soil water retention, and other soil properties (Amann and Hartmann, 2019; Anda et al., 2015; Beerling et al., 2018; Garcia et al., 2020; Hartmann and Kempe, 2008; Hartmann et al., 2013; Leonardos et al., 1987; Nkouathio et al., 2008; Van Straaten, 2006). EW effectiveness as a soil conditioner and means of plant nutrition correlates to the rate of nutrient supply by the rock minerals (i.e., the weathering rates). Lower weathering rates than the plant nutrient demand result in poor nutrient supply, which consequently limits the plant growth (Harley and Gilkes, 2000) if EW is the sole source of the respective nutrient. Therefore, the plant response depends on the selected plant species and the individual weathering rates of minerals in selected rocks. Soil exchangeable K and soil available P decrease might be traced back to P-fixation (Silva et al., 2013) or to the use of rocks with low P content since Carvalho (2012) and Silva et al. (2013) used Gneiss and Granite respectively in their experiments, which commonly share low P content relative to basic rocks (e.g., Basalt; Porder and Ramachandran, 2013). Besides that, the used Gneiss and Granite have high content of K-feldspars (Harley and Gilkes, 2000). Most of the bound K in K-feldspars are nearly unavailable for plants (Bakken et al., 1997) due to K-feldspars low dissolution rates (Zhang et al., 2018). However, hydrothermal treatment can make the bound K in K-feldspars available to plants (Liu et al., 2015; Ma et al., 2016a; Ma et al., 2016b).

Plant properties were negatively affected in some cases (Fig. 17, Appendix H Table S11) probably due to nutrient limitation (Bakri et al., 2017; Carvalho, 2012; de Resende et al., 2006; Feiden, 1991; Hinsinger et al., 1996) occasioned by the low weathering rates of used rock powder (Carvalho, 2012; Feiden, 1991) or by the release of some trace element responsible for hindering plant growth (Athar and Ahmad, 2002; Diaconu et al., 2020). Autochthonous microorganisms can positively influence the K and P release (Carvalho, 2012) and the use of solubilizing microorganisms can raise weathering rates, and consequently nutrient availability (Khan et al., 2007; Meena et al., 2016; Meena et al., 2014). Additional solutions to overcome nutrient limitation would be to rise application rates of rock powder and coapplication with industrial fertilizers (Bakri et al., 2017; Bolland and Baker, 2000; Carvalho, 2012; Feiden, 1991; Leonardos et al., 1987) or other sustainable techniques (Garcia et al., 2018; Nair, 2007) that could include organic fertilizers application.

There is an apparent discrepancy in the results for dry total plant and dry shoot mass, after applying rocks with grains passing through sieve meshes < 0.053 mm (~ -15 % and ~ -7 % decrease, respectively) and acid rocks (40 % and ~ 56 % gain, respectively). Based on the confidence intervals, which are small, and on the number of used samples (n), the statistical power for acid rock application on dry total plant mass and dry shoot mass is greater than that for rocks with grains passing through sieve meshes < 0.053 mm. This apparent discrepancy and uncertainty of the role of the grain sizes might be solved by increasing numbers of experiments.

In general, the positive response of plant growth and yield after rock powder application (Fig. 17, Appendix H Table S11) is related to positive changes in soil properties. Adding rock powder could positively affect the soil pH, exchangeable K and available P (Fig. 18, Appendix H Table S12). Increasing soil pH may have contributed to the iron and aluminum hydrous-oxides transient negative surface charges to become higher, since they are mainly sensitive to soil pH and ionic strength of solution, directly influencing the soil CEC (Seaman and Roberts, 2012) and nutrient retention.

The soil pH improvement is probably related to Mg^{2+} , Ca^{2+} , K^+ , and Na^+ release after rock powder application and to alkalinity gain as HCO_3^- and CO_3^{2-} that would also boost the ionic strength of soil solution (Hartmann et al., 2013). Different authors have seen that near neutral pH conditions can be reached after basalt application on acidic

soils (Anda et al., 2015) and significant positive effects is observed for basic rocks being deployed (Fig. 18). This would make, as for biochar discussed above, macro- (e.g., Mg, Ca, K, P, and S), and micronutrients (e.g., B, Mo, Cu, Fe, Mn, Zn, Ni) available for plant nutrition (Brady, 1984).

The weathering process of primary minerals result in the genesis of clay and hydrous-oxides minerals (Wilson, 2004). Clay and hydrous-oxides minerals have the potential to adsorb organic matter onto their surfaces, which will stabilize organic matter (Saidy et al., 2012; Wiseman and Püttmann, 2006). The bound organic matter can potentially influence the CEC of soils (Seaman and Roberts, 2012) since the CEC of soil organic matter is greater than that of clay minerals (Parfitt et al., 1995). However, further research on the potential of EW on soil organic matter stabilization and how biomass response is affected by it is necessary to quantify the impact of EW on soil carbon sequestration and climate change.

Rock powder application significantly increased the biomass yield for the different soil textures (Fig. 17, Appendix H Table S11). However, the dry total plant and dry shoot mass response is positive only for applying rock powder to coarse textured soils. *Hevea brasiliensis* (rubber tree) planted in a fine (clay) soil had a negative plant response compared to control after applying 5 – 20 t basalt ha⁻¹ (grain size < 0.01 mm); nevertheless, increasing the application to 30 t basalt ha⁻¹ raised the dry total plant and dry shoot mass (Bakri et al., 2017). Maize and Wheat planted in a coarse (sand) soil also registered a decline in plant properties after granite application (grain size < 2 mm), but they increased for experiments with added fertilizers (Bamberg et al., 2013; Bolland and Baker, 2000). Therefore, in our case, the decrease in plant response for the three different crops are probably related to low nutrient release of added rock powder (Fig. 17) rather than changes in the drainage condition of soils. However, experiments are necessary to properly understand the effects on biomass growth influenced by changes in nutrient availability and drainage condition of soils.

4.5.3. Potential benefits for biochar and EW coapplication

A portfolio of NETs, rather than a single technology, is indicated to minimize unwanted effects on ecosystems (Fuss, 2017; Fuss et al., 2018). Since the land-based NETs share the same environmental compartment, coapplication of these NETs can result in benefits (Amann and Hartmann, 2019; Beerling et al., 2018). EW can potentially supply nutrients for afforestation or reforestation (AR) and grass like miscanthus for bioenergy with carbon capture and storage (BECCS) reducing or even replacing the use of industrial fertilizers in some cases (Garcia et al., 2020). Applying biochar and EW in combination might result in synergetic effects for both technologies but now neither laboratory nor field experiments have focused on these potentials.

Positive effects of EW on exchangeable K and available P are more persistent than the effects on soil CEC and pH (Fig. 18). While for biochar, there is a tendency of decreasing positive effects on plant growth with time, which demands repeated application with lower annual dosages over the years to sustain a constant plant growth (Fig. 15 and Fig. 16). Positive yield effects due to rock powder application increase with time (Fig. 17). Therefore, coapplication of EW and biochar may be advantageous for plant effects and soil properties either applied with one singular dose or applied repeatedly with cumulative effects since the observed long-term effect of EW may positively contribute to biochar and the short-term effect of biochar may positively contribute to EW.

Biochar was shown to stabilize and increase soil organic carbon over the long-term (Blanco-Canqui et al., 2019; Weng et al., 2017) while EW accumulates atmospheric carbon through (bi)carbonate formation equally over the long-term (Beerling et al., 2018; Hartmann et al., 2013). The CDR potential of both application methods is thus increasing over time and it is likely that their coapplication mutually enhances the two different CDR-effects. As biochar improves soil aeration and water holding capacity (WHC; Quin et al., 2014) it will certainly foster the

weathering of the applied minerals via soil moisture improvement and related increase in soil-pCO₂ if within the favorable range (Romero-Mujalli et al., 2018). Also, biochar increases soil microbial activity (Zhou et al., 2017), which could further enhance the weathering of rock powder. Specifically, biochar can promote lithotrophic microbial metabolisms by serving as an electron shuttle between microbes and solid minerals (Kappler et al., 2014). EW delivers macro- and micronutrients necessary for the formation of soil organic matter (SOM). Systematic trials with different soils and coapplication of different biochars and rock powders at different rates are necessary to reveal the underlying mechanisms. This should include microcosm studies on the interaction of biochar, rock powder, and microorganisms.

EW is more effective to increase the yield of plants, while biochar could affect more other plant and soil properties (cp. summary from Fig. 15 with Fig. 17 and the values from Appendix H Table S9 with Table S11). EW's positive effects on soil pH, and available P were higher than that of biochar while biochar could increase CEC, and soil exchangeable K more than EW (cp. summary from Fig. 16 with Fig. 18 and the values from Appendix H Table S10 with Table S12) and additionally built up SOM. Therefore, this indicates that coapplication of both NETs may magnify the already observed positive effects of each NET on soil and plant properties. However, laboratory and field trials are necessary to check this hypothesis and to properly estimate the boundaries of the system (i.e., application ratios of biochar and EW, the application rates of the mixture, changes in nutrient fluxes, water percolation through soil profile, and plant-available water). Additionally, laboratory and field trials on coapplication of EW and biochar would allow to improve the comprehension on which application technic is the most adequate for a specific application scale and location (e.g., first applying biochar and later on EW or vice versa; singular or repeated coapplication of EW and biochar; combining biochar and rock powder as composting additive or bedding material in animal farming, and co-pyrolysis of biomass and rock powder).

Rock powder and other amendments can be used for enhancing biochar with nutrients (Kammann et al., 2015; Ye et al., 2016) and biochar enhancement could be done by composting it with animal manures and rock powder. Ye et al. (2016) torrefied the mixture of biochar, animal manure, and basalt powder at temperatures of 220°C for 3 h while Kammann et al. (2015) composted biochar with animal manures and rock powder for six weeks with thermophilic phase reaching temperatures of 60–70 °C. In both methods, the high temperatures might have favored the release of nutrients from rock powder since temperature is one of the mechanisms controlling weathering rates. Besides the use of rock powder as a source of nutrients for enhancing biochars, weathering rates might get enhanced (Arcand and Schneider, 2006) due to positive impacts of biochar on arbuscular mycorrhizas (Vanek and Lehmann, 2015) in cases that biochar is firstly deployed and EW is used as a source of macro- and micronutrients to re-load the already deployed biochar.

Carvalho (2012) found that the trace elements (Cd, Cr, Pb, and Ni) content in soil did not increase after applying different rocks and that the soil trace elements content remained well below the thresholds for non-contaminated soils. de Souza et al. (2013b) found no negative effects of rock powder on earthworm growth. Even if the risk of trace elements availability after rock powder application is low, biochar can immobilize trace elements in soils (Chen et al., 2018) and be co-deployed with rock powder as a protective measure to avoid its potential release (Amann and Hartmann, 2019). Another potential co-benefit of applying both terrestrial negative emission technologies may be the stabilization of biochar. Rock powder dissolution results in genesis of clay minerals like kaolinite, and of iron and or aluminum hydrous-oxides (Wilson, 2004), which can stabilize biochar by avoiding oxidation and biological degradation (Yang et al., 2018; Yang et al., 2016). However, further research is necessary to quantify to which extent the genesis of clay minerals due to weathering of primary minerals, to extra input of

ions (Mg^{2+} , Ca^{2+} , K^+ , SiO_4^{4-} , Al^{3+} , etc.), and to changes of soil hydraulic properties can contribute to the stabilization of soil organic matter and biochar.

4.5.4. Guidelines for biochar and EW experiments

Soils temporal and spatial heterogeneity is high and homogeneous environments rarely exist in nature (Hutchings et al., 2003). The heterogeneity of biochar and rock powder is high as well, especially concerning the physico-chemical properties of them. To reach the Paris climate agreement targets, early and moderate application of NET for CDR should be considered (Obersteiner et al., 2018), increasing the research on NET. Therefore, this study can be updated and enhanced periodically in the upcoming years. Reporting all the data in tabular format as a supplementary file, rather than only in figures, would significantly contribute to further systematic reviews.

Detailed reports of experimental setup and conditions together with consistent data description will be necessary. Reporting the mean, standard deviations or standard errors, *p-tests*, together with sample number of all treatments and control experiments for measured soil (pH, CEC, exchangeable K, and available P) and plant properties (dry total plant and dry shoot mass, main stem diameter, plant height, and yield) would considerably improve future systematic reviews. Besides that, reporting normality tests or some other statistical parameter to know the output distribution (e.g., kurtosis, skewness, and minimum and maximum values for variability and median, and mode for central tendency) would allow to determine if the data set is well modeled by a normal distribution.

Additional information on soil bulk density, porosity, surface area, soil hydraulic conductivity, plant-available water, soil aggregate stability, microbial activity, release and mobility of trace elements and PAHs, macro- (e.g., Mg, Ca, K, P, and S), and micronutrients (e.g., B, Mo, Cu, Fe, Mn, Zn, Ni) stocks before and after biochar and or enhanced silicate rock weathering application, and long-term experiments (≥ 5 years) would considerably contribute to fully understand the effects of these NETs on soil ecosystem and biomass growth. Also, rock powder and biochar need to be analysed properly, for the latter we strongly recommend analysis according to the guidelines of the European Biochar Certificate (EBC, 2012).

During our analysis, an important observation was that sometimes different rock powders or biochar shared the same experimental factor (e.g. for experiments with running times of up to three months biochar with different pyrolysis temperatures and different feedstocks were selected or different rock chemistry (basic and acidic) for a specific grain size were selected) resulting in an under- or overestimation of the effects after biochar or rock powder application. A potential solution for this is to perform experiments with a cascade or matrix configuration either for EW or biochar (e.g., for EW use basic rocks ground in different grain sizes, application rates, for each soil texture, rather than perform experiments with acid rocks and so on) to test all potential combinations for experimental setups.

4.6. Conclusions

Different studies have individually shown the effects of applying rock powder or biochar to plant and soil properties under specific experimental setups and climate regimes. However, an investigation on the effects of applying EW or biochar accounting for specific or more generalized setups for a range of climatic zones, from temperate to tropical and subtropical environments was missing. For the first time in the literature, the potential effects of biochar and EW on soil and plant properties were compared, either for specific variables that control the plant and soil response or for a more general configuration.

This systematic review shows that each selected experimental factor has different influence on each of the investigated soil or plant property after biochar or EW application, highlighting the complexity of mechanisms

governing the response of a selected soil or plant properties. Therefore, a general application setup to optimize plant and soil responses for any scale and location is unlikely to exist.

Generally, positive effects of EW on yield were higher, while biochar could effectively contribute more to the dry total plant and dry shoot mass, main stem diameter, and plant height. EW positive effects on soil pH, and available P were higher than that of biochar while biochar could increase CEC and soil exchangeable K more than EW. Thus, EW and biochar coapplication may have complementary effects. Additionally, EW changes to soil and plant properties tend to be greater in the long-term (three years) than the plant growth enhancing effects of biochar, which had stronger short-term (up to six months) effects. The biochar-induced promotion of soil microbial activity might have synergetic effect on EW. Therefore, coapplication of EW and biochar may reestablish the short- and long-term soil nutrient pools and can be a solution to the cases that the plant nutrient requirement rates surpasses the nutrient release rates of rock powder.

The different experimental factors used in this review could be adapted to meet the nutritional needs of local soil and specific plant species. The combined application of EW and biochar have the potential to be used as soil ameliorant for AR and for plantations for bioenergy or crop production, while in addition optimizing or partly replacing the use of industrial fertilizers (Amann & Hartmann, 2019). This would be necessary especially in cases where soil and atmospheric nutrient supply cannot cope with biomass nutrient requirements (Garcia et al., 2018; Garcia et al., 2020).

The longevity and the magnitude of effects on soil and plant properties due to biochar or EW application at a specific area cannot be predicted by this work. Experiments taking five years or more either at laboratory or field scale are necessary to evaluate the sustainability of effects on selected soil and plant properties after EW and biochar application. Laboratory or field research on coapplication of EW and biochar as NET and the related changes in soil and plant properties were so far not identified. Since it is unlikely that a single NET will sustainably contribute to reach Paris agreement goals to limit temperature rise at the end of this century (Amann and Hartmann, 2019; Beerling et al., 2018; Minx et al., 2018), further research should focus on effects of coapplication of EW and biochar on plant and soil properties. To anticipate side-effects and for a more sustainable biochar and EW implementation policy at any location and scale, a more complete understanding of the different mechanisms governing soil, ecological, and biological functions is important.

5. Synthesis

Integrated assessment models only consider the individual and large-scale deployment of NET, which impacts landscape configuration, water and nutrient cycles. Thus, to reach a long-term and sustainable CDR, the potential synergies between different NETs needed to be assessed. In this thesis, the potential coapplication of enhanced silicate rock weathering with other terrestrial NETs was examined with regard to probable effects on soil nutrient pools, soil physical and chemical properties, and plant response. Therefore, different databases and numerical model outputs were used to evaluate geogenic nutrient budgets of forests and the nutrient export by harvest rates. Once the preliminary evaluation was concluded, projections of EW deployment to resupply exported nutrients or to close potential negative nutrient budgets and its effects on soil and plant properties and potential CDR were assessed.

In chapter 2 of the thesis, the potential geogenic nutrient supply was estimated and compared to the projected nutrient export by different harvest rates of U.S. timberland forests. As an attempt to decrease net carbon dioxide emissions (Kazagic et al., 2016), intensive harvest rates of forest biomass may be necessary for bioenergy generation (Lauri et al., 2014). However, only a few studies have investigated the effects of nutrient limitations in biomass production for future bioenergy demand. Thus, it was hypothesized that nutrient export by harvest will not be compensated by atmospheric deposition and mineral weathering supply (i.e., geogenic nutrient supply). Either for spatially explicit nutrient budgets considering actual harvest rates or for projected nutrient export boosted by intensive harvesting to meet a future bioenergy demand, this new analysis revealed that the harvest nutrient export exceeded geogenic nutrient supply for most of U.S. timberland areas. Overall, the projected nutrient limitation within U.S. timberland forests depended on the spatial correlation between the lithological composition, climate, and weathering rates, but it followed the order $P > K > Ca > Mg$.

It was concluded that the limiting kinetics in geogenic nutrient supply was the cause of the estimated negative nutrient budgets for projected and spatially explicit harvest rates. Consequently, the expected biomass growth rates for an intensive harvest scenario may be restrained. Thus, chapter 2 highlights that negative nutrient budgets can be avoided by providing an external source of nutrients (e.g., natural rock products) and other sustainable forest managements. Therefore, the new analysis presented in chapter 2 can be used to guide future forest management practices in U.S. timberland forests. However, proper knowledge on spatially explicit limitations on forest biomass growth rates is still missing at global scale, as well as the biomass amount produced by closing nutritional gaps.

The use of ground rocks as EW to actively sequester atmospheric carbon dioxide, supply nutrients for biomass production, and the related effects to soil hydrology were evaluated in chapter 3 by using the output from well established numerical models, different databases, and by pedotransfer functions. Based on the findings of chapter 2, P is the main nutrient limiting U.S. timberland forests regrowth and it is a limiting nutrient in a wide range of ecosystems (Elser et al., 2007). However, geogenic P supply is a factor rarely included in climate afforestation- reforestation models. Thus, the potential reduction in projected carbon dioxide removal by forests was studied by performing a global P budget for an N-stock-based P demand from different AR scenarios. The AR scenarios accounted for natural N supply and for N fertilization. If N is not limiting the biomass production, P limitation can cause an average C reduction of 19 – 47 % for an optimistic and a conservative geogenic P supply scenario, respectively. This can potentially lead to considerable divergences between predictions of carbon sequestration estimated by climate AR models and real carbon sequestration by AR practices.

To reach climate targets, constant harvest rates of bioenergy grass are going to be necessary over the years for bioenergy generation. Thus, a sustainable bioenergy grass plantation is possible only if the nutrients exported by

harvest are replenished, otherwise a decrease in harvest rate is expected. The new findings suggest that when compared to other rocks, basalt powder is more efficient to replace or reduce the use of industrial fertilizers either for AR or for bioenergy grasses for BECCS. This is because of the higher chemical P content, the relative fast weathering rate, and the equilibrated supply of Ca, K, and Mg of basalt powder.

Assessing the effects of large-scale deployment of basalt powder to topsoil hydrology reveal that plant-available water can be enhanced. The texture of deployed rock powder not only affect the nutrient fluxes, but it will also influence the impacts on soil hydrology together with the initial soil texture. Soil texture is unlikely to be changed through agronomic practices (Sullivan, 2000). However, it could be demonstrated by this thesis that deploying EW into topsoils may change the hydraulic properties, especially at the rooting zone (~30 cm depth). This is an important characteristic of EW not explored before, since under a future scenario of climate change, EW can potentially mitigate or alleviate drought effects to a certain extent within areas used for AR or bioenergy plantation. Furthermore, it was seen in chapter 3 that a general picture of potential effects of combining terrestrial NETs, derived from already published individual data is necessary. Thus, to better assess the global potential of combining terrestrial NETs with EW, the related physical, chemical, and physico-chemical changes of soil influenced by different EW deployment rates should be considered in such reviews.

Hence, the effects of rock powder or biochar deployment on plant and soil properties were discussed in chapter 4 by a systematic review. After the selection criteria, 63 and 26 peer-reviewed articles were usable for biochar and EW, respectively. The selected studies covered a range of edaphoclimatic conditions. Each of these studies could successfully show the effects of applying rock powder or biochar to plant and soil properties under specific experimental setups and climate regimes. However, the new results in chapter 4 allowed for generalized effects on soil and plant properties after deploying EW or biochar. For the first time, the potential effects of biochar and EW on soil and plant properties were compared, either for a more simplified configuration or for specific experimental factors (i.e., deployment rates, soil texture, experiment duration, field or laboratory experiment, etc.) that control the plant and soil response.

The new quantitative analysis revealed that different mechanisms influencing the plant and soil response either after biochar or EW deployment are complex. Therefore, a general deployment setup to optimize plant and soil response for any scale and location is unlikely to exist. However, the different experimental factors discussed in chapter 4 could be adapted to meet the nutritional needs of local soil and specific plant species. This potential of EW and biochar was suggested by different authors (Amann and Hartmann, 2019); nonetheless, in chapter 4, the effects on soil and plant properties after deploying EW or biochar are quantitatively shown. Moreover, once EW is deployed, weathering of pristine minerals starts and the genesis of clay minerals and iron hydrous-oxides may occur (Wilson, 2004), which has the potential to stabilize soil organic matter (Saidy et al., 2012) or biochar (Yang et al., 2018; Yang et al., 2016).

In general, the new results reveal that applying EW caused higher yields of plants, greater positive effects on soil pH, and available P than after deploying biochar. The findings also show that after deploying biochar, a greater increase in dry total plant and dry shoot mass, main stem diameter, plant height, cation exchange capacity, and soil exchangeable K than after deploying EW occurred. However, negative effects cannot be ruled out. Furthermore, it was seen that EW changes to soil and plant properties tend to be greater in the long-term (40 months) than the effects of biochar, which had greater short-term (up to six months) effects. This new finding is an important characteristic suggesting that co-deployment of biochar and EW do not compete and will enhance the short- and long-term soil nutrient pools. Therefore, the combined application of EW and biochar have the potential to be used

as soil ameliorant for AR and for plantations for bioenergy or crops for food production, while in addition optimizing or replacing in part the use of industrial fertilizers. Nonetheless, co-deployment of EW and biochar has been less explored even though it may optimize the plant nutrient availability of both technologies.

This thesis shows that additionally to the carbon dioxide removal potential, EW acts as a long-term balanced nutrient source for AR, bioenergy grass plantations for BECCS, or for agricultural plantations. Therefore, it enhances the comprehension on potential synergies of coapplication of EW with these NETs. Furthermore, it was identified the potential of EW to stabilize soil organic matter and as a long-term nutrient source for coapplication techniques with biochar. However, only a few authors have focused on these potentials. For that reason, future laboratory or field studies have to be developed as suggested in chapter 4. They need to focus on the effects of EW and biochar coapplication on plants and soil properties, quantify the capacity of soil organic matter stabilization by EW and its consequent effects to soil carbon sequestration and to global climate. Additionally, the effects of EW and biochar coapplication on soil microorganisms and microbial activity have to be studied since different authors identified positive effects either after EW or biochar application to soil.

6. Bibliography

- 14688-1:2002, I., 2002. 14688-1: 2002: Geotechnical investigation and testing–Identification and classification of soil–Part 1: Identification and description. International Organization for Standardization, Geneva.
- Abbas, F. et al., 2017. Agroforestry: a sustainable environmental practice for carbon sequestration under the climate change scenarios—a review. *Environmental Science and Pollution Research*, 24(12): 11177-11191.
- Abdel-Shafy, H.I., Mansour, M.S.M., 2016. A review on polycyclic aromatic hydrocarbons: Source, environmental impact, effect on human health and remediation. *Egyptian Journal of Petroleum*, 25(1): 107-123.
- Abujabhah, I.S., Bound, S.A., Doyle, R., Bowman, J.P., 2016. Effects of biochar and compost amendments on soil physico-chemical properties and the total community within a temperate agricultural soil. *Applied Soil Ecology*, 98: 243-253.
- Achat, D.L., Augusto, L., Gallet-Budynek, A., Loustau, D., 2016. Future challenges in coupled C–N–P cycle models for terrestrial ecosystems under global change: a review. *Biogeochemistry*, 131(1): 173-202.
- Achat, D.L., Fortin, M., Landmann, G., Ringeval, B., Augusto, L., 2015. Forest soil carbon is threatened by intensive biomass harvesting. *Sci Rep*, 5: 15991.
- Agbna, G.H.D. et al., 2017. Effects of deficit irrigation and biochar addition on the growth, yield, and quality of tomato. *Scientia Horticulturae*, 222: 90-101.
- Agegnehu, G., Bass, A.M., Nelson, P.N., Bird, M.I., 2016a. Benefits of biochar, compost and biochar–compost for soil quality, maize yield and greenhouse gas emissions in a tropical agricultural soil. *Science of The Total Environment*, 543: 295-306.
- Agegnehu, G. et al., 2015a. Biochar and biochar-compost as soil amendments: Effects on peanut yield, soil properties and greenhouse gas emissions in tropical North Queensland, Australia. *Agriculture, Ecosystems & Environment*, 213: 72-85.
- Agegnehu, G., Bird, M.I., Nelson, P.N., Bass, A.M., 2015b. The ameliorating effects of biochar and compost on soil quality and plant growth on a Ferralsol. *Soil Research*, 53(1): 1-12.
- Agegnehu, G., Nelson, P.N., Bird, M.I., 2016b. The effects of biochar, compost and their mixture and nitrogen fertilizer on yield and nitrogen use efficiency of barley grown on a Nitisol in the highlands of Ethiopia. *Science of The Total Environment*, 569-570: 869-879.
- Allen, R.L., 1846. A brief compend of American agriculture. Saxton & Miles.
- Amann, T., Hartmann, J., 2019. Ideas and perspectives: Synergies from co-deployment of negative emission technologies. *Biogeosciences*, 16(15): 2949-2960.
- Ameloot, N., Graber, E.R., Verheijen, F.G.A., De Neve, S., 2013. Interactions between biochar stability and soil organisms: review and research needs. *European Journal of Soil Science*, 64(4): 379-390.
- Amendola, C. et al., 2017. Short-term effects of biochar on grapevine fine root dynamics and arbuscular mycorrhizae production. *Agriculture, Ecosystems & Environment*, 239: 236-245.
- Amiotte Suchet, P., Probst, J.L., Ludwig, W., 2003. Worldwide distribution of continental rock lithology: Implications for the atmospheric/soil CO₂ uptake by continental weathering and alkalinity river transport to the oceans. *Global Biogeochemical Cycles*, 17(2).
- Amoakwah, E., Frimpong, K.A., Arthur, E., 2017. Corn Cob Biochar Improves Aggregate Characteristics of a Tropical Sandy Loam. *Soil Science Society of America Journal*, 81(5): 1054-1063.
- Ampelli, C., Perathoner, S., Centi, G., 2015. CO₂ utilization: an enabling element to move to a resource- and energy-efficient chemical and fuel production. *Philosophical Transactions of the Royal Society A: Mathematical, Physical and Engineering Sciences*, 373(2037): 2037.
- Anda, M., Shamshuddin, J., Fauziah, C.I., 2013. Increasing negative charge and nutrient contents of a highly weathered soil using basalt and rice husk to promote cocoa growth under field conditions. *Soil & Tillage Research*, 132: 1-11.
- Anda, M., Shamshuddin, J., Fauziah, C.I., 2015. Improving chemical properties of a highly weathered soil using finely ground basalt rocks. *Catena*, 124: 147-161.
- Anda, M., Shamshuddin, J., Fauziah, C.I., Omar, S.R.S., 2009. Dissolution of Ground Basalt and Its Effect on Oxisol Chemical Properties and Cocoa Growth. *Soil Science*, 174(5): 264-271.
- Anderson, K., Peters, G., 2016. The trouble with negative emissions. *Science*, 354(6309): 182-183.
- Appelo, C.A.J., Postma, D., 2005. *Geochemistry, Groundwater and Pollution*, Second Edition. CRC Press.
- Arcand, M.M., Schneider, K.D., 2006. Plant- and microbial-based mechanisms to improve the agronomic effectiveness of phosphate rock: a review. *Anais da Academia Brasileira de Ciências*, 78: 791-807.
- Arif, M. et al., 2017. Biochar improves phosphorus use efficiency of organic-inorganic fertilizers, maize-wheat productivity and soil quality in a low fertility alkaline soil. *Field Crops Research*, 214: 25-37.
- Arshad, M., St. Arnaud, R., Huang, P., 1972. Dissolution of trioctahedral layer silicates by ammonium oxalate, sodium dithionite–citrate–bicarbonate, and potassium pyrophosphate. *Canadian Journal of Soil Science*, 52(1): 19-26.

- Aslyng, H., 1976. Klima, jord og planter. *Kulturteknik I*, 5: 368.
- Athar, R., Ahmad, M., 2002. Heavy Metal Toxicity: Effect on Plant Growth and Metal Uptake by Wheat, and on Free Living Azotobacter. *Water, Air, and Soil Pollution*, 138(1): 165-180.
- Augusto, L., Achat, D.L., Jonard, M., Vidal, D., Ringeval, B., 2017. Soil parent material-A major driver of plant nutrient limitations in terrestrial ecosystems. *Global Change Biol*, 23: 3808-3824.
- Augusto, L., Bakker, M.R., Meredieu, C., 2008. Wood ash applications to temperate forest ecosystems—potential benefits and drawbacks. *Plant and Soil*, 306(1-2): 181-198.
- Backer, R.G.M., Schwinghamer, T.D., Whalen, J.K., Seguin, P., Smith, D.L., 2016. Crop yield and SOC responses to biochar application were dependent on soil texture and crop type in southern Quebec, Canada. *Journal of Plant Nutrition and Soil Science*, 179(3): 399-408.
- Bakken, A.K., Gautneb, H., Myhr, K., 1997. Plant available potassium in rocks and mine tailings with biotite, nepheline and K-feldspar as K-bearing minerals. *Acta Agriculturae Scandinavica, Section B — Soil & Plant Science*, 47(3): 129-134.
- Bakri, A., Mokhatar, S.J., Daud, N.W., 2017. Physiological and morphological responses of rubber (*hevea brasiliensis*) rrim 3001 to different rates of basalt application. *J. Trop. Plant Physiol*, 9: 24-35.
- Bamberg, A.L. et al., 2013. Desempenho agrônômico de fontes minerais e orgânicas de nutrientes para as culturas de milho e trigo, II Congresso Brasileiro de Rochagem, pp. 24.
- Bamminger, C. et al., 2016. Short-term response of soil microorganisms to biochar addition in a temperate agroecosystem under soil warming. *Agriculture, Ecosystems & Environment*, 233: 308-317.
- Bandara, T. et al., 2017. Efficacy of woody biomass and biochar for alleviating heavy metal bioavailability in serpentine soil. *Environmental Geochemistry and Health*, 39(2): 391-401.
- Bass, A.M., Bird, M.I., Kay, G., Muirhead, B., 2016. Soil properties, greenhouse gas emissions and crop yield under compost, biochar and co-composted biochar in two tropical agronomic systems. *Science of The Total Environment*, 550: 459-470.
- Batjes, N., 2005. ISRIC-WISE global data set of derived soil properties on a 0.5 by 0.5 degree grid (version 3.0), ISRIC – World Soil Information.
- Bear, J., 1972. Dynamics of fluids in porous media. American Elsevier., New York.
- Beech, E., Rivers, M., Oldfield, S., Smith, P., 2017. GlobalTreeSearch: The first complete global database of tree species and country distributions. *Journal of Sustainable Forestry*, 36(5): 454-489.
- Beerling, D.J. et al., 2018. Farming with crops and rocks to address global climate, food and soil security. *Nature Plants*, 4(3): 138-147.
- Bennett, P.C., Rogers, J.R., Choi, W.J., Hiebert, F.K., 2001. Silicates, Silicate Weathering, and Microbial Ecology. *Geomicrobiology Journal*, 18(1): 3-19.
- Beringer, T., Lucht, W., Schaphoff, S., 2011. Bioenergy production potential of global biomass plantations under environmental and agricultural constraints. *Global Change Biology Bioenergy*, 3(4): 299-312.
- Berner, A.R., Lasaga, A.C., Garrels, R.M., 1983. The carbonate-silicate geochemical cycle and its effect on atmospheric carbon dioxide over the past 100 million years. *Am J Sci*, 283: 641-683.
- Berner, R.A., 1997. The Rise of Plants and Their Effect on Weathering and Atmospheric CO₂. *Science*, 276(5312): 544-546.
- Betts, R.A., 2000. Offset of the potential carbon sink from boreal forestation by decreases in surface albedo. *Nature*, 408(6809): 187-190.
- Betts, R.A., Falloon, P.D., Goldewijk, K.K., Ramankutty, N., 2007. Biogeophysical effects of land use on climate: Model simulations of radiative forcing and large-scale temperature change. *Agricultural and Forest Meteorology*, 142(2): 216-233.
- Beyer, W., 1964. Zur bestimmung der wasserdurchlässigkeit von kiesen und sanden aus der kornverteilungskurve. *WWT*, 14(6): 165-168.
- Bird, M.I., Wurster, C.M., de Paula Silva, P.H., Bass, A.M., De Nys, R., 2011. Algal biochar—production and properties. *Bioresource technology*, 102(2): 1886-1891.
- Bissonnais, Y.L., Singer, M.J., 1992. Crusting, Runoff, and Erosion Response to Soil Water Content and Successive Rainfalls. *Soil Science Society of America Journal*, 56(6): 1898-1903.
- Blanco-Canqui, H., Laird, D., Heaton, E., Rathke, S., Sharma Acharya, B., 2019. Soil carbon increased by twice the amount of biochar carbon applied after six years: Field evidence of negative priming. *GCB Bioenergy*.
- Boateng, A.A., Garcia-Perez, M., Mašek, O.e., Brown, R., del Campo, B., 2015. Biochar production technology, Biochar for environmental management. Routledge, pp. 95-120.
- Bodirsky, B.L. et al., 2012. N₂O emissions from the global agricultural nitrogen cycle – current state and future scenarios. *Biogeosciences*, 9(10): 4169-4197.
- Boersma, M., Wrobel-Tobiszewska, A., Murphy, L., Eyles, A., 2017. Impact of biochar application on the productivity of a temperate vegetable cropping system. *New Zealand Journal of Crop and Horticultural Science*, 45(4): 277-288.
- Bolland, M.D.A., Baker, M.J., 2000. Powdered granite is not an effective fertilizer for clover and wheat in sandy soils from Western Australia. *Nutrient Cycling in Agroecosystems*, 56(1): 59-68.

- Bondeau, A. et al., 2007. Modelling the role of agriculture for the 20th century global terrestrial carbon balance. *Global Change Biology*, 13(3): 679-706.
- Bonsch, M. et al., 2016. Trade-offs between land and water requirements for large-scale bioenergy production. *Global Change Biology Bioenergy*, 8(1): 11-24.
- Borchard, N. et al., 2019. Biochar, soil and land-use interactions that reduce nitrate leaching and N₂O emissions: A meta-analysis. *Science of The Total Environment*, 651: 2354-2364.
- Borenstein, M., Hedges, L.V., Higgins, J.P., Rothstein, H.R., 2010. A basic introduction to fixed-effect and random-effects models for meta-analysis. *Research synthesis methods*, 1(2): 97-111.
- Borenstein, M., Hedges, L.V., Higgins, J.P., Rothstein, H.R., 2011. *Introduction to meta-analysis*. John Wiley & Sons.
- Börker, J., Hartmann, J., Romero-Mujalli, G., Li, G., 2019. Aging of basalt volcanic systems and decreasing CO₂ consumption by weathering. *Earth Surf. Dynam.*, 7(1): 191-197.
- Bowen, M.E., McAlpine, C.A., House, A.P.N., Smith, G.C., 2007. Regrowth forests on abandoned agricultural land: A review of their habitat values for recovering forest fauna. *Biological Conservation*, 140(3): 273-296.
- Boysen, L.R., Lucht, W., Gerten, D., 2017a. Trade-offs for food production, nature conservation and climate limit the terrestrial carbon dioxide removal potential. *Global Change Biology*, 23(10): 4303-4317.
- Boysen, L.R. et al., 2017b. The limits to global-warming mitigation by terrestrial carbon removal. *Earth's Future*, 5(5): 463-474.
- Brady, N.C., 1984. *The nature and properties of soils*, 9. Macmillan, NY.
- Brannvall, E., Wolters, M., Sjoblom, R., Kumpiene, J., 2015. Elements availability in soil fertilized with pelletized fly ash and biosolids. *J Environ Manage*, 159: 27-36.
- Bruun, E.W., Petersen, C.T., Hansen, E., Holm, J.K., Hauggaard-Nielsen, H., 2014. Biochar amendment to coarse sandy subsoil improves root growth and increases water retention. *Soil Use and Management*, 30(1): 109-118.
- Cadoux, S., Riche, A.B., Yates, N.E., Machet, J.-M., 2012. Nutrient requirements of *Miscanthus x giganteus*: Conclusions from a review of published studies. *Biomass and Bioenergy*, 38: 14-22.
- Calabrese, S., Porporato, A., Parolari, A.J., 2017. Hydrologic transport of dissolved inorganic carbon and its control on chemical weathering. *Journal of Geophysical Research: Earth Surface*, 122(10): 2016-2032.
- Cánovas, C.R. et al., 2019. Mineral reactivity in sulphide mine wastes: influence of mineralogy and grain size on metal release. *European Journal of Mineralogy*, 31(2): 263-273.
- Cao, L., Caldeira, K., 2010. Atmospheric carbon dioxide removal: long-term consequences and commitment. *Environmental Research Letters*, 5(2): 024011.
- Carrier, W.D.I., 2003. Goodbye, hazen; hello, kozeny-carman. *Journal of geotechnical and geoenvironmental engineering*, 129(11): 1054-1056.
- Carvalho, A.M.X.d., 2012. Rochagem e suas interações no ambiente solo: contribuições para aplicação em agroecossistemas sob manejo agroecológico. 2012. 116p, Tese (Doutorado)-Curso de Solos e Nutrição de Plantas, Universidade Federal ...
- Casey, W.H., Bunker, B., 1990. Leaching of minerals and glass surface during dissolution. *Mineral-water interface geochemistry*: 397-426.
- Castaldi, S. et al., 2011. Impact of biochar application to a Mediterranean wheat crop on soil microbial activity and greenhouse gas fluxes. *Chemosphere*, 85(9): 1464-1471.
- Chan, K.Y., Van Zwieten, L., Meszaros, I., Downie, A., Joseph, S., 2007. Agronomic values of greenwaste biochar as a soil amendment. *Soil Research*, 45(8): 629-634.
- Chan, K.Y., Van Zwieten, L., Meszaros, I., Downie, A., Joseph, S., 2008. Using poultry litter biochars as soil amendments. *Soil Research*, 46(5): 437-444.
- Change, I.P.o.C., 2014. *Climate Change 2013 – The Physical Science Basis: Working Group I Contribution to the Fifth Assessment Report of the Intergovernmental Panel on Climate Change*. Cambridge University Press, Cambridge.
- Changxun, G., Zhiyong, P., Shu'ang, P., 2016. Effect of biochar on the growth of *Poncirus trifoliata* (L.) Raf. seedlings in Gannan acidic red soil. *Soil Science and Plant Nutrition*, 62(2): 194-200.
- Chen, D. et al., 2018. Effects of biochar on availability and plant uptake of heavy metals – A meta-analysis. *Journal of Environmental Management*, 222: 76-85.
- Chen, J. et al., 2016. Change in active microbial community structure, abundance and carbon cycling in an acid rice paddy soil with the addition of biochar. *European Journal of Soil Science*, 67(6): 857-867.
- Chen, Y., Shinogi, Y., Taira, M., 2010. Influence of biochar use on sugarcane growth, soil parameters, and groundwater quality. *Soil Research*, 48(7): 526-530.
- Cheng, C.-H., Lehmann, J., Thies, J.E., Burton, S.D., Engelhard, M.H., 2006. Oxidation of black carbon by biotic and abiotic processes. *Organic Geochemistry*, 37(11): 1477-1488.
- Chesworth, W., van Straaten, P., Semoka, J.M.R., 1989. *Agrogeology in East Africa: the Tanzania-Canada project*. *Journal of African Earth Sciences (and the Middle East)*, 9(2): 357-362.

- Chintala, R., Mollinedo, J., Schumacher, T.E., Malo, D.D., Julson, J.L., 2014. Effect of biochar on chemical properties of acidic soil. *Archives of Agronomy and Soil Science*, 60(3): 393-404.
- Christman, Z.J., Rogan, J., 2012. Error Propagation in Raster Data Integration. *Photogrammetric Engineering & Remote Sensing*, 78(6): 617-624.
- Christophel, D., Spengler, S., Schmidt, B., Ewald, J., Prietzel, J., 2013. Customary selective harvesting has considerably decreased organic carbon and nitrogen stocks in forest soils of the Bavarian Limestone Alps. *Forest Ecology and Management*, 305: 167-176.
- Ciceri, D., de Oliveira, M., Stokes, R.M., Skorina, T., Allanore, A., 2017. Characterization of potassium agrominerals: Correlations between petrographic features, comminution and leaching of ultrapotassic syenites. *Minerals Engineering*, 102: 42-57.
- Clarkson, D.T., Hanson, J.B., 1980. The Mineral Nutrition of Higher Plants. *Annual Review of Plant Physiology*, 31(1): 239-298.
- Cornelissen, G. et al., 2013. Biochar effect on maize yield and soil characteristics in five conservation farming sites in Zambia. *Agronomy*, 3(2): 256-274.
- Cornelissen, G. et al., 2016. Emissions and char quality of flame-Curtain" Kon Tiki" kilns for farmer-scale charcoal/biochar production. *PloS one*, 11(5).
- Cornelissen, S., Koper, M., Deng, Y.Y., 2012. The role of bioenergy in a fully sustainable global energy system. *Biomass and Bioenergy*, 41: 21-33.
- Coroneos, C., Hinsinger, P., Gilkes, R.J., 1996. Granite powder as a source of potassium for plants: a glasshouse bioassay comparing two pasture species. *Fertilizer research*, 45(2): 143-152.
- Council, N.R., 2010. *Advancing the Science of Climate Change*. The National Academies Press.
- Council, N.R., 2015. *Climate Intervention: Carbon Dioxide Removal and Reliable Sequestration*. The National Academies Press, Washington, DC, 154 pp.
- Crane-Droesch, A., Abiven, S., Jeffery, S., Torn, M.S., 2013. Heterogeneous global crop yield response to biochar: a meta-regression analysis. *Environmental Research Letters*, 8(4): 044049.
- Creutzig, F., 2016. Economic and ecological views on climate change mitigation with bioenergy and negative emissions. *Global Change Biology Bioenergy*, 8(1): 4-10.
- Croke, J., Hairsine, P., Fogarty, P., 1999. Runoff generation and re-distribution in logged eucalyptus forests, south-eastern Australia. *Journal of Hydrology*, 216(1-2): 56-77.
- Crowley, K.F. et al., 2012. Do Nutrient Limitation Patterns Shift from Nitrogen Toward Phosphorus with Increasing Nitrogen Deposition Across the Northeastern United States? *Ecosystems*, 15(6): 940-957.
- Cruz-Paredes, C. et al., 2017. Risk assessment of replacing conventional P fertilizers with biomass ash: Residual effects on plant yield, nutrition, cadmium accumulation and mycorrhizal status. *Sci Total Environ*, 575: 1168-1176.
- Curaqueo, G., Meier, S., Khan, N., Cea, M., Navia, R., 2014. Use of biochar on two volcanic soils: effects on soil properties and barley yield. *Journal of soil science and plant nutrition*, 14: 911-924.
- da Silva, A., Almeida, J.A., Schmitt, C., do Amarante, C.V., 2012. Fertilidade do solo e desenvolvimento de feijão comum em resposta adubação com pó de basalto. *Revista Brasileira de Ciências Agrárias*, 7(4): 548-554.
- de Resende, Á.V. et al., 2006. Rochas como fontes de potássio e outros nutrientes para culturas anuais. *Revista Espaço e Geografia*, 9(1).
- de Richter, R., Ming, T., Davies, P., Liu, W., Caillol, S., 2017. Removal of non-CO2 greenhouse gases by large-scale atmospheric solar photocatalysis. *Progress in Energy and Combustion Science*, 60: 68-96.
- de Souza, F.P., de Souza Martins, E., Krahl, L.L., Hurtado, S.M.C., 2013a. Efeito da aplicação do pó de rocha na recuperação de uma pastagem cultivada.
- de Souza, M.E.P. et al., 2013b. Vermicomposting with rock powder increases plant growth. *Applied Soil Ecology*, 69: 56-60.
- De Tender, C.A. et al., 2016. Biological, physicochemical and plant health responses in lettuce and strawberry in soil or peat amended with biochar. *Applied Soil Ecology*, 107: 1-12.
- De Turk, E.E., 1919. Potassium-bearing minerals as a source of potassium for plant growth. University of Illinois.
- Dean, C., Kirkpatrick, J.B., Friedland, A.J., 2017. Conventional intensive logging promotes loss of organic carbon from the mineral soil. *Glob Chang Biol*, 23(1): 1-11.
- Delattin, F., Bram, S., De Ruyck, J., 2006. Co-Utilization of Biomass and Natural Gas in an Existing Powerplant Through Primary Steam Reforming of Natural Gas, *ASME Turbo Expo 2006: Power for Land, Sea, and Air*. American Society of Mechanical Engineers, pp. 295-299.
- Diaconu, M. et al., 2020. Characterization of heavy metal toxicity in some plants and microorganisms—A preliminary approach for environmental bioremediation. *New Biotechnology*, 56: 130-139.
- Dietrich, J.P. et al., 2018. *MAGPIE – An Open Source land-use modeling framework – Version 4.0*.
- Dietrich, J.P., Schmitz, C., Lotze-Campen, H., Popp, A., Müller, C., 2014. Forecasting technological change in agriculture—an endogenous implementation in a global land use model. *Technological Forecasting and Social Change*, 81: 236-249.

- Dietrich, J.P. et al., 2012. Measuring agricultural land-use intensity—A global analysis using a model-assisted approach. *Ecological Modelling*, 232: 109-118.
- Dietzen, C., Harrison, R., Michelsen-Correa, S., 2018. Effectiveness of enhanced mineral weathering as a carbon sequestration tool and alternative to agricultural lime: An incubation experiment. *International Journal of Greenhouse Gas Control*, 74: 251-258.
- DIN, 1996. Prüfung fester Brennstoffe - Preßlinge aus naturbelassenem Holz - Anforderungen und Prüfung. Beuth, Germany, pp. 4.
- Ding, Y. et al., 2016. Biochar to improve soil fertility. A review. *Agronomy for Sustainable Development*, 36(2): 36.
- Doetterl, S. et al., 2018. Links among warming, carbon and microbial dynamics mediated by soil mineral weathering. *Nature Geoscience*, 11(8): 589-593.
- Dong, D. et al., 2015. Effects of biochar amendment on rice growth and nitrogen retention in a waterlogged paddy field. *Journal of Soils and Sediments*, 15(1): 153-162.
- Dong, D. et al., 2013. Responses of methane emissions and rice yield to applications of biochar and straw in a paddy field. *Journal of Soils and Sediments*, 13(8): 1450-1460.
- Dooley, K., Christoff, P., Nicholas, K.A., 2018. Co-producing climate policy and negative emissions: trade-offs for sustainable land-use. *Global Sustainability*, 1: e3.
- Drake, J.A., Cavagnaro, T.R., Cunningham, S.C., Jackson, W.R., Patti, A.F., 2016. Does Biochar Improve Establishment of Tree Seedlings in Saline Sodic Soils? *Land Degradation & Development*, 27(1): 52-59.
- Du, E. et al., 2020. Global patterns of terrestrial nitrogen and phosphorus limitation. *Nature Geoscience*.
- Duchesne, L., Houle, D., 2008. Impact of nutrient removal through harvesting on the sustainability of the boreal forest. *Ecological Applications*, 18(7): 1642-1651.
- Earle, S., 2018. Physical geology.
- EBC, 2012. European Biochar Certificate—Guidelines for A Sustainable Production of Biochar. European Biochar Foundation (EBC), Arbaz, Switzerland. Version 6.2 E of 04th February 2016 [online].
- Edenhofer, O., 2015. Climate change 2014: mitigation of climate change, 3. Cambridge University Press.
- Edwards, D.P. et al., 2017. Climate change mitigation: potential benefits and pitfalls of enhanced rock weathering in tropical agriculture. *Biology letters*, 13(4): 7.
- Ehlers, W., Goss, M., 2016. Water dynamics in plant production. CABI.
- Ehrig, R., Behrendt, F., 2013. Co-firing of imported wood pellets – An option to efficiently save CO₂ emissions in Europe? *Energy Policy*, 59: 283-300.
- El-Naggar, A. et al., 2018. Biochar influences soil carbon pools and facilitates interactions with soil: A field investigation. *Land Degradation & Development*, 29(7): 2162-2171.
- Elser, J.J. et al., 2007. Global analysis of nitrogen and phosphorus limitation of primary producers in freshwater, marine and terrestrial ecosystems. *Ecology Letters*, 10(12): 1135-1142.
- Erhart, J., 2009. Efeito do pó de basalto nas propriedades químicas do solo e nutrição da videira (Cabernet sauvignon).
- Eurostat, 2016. Agriculture, forestry and fishery statistics, Eurostat, Luxembourg.
- Fageria, N.K., Baligar, V.C., 2008. Chapter 7 Ameliorating Soil Acidity of Tropical Oxisols by Liming For Sustainable Crop Production, *Advances in Agronomy*. Academic Press, pp. 345-399.
- Fagernäs, L., Kuoppala, E., Simell, P., 2012. Polycyclic aromatic hydrocarbons in birch wood slow pyrolysis products. *Energy & Fuels*, 26(11): 6960-6970.
- FAO, 2015. FAO - Food and Agriculture Organization of the United Nations: 2014 Global Forest Products Facts and Figures.
- Feiden, A., 1991. Efeito de doses crescentes de po de rocha basáltica sobre a absorção de macro e micronutrientes pela cultura do trigo.
- Fertilizer Technology Research Centre, 2016. Technical Bulletin: Fertilizer and Soil Acidity. In: McLaughlin, M. (Editor). The University of Adelaide
- Fischer, G., Shah, M., van Velthuizen, H., Nachtergaele, F.O., 2001. Global agro-ecological assessment for agriculture in the 21st century, International Institute for Applied Systems Analysis, Luxemburg, Austria.
- Fishkis, O., Ingwersen, J., Lamers, M., Denysenko, D., Streck, T., 2010. Phytolith transport in soil: A field study using fluorescent labelling. *Geoderma*, 157(1): 27-36.
- Foote, J.A., Boutton, T.W., Scott, D.A., 2015. Soil C and N storage and microbial biomass in US southern pine forests: Influence of forest management. *Forest Ecology and Management*, 355: 48-57.
- Foster, E.J., Hansen, N., Wallenstein, M., Cotrufo, M.F., 2016. Biochar and manure amendments impact soil nutrients and microbial enzymatic activities in a semi-arid irrigated maize cropping system. *Agriculture, Ecosystems & Environment*, 233: 404-414.
- Freire, M., Lopes, H., Tarelho, L.A., 2015. Critical aspects of biomass ashes utilization in soils: Composition, leachability, PAH and PCDD/F. *Waste Manag*, 46: 304-15.
- Fuss, S., 2017. The 1.5 C target, political implications, and the role of BECCS, *Oxford Research Encyclopedia of Climate Science*.

- Fuss, S. et al., 2018. Negative emissions—Part 2: Costs, potentials and side effects. *Environmental Research Letters*, 13(6): 063001.
- Gaillardet, J., Dupré, B., Louvat, P., Allegre, C., 1999. Global silicate weathering and CO₂ consumption rates deduced from the chemistry of large rivers. *Chemical geology*, 159(1-4): 3-30.
- Gaiser, T., Graef, F.C., Carvalho, J., 2000. Water retention characteristics of soils with contrasting clay mineral composition in semi-arid tropical regions. *Soil Research*, 38(3): 523-536.
- Garcia, W.d.O., Amann, T., Hartmann, J., 2018. Increasing biomass demand enlarges negative forest nutrient budget areas in wood export regions. *Scientific Reports*, 8(1): 5280.
- Garcia, W.d.O. et al., 2020. Impacts of enhanced weathering on biomass production for negative emission technologies and soil hydrology. *Biogeosciences*, 17(7): 2107-2133.
- Gaus, I., 2010. Role and impact of CO₂-rock interactions during CO₂ storage in sedimentary rocks. *International Journal of Greenhouse Gas Control*, 4(1): 73-89.
- Genesio, L. et al., 2012. Surface albedo following biochar application in durum wheat. *Environmental Research Letters*, 7(1): 014025.
- Gijsman, A.J., Jagtap, S.S., Jones, J.W., 2002. Wading through a swamp of complete confusion: how to choose a method for estimating soil water retention parameters for crop models. *European Journal of Agronomy*, 18(1): 77-106.
- Gilkes, R., Young, R., Quirk, J., 1973. Artificial Weathering of Oxidized Biotite: I. Potassium Removal by Sodium Chloride and Sodium Tetraphenylboron Solutions 1. *Soil Science Society of America Journal*, 37(1): 25-28.
- Gillman, G.P., 1980. The Effect of Crushed Basalt Scoria on the Cation Exchange Properties of a Highly Weathered Soil 1. *Soil Science Society of America Journal*, 44: 465-468.
- Glaser, B., Haumaier, L., Guggenberger, G., Zech, W., 2001. The 'Terra Preta' phenomenon: a model for sustainable agriculture in the humid tropics. *Naturwissenschaften*, 88(1): 37-41.
- Glaser, B., Lehmann, J., Zech, W., 2002. Ameliorating physical and chemical properties of highly weathered soils in the tropics with charcoal – a review. *Biology and Fertility of Soils*, 35(4): 219-230.
- Glaser, B., Lehr, V.-I., 2019. Biochar effects on phosphorus availability in agricultural soils: A meta-analysis. *Scientific reports*, 9.
- Goddéris, Y. et al., 2006. Modelling weathering processes at the catchment scale: The WITCH numerical model. *Geochimica et Cosmochimica Acta*, 70(5): 1128-1147.
- Goll, D.S. et al., 2012. Nutrient limitation reduces land carbon uptake in simulations with a model of combined carbon, nitrogen and phosphorus cycling. *Biogeosciences*, 9: 3547-3569.
- Goll, D.S., Joetzer, E., Huang, M., Ciais, P., 2018. Low Phosphorus Availability Decreases Susceptibility of Tropical Primary Productivity to Droughts. *Geophysical Research Letters*, 45(16): 8231-8240.
- Goll, D.S., Moosdorf, N., Hartmann, J., Brovkin, V., 2014. Climate-driven changes in chemical weathering and associated phosphorus release since 1850: Implications for the land carbon balance. *Geophysical Research Letters*, 41(10): 3553-3558.
- Goll, D.S. et al., 2017. Carbon-nitrogen interactions in idealized simulations with JSBACH (version 3.10). *Geoscientific Model Development*, 10: 2009-2030.
- Goswami, S. et al., 2018. Phosphorus limitation of aboveground production in northern hardwood forests. *Ecology*, 99(2): 438-449.
- Grand, S., Hudson, R., Lavkulich, L.M., 2014. Effects of forest harvest on soil nutrients and labile ions in Podzols of southwestern Canada: Mean and dispersion effects. *Catena*, 122: 18-26.
- Grathwohl, P., 2014. On equilibration of pore water in column leaching tests. *Waste Management*, 34(5): 908-918.
- Grecco, M. et al., 2013. Efeito de rochas moídas e torta de tungue sobre a concentração e acumulação de nutrientes na parte aérea de plantas de milho (*Zea mays*), *Anais do Congresso Brasileiro de Rochagem, Poços de Caldas, MG*.
- Guo, X., Li, H., Chen, H., 2017. The Effects of Biochar and Intercropping on the Cd, Cr and Zn Speciation in Soils and Plant Uptake by *Machilus pauhoi*. *Bulletin of Environmental Contamination and Toxicology*, 98(4): 574-581.
- Hagemann, N. et al., 2017a. Organic coating on biochar explains its nutrient retention and stimulation of soil fertility. *Nature communications*, 8(1): 1-11.
- Hagemann, N., Kammann, C.I., Schmidt, H.-P., Kappler, A., Behrens, S., 2017b. Nitrate capture and slow release in biochar amended compost and soil. *PloS one*, 12(2).
- Hagemann, N. et al., 2018. Activated carbon, biochar and charcoal: linkages and synergies across pyrogenic carbon's ABCs. *Water*, 10(2): 182.
- Hahn, J., Schardt, M., Wolf, B., F., S., Mergler, F., 2014. Scheitholz – Produktion, Lagerung, Kennzahlen. In: (LWF), B.L.f.W.u.F. (Editor). *Druckerei Lanzinger GbR, Oberbergkirchen*.
- Haider, G., Steffens, D., Moser, G., Müller, C., Kammann, C.I., 2017. Biochar reduced nitrate leaching and improved soil moisture content without yield improvements in a four-year field study. *Agriculture, Ecosystems & Environment*, 237: 80-94.

- Hall, J.M., Van Holt, T., Daniels, A.E., Balthazar, V., Lambin, E.F., 2012. Trade-offs between tree cover, carbon storage and floristic biodiversity in reforesting landscapes. *Landscape Ecology*, 27(8): 1135-1147.
- Harley, A., Gilkes, R., 2000. Factors influencing the release of plant nutrient elements from silicate rock powders: a geochemical overview. *Nutrient Cycling in Agroecosystems*, 56(1): 11-36.
- Harter, J. et al., 2016. Soil biochar amendment shapes the composition of N₂O-reducing microbial communities. *Science of the Total Environment*, 562: 379-390.
- Hartmann, J., Jansen, N., Dürr, H.H., Kempe, S., Köhler, P., 2009. Global CO₂-consumption by chemical weathering: What is the contribution of highly active weathering regions? *Global and Planetary Change*, 69(4): 185-194.
- Hartmann, J., Jansen, N., Kempe, S., Dürr, H.H., 2007. Geochemistry of the river Rhine and the upper Danube: Recent trends and lithological influence on baselines. *Journal of Environmental Science for Sustainable Society*, 1: 39-46.
- Hartmann, J., Kempe, S., 2008. What is the maximum potential for CO₂ sequestration by "stimulated" weathering on the global scale? *Naturwissenschaften*, 95(12): 1159-64.
- Hartmann, J., Lauerwald, R., Moosdorf, N., 2014a. A brief overview of the GLObal RIVER CHEmistry Database, GLORICH. *Geochemistry of the Earth's Surface Ges-10*, 10: 23-27.
- Hartmann, J., Moosdorf, N., 2012. The new global lithological map database GLiM: A representation of rock properties at the Earth surface. *Geochemistry, Geophysics, Geosystems*, 13(12): n/a-n/a.
- Hartmann, J., Moosdorf, N., Lauerwald, R., Hinderer, M., West, A.J., 2014b. Global chemical weathering and associated P-release - The role of lithology, temperature and soil properties. *Chemical Geology*, 363(0): 145-163.
- Hartmann, J. et al., 2013. Enhanced chemical weathering as a geoengineering strategy to reduce atmospheric carbon dioxide, supply nutrients, and mitigate ocean acidification. *Reviews of Geophysics*, 51(2): 113-149.
- Hayes, N.R., Buss, H.L., Moore, O.W., Krám, P., Pancost, R.D., 2020. Controls on granitic weathering fronts in contrasting climates. *Chemical Geology*, 535: 119450.
- Haynes, R.J., Swift, R.S., 1986. Effects of soil acidification and subsequent leaching on levels of extractable nutrients in a soil. *Plant and Soil*, 95(3): 327-336.
- He, Y., Shen, Q., Kong, H., Xiong, Y., Wang, X., 2005. Effect of soil moisture content and phosphorus application on phosphorus nutrition of rice cultivated in different water regime systems. *Journal of plant nutrition*, 27(12): 2259-2272.
- He, Y., Zhu, Y., Smith, S., Smith, F., 2002. Interactions between soil moisture content and phosphorus supply in spring wheat plants grown in pot culture.
- Hedges, L.V., Gurevitch, J., Curtis, P.S., 1999. The meta-analysis of response ratios in experimental ecology. *Ecology*, 80(4): 1150-1156.
- Hensel, J., 1894. *Bread from Stones: A New and Rational System of Land Fertilization and Physical Regeneration*. AJ Tafel.
- Herbert, D.A., Fownes, J.H., 1995. Phosphorus limitation of forest leaf area and net primary production on a highly weathered soil. *Biogeochemistry*, 29(3): 223-235.
- Hering, J., Stum, W., 1990. Oxidative and reductive dissolution of minerals. *Rev. Mineral.*, 23: 427-465.
- Hesterberg, D., 1993. Effects of stopping liming on abandoned agricultural land. *Land Degradation & Development*, 4(4): 257-267.
- Higgins, J.P., Green, S., 2011. *Cochrane handbook for systematic reviews of interventions*, 4. John Wiley & Sons.
- Hinsinger, P., Bolland, M.D.A., Gilkes, R.J., 1996. Silicate rock powder: effect on selected chemical properties of a range of soils from Western Australia and on plant growth as assessed in a glasshouse experiment. *Fertilizer research*, 45(1): 69-79.
- Holdren Jr, G.R., Speyer, P.M., 1985. Reaction rate-surface area relationships during the early stages of weathering—I. Initial observations. *Geochimica et Cosmochimica Acta*, 49(3): 675-681.
- Holtan, H., Kamp-Nielsen, L., Stuanes, A.O., 1988. Phosphorus in Soil, Water and Sediment: An Overview. In: Persson, G., Jansson, M. (Eds.), *Phosphorus in Freshwater Ecosystems*. Developments in Hydrobiology. Springer, Dordrecht, pp. 19-34.
- Honcamp, F., 1910. Über den Wert des Phonolitmehles (Kalisilikat) als Düngemittel. *Zentralbl. f. Agr.-Chemie*, 39: 224.
- Hoogwijk, M., Faaij, A., Eickhout, B., de Vries, B., Turkenburg, W., 2005. Potential of biomass energy out to 2100, for four IPCC SRES land-use scenarios. *Biomass and Bioenergy*, 29(4): 225-257.
- Hopkins, W.G., Hüner, N.P.A., 2008. *Introduction to plant physiology*. John Wiley and Sons.
- Hossain, M.K., Strezov, V., Nelson, P.F., 2015. Comparative Assessment of the Effect of Wastewater Sludge Biochar on Growth, Yield and Metal Bioaccumulation of Cherry Tomato. *Pedosphere*, 25(5): 680-685.
- Houghton, J.T. et al., 2001. *Climate change 2001: the scientific basis*. The Press Syndicate of the University of Cambridge.

- Hu, Y.-L., Wu, F.-P., Zeng, D.-H., Chang, S.X., 2014. Wheat straw and its biochar had contrasting effects on soil C and N cycling two growing seasons after addition to a Black Chernozemic soil planted to barley. *Biology and Fertility of Soils*, 50(8): 1291-1299.
- Huber, C. et al., 2010. Ion concentrations and fluxes of seepage water before and after clear cutting of Norway spruce stands at Ballyhooly, Ireland, and Höglwald, Germany. *Biogeochemistry*, 101(1-3): 7-26.
- Humpenöder, F. et al., 2014. Investigating afforestation and bioenergy CCS as climate change mitigation strategies. *Environmental Research Letters*, 9(6): 064029.
- Hurttt, G.C. et al., 2011. Harmonization of land-use scenarios for the period 1500–2100: 600 years of global gridded annual land-use transitions, wood harvest, and resulting secondary lands. *Climatic Change*, 109(1).
- Hutchings, M.J., John, E.A., Wijesinghe, D.K., 2003. Toward understanding the consequences of soil heterogeneity for plant populations and communities. *Ecology*, 84(9): 2322-2334.
- IFA, 2017. IFA- International Fertilizer Association database.
- IGBP-DIS, S., 1998. A program for creating global soil-property databases. IGBP Global Soils Data Task, France.
- Inal, A., Gunes, A., Sahin, O., Taskin, M.B., Kaya, E.C., 2015. Impacts of biochar and processed poultry manure, applied to a calcareous soil, on the growth of bean and maize. *Soil Use and Management*, 31(1): 106-113.
- Irfan, M. et al., 2019. Response of soil microbial biomass and enzymatic activity to biochar amendment in the organic carbon deficient arid soil: a 2-year field study. *Arabian Journal of Geosciences*, 12(3): 95.
- Irvine, T., Baragar, W., 1971. A guide to the chemical classification of the common volcanic rocks. *Canadian journal of earth sciences*, 8(5): 523-548.
- Jeffery, S. et al., 2017. Biochar boosts tropical but not temperate crop yields. *Environmental Research Letters*, 12(5): 053001.
- Ji, C. et al., 2020. Differential responses of soil N₂O to biochar depend on the predominant microbial pathway. *Applied Soil Ecology*, 145.
- Jien, S.-H., Wang, C.-S., 2013. Effects of biochar on soil properties and erosion potential in a highly weathered soil. *CATENA*, 110: 225-233.
- Jobbágy, E.G., Jackson, R.B., 2001. The distribution of soil nutrients with depth: Global patterns and the imprint of plants. *Biogeochemistry*, 53(1): 51-77.
- Johannessen, S.C., Macdonald, R.W., 2016. Geoengineering with seagrasses: is credit due where credit is given? *Environmental Research Letters*, 11(11): 113001.
- John, D.S., Lori, S., Juliette, N.R.-V., 2018. Does replacing coal with wood lower CO₂ emissions? Dynamic lifecycle analysis of wood bioenergy. *Environmental Research Letters*, 13(1): 015007.
- Johnson, A.H., Frizano, J., Vann, D.R., 2003. Biogeochemical implications of labile phosphorus in forest soils determined by the Hedley fractionation procedure. *Oecologia*, 135(4): 487-499.
- Jonard, M. et al., 2015. Tree mineral nutrition is deteriorating in Europe. *Glob Chang Biol*, 21(1): 418-30.
- Jonard, M. et al., 2012. Deterioration of Norway spruce vitality despite a sharp decline in acid deposition: a long-term integrated perspective. *Global Change Biology*, 18(2): 711-725.
- Jones, D.L., Rousk, J., Edwards-Jones, G., DeLuca, T.H., Murphy, D.V., 2012. Biochar-mediated changes in soil quality and plant growth in a three year field trial. *Soil Biology and Biochemistry*, 45: 113-124.
- Jones, S. et al., 2016. Biochar and compost amendments enhance copper immobilisation and support plant growth in contaminated soils. *Journal of Environmental Management*, 171: 101-112.
- Joseph, S. et al., 2018. Microstructural and associated chemical changes during the composting of a high temperature biochar: Mechanisms for nitrate, phosphate and other nutrient retention and release. *Science of The Total Environment*, 618: 1210-1223.
- Kammann, C.I. et al., 2015. Plant growth improvement mediated by nitrate capture in co-composted biochar. *Scientific Reports*, 5(1): 11080.
- Kang, Y., Khan, S., Ma, X., 2009. Climate change impacts on crop yield, crop water productivity and food security – A review. *Progress in Natural Science*, 19(12): 1665-1674.
- Kantola, I.B., Masters, M.D., Beerling, D.J., Long, S.P., DeLucia, E.H., 2017. Potential of global croplands and bioenergy crops for climate change mitigation through deployment for enhanced weathering. *Biology Letters*, 13(4): 302.
- Kappler, A. et al., 2014. Biochar as an electron shuttle between bacteria and Fe (III) minerals. *Environmental Science & Technology Letters*, 1(8): 339-344.
- Kazagic, A., Music, M., Smajevic, I., Ademovic, A., Redzic, E., 2016. Possibilities and sustainability of "biomass for power" solutions in the case of a coal-based power utility. *Clean Technologies and Environmental Policy*, 18(6): 1675-1683.
- Keith, A., Singh, B., Dijkstra, F.A., 2015. Biochar reduces the rhizosphere priming effect on soil organic carbon. *Soil Biology and Biochemistry*, 88: 372-379.
- Kelly, C.N. et al., 2015. Switchgrass Biochar Effects on Plant Biomass and Microbial Dynamics in Two Soils from Different Regions. *Pedosphere*, 25(3): 329-342.
- Kempe, S., 1979. Carbon in the rock cycle. *The global carbon cycle*, 380: 343-375.

- Keys, K., Noseworthy, J.D., Ogilvie, J., Burton, D.L., Arp, P.A., 2016. A Simple Geospatial Nutrient Budget Model for Assessing Forest Harvest Sustainability across Nova Scotia, Canada. *Open Journal of Forestry*, 06(05): 420-444.
- Khan, M.S., Zaidi, A., Wani, P.A., 2007. Role of phosphate-solubilizing microorganisms in sustainable agriculture — A review. *Agronomy for Sustainable Development*, 27(1): 29-43.
- Kizito, S. et al., 2019. Role of Nutrient-Enriched Biochar as a Soil Amendment during Maize Growth: Exploring Practical Alternatives to Recycle Agricultural Residuals and to Reduce Chemical Fertilizer Demand. *Sustainability*, 11(11): 3211.
- Knust, C., Schua, K., Feger, K.-H., 2016. Estimation of Nutrient Exports Resulting from Thinning and Intensive Biomass Extraction in Medium-Aged Spruce and Pine Stands in Saxony, Northeast Germany. *Forests*, 7(12).
- Kracher, D., 2017. Nitrogen-Related Constraints of Carbon Uptake by Large-Scale Forest Expansion: Simulation Study for Climate Change and Management Scenarios. *Earth's Future*, 5(11): 1102-1118.
- Kraxner, F. et al., 2017. Mapping certified forests for sustainable management - A global tool for information improvement through participatory and collaborative mapping. *Forest Policy and Economics*, 83: 10-18.
- Krevor, S. et al., 2015. Capillary trapping for geologic carbon dioxide storage – From pore scale physics to field scale implications. *International Journal of Greenhouse Gas Control*, 40: 221-237.
- Kronberg, B.I., 1977. The geochemistry of some Brazilian soils and geochemical considerations for agriculture on highly leached soils.
- Kuśmierz, M., Oleszczuk, P., 2014. Biochar production increases the polycyclic aromatic hydrocarbon content in surrounding soils and potential cancer risk. *Environmental Science and Pollution Research*, 21(5): 3646-3652.
- Kvakić, M. et al., 2018. Quantifying the Limitation to World Cereal Production Due To Soil Phosphorus Status. *Global Biogeochemical Cycles*, 32(1): 143-157.
- La Scala, N., Bolonhezi, D., Pereira, G.T., 2006. Short-term soil CO₂ emission after conventional and reduced tillage of a no-till sugar cane area in southern Brazil. *Soil and Tillage Research*, 91(1): 244-248.
- Laboratory, E.S.R., 2019. Trends in Atmospheric Carbon Dioxide.
- Laboratory, F.P., 2010. Wood handbook—Wood as an engineering material. General Technical Report FPL-GTR-190, U.S. Department of Agriculture, Forest Service, Forest Products Laboratory.
- Laghari, M. et al., 2016. Fast pyrolysis biochar from sawdust improves the quality of desert soils and enhances plant growth. *Journal of the Science of Food and Agriculture*, 96(1): 199-206.
- Laghari, M. et al., 2015. Effects of biochar application rate on sandy desert soil properties and sorghum growth. *CATENA*, 135: 313-320.
- Landeweert, R., Hoffland, E., Finlay, R.D., Kuyper, T.W., van Breemen, N., 2001. Linking plants to rocks: ectomycorrhizal fungi mobilize nutrients from minerals. *Trends in Ecology & Evolution*, 16(5): 248-254.
- Lasaga, A.C., Soler, J.M., Ganor, J., Burch, T.E., Nagy, K.L., 1994. Chemical weathering rate laws and global geochemical cycles. *Geochimica et Cosmochimica Acta*, 58(10): 2361-2386.
- Lauri, P. et al., 2014. Woody biomass energy potential in 2050. *Energy Policy*, 66(Supplement C): 19-31.
- LeCroy, C., Masiello, C.A., Rudgers, J.A., Hockaday, W.C., Silberg, J.J., 2013. Nitrogen, biochar, and mycorrhizae: Alteration of the symbiosis and oxidation of the char surface. *Soil Biology and Biochemistry*, 58: 248-254.
- Lee, S.S., Shah, H.S., Awad, Y.M., Kumar, S., Ok, Y.S., 2015. Synergy effects of biochar and polyacrylamide on plants growth and soil erosion control. *Environmental Earth Sciences*, 74(3): 2463-2473.
- Lehmann, J., 2007. Bio-energy in the black. *Frontiers in Ecology and the Environment*, 5(7): 381-387.
- Lehmann, J., Gaunt, J., Rondon, M., 2006. Bio-char sequestration in terrestrial ecosystems—a review. *Mitigation and adaptation strategies for global change*, 11(2): 403-427.
- Lehmann, J. et al., 2011. Biochar effects on soil biota - A review. *Soil Biology & Biochemistry*, 43(9): 1812-1836.
- Lempp, P., 2013. Biomass Co-firing in Coal Power Plants, IEA-ETSAP and IRENA, Technology-Policy Brief E21.
- Lenton, T.M., 2010. The potential for land-based biological CO₂ removal to lower future atmospheric CO₂ concentration. *Carbon Management*, 1(1): 145-160.
- Lenton, T.M., 2014. The global potential for carbon dioxide removal. In: Harrison, R.M., Hester, R.E. (Eds.), *Geoengineering of the Climate System*. Cambridge, The Royal Society of Chemistry, London, pp. 52-79.
- Lenton, T.M., Britton, C., 2006. Enhanced carbonate and silicate weathering accelerates recovery from fossil fuel CO₂ perturbations. *Global Biogeochemical Cycles*, 20(3).
- Leonardos, O., Fyfe, W., Kronberg, B., 1976. Rochagem: O método de aumento da fertilidade em solos lixiviados e arenosos, Congresso Brasileiro de Geologia, pp. 137-145.
- Leonardos, O., Imaña, J., Flor, H., Kronberg, B., Fyfe, W., 1982. Nutrient recharge of laterites using basalt powder, 2nd Int. Sem. Lateritisation processes IUGS/UNESCO, pp. 66.
- Leonardos, O.H., Fyfe, W.S., Kronberg, B.I., 1987. The use of ground rocks in laterite systems: An improvement to the use of conventional soluble fertilizers? *Chemical Geology*, 60(1): 361-370.

- Lewandowski, T.E., Forrester, J.A., Mladenoff, D.J., D'Amato, A.W., Palik, B.J., 2016. Response of the soil microbial community and soil nutrient bioavailability to biomass harvesting and reserve tree retention in northern Minnesota aspen-dominated forests. *Applied Soil Ecology*, 99: 13-20.
- Li, C. et al., 2018. Impact of biochar addition on soil properties and water-fertilizer productivity of tomato in semi-arid region of Inner Mongolia, China. *Geoderma*, 331: 100-108.
- Li, J.-G., Dong, Y.-H., 2013. Effect of a rock dust amendment on disease severity of tomato bacterial wilt. *Antonie van Leeuwenhoek*, 103(1): 11-22.
- Liang, F., Li, G.-t., Lin, Q.-m., Zhao, X.-r., 2014. Crop Yield and Soil Properties in the First 3 Years After Biochar Application to a Calcareous Soil. *Journal of Integrative Agriculture*, 13(3): 525-532.
- Lin, X.W. et al., 2015. Effects of biochar application on greenhouse gas emissions, carbon sequestration and crop growth in coastal saline soil. *European Journal of Soil Science*, 66(2): 329-338.
- Liu, S., Han, C., Liu, J., Li, H., 2015. Hydrothermal decomposition of potassium feldspar under alkaline conditions. *Rsc Advances*, 5(113): 93301-93309.
- Liu, X.-H., Zhang, X.-C., 2012. Effect of Biochar on pH of Alkaline Soils in the Loess Plateau: Results from Incubation Experiments. *International Journal of Agriculture & Biology*, 14(5).
- Lorenz, S., Kasang, D., Lohmann, G., 2007. Global water cycle and climate change, *Global change: Enough water for all? Wissenschaftliche Auswertungen*, pp. 157-161.
- Lotze-Campen, H. et al., 2008. Global food demand, productivity growth, and the scarcity of land and water resources: a spatially explicit mathematical programming approach. *Agricultural Economics*, 39(3): 325-338.
- Luz, P.H.d.C. et al., 2013. Avaliação do desempenho do fonólito via mineral e no enriquecimento da torta de filtro em soqueira de cana-de-açúcar. *Anais*.
- Ma, X., Ma, H., Yang, J., 2016a. Sintering Preparation and Release Properties of K₂MgSi₃O₈ Slow-Release Fertilizer Using Biotite Acid-Leaching Residues as Silicon Source. *Industrial & Engineering Chemistry Research*, 55(41): 10926-10931.
- Ma, X., Yang, J., Ma, H., Liu, C., 2016b. Hydrothermal extraction of potassium from potassic quartz syenite and preparation of aluminum hydroxide. *International Journal of Mineral Processing*, 147: 10-17.
- Macdonald, L.M., Farrell, M., Zwieten, L.V., Krull, E.S., 2014. Plant growth responses to biochar addition: an Australian soils perspective. *Biology and Fertility of Soils*, 50(7): 1035-1045.
- Madaras, M., Mayerová, M., Kulháněk, M., Koubová, M., Faltus, M., 2013. Waste silicate minerals as potassium sources: a greenhouse study on spring barley. *Archives of Agronomy and Soil Science*, 59(5): 671-683.
- Madsen, H.B., 1985. Distribution of spring barley roots in Danish soils, of different texture and under different climatic conditions. *Plant and Soil*, 88(1): 31-43.
- Mahowald, N. et al., 2008. Global distribution of atmospheric phosphorus sources, concentrations and deposition rates, and anthropogenic impacts. *Global Biogeochemical Cycles*, 22(4): n/a-n/a.
- Manning, D.A.C., 2010. Mineral sources of potassium for plant nutrition. A review. *Agronomy for Sustainable Development*, 30(2): 281-294.
- Mantau, U. et al., 2010. Real potential for changes in growth and use of EU forests. Hamburg: EUwood, Methodology report.
- Martinsen, V. et al., 2014. Farmer-led maize biochar trials: Effect on crop yield and soil nutrients under conservation farming. *Journal of Plant Nutrition and Soil Science*, 177(5): 681-695.
- Mbow, C. et al., 2014. Agroforestry solutions to address food security and climate change challenges in Africa. *Current Opinion in Environmental Sustainability*, 6: 61-67.
- McHenry, M.P., 2011. Soil Organic Carbon, Biochar, and Applicable Research Results for Increasing Farm Productivity under Australian Agricultural Conditions. *Communications in Soil Science and Plant Analysis*, 42(10): 1187-1199.
- Meena, V.S. et al., 2016. Potassium-Solubilizing Microorganism in Evergreen Agriculture: An Overview. In: Meena, V.S., Maurya, B.R., Verma, J.P., Meena, R.S. (Eds.), *Potassium Solubilizing Microorganisms for Sustainable Agriculture*. Springer India, New Delhi, pp. 1-20.
- Meena, V.S., Maurya, B.R., Verma, J.P., 2014. Does a rhizospheric microorganism enhance K⁺ availability in agricultural soils? *Microbiological Research*, 169(5): 337-347.
- Melo, V.F., UChôa, S.C.P., Dias, F.O., Barbosa, G.F., 2012. Doses de basalto moído nas propriedades químicas de um Latossolo Amarelo distrófico da savana de Roraima. *Acta Amazonica*, 42(4).
- Menge, D.N.L., Hedin, L.O., Pacala, S.W., 2012. Nitrogen and Phosphorus Limitation over Long-Term Ecosystem Development in Terrestrial Ecosystems. *PLoS ONE*, 7(8): e42045.
- Mersi, W.V., Kuhnert-Finkernagel, R., Schinner, F., 1992. The influence of rock powders on microbial activity of three forest soils. *Zeitschrift für Pflanzenernährung und Bodenkunde*, 155(1): 29-33.
- Mete, F.Z., Mia, S., Dijkstra, F.A., Abuyusuf, M., Hossain, A.S.M.I., 2015. Synergistic Effects of Biochar and NPK Fertilizer on Soybean Yield in an Alkaline Soil. *Pedosphere*, 25(5): 713-719.
- Metz, B., Davidson, O., Bosch, P., Dave, R., Meyer, L., 2007. *Climate change 2007: Mitigation of climate change*. Cambridge Univ. Press.

- Mickan, B.S., Abbott, L.K., Stefanova, K., Solaiman, Z.M., 2016. Interactions between biochar and mycorrhizal fungi in a water-stressed agricultural soil. *Mycorrhiza*, 26(6): 565-574.
- Minagawa, J., 2009. Chapter 14 - Light-Harvesting Proteins. In: Harris, E.H., Stern, D.B., Witman, G.B. (Eds.), *The Chlamydomonas Sourcebook (Second Edition)*. Academic Press, London, pp. 503-539.
- Ming, T., de_Richter, R., Shen, S., Caillol, S., 2016. Fighting global warming by greenhouse gas removal: destroying atmospheric nitrous oxide thanks to synergies between two breakthrough technologies. *Environmental Science and Pollution Research*, 23(7): 6119-6138.
- Minx, J.C. et al., 2018. Negative emissions—Part 1: Research landscape and synthesis. *Environmental Research Letters*, 13(6): 063001.
- Mitchell, M. et al., 2018. markummittchell/engage-digitizer: Version 10.6 Support for Flathub (Version v10.6).
- Mohr, C.H., Coppus, R., Iroume, A., Huber, A., Bronstert, A., 2013. Runoff generation and soil erosion processes after clear cutting. *Journal of Geophysical Research-Earth Surface*, 118(2): 814-831.
- Mohr, C.H. et al., 2014. Seasonal logging, process response, and geomorphic work. *Earth Surface Dynamics*, 2(1): 117-125.
- Moon, S., Chamberlain, C.P., Hilley, G.E., 2014. New estimates of silicate weathering rates and their uncertainties in global rivers. *Geochimica et Cosmochimica Acta*, 134: 257-274.
- Müller, C., Robertson, R.D., 2013. Projecting future crop productivity for global economic modeling. *Agricultural Economics*, 45(1): 37-50.
- Munkholm, L.J., Schjønnning, P., Sørensen, H., 2003. Jordpakning og mekanisk løsning på grovsandet jord, Ministeriet for Fødevarer, Landbrug og Fiskeri,, Viborg.
- Myhre, G. et al., 2013. Anthropogenic and Natural Radiative Forcing. *Climate Change 2013: The Physical Science Basis. Contribution of Working Group I to the Fifth Assessment Report of the Intergovernmental Panel on Climate Change*, 659–740. Cambridge: Cambridge University Press.
- Nair, P.R., 2007. The coming of age of agroforestry. *Journal of the Science of Food and Agriculture*, 87(9): 1613-1619.
- Nelissen, V., Saha, B.K., Ruyschaert, G., Boeckx, P., 2014. Effect of different biochar and fertilizer types on N₂O and NO emissions. *Soil Biology and Biochemistry*, 70: 244-255.
- Nguyen, T.T.N. et al., 2018. The effects of short term, long term and reapplication of biochar on soil bacteria. *Science of The Total Environment*, 636: 142-151.
- Nkouathio, D.G. et al., 2008. Utilisation des roches volcaniques pour la remineralisation des sols ferrallitiques des regions tropicales. Cas des pyroclastites basaltiques du graben de Tombel (Ligne volcanique du Cameroun). *Bull. Soc. Vaudoise Sci. Nat.*: 14.
- Noordin, W., Zulkefly, S., Shamshuddin, J., Hanafi, M., 2017. Improving soil chemical properties and growth performance of hevea brasiliensis through basalt application. *International Proceedings of IRC 2017*, 1(1): 308-323.
- Nunes, J.M.G., Kautzmann, R.M., Oliveira, C., 2014. Evaluation of the natural fertilizing potential of basalt dust wastes from the mining district of Nova Prata (Brazil). *Journal of Cleaner Production*, 84: 649-656.
- O'Toole, A. et al., 2016. Current and future applications for biochar. *Biochar in European Soils and Agriculture: Science and Practice*. Abington: Taylor & Francis Group: 253-280.
- Obersteiner, M. et al., 2018. How to spend a dwindling greenhouse gas budget. *Nature Climate Change*, 8(1): 7-10.
- Olness, A., Archer, D., 2005. Effect of organic carbon on available water in soil. *Soil Science*, 170(2): 90-101.
- Olsen, M., 1958. Orienterende forsøg vedrørende jordens dybdebehandling, Hedeselskabets Forskningsvirksomhed, Viborg.
- Olsson, B.A., Åkerblom, S., Bishop, K., Eklöf, K., Ring, E., 2017. Does the harvest of logging residues and wood ash application affect the mobilization and bioavailability of trace metals? *Forest Ecology and Management*, 383: 61-72.
- Olsson, O., Hillring, B., 2012. 5.06 - A Global Bioenergy Market. In: Sayigh, A. (Ed.), *Comprehensive Renewable Energy*. Elsevier, Oxford, pp. 75-85.
- Omondi, M.O. et al., 2016. Quantification of biochar effects on soil hydrological properties using meta-analysis of literature data. *Geoderma*, 274: 28-34.
- Oren, R. et al., 2001. Soil fertility limits carbon sequestration by forest ecosystems in a CO₂-enriched atmosphere. *Nature*, 411(6836): 469-72.
- Ortiz, C.A., Lundblad, M., Lundstrom, A., Stendahl, J., 2014. The effect of increased extraction of forest harvest residues on soil organic carbon accumulation in Sweden. *Biomass & Bioenergy*, 70: 230-238.
- Panhwar, Q., Naher, U., Shamshuddin, J., Othman, R., Ismail, M., 2016. Applying Limestone or Basalt in Combination with Bio-Fertilizer to Sustain Rice Production on an Acid Sulfate Soil in Malaysia. *Sustainability*, 8(7): 700.
- Pardo, L.H., Robin-Abbott, M., Duarte, N., Miller, E., K., 2005. *Tree Chemistry Database (Version 1.0)*, United States Department of Agriculture, NE-324. Newtown Square PA.

- Paré, D. et al., 2013. Estimating stand-scale biomass, nutrient contents, and associated uncertainties for tree species of Canadian forests. *Canadian Journal of Forest Research*, 43(11).
- Parfitt, R.L., Giltrap, D.J., Whitton, J.S., 1995. Contribution of organic matter and clay minerals to the cation exchange capacity of soils. *Communications in Soil Science and Plant Analysis*, 26(9-10): 1343-1355.
- Park, J.H., Choppala, G.K., Bolan, N.S., Chung, J.W., Chuasavathi, T., 2011. Biochar reduces the bioavailability and phytotoxicity of heavy metals. *Plant and soil*, 348(1-2): 439.
- Pfister, M., Saha, S., 2017. Effects of biochar and fertilizer management on sunflower (*Helianthus annuus* L.) feedstock and soil properties. *Archives of Agronomy and Soil Science*, 63(5): 651-662.
- Phillips, T., Watmough, S.A., 2012. A nutrient budget for a selection harvest: implications for long-term sustainability. *Canadian Journal of Forest Research-Revue Canadienne De Recherche Forestiere*, 42(12): 2064-2077.
- Pierce, S.K., Curtis, N.E., 2012. Chapter four - Cell Biology of the Chloroplast Symbiosis in Sacoglossan Sea Slugs. In: Jeon, K.W. (Ed.), *International Review of Cell and Molecular Biology*. Academic Press, pp. 123-148.
- Pontius, R., 2000. Quantification error versus location error in comparison of categorical maps. *Photogrammetric Engineering and Remote Sensing*, 66(5): 540-540.
- Popp, A. et al., 2017. Land-use futures in the shared socio-economic pathways. *Global Environmental Change*, 42: 331-345.
- Popp, A., Lotze-Campen, H., Bodirsky, B., 2010. Food consumption, diet shifts and associated non-CO2 greenhouse gases from agricultural production. *Global Environmental Change*, 20(3): 451-462.
- Popp, A. et al., 2011. On sustainability of bioenergy production: Integrating co-emissions from agricultural intensification. *Biomass and Bioenergy*, 35(12): 4770-4780.
- Porder, S., Hilley, G.E., 2011. Linking chronosequences with the rest of the world: predicting soil phosphorus content in denuding landscapes. *Biogeochemistry*, 102(1): 153-166.
- Porder, S., Ramachandran, S., 2013. The phosphorus concentration of common rocks—a potential driver of ecosystem P status. *Plant and soil*, 367(1-2): 41-55.
- Pratiwi, E.P.A., Shinogi, Y., 2016. Rice husk biochar application to paddy soil and its effects on soil physical properties, plant growth, and methane emission. *Paddy and Water Environment*, 14(4): 521-532.
- Program, N.A.D., 2016. Total Deposition Maps, v2016.01.
- Quin, P.R. et al., 2014. Oil mallee biochar improves soil structural properties—a study with x-ray micro-CT. *Agriculture, ecosystems & environment*, 191: 142-149.
- Rajkovich, S. et al., 2012. Corn growth and nitrogen nutrition after additions of biochars with varying properties to a temperate soil. *Biology and Fertility of Soils*, 48(3): 271-284.
- Ranger, J., Turpault, M.P., 1999. Input-output nutrient budgets as a diagnostic tool for sustainable forest management. *Forest Ecology and Management*, 122(1-2): 139-154.
- Raymond, P.A., Hamilton, S.K., 2018. Anthropogenic influences on riverine fluxes of dissolved inorganic carbon to the oceans. *Limnology and Oceanography Letters*, 3(3): 143-155.
- Reick, C.H., Raddatz, T., Brovkin, V., Gayler, V., 2013. Representation of natural and anthropogenic land cover change in MPI-ESM. *Journal of Advances in Modeling Earth Systems*, 5(3): 459-482.
- Reicosky, D.C., 1997. Tillage-induced CO2 emission from soil. *Nutrient Cycling in Agroecosystems*, 49(1): 273-285.
- Ren21, 2017. *Renewables 2017 - Global Status Report*, REN21, Paris: REN21 Secretariat.
- Renforth, P., 2012. The potential of enhanced weathering in the UK. *International Journal of Greenhouse Gas Control*, 10: 229-243.
- Renforth, P., von Strandmann, P.A.E.P., Henderson, G.M., 2015. The dissolution of olivine added to soil: Implications for enhanced weathering. *Applied Geochemistry*, 61: 109-118.
- Ringeval, B. et al., 2019. Insights on nitrogen and phosphorus co-limitation in global croplands from theoretical and modelling fertilization experiments. *Biogeosciences Discuss.*, 2019: 1-35.
- RISI, 2015. *Global Pellet Demand Outlook Study 2015*.
- Roberts, D.A., Paul, N.A., Dworjany, S.A., Bird, M.I., De Nys, R., 2015. Biochar from commercially cultivated seaweed for soil amelioration. *Scientific reports*, 5: 9665.
- Robertson, S.J., Rutherford, P.M., López-Gutiérrez, J.C., Massicotte, H.B., 2012. Biochar enhances seedling growth and alters root symbioses and properties of sub-boreal forest soils. *Canadian Journal of Soil Science*, 92(2): 329-340.
- Rockström, J. et al., 2009. A safe operating space for humanity. *Nature*, 461: 472-475.
- Rogers, J.R., Bennett, P.C., 2004. Mineral stimulation of subsurface microorganisms: release of limiting nutrients from silicates. *Chemical Geology*, 203(1): 91-108.
- Romero-Mujalli, G., Hartmann, J., Börker, J., Gaillardet, J., Calmels, D., 2018. Ecosystem controlled soil-rock pCO2 and carbonate weathering – Constraints by temperature and soil water content. *Chemical Geology*, 527.

- Rossato, L. et al., 2017. Impact of Soil Moisture on Crop Yields over Brazilian Semiarid. *Frontiers in Environmental Science*, 5(73).
- Rousk, J., Dempster, D.N., Jones, D.L., 2013. Transient biochar effects on decomposer microbial growth rates: evidence from two agricultural case-studies. *European Journal of Soil Science*, 64(6): 770-776.
- Royer, D.L., Berner, R.A., Montañez, I.P., Tabor, N.J., Beerling, D.J., 2004. CO₂ as a primary driver of phanerozoic climate. *GSA today*, 14(3): 4-10.
- Rutigliano, F.A. et al., 2014. Effect of biochar addition on soil microbial community in a wheat crop. *European Journal of Soil Biology*, 60: 9-15.
- Sachse, J., 1927. Über die Aufnahme von Nährstoffen aus einem gemahlenen Basalt durch die Pflanze. *Zeitschrift für Pflanzenernährung, Düngung, Bodenkunde*, 9(4): 193-223.
- Sadras, V.O., Milroy, S.P., 1996. Soil-water thresholds for the responses of leaf expansion and gas exchange: A review. *Field Crops Research*, 47(2): 253-266.
- Saidy, A.R. et al., 2012. Effects of clay mineralogy and hydrous iron oxides on labile organic carbon stabilisation. *Geoderma*, 173-174: 104-110.
- Sairam, R., 2011. Physiology of waterlogging tolerance in plants, National Seminar on Sustainable Crop Productivity through Physiological Interventions, Matunga, Mumbai, pp. 9.
- Sanz Scovino, J.I., Rowell, D.L., 1988. The use of feldspars as potassium fertilizers in the savannah of Colombia. *Fertilizer research*, 17(1): 71-83.
- Sarbas, B., 2008. The GEOROC Database as Part of a Growing Geoinformatics Network. In: Brady, S.R., Sinha, A.K., Gundersen, L.C. (Editors), *Geoinformatics 2008—Data to Knowledge*. USGS, Potsdam, pp. 42 - 43.
- Saxena, J., Rana, G., Pandey, M., 2013. Impact of addition of biochar along with *Bacillus* sp. on growth and yield of French beans. *Scientia Horticulturae*, 162: 351-356.
- Saxton, K., Rawls, W.J., Romberger, J., Papendick, R., 1986. Estimating generalized soil-water characteristics from texture I. *Soil Science Society of America Journal*, 50(4): 1031-1036.
- Saxton, K.E., Rawls, W.J., 2006. Soil water characteristic estimates by texture and organic matter for hydrologic solutions. *Soil science society of America Journal*, 70(5): 1569-1578.
- Schaap, M.G., Leij, F.J., van Genuchten, M.T., 2001. rosetta: a computer program for estimating soil hydraulic parameters with hierarchical pedotransfer functions. *Journal of Hydrology*, 251(3): 163-176.
- Schmidt, H.-P. et al., 2018. Pyrogenic carbon capture and storage. *GCB Bioenergy*, 0(0): 19.
- Schmidt, H.-P., Hagemann, N., Draper, K., Kammann, C., 2019. The use of biochar in animal feeding. *PeerJ*, 7: e7373.
- Schmidt, H.P., Pandit, B.H., Cornelissen, G., Kammann, C.I., 2017. Biochar-based fertilization with liquid nutrient enrichment: 21 field trials covering 13 crop species in Nepal. *Land Degradation & Development*, 28(8): 2324-2342.
- Schmidt, H.P., Taylor, P., Eglise, A., Arbaz, C., 2014. Kon-Tiki flame curtain pyrolysis for the democratization of biochar production. *Biochar J*, 1: 14-24.
- Schroeder, P., 1992. Carbon storage potential of short rotation tropical tree plantations. *Forest Ecology and Management*, 50(1): 31-41.
- Schuiling, R.D., Krijgsman, P., 2006. Enhanced Weathering: An Effective and Cheap Tool to Sequester CO₂. *Climatic Change*, 74(1): 349-354.
- Schwede, D.B., Lear, G.G., 2014. A novel hybrid approach for estimating total deposition in the United States. *Atmospheric Environment*, 92: 207-220.
- Seaman, J.C., Roberts, K.A., 2012. Radionuclide Fate and Transport in Terrestrial Environments. *Encyclopedia of Sustainability Science and Technology*: 8597-8634.
- Service, U.S.F., 2016. U.S. Forest Service - Timber Harvests. US Forest Service, Department of Agriculture - <https://www.fs.fed.us/forestmanagement/products/cut-sold/index.shtml> - downloaded on 05.12.2016.
- Sharpley, A., 2000. Phosphorus availability. CRC Press. Boca Raton Florida. pp. D18-D37, pp. D18-D30.
- Shen, J. et al., 2011. Phosphorus Dynamics: From Soil to Plant. *Plant Physiology*, 156(3): 997-1005.
- Sherman, A., 2012. Pellet Fuel Quality, Delivery, and Storage, Vermont Woodchip and Pellet Heating Conference, Biomass Energy Resource Center.
- Sikkema, R., Junginger, M., Pichler, W., Hayes, S., Faaij, A.P.C., 2010. The international logistics of wood pellets for heating and power production in Europe: Costs, energy-input and greenhouse gas balances of pellet consumption in Italy, Sweden and the Netherlands. *Biofuels Bioproducts & Biorefining-Biofpr*, 4(2): 132-153.
- Sikkema, R. et al., 2011. The European wood pellet markets: current status and prospects for 2020. *Biofuels, Bioproducts and Biorefining*, 5(3): 250-278.
- Sillmann, J., Kharin, V.V., Zwiers, F.W., Zhang, X., Bronaugh, D., 2013. Climate extremes indices in the CMIP5 multimodel ensemble: Part 2. Future climate projections. *Journal of Geophysical Research: Atmospheres*, 118(6): 2473-2493.

- Silva, B., Paradelo, R., Vázquez, N., García-Rodeja, E., Barral, M.T., 2013. Effect of the addition of granitic powder to an acidic soil from Galicia (NW Spain) in comparison with lime. *Environmental earth sciences*, 68(2): 429-437.
- Singh, B., Schulze, D., 2015. Soil minerals and plant nutrition. *Nature Education Knowledge*, 6(1): 1.
- Smeets, E.M.W., Faaij, A.P.C., 2007. Bioenergy potentials from forestry in 2050. *Climatic Change*, 81(3): 353-390.
- Smith, P., 2012. Agricultural greenhouse gas mitigation potential globally, in Europe and in the UK: what have we learnt in the last 20 years? *Global Change Biology*, 18(1): 35-43.
- Smith, P. et al., 2019. Land-Management Options for Greenhouse Gas Removal and Their Impacts on Ecosystem Services and the Sustainable Development Goals. *Annual Review of Environment and Resources*, 44(1): 255-286.
- Smith, P. et al., 2016. Biophysical and economic limits to negative CO₂ emissions. *Nature Clim. Change*, 6(1): 42-50.
- Smith, P. et al., 2015. Biophysical and economic limits to negative CO₂ emissions. *Nature Climate Change*, 6: 42-50.
- Smith, W.K., Zhao, M., Running, S.W., 2012. Global Bioenergy Capacity as Constrained by Observed Biospheric Productivity Rates. *BioScience*, 62(10): 911-922.
- Smolander, A., Kitunen, V., Tamminen, P., Kukkola, M., 2010. Removal of logging residue in Norway spruce thinning stands: Long-term changes in organic layer properties. *Soil Biology and Biochemistry*, 42(8): 1222-1228.
- Sonntag, S., Pongratz, J., Reick, C.H., Schmidt, H., 2016. Reforestation in a high-CO₂ world—Higher mitigation potential than expected, lower adaptation potential than hoped for. *Geophysical Research Letters*, 43(12): 6546-6553.
- Stefánsson, A., Gíslason, S.R., Arnórsson, S., 2001. Dissolution of primary minerals in natural waters: II. Mineral saturation state. *Chemical Geology*, 172(3-4): 251-276.
- Stolaroff, J.K. et al., 2012. Review of Methane Mitigation Technologies with Application to Rapid Release of Methane from the Arctic. *Environmental Science & Technology*, 46(12): 6455-6469.
- Straaten, P.v., 2007. *Agrogeology: the use of rocks for crops*. Ed. Enviroquest Ltd, 440 pp.
- Strefler, J., Amann, T., Bauer, N., Kriegler, E., Hartmann, J., 2018. Potential and costs of Carbon Dioxide Removal by Enhanced Weathering of rocks. *Environmental Research Letters*.
- Sullivan, P., 2000. Drought resistant soils. ATTRA.
- Sun, Y. et al., 2017. Diagnosing phosphorus limitations in natural terrestrial ecosystems in carbon cycle models. *Earth's Future*.
- Survey, U.F.S.U.S.G., 2000. *Forest Cover Types, Forest Cover Types*. U.S. Geological Survey, Reston, VA.
- Swanback, T.R., 1950. Granite stone meal as a source of potash for tobacco. *Bulletin. Connecticut Agricultural Experiment Station*, 536.
- Tanner, E.V.J., Vitousek, P.M., Cuevas, E., 1998. Experimental investigation of nutrient limitation of forest growth on wet tropical mountains. *Ecology*, 79(1): 10-22.
- Taylor, L.L. et al., 2009. Biological weathering and the long-term carbon cycle: integrating mycorrhizal evolution and function into the current paradigm. *Geobiology*, 7(2): 171-91.
- Taylor, L.L. et al., 2015. Enhanced weathering strategies for stabilizing climate and averting ocean acidification. *Nature Climate Change*, 6(4): 402-406.
- Theodoro, S.H., de Souza Martins, E., Fernandes, M.M., de Carvalho, A.M.X., 2013. Nota do Comitê organizador, II Congresso Brasileiro de Rochagem, Poços de Caldas - MG.
- Thiffault, E. et al., 2011. Effects of forest biomass harvesting on soil productivity in boreal and temperate forests—a review. *Environmental Reviews*, 19(NA): 278-309.
- Thomson, A.M. et al., 2011. RCP4.5: a pathway for stabilization of radiative forcing by 2100. *Climatic Change*, 109(1): 77-94.
- Tokimatsu, K., Yasuoka, R., Nishio, M., 2017. Global zero emissions scenarios: The role of biomass energy with carbon capture and storage by forested land use. *Applied Energy*, 185: 1899-1906.
- Trivedi, N.S., Mandavgane, S.A., Mehete, S., Kulkarni, B.D., 2016. Characterization and valorization of biomass ashes. *Environ Sci Pollut Res Int*, 23(20): 20243-20256.
- Uhlig, D., Schuessler, J.A., Bouchez, J., Dixon, J.L., von Blanckenburg, F., 2017. Quantifying nutrient uptake as driver of rock weathering in forest ecosystems by magnesium stable isotopes. *Biogeosciences*, 14(12): 3111-3128.
- Uhlig, D., von Blanckenburg, F., 2019. How Slow Rock Weathering Balances Nutrient Loss During Fast Forest Floor Turnover in Montane, Temperate Forest Ecosystems. *Frontiers in Earth Science*, 7(159).
- Upadhyay, K.P., George, D., Swift, R.S., Galea, V., 2014. The Influence of Biochar on Growth of Lettuce and Potato. *Journal of Integrative Agriculture*, 13(3): 541-546.
- Uroz, S., Calvaruso, C., Turpault, M.-P., Frey-Klett, P., 2009. Mineral weathering by bacteria: ecology, actors and mechanisms. *Trends in Microbiology*, 17(8): 378-387.

- Vaccari, F.P. et al., 2011. Biochar as a strategy to sequester carbon and increase yield in durum wheat. *European Journal of Agronomy*, 34(4): 231-238.
- Vaccari, F.P. et al., 2015. Biochar stimulates plant growth but not fruit yield of processing tomato in a fertile soil. *Agriculture, Ecosystems & Environment*, 207: 163-170.
- Vadeboncoeur, M.A., Hamburg, S.P., Yanai, R.D., Blum, J.D., 2014. Rates of sustainable forest harvest depend on rotation length and weathering of soil minerals. *Forest Ecology and Management*, 318: 194-205.
- Van Straaten, P., 2006. Farming with rocks and minerals: challenges and opportunities. *An Acad Bras Cienc*, 78(4): 731-47.
- Vanek, S.J., Lehmann, J., 2015. Phosphorus availability to beans via interactions between mycorrhizas and biochar. *Plant and Soil*, 395(1): 105-123.
- Vangansbeke, P. et al., 2015. Strong negative impacts of whole tree harvesting in pine stands on poor, sandy soils: A long-term nutrient budget modelling approach. *Forest Ecology and Management*, 356: 101-111.
- Velbel, M., Taylor, A., Romero, N., 1990. Effect of temperature on feldspar weathering rates in alpine and non-alpine watersheds, *Geol. Soc. Am. Abstr. Program*, pp. 49.
- Vengosh, A., 2003. 9.09 - Salinization and Saline Environments. In: Holland, H.D., Turekian, K.K. (Eds.), *Treatise on Geochemistry*. Pergamon, Oxford, pp. 1-35.
- Vergutz, L., Manzoni, S., Porporato, A., Novais, R.F., Jackson, R.B., 2012. A Global Database of Carbon and Nutrient Concentrations of Green and Senesced Leaves. ORNL Distributed Active Archive Center.
- Vichi, M., Navarra, A., Fogli, P.G., 2013. Adjustment of the natural ocean carbon cycle to negative emission rates. *Climatic Change*, 118(1): 105-118.
- Vienken, T., Dietrich, P., 2011. Field evaluation of methods for determining hydraulic conductivity from grain size data. *Journal of Hydrology*, 400(1-2): 58-71.
- Vitousek, P.M. et al., 1997. Human alteration of the global nitrogen cycle: sources and consequences. *Ecological applications*, 7(3): 737-750.
- Vitousek, P.M., Porder, S., Houlton, B.Z., Chadwick, O.A., 2010. Terrestrial phosphorus limitation: mechanisms, implications, and nitrogen–phosphorus interactions. *Ecological Applications*, 20(1): 5-15.
- von Liebig, J.F., Playfair, L.P.B., 1843. *Chemistry in its application to agriculture and physiology*. JM Campbell.
- Von Wilpert, K., Lukes, M., 2003. Ecochemical effects of phonolite rock powder, dolomite and potassium sulfate in a spruce stand on an acidified glacial loam. *Nutrient Cycling in Agroecosystems*, 65(2): 115-127.
- Waldbauer, J.R., Chamberlain, C.P., 2005. Influence of uplift, weathering, and base cation supply on past and future CO₂ levels, A history of atmospheric CO₂ and its effects on Plants, Animals, and Ecosystems. Springer, pp. 166-184.
- Walker, J.C., Hays, P., Kasting, J.F., 1981. A negative feedback mechanism for the long-term stabilization of Earth's surface temperature. *Journal of Geophysical Research: Oceans*, 86(C10): 9776-9782.
- Wall, A., Hytönen, J., 2011. The long-term effects of logging residue removal on forest floor nutrient capital, foliar chemistry and growth of a Norway spruce stand. *Biomass and Bioenergy*, 35(8): 3328-3334.
- Wang, H. et al., 2020. Biochar Mitigates Greenhouse Gas Emissions from an Acidic Tea Soil. *Polish Journal of Environmental Studies*, 29(1): 323-330.
- Wang, J., Xiong, Z., Kuzyakov, Y., 2016a. Biochar stability in soil: meta-analysis of decomposition and priming effects. *GCB Bioenergy*, 8(3): 512-523.
- Wang, R. et al., 2017. Global forest carbon uptake due to nitrogen and phosphorus deposition from 1850 to 2100. *Global Change Biology*, 23(11): 4854-4872.
- Wang, Y., Li, M., 2018. Role of Biochar Amendment on Soil Carbon Mineralization and Microbial Biomass. *Journal of Geoscience and Environment Protection*, Vol.06No.11: 8.
- Wang, Y., Wei, Y., Sun, J., 2016b. Biochar Application Promotes Growth Parameters of Soybean and Reduces the Growth Difference. *Communications in Soil Science and Plant Analysis*, 47(12): 1493-1502.
- Wang, Y.P., Law, R.M., Pak, B., 2010. A global model of carbon, nitrogen and phosphorus cycles for the terrestrial biosphere. *Biogeosciences*, 7(7): 2261-2282.
- Weerasuriya, T.J., Pushpakumara, S., Cooray, P.I., 1993. Acidulated pegmatitic mica: A promising new multi-nutrient mineral fertilizer. *Fertilizer research*, 34(1): 67-77.
- Weng, Z.H. et al., 2017. Biochar built soil carbon over a decade by stabilizing rhizodeposits. *Nature Climate Change*, 7(5): 371-376.
- Werner, C., Schmidt, H., Gerten, D., Lucht, W., Kammann, C., 2018. Biogeochemical potential of biomass pyrolysis systems for limiting global warming to 1.5 C. *Environmental Research Letters*, 13(4): 044036.
- Whitfield, C.J., Reid, C., 2013. Predicting surface area of coarse-textured soils: Implications for weathering rates. *Canadian Journal of Soil Science*, 93(5): 621-630.
- Wilson, M., 2004. Weathering of the primary rock-forming minerals: processes, products and rates. *Clay Minerals*, 39(3): 233-266.
- Winter, J.D., 2001. *An Introduction to Igneous and Metamorphic Petrology*. Prentice Hall, Upper Saddle River, NJ, 347 pp.

- Wiseman, C.L.S., Püttmann, W., 2006. Interactions between mineral phases in the preservation of soil organic matter. *Geoderma*, 134(1): 109-118.
- Wösten, J.H.M., Pachepsky, Y.A., Rawls, W.J., 2001. Pedotransfer functions: bridging the gap between available basic soil data and missing soil hydraulic characteristics. *Journal of Hydrology*, 251(3): 123-150.
- Wright, S.J. et al., 2011. Potassium, phosphorus, or nitrogen limit root allocation, tree growth, or litter production in a lowland tropical forest. *Ecology*, 92(8): 1616-1625.
- Wu, H. et al., 2017. The interactions of composting and biochar and their implications for soil amendment and pollution remediation: a review. *Critical Reviews in Biotechnology*, 37(6): 754-764.
- Xu, N., Tan, G., Wang, H., Gai, X., 2016. Effect of biochar additions to soil on nitrogen leaching, microbial biomass and bacterial community structure. *European Journal of Soil Biology*, 74: 1-8.
- Yang, F. et al., 2018. Kaolinite Enhances the Stability of the Dissolvable and Undissolvable Fractions of Biochar via Different Mechanisms. *Environmental Science & Technology*, 52(15): 8321-8329.
- Yang, F., Zhao, L., Gao, B., Xu, X., Cao, X., 2016. The Interfacial Behavior between Biochar and Soil Minerals and Its Effect on Biochar Stability. *Environmental Science & Technology*, 50(5): 2264-2271.
- Yang, X., Post, W.M., Thornton, P.E., Jain, A.K., 2014a. Global Gridded Soil Phosphorus Distribution Maps at 0.5-degree Resolution. ORNL Distributed Active Archive Center.
- Yang, X., Thornton, P.E., Ricciuto, D.M., Post, W.M., 2014b. The role of phosphorus dynamics in tropical forests – a modeling study using CLM-CNP. *Biogeosciences*, 11(6): 1667-1681.
- Yasunari, T., 2020. The Uplift of the Himalaya-Tibetan Plateau and Human Evolution: An Overview on the Connection Among the Tectonics, Eco-Climate System and Human Evolution During the Neogene Through the Quaternary Period. In: Dimri, A.P., Bookhagen, B., Stoffel, M., Yasunari, T. (Eds.), *Himalayan Weather and Climate and their Impact on the Environment*. Springer International Publishing, Cham, pp. 281-305.
- Ye, J. et al., 2016. A Combination of Biochar–Mineral Complexes and Compost Improves Soil Bacterial Processes, Soil Quality, and Plant Properties. *Frontiers in Microbiology*, 7(372).
- Yousefpour, R., Nabel, J.E., Pongratz, J., 2019. Simulating growth-based harvest adaptive to future climate change. *Biogeosciences*, 16: 241-254.
- Yuan, J.-H., Xu, R.-K., Zhang, H., 2011. The forms of alkalis in the biochar produced from crop residues at different temperatures. *Bioresource technology*, 102(3): 3488-3497.
- Zaehle, S., Dalmonech, D., 2011. Carbon–nitrogen interactions on land at global scales: current understanding in modelling climate biosphere feedbacks. *Current Opinion in Environmental Sustainability*, 3(5): 311-320.
- Zhang, G., Kang, J., Wang, T., Zhu, C., 2018. Review and outlook for agromineral research in agriculture and climate mitigation. *Soil Research*, 56(2): 113-122.
- Zhao, X. et al., 2014. Effects of crop-straw biochar on crop growth and soil fertility over a wheat-millet rotation in soils of China. *Soil Use and Management*, 30(3): 311-319.
- Zhou, H. et al., 2018. Short-term biochar manipulation of microbial nitrogen transformation in wheat rhizosphere of a metal contaminated Inceptisol from North China plain. *Science of The Total Environment*, 640-641: 1287-1296.
- Zhou, H. et al., 2017. Changes in microbial biomass and the metabolic quotient with biochar addition to agricultural soils: A Meta-analysis. *Agriculture, Ecosystems & Environment*, 239: 80-89.
- Zhu, L.-x., Xiao, Q., Shen, Y.-f., Li, S.-q., 2017. Microbial functional diversity responses to 2 years since biochar application in silt-loam soils on the Loess Plateau. *Ecotoxicology and Environmental Safety*, 144: 578-584.
- Zhu, Q.-H., Peng, X.-H., Huang, T.-Q., Xie, Z.-B., Holden, N.M., 2014. Effect of Biochar Addition on Maize Growth and Nitrogen Use Efficiency in Acidic Red Soils. *Pedosphere*, 24(6): 699-708.

Appendix

A. Personal contribution to listed publications

Garcia, W. de O., Amann, T., and Hartmann, J.: Increasing biomass demand enlarges negative forest nutrient budget areas in wood export regions, *Scientific Reports*, 8, 5280, 10.1038/s41598-018-22728-5, 2018.

The author of this thesis actively participated on the study design, subsequent discussions, planning and writing, did the geochemical data compilation and all the calculations necessary for nutrient budgets.

Minx, J. C., Lamb, W. F., Callaghan, M. W., Fuss, S., Hilaire, J., Creutzig, F., Amann, T., Beringer, T., **Garcia, W. de O.**, and Hartmann, J.: Negative emissions—Part 1: Research landscape and synthesis, *Environmental Research Letters*, 13, 063001, 2018.

The author of this thesis actively participated on the writing and data collection for enhanced silicate rock Weathering and Ocean Fertilization for the review.

Fuss, S., Minx, J. C., Lamb, W. F., Callaghan, M. W., Hilaire, J., Creutzig, F., Amann, T., Beringer, T., **Garcia, W. de O.**, Hartmann, J., Khanna, T., Luderer, G., Nemet F, G., Rogelj, J., Smith, P., Vicente Vicente, J. L., Wilcox, J., and del Mar Zamora Dominguez, M.: Negative emissions—Part 2: Costs, potentials and side effects, *Environmental Research Letters*, 13, 063001, 2018.

The author of this thesis actively participated on the design, subsequent discussions, planning and writing of subsections 3.4 and 3.5.

Amann, T., Hartmann, J., Struyf, E., **Garcia, W. de O.**, Fischer, E. K., Janssens, I., Meire, P., and Schoelynck, J.: Enhanced Weathering and related element fluxes – a cropland mesocosm approach, *Biogeosciences*, 17, 103-119, 10.5194/bg-17-103-2020, 2020.

The author of this thesis contributed to the discussion of trace elements subsection 4.3.

Garcia, W. de O., Amann, T., Hartmann, J., Karstens, K., Popp, A., Boysen, L. R., Smith, P., and Goll, D.: Impacts of enhanced weathering on biomass production for negative emission technologies and soil hydrology, *Biogeosciences*, 17, 2107-2133, 10.5194/bg-17-2107-2020, 2020

The author of this thesis actively participated on the study design, subsequent discussions, planning and writing, compiled all the used data and conducted all the necessary calculations.

Garcia, W. de O., Amann, T., and Hartmann, J., Romero-Mujalli, G., Schmidt, H.-P., Hagemann, N.: Systematic Review: Effects of Biochar and terrestrial enhanced silicate rock weathering on soil and plant properties. (*in prep.*)

The author of this thesis compiled all the used data, implemented the statistical model and was responsible for the study design and writing the article.

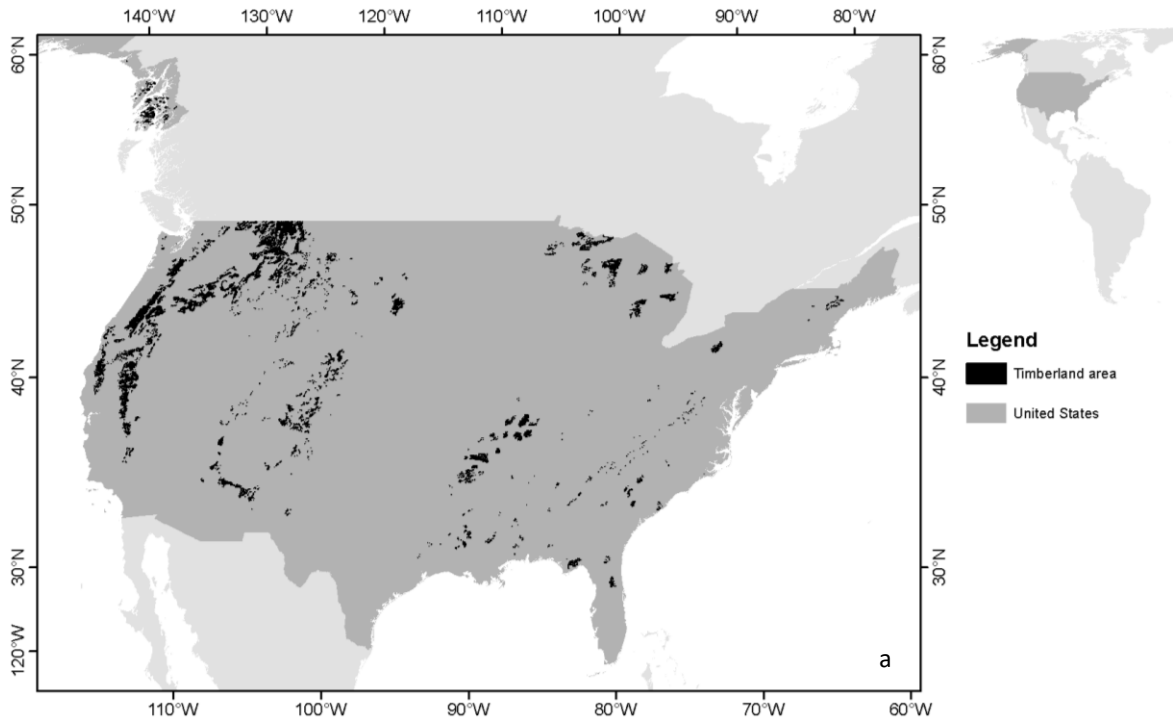
Spatially explicit nutrient budget for whole-tree harvest/clear-cut was investigated. The whole-tree nutrient contribution was accounted by the nutrient content sum within: dead wood, stem, bole, branch, twig, and foliage based on each compartment fraction. The spatially averaged nutrient loss and supply diagrams are presented in the main text and are used for estimating specific harvest rates nutritional requirements (no spatial distribution considered) by visualizing the harvest rate nutrient losses and the possible geogenic (weathering plus atmospheric deposition) nutrient supply from different lithological classes.

Detailed calculation procedures for spatially explicit nutrient budgets and spatially averaged diagrams are described in the sections B) the nutrient loss, C) the nutrient supply, and D) presenting the spatially explicit analysis for deficits per considered nutrient, in addition to the diagrams presented in the main text.

B. Timberland wood composition and nutrient loss

Spatially explicit information for timberland area and harvest rates were obtained from a U.S. Forest Service Service (2016) shapefile (Fig. S 1a). The spatially explicit harvest rates are divided in seven classes with minima and maxima harvest rate values according to U.S. Forest Service¹ as follow: <140, 140 – 343, 350 – 588, 595 – 833, 840 – 1148, 1154 – 1571 and >1574 m³ km⁻². One considered group for analysis represents minimal harvest rates per class with: 70 (the minimum reported value half), 140, 350, 595, 840, 1155 and 1575 m³ km⁻². The second group represents the maximal harvest rates per class: 139 (for <140), 343, 588, 833, 1148, 1567 and 3150 m³ km⁻² (with 3150 m³ km⁻² being 2 times higher than 1574 m³ km⁻², the reported upper boundary). The practiced harvest rates for minimum and maximum nutrient loss were used in $Class_i$ from Eq. (7) in the main text for quantifying the spatially explicit nutrient loss and for diagrams representing harvest rate averaged nutrient loss (Fig. S 1b).

To assess the spatially explicit tree-species within timberland areas, the timberland distribution shapefile was merged with the forest cover type raster-file from the U.S. Forest Service & U.S. Geological Survey (2000). The 22 tree-species identified within the mapped timberland area had the chemical composition derived from the Tree Chemistry Database (Pardo et al., 2005). The green wood density was derived from the U.S. Forest Products Laboratory (2010) for each of 22 tree-species. In some localities, more than one tree-species was described within an area, which originates a composed tree-species name (e.g., Fir-Spruce). In those cases, all data concerning the different tree-species were used to calculate the 25th and the 75th quartiles and median values for tree chemistry and density. When a tree-species could not be identified within the chemistry or density databases, values assuming the 25th/75th quartiles and median of all trees in the databases were used (Fig. S 2). This occurred for the Chaparral, Douglas-fir, Elm-ash-cottonwood, Hemlock-Sitka spruce, Larch, Oak-hickory, Redwood, Loblolly-shortleaf-pine and Pinyon-juniper entries for chemistry and Pinyon-juniper, entries for density (Table S 1).



Spatially explicit timberland harvest statistics

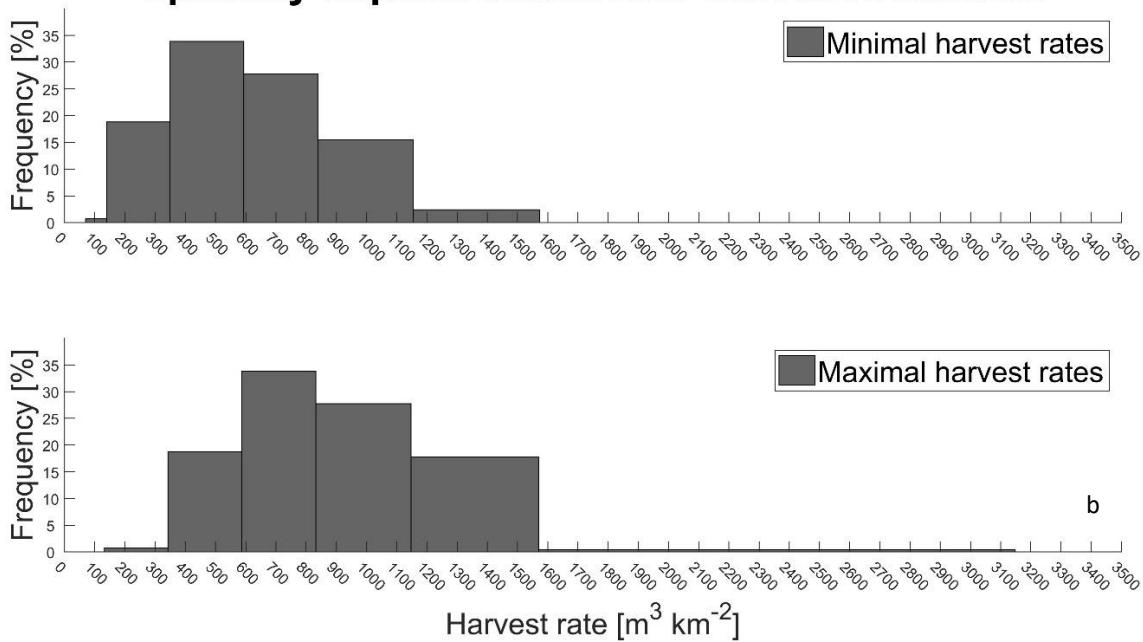


Fig. S 1: a) Timberland distribution area according to U.S. Forest Service (2016) across the continental U.S. (total area: 37,536 km²). Pixel outline width border of 0.01. Map generated with ESRI ArcGIS ver. 10.3.1 (<http://www.esri.com>). b) Minimal and maximal harvest rate frequencies considering U.S. Forest Service (Service, 2016) explicit data. Within the minimal harvest rate group, the most frequent harvest rates are 350 and 595 m³ km⁻². For the maximum harvest rate group, 588 and 833 m³ km⁻² are the most frequent harvest rates.

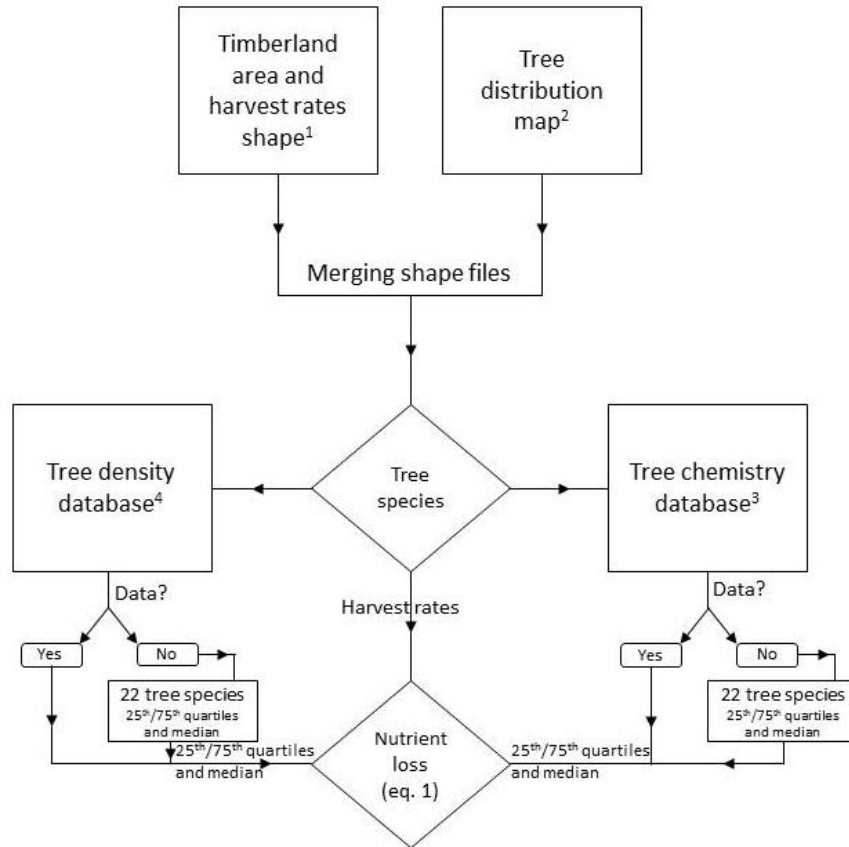


Fig. S 2: Workflow for obtaining the spatially explicit 25th and the 75th quartiles and median nutrient loss within timberland areas by using spatially explicit harvest rates, whole tree-species chemistry and density database for green wood. For the spatially averaged diagrams, the previous steps were followed, but instead of using spatially explicit harvest rates, the values within minimal and maximal harvest rate groups were used for each one of the 22 tree-species. The final values were averaged and used on the diagrams.

B1) Compartment weighted chemical composition per considered tree-species

Information concerning the chemistry and mass fraction for the following tree compartments were available: dead wood, stem, bole, branch, twig, and foliage. For the considered timberland clear-cut scenarios, the whole-tree chemical composition was estimated by Eq. (S 1):

$$C_w = \text{perct}\left(\frac{\sum(tf \cdot tcc)}{100}\right), \quad (\text{S } 1)$$

Where C_w is the exported whole-tree chemistry fraction (Table S 1) for the 25th and the 75th quartiles and median of each nutrient w [-] within the chosen tree-species. The 25th and the 75th quartiles and median values were obtained considering all the tree compartments listed before (Table S 2) for ‘n’ samples (Table S 1). C_w is used in Eq. (6). tcc [weight-%] is the tree compartment chemistry of nutrient w (e.g., twig, *etc.*) and tf [-] (Table S 3) is the tree compartment fraction (e.g., twig, *etc.*). tcc and tf were derived from tree chemistry database (Pardo et al., 2005).

B2) Estimating the spatially explicit element loss and applied minima and maxima scenarios

Minima and maxima spatially explicit nutrient loss N_l (Eq. (6)) using harvested biomass area normalized mass M_l (Eq. (7)) was estimated by using the following parameter settings affecting the elements’ export rate:

1) The 25th and the 75th quartiles from the spatially explicit exported whole nutrient fraction C_w [-] (Eq. (S 1)) per tree-species and considered element are used here as respectively minima and maxima values for the discussion (cf., Table S 1).

2) Minima and maxima values of each spatially explicit harvest rate class $Class_i$ [$m^3 km^{-2}$] named above (cf., First paragraph Appendix B).

3) The 25th and the 75th quartiles from wood density ρ_{wood} [$kg m^{-3}$] per tree-species used as minima and maxima case values for the discussion (cf., Table S 1).

Sometimes a mismatching between geospatial information sources was observed. Areas were marked as non-forest within the forest type map (Survey, 2000) despite of mapped presence of timberland by the U.S. Forest Service (Service, 2016). In this case, the 25th and the 75th quartiles and median values for whole-tree chemical composition and green wood density of all the 22 considered tree-species were assumed, which were then multiplied by the minimum or maximum spatially explicit harvest rates reported for the mapped timberland area.

B3) Estimating the nutrient loss for different harvest rates

Like the spatially explicit nutrient loss, the nutrient loss for a harvest rate was calculated by Eq. (6) and Eq. (7). Minimal and maximal harvest rate groups' values (cf., First paragraph Appendix B) were used as harvest rate class ($Class_i$ in Eq. (7)), allowing for an analysis that does not consider spatially explicit data. The reported 25th and the 75th quartiles and median green wood density values of each tree-species within timberland area were used as ρ_{wood} (Table S 1). The 25th and the 75th quartiles and median values for whole-tree chemical compound fraction for each tree-species were used as C_w (Table S 1). Minima and maxima values for nutrient loss were obtained for all 22-tree-species. The nutrient losses of each harvest rate and tree-species were grouped together and averaged. The resulting value was used for nutrient loss prediction. In the main text Fig. 1 and Fig. 2, harvest rate nutrient losses are presented by the grey horizontal boxes.

Table S 1: Exported nutrient content statistics for each tree-specie for clear-cut obtained by equation SI-1, considering the nutrient content within dead wood, stem, bole, branch, twig, and foliage. Wood density for 25th, 75th quartiles and median of each considered tree-specie.

	Ca ³				Mg ³				K ³				P ³				Density ρ_{wood}^4									
Unit	[WT%]																				[kg m ⁻³]					
Tree specie	25 th	med	75 th	n	25 th	med	75 th	n	25 th	med	75 th	N	25 th	med	75 th	n	25 th	med	75 th	n	n_tf	n_tcc				
Aspen-birch	0.22	0.30	2.02	10	0.03	0.04	0.07	10	0.08	0.14	0.20	10	0.03	0.03	0.03	10	424	453	474	5	10	10				
Chaparral*	0.20	0.28	0.35	26	0.02	0.03	0.04	26	0.06	0.09	0.12	26	0.01	0.03	0.03	26	460	460	460	1	0	0				
Douglas-fir*	0.20	0.28	0.35	26	0.02	0.03	0.04	26	0.06	0.09	0.12	26	0.01	0.03	0.03	26	450	455	460	4	0	0				
Elm-ash-cottonwood*	0.20	0.28	0.35	26	0.02	0.03	0.04	26	0.06	0.09	0.12	26	0.01	0.03	0.03	26	421	440	479	11	0	0				
Fir-spruce	0.15	0.27	0.32	9	0.02	0.03	0.03	9	0.05	0.09	0.11	9	0.01	0.03	0.04	9	333	365	371	12	9	9				
Hemlock-Sitka spruce*	0.20	0.28	0.35	26	0.02	0.03	0.04	26	0.06	0.09	0.12	26	0.01	0.03	0.03	26	370	403	404	11	0	0				
Larch*	0.20	0.28	0.35	26	0.02	0.03	0.04	26	0.06	0.09	0.12	26	0.01	0.03	0.03	26	480	480	480	1	0	0				
Loblolly-shortleaf pine*	0.20	0.28	0.35	26	0.02	0.03	0.04	26	0.06	0.09	0.12	26	0.01	0.03	0.03	26	380	430	470	32	0	0				
Lodgepole pine	0.09	0.23	0.37	4	0.02	0.02	0.03	4	0.03	0.05	0.06	4	0.01	0.02	0.03	4	380	430	470	16	4	4				
Longleaf-slash pine	0.09	0.23	0.37	4	0.02	0.02	0.03	4	0.03	0.05	0.06	4	0.01	0.02	0.03	4	380	430	470	32	4	4				
Maple-beech-birch	0.20	0.22	0.28	7	0.02	0.03	0.03	7	0.06	0.09	0.11	7	0.01	0.02	0.03	7	499	533	559	9	7	7				
Oak-gum-cypress	0.27	0.27	0.27	1	0.03	0.03	0.03	1	0.09	0.09	0.09	1	0.03	0.03	0.03	1	490	500	510	18	1	1				
Oak-hickory*	0.20	0.28	0.35	26	0.02	0.03	0.04	26	0.06	0.09	0.12	26	0.01	0.03	0.03	26	580	598	620	25	0	0				
Oak-pine	0.09	0.23	0.37	4	0.02	0.02	0.03	4	0.03	0.05	0.06	4	0.01	0.02	0.03	4	470	505	535	33	4	4				
Pinyon-juniper*	0.20	0.28	0.35	26	0.02	0.03	0.04	26	0.06	0.09	0.12	26	0.01	0.03	0.03	26	380	460	560	117	0	0				
Ponderosa pine	0.09	0.23	0.37	4	0.02	0.02	0.03	4	0.03	0.05	0.06	4	0.01	0.02	0.03	4	380	430	470	16	4	4				
Redwood*	0.20	0.28	0.35	26	0.02	0.03	0.04	26	0.06	0.09	0.12	26	0.01	0.03	0.03	26	350	380	440	3	0	0				
Spruce-fir	0.15	0.27	0.32	9	0.02	0.03	0.03	9	0.05	0.09	0.11	9	0.01	0.03	0.04	9	333	365	371	12	9	9				
Western hardwoods	0.09	0.23	0.37	4	0.02	0.02	0.03	4	0.03	0.05	0.06	4	0.01	0.02	0.03	4	427	435	443	20	4	4				
Western white pine	0.09	0.23	0.37	4	0.02	0.02	0.03	4	0.03	0.05	0.06	4	0.01	0.02	0.03	4	380	430	470	16	4	4				
White-red-jack pine	0.17	0.35	0.39	3	0.02	0.03	0.03	3	0.03	0.06	0.06	3	0.01	0.03	0.03	3	380	430	470	48	3	3				
Alaska Spruce-birch	0.21	0.26	0.29	10	0.02	0.03	0.03	10	0.06	0.09	0.10	10	0.03	0.03	0.03	10	414	460	480	8	10	10				

n is the number of samples used in the statistic. The values for Ca, Mg, K, and P correspond to C_w in main text equation 1. For areas with more than one tree-species 25th/75th and median values were used as C_w . *Trees without tree compartment fraction information, in those cases, average C_w values were used. n_tf and n_tcc correspond to the number of trees with tree compartment fraction information and tree compartment chemistry respectively. 3 - (Pardo et al., 2005); 4 - (Laboratory, 2010).

Table S 2: Whole tree chemistry. Values obtained considering the nutrient content and fraction of different tree compartments (equation SI-01). Each row represents the calculated fraction of different trees using the Tree Chemistry Database³. The raw table is given in the excel supplement.

Tree specie	Ca	Mg	K	P
Unit	[-]			
Aspen-birch	2.6E-03	3.8E-04	8.9E-04	3.0E-04
	1.7E-03	1.9E-04	4.0E-04	9.8E-05
	2.2E-03	2.8E-04	6.4E-04	2.7E-04
	2.1E-03	2.3E-04	1.1E-03	2.7E-04
	3.4E-03	4.7E-04	1.8E-03	3.2E-04
	2.7E-03	3.0E-04	8.2E-04	1.4E-04
	5.2E-02	5.8E-04	2.0E-03	3.2E-04
	3.6E-02	8.7E-04	7.1E-03	4.8E-04
	2.0E-02	7.2E-04	1.9E-03	3.5E-04
3.7E-03	6.7E-04	2.2E-03	3.6E-04	
Chaparral*	-	-	-	-
Douglas-fir*	-	-	-	-
Elm-ash-cottonwood*	-	-	-	-
Fir-spruce	1.6E-03	2.1E-04	9.2E-04	9.7E-05
	3.1E-03	4.0E-04	1.6E-03	4.6E-04
	3.0E-05	3.8E-06	2.0E-05	7.4E-06
	4.9E-03	2.3E-04	6.3E-04	7.8E-04
	3.5E-03	2.9E-04	1.2E-03	3.9E-04
	1.3E-03	1.1E-04	2.7E-04	7.5E-05
	2.6E-03	2.8E-04	8.7E-04	2.5E-04
	2.9E-03	3.2E-04	9.2E-04	2.6E-04
	2.7E-03	2.7E-04	1.0E-03	2.8E-04
Hemlock-Sitka spruce*	-	-	-	-
Larch*	-	-	-	-

Table S 2: Whole tree chemistry. Values obtained considering the nutrient content and fraction of different tree compartments (equation SI-01). Each row represents the calculated fraction of different trees using the Tree Chemistry Database³. The raw table is given in the excel supplement.

Tree specie	Ca	Mg	K	P
Unit	[-]			
Loblolly-shortleaf pine*	-	-	-	-
Lodgepole pine	1.1E-03	1.6E-04	1.9E-04	9.3E-05
	4.0E-03	2.9E-04	5.8E-04	3.1E-04
	3.5E-03	3.2E-04	5.7E-04	3.2E-04
	7.8E-04	1.6E-04	3.7E-04	9.4E-05
Longleaf-slash pine	1.1E-03	1.6E-04	1.9E-04	9.3E-05
	4.0E-03	2.9E-04	5.8E-04	3.1E-04
	3.5E-03	3.2E-04	5.7E-04	3.2E-04
	7.8E-04	1.6E-04	3.7E-04	9.4E-05
Maple-beech-birch	2.0E-03	1.8E-04	5.8E-04	1.0E-04
	2.8E-03	2.6E-04	1.1E-03	2.2E-04
	3.1E-03	3.7E-04	1.1E-03	2.3E-04
	2.6E-03	3.8E-04	8.9E-04	3.0E-04
	1.7E-03	1.9E-04	4.0E-04	9.8E-05
	2.2E-03	2.8E-04	6.4E-04	2.7E-04
Oak-gum-cypress	2.1E-03	2.3E-04	1.1E-03	2.7E-04
	2.7E-03	3.2E-04	8.5E-04	2.6E-04
Oak-hickory*	-	-	-	-
Oak-pine	1.1E-03	1.6E-04	1.9E-04	9.3E-05
	4.0E-03	2.9E-04	5.8E-04	3.1E-04
	3.5E-03	3.2E-04	5.7E-04	3.2E-04
	7.8E-04	1.6E-04	3.7E-04	9.4E-05
Pinyon-juniper*	-	-	-	-
Ponderosa pine	1.1E-03	1.6E-04	1.9E-04	9.3E-05

Table S 2: Whole tree chemistry. Values obtained considering the nutrient content and fraction of different tree compartments (equation SI-01). Each row represents the calculated fraction of different trees using the Tree Chemistry Database³. The raw table is given in the excel supplement.

Tree specie	Ca	Mg	K	P
Unit	[-]			
	4.0E-03	2.9E-04	5.8E-04	3.1E-04
	3.5E-03	3.2E-04	5.7E-04	3.2E-04
	7.8E-04	1.6E-04	3.7E-04	9.4E-05
Redwood*	-	-	-	-
Spruce-fir	1.6E-03	2.1E-04	9.2E-04	9.7E-05
	3.1E-03	4.0E-04	1.6E-03	4.6E-04
	3.0E-05	3.8E-06	2.0E-05	7.4E-06
	4.9E-03	2.3E-04	6.3E-04	7.8E-04
	3.5E-03	2.9E-04	1.2E-03	3.9E-04
	1.3E-03	1.1E-04	2.7E-04	7.5E-05
	2.6E-03	2.8E-04	8.7E-04	2.5E-04
	2.9E-03	3.2E-04	9.2E-04	2.6E-04
	2.7E-03	2.7E-04	1.0E-03	2.8E-04
Western hardwoods	1.1E-03	1.6E-04	1.9E-04	9.3E-05
	4.0E-03	2.9E-04	5.8E-04	3.1E-04
	3.5E-03	3.2E-04	5.7E-04	3.2E-04
	7.8E-04	1.6E-04	3.7E-04	9.4E-05
Western white pine	1.1E-03	1.6E-04	1.9E-04	9.3E-05
	4.0E-03	2.9E-04	5.8E-04	3.1E-04
	3.5E-03	3.2E-04	5.7E-04	3.2E-04
	7.8E-04	1.6E-04	3.7E-04	9.4E-05
White-red-jack pine	1.1E-03	1.6E-04	1.9E-04	9.3E-05
	4.0E-03	2.9E-04	5.8E-04	3.1E-04
	3.5E-03	3.2E-04	5.7E-04	3.2E-04

Table S 2: Whole tree chemistry. Values obtained considering the nutrient content and fraction of different tree compartments (equation SI-01). Each row represents the calculated fraction of different trees using the Tree Chemistry Database³. The raw table is given in the excel supplement.

Tree specie	Ca	Mg	K	P
Unit	[-]			
Alaska Spruce-birch	2.6E-03	3.8E-04	8.9E-04	3.0E-04
	1.7E-03	1.9E-04	4.0E-04	9.8E-05
	2.2E-03	2.8E-04	6.4E-04	2.7E-04
	2.1E-03	2.3E-04	1.1E-03	2.7E-04
	4.9E-03	2.3E-04	6.3E-04	7.8E-04
	3.5E-03	2.9E-04	1.2E-03	3.9E-04
	1.3E-03	1.1E-04	2.7E-04	7.5E-05
	2.6E-03	2.8E-04	8.7E-04	2.5E-04
	2.9E-03	3.2E-04	9.2E-04	2.6E-04
	2.7E-03	2.7E-04	1.0E-03	2.8E-04
All trees	1.6E-03	2.1E-04	9.2E-04	9.7E-05
	3.1E-03	4.0E-04	1.6E-03	4.6E-04
	1.1E-03	1.6E-04	1.9E-04	9.3E-05
	4.0E-03	2.9E-04	5.8E-04	3.1E-04
	3.5E-03	3.2E-04	5.7E-04	3.2E-04
	7.8E-04	1.6E-04	3.7E-04	9.4E-05
	2.0E-03	1.8E-04	5.8E-04	1.0E-04
	2.8E-03	2.6E-04	1.1E-03	2.2E-04
	3.1E-03	3.7E-04	1.1E-03	2.3E-04
	1.7E-03	1.9E-04	4.0E-04	9.8E-05
2.2E-03	2.8E-04	6.4E-04	2.7E-04	
2.1E-03	2.3E-04	1.1E-03	2.7E-04	
3.0E-05	3.8E-06	2.0E-05	7.4E-06	
4.9E-03	2.3E-04	6.3E-04	7.8E-04	

Table S 2: Whole tree chemistry. Values obtained considering the nutrient content and fraction of different tree compartments (equation SI-01). Each row represents the calculated fraction of different trees using the Tree Chemistry Database³. The raw table is given in the excel supplement.

Tree specie	Ca	Mg	K	P
Unit	[-]			
	3.5E-03	2.9E-04	1.2E-03	3.9E-04
	1.3E-03	1.1E-04	2.7E-04	7.5E-05
	2.6E-03	2.8E-04	8.7E-04	2.5E-04
	2.9E-03	3.2E-04	9.2E-04	2.6E-04
	2.7E-03	2.7E-04	1.0E-03	2.8E-04
	3.4E-03	4.7E-04	1.8E-03	3.2E-04
	2.7E-03	3.0E-04	8.2E-04	1.4E-04
	5.2E-02	5.8E-04	2.0E-03	3.2E-04
	3.6E-02	8.7E-04	7.1E-03	4.8E-04
	2.0E-02	7.2E-04	1.9E-03	3.5E-04
	3.7E-03	6.7E-04	2.2E-03	3.6E-04
	2.7E-03	3.2E-04	8.5E-04	2.6E-04

Tree-species without information concerning chemistry or fractions. In these cases, the information concerning all tree-species within interest area, which had values for element fractions and chemistry, was used. All tree-species values are reported in this table as "All trees" and they were used for trees with asterisk ().

Table S 3: Tree compartment fraction. Values used for quantifying the nutrient fractions for whole-tree harvest. Each row represents a different compartment fraction based from different samples³. The raw table is given in the excel supplement.

Tree specie	Dead wood	Stem	Bark	Bole	Branch	Twig	Foliage
Unit	[-]						
	0.016	0	0.086	0.661	0.215	0	0.022
	0.006	0	0.113	0.646	0.199	0.036	0
	0.021	0	0.107	0.684	0.169	0	0.019
	0	0	0.108	0.727	0.142	0	0.023
Aspen-birch	0.051	0	0.152	0.583	0.191	0	0.023
	0.036	0	0.156	0.661	0.124	0.024	0
	0.013	0	0.241	0.607	0.095	0.012	0.032
	0.059	0	0.219	0.487	0.168	0.02	0.047
	0.054	0	0.191	0.591	0.138	0.008	0.018
	0.053	0	0.176	0.584	0.166	0	0.021
Chaparral*	-	-	-	-	-	-	-
Douglas-fir*	-	-	-	-	-	-	-
Elm-ash-cottonwood*	-	-	-	-	-	-	-
	0.067	0	0.082	0.559	0.12	0.172	0
	0.06	0.018	0.093	0.486	0.188	0	0.158
	0	0	0	0	0.0023	0	0.0022
	0.106	0	0.102	0.402	0.228	0	0.161
Fir-spruce	0.12	0	0.05	0.56	0.15	0	0.12
	0.125	0	0.061	0.486	0.162	0.167	0
	0.079	0.014	0.08	0.636	0.114	0	0.077
	0.089	0.015	0.084	0.575	0.158	0	0.085
	0.047	0.018	0.091	0.621	0.128	0	0.095
Hemlock-Sitka spruce*	-	-	-	-	-	-	-

Table S 3: Tree compartment fraction. Values used for quantifying the nutrient fractions for whole-tree harvest. Each row represents a different compartment fraction based from different samples³. The raw table is given in the excel supplement.

Tree specie	Dead wood	Stem	Bark	Bole	Branch	Twig	Foliage
Unit	[-]						
Larch*	-	-	-	-	-	-	-
Loblolly-shortleaf pine*	-	-	-	-	-	-	-
Lodgepole pine	0.017	0	0.063	0.756	0.114	0.05	0
	0.06	0	0.1	0.57	0.18	0	0.09
	0.106	0	0.119	0.542	0.137	0	0.096
	0.065	0	0.086	0.609	0.178	0.061	0
Longleaf-slash pine	0.017	0	0.063	0.756	0.114	0.05	0
	0.06	0	0.1	0.57	0.18	0	0.09
	0.106	0	0.119	0.542	0.137	0	0.096
	0.065	0	0.086	0.609	0.178	0.061	0
Maple-beech-birch	0.023	0	0.085	0.64	0.198	0.055	0
	0.032	0	0.088	0.68	0.18	0	0.02
	0.025	0	0.086	0.684	0.185	0	0.02
	0.016	0	0.086	0.661	0.215	0	0.022
	0.006	0	0.113	0.646	0.199	0.036	0
	0.021	0	0.107	0.684	0.169	0	0.019
	0	0	0.108	0.727	0.142	0	0.023
Oak-gum-cypress	0	0.033	0.078	0.801	0.088	0	0
Oak-hickory*	-	-	-	-	-	-	-
Oak-pine	0.017	0	0.063	0.756	0.114	0.05	0
	0.06	0	0.1	0.57	0.18	0	0.09
	0.106	0	0.119	0.542	0.137	0	0.096
	0.065	0	0.086	0.609	0.178	0.061	0

Table S 3: Tree compartment fraction. Values used for quantifying the nutrient fractions for whole-tree harvest. Each row represents a different compartment fraction based from different samples³. The raw table is given in the excel supplement.

Tree specie	Dead wood	Stem	Bark	Bole	Branch	Twig	Foliage
Unit	[-]						
Pinyon-juniper*	-	-	-	-	-	-	-
Ponderosa pine	0.017	0	0.063	0.756	0.114	0.05	0
	0.06	0	0.1	0.57	0.18	0	0.09
	0.106	0	0.119	0.542	0.137	0	0.096
	0.065	0	0.086	0.609	0.178	0.061	0
Redwood*	-	-	-	-	-	-	-
Spruce-fir	0.067	0	0.082	0.559	0.12	0.172	0
	0.06	0.018	0.093	0.486	0.188	0	0.158
	0	0	0	0	0.0023	0	0.0022
	0.106	0	0.102	0.402	0.228	0	0.161
	0.12	0	0.05	0.56	0.15	0	0.12
	0.125	0	0.061	0.486	0.162	0.167	0
	0.079	0.014	0.08	0.636	0.114	0	0.077
0.089	0.015	0.084	0.575	0.158	0	0.085	
Western hardwoods	0.047	0.018	0.091	0.621	0.128	0	0.095
	0.017	0	0.063	0.756	0.114	0.05	0
	0.06	0	0.1	0.57	0.18	0	0.09
	0.106	0	0.119	0.542	0.137	0	0.096
Western white pine	0.065	0	0.086	0.609	0.178	0.061	0
	0.017	0	0.063	0.756	0.114	0.05	0
	0.06	0	0.1	0.57	0.18	0	0.09
	0.106	0	0.119	0.542	0.137	0	0.096
	0.065	0	0.086	0.609	0.178	0.061	0
	0.017	0	0.063	0.756	0.114	0.05	0

Table S 3: Tree compartment fraction. Values used for quantifying the nutrient fractions for whole-tree harvest. Each row represents a different compartment fraction based from different samples³. The raw table is given in the excel supplement.

Tree specie	Dead wood	Stem	Bark	Bole	Branch	Twig	Foliage
Unit	[-]						
White-red-jack pine	0.06	0	0.1	0.57	0.18	0	0.09
	0.106	0	0.119	0.542	0.137	0	0.096
Alaska Spruce-birch	0.016	0	0.086	0.661	0.215	0	0.022
	0.006	0	0.113	0.646	0.199	0.036	0
	0.021	0	0.107	0.684	0.169	0	0.019
	0	0	0.108	0.727	0.142	0	0.023
	0.106	0	0.102	0.402	0.228	0	0.161
	0.12	0	0.05	0.56	0.15	0	0.12
	0.125	0	0.061	0.486	0.162	0.167	0
	0.079	0.014	0.08	0.636	0.114	0	0.077
	0.089	0.015	0.084	0.575	0.158	0	0.085
	0.047	0.018	0.091	0.621	0.128	0	0.095
	All trees	0.067	0	0.082	0.559	0.12	0.172
0.06		0.018	0.093	0.486	0.188	0	0.158
0.017		0	0.063	0.756	0.114	0.05	0
0.06		0	0.1	0.57	0.18	0	0.09
0.106		0	0.119	0.542	0.137	0	0.096
0.065		0	0.086	0.609	0.178	0.061	0
0.023		0	0.085	0.64	0.198	0.055	0
0.032		0	0.088	0.68	0.18	0	0.02
0.025		0	0.086	0.684	0.185	0	0.02
0.006		0	0.113	0.646	0.199	0.036	0
0.021		0	0.107	0.684	0.169	0	0.019

Table S 3: Tree compartment fraction. Values used for quantifying the nutrient fractions for whole-tree harvest. Each row represents a different compartment fraction based from different samples³. The raw table is given in the excel supplement.

Tree specie	Dead wood	Stem	Bark	Bole	Branch	Twig	Foliage
Unit	[-]						
	0	0	0.108	0.727	0.142	0	0.023
	0	0	0	0	0.0023	0	0.0022
	0.106	0	0.102	0.402	0.228	0	0.161
	0.12	0	0.05	0.56	0.15	0	0.12
	0.125	0	0.061	0.486	0.162	0.167	0
	0.079	0.014	0.08	0.636	0.114	0	0.077
	0.089	0.015	0.084	0.575	0.158	0	0.085
	0.047	0.018	0.091	0.621	0.128	0	0.095
	0.051	0	0.152	0.583	0.191	0	0.023
	0.036	0	0.156	0.661	0.124	0.024	0
	0.013	0	0.241	0.607	0.095	0.012	0.032
	0.059	0	0.219	0.487	0.168	0.02	0.047
	0.054	0	0.191	0.591	0.138	0.008	0.018
	0.053	0	0.176	0.584	0.166	0	0.021
	0	0.033	0.078	0.801	0.088	0	0

Tree-species without information concerning chemistry or fractions. In these cases, information concerning all tree-species within interest area, which had values for element fractions and chemistry, was used. All tree-species values are reported in this table as "All trees" and they were used for obtaining the 25th/75th and median nutrient values of trees marked by an asterisk ().

C. Nutrient Supply

For timberland areas, total atmospheric deposition rates and weathering nutrient supply are considered as different nutrient sources. For regions in which the weathering rates reported by Hartmann et al. (2014b) were low (Fig. S 7), or depending on the lithological class geochemistry, atmospheric deposition is the main Ca, Mg, K, and P source to the system. To show the nutrient contribution from the different sources, maps for the difference between the atmospheric deposition rates and weathering nutrient fluxes are presented (Fig. S 9a –Fig. S 16a). Special attention was given to the nutrient source contribution within timberland areas. Extra frequency diagrams presenting the atmospheric or weathering nutrient contribution within timberland areas are given in (Fig. S 9a – Fig. S 16a).

C1) Total atmospheric deposition

Total (wet + dry) atmospheric chemical deposition maps from the National Atmospheric Deposition Program (2016), cf., Schwede and Lear (2014), were used to quantify the median U.S. continental atmospheric deposition. Ca, Mg, and K were the considered elements for a deposition range for years 2000 to 2015 (Fig. S 3 to Fig. S 5) was considered. The respective Mg, Ca, and K minima and maxima deposition values are: $5.5 - 1.7 \times 10^3$, $21 - 2.7 \times 10^3$, and $6.2 - 2.7 \times 10^2 \text{ kg km}^{-2} \text{ a}^{-1}$. The atmospheric deposition is spatially heterogeneous, but patterns are identifiable. For Ca, the highest depositions occur, in their majority, within longitudes 100°W and 120°W . While the atmospheric deposition for K is higher on the U.S. Eastern part, comprehending longitudes between 80°W and 120°W . For Mg, the highest atmospheric deposition concentrations are observed over the entire U.S. coast. Phosphorus total deposition (Mahowald et al., 2008) was obtained from a global simulation. The reported depositional values within U.S. were $0.1 - 4.1 \text{ kg km}^{-2} \text{ a}^{-1}$, with the highest values located on the Eastern U.S. (Fig. S 6).

Resulting median Ca, Mg, K, and P raster files (Fig. S 3 to Fig. S 6) were overlaid to the timberland distribution maps (Fig. S 2) and to the GLIM database to obtain the interest area atmospheric deposition values. By this, it was possible to quantify the spatially explicit and averaged atmospheric nutrient deposition rates within each lithological class.

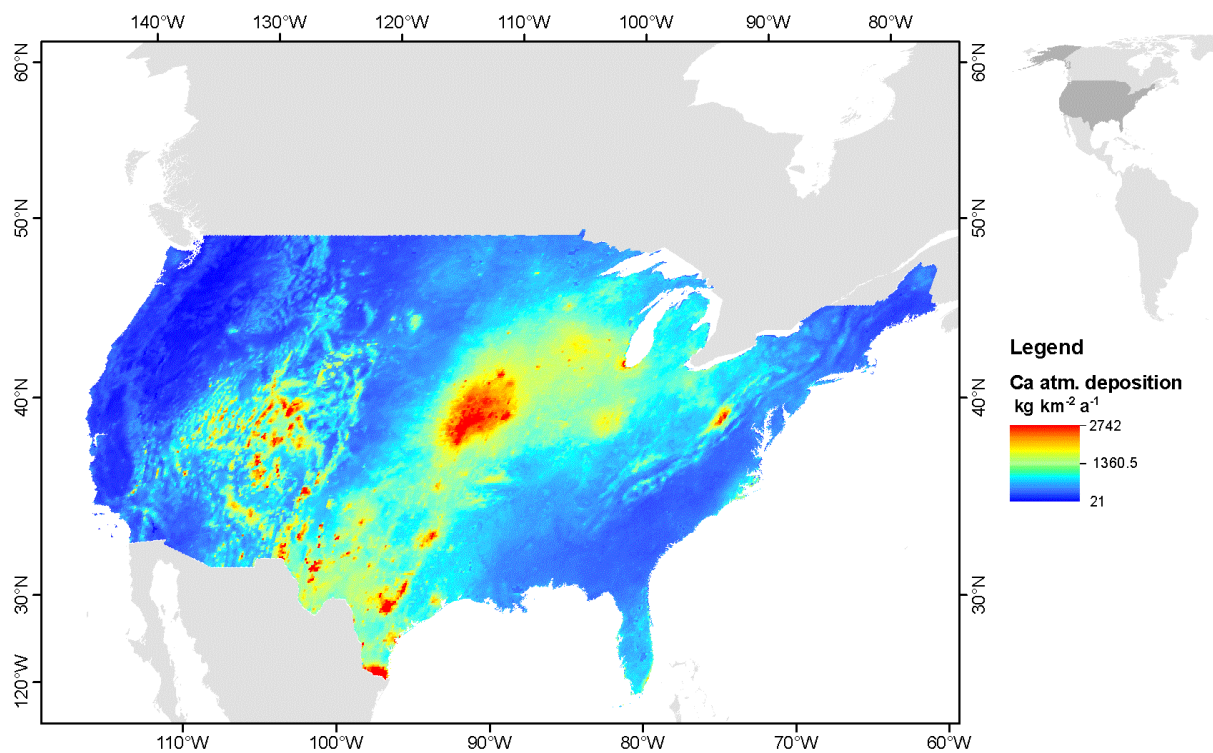


Fig. S 3: Total atmospheric Ca deposition [$\text{kg km}^{-1} \text{a}^{-1}$] for U.S. (National Atmospheric Deposition Program, 2016). Map generated with ESRI ArcGIS ver. 10.3.1 (<http://www.esri.com>).

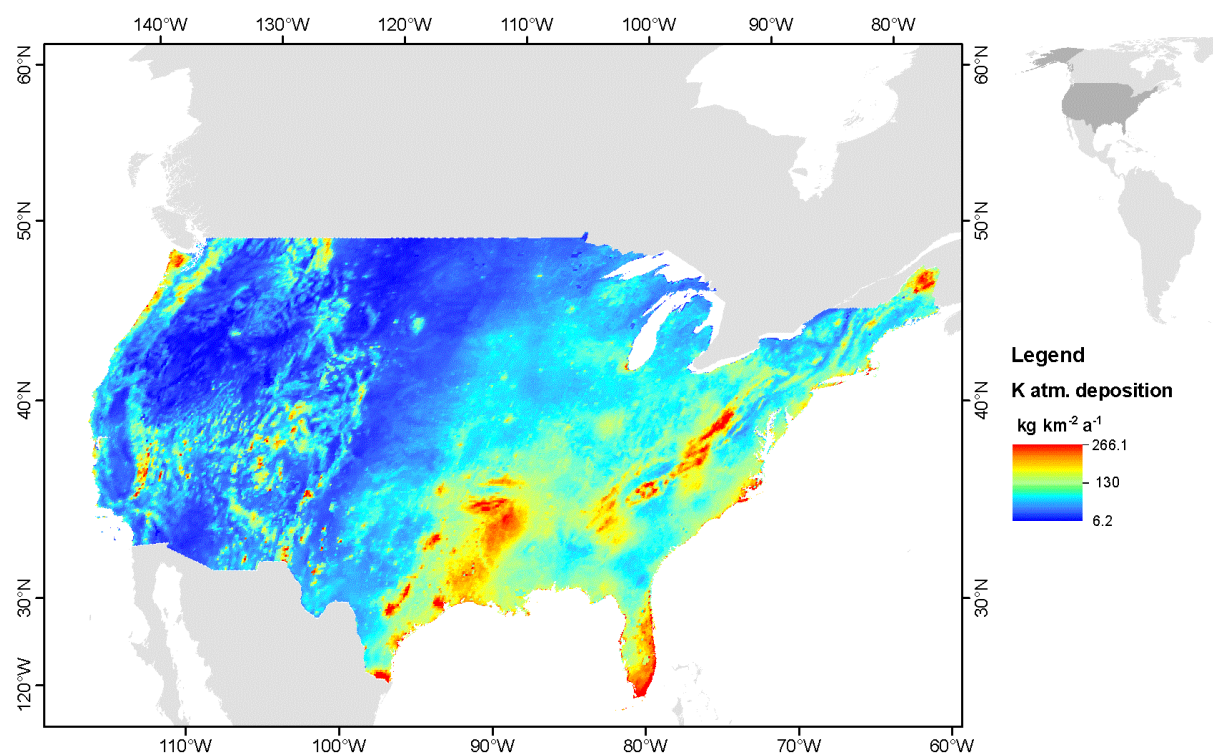


Fig. S 4: Total atmospheric K deposition [$\text{kg km}^{-1} \text{a}^{-1}$] for U.S. (National Atmospheric Deposition Program, 2016). Map generated with ESRI ArcGIS ver. 10.3.1 (<http://www.esri.com>).

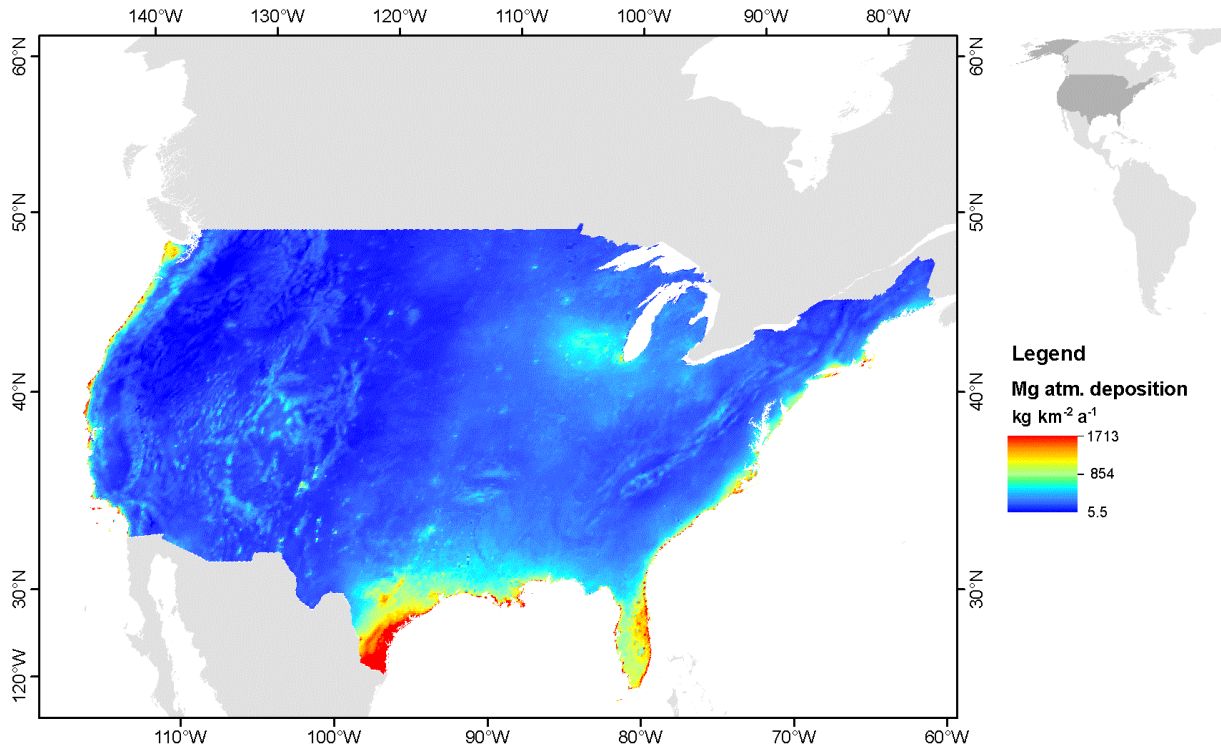


Fig. S 5: Total atmospheric Mg deposition [$\text{kg km}^{-2} \text{a}^{-1}$] for U.S. (National Atmospheric Deposition Program, 2016). Map generated with ESRI ArcGIS ver. 10.3.1 (<http://www.esri.com>).

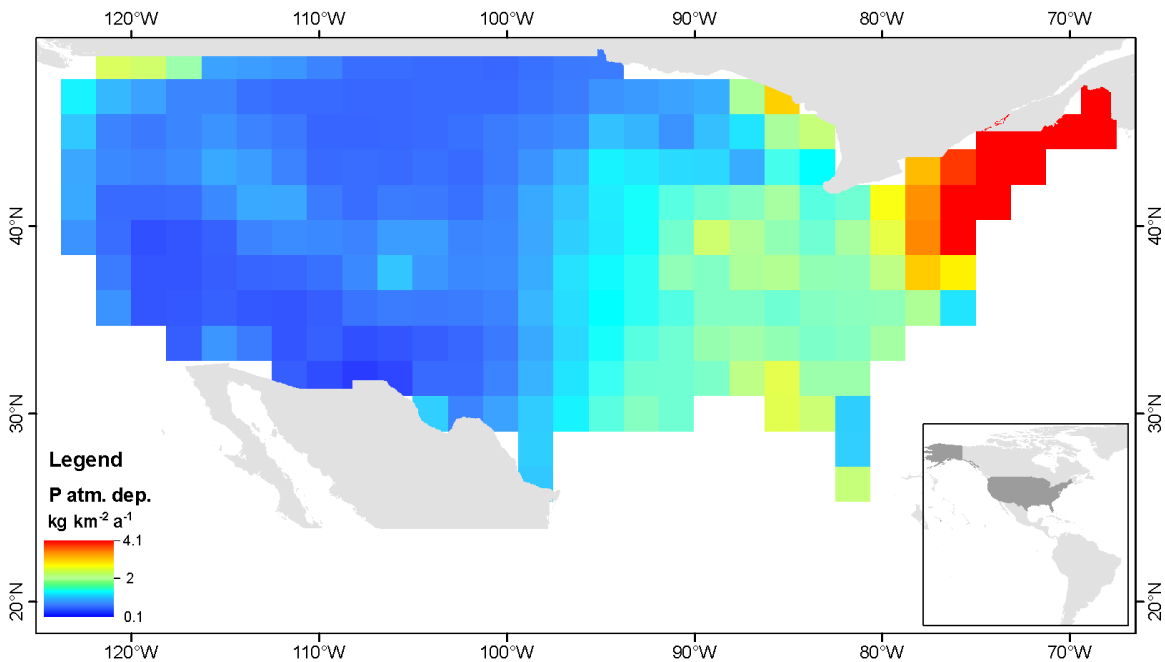


Fig. S 6: Atmospheric P deposition [$\text{kg km}^{-2} \text{a}^{-1}$] for U.S. extracted from (Mahowald et al., 2008). Map generated with ESRI ArcGIS ver. 10.3.1 (<http://www.esri.com>).

C2) Weathering Rates (WR)

Weathering rates were used (corresponding to Eq. (8) WR_{calc}) from the Hartmann et al. (2014b) model framework. Weathering rates provide a maximum and minimum range, representing fresh and easily weatherable lithology (no soil shielding effect) and locations where weathering is, by soil shielding effects, comparable to humid tropical conditions with depleted soils overlaying the considered lithology. Weathering rates were obtained by overlaying the timberland area shape file (black areas Fig. S 1) to the weathering rate raster file (Fig. S 7).

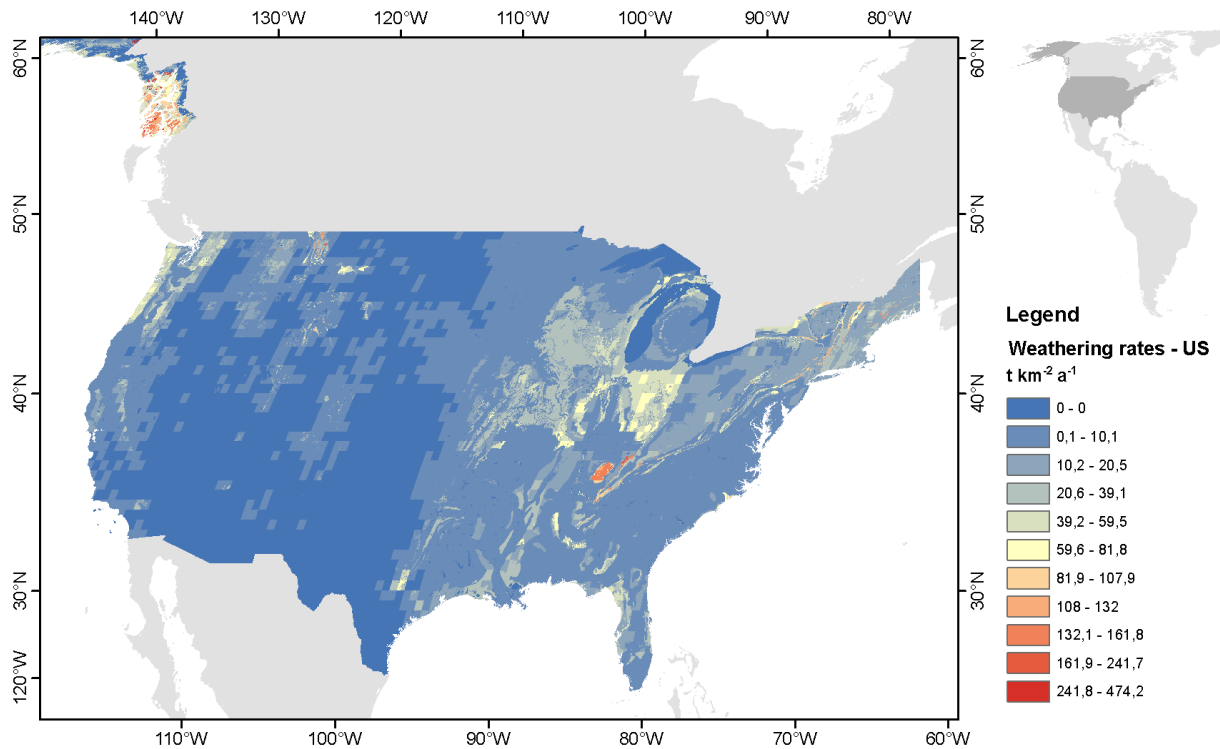


Fig. S 7: Weathering rates [$t\ km^{-2}\ a^{-1}$] across continental U.S. obtained from Hartmann et al. (2014b), WR as Si+Ca+Mg+Na+K. Map generated with ESRI ArcGIS ver. 10.3.1 (<http://www.esri.com>).

C3) Lithological classes' geochemical composition

Spatial rock class distribution within timberland areas for the twelve studied lithological classes was obtained by overlaying the timberland area shapefile (black areas Fig. S 1) to the GLIM database (Hartmann and Moosdorf, 2012). Typical geochemical composition ranges using median and the 25th and 75th percentiles from the GEOROCK database (Sarbas, 2008) and data for whole-rock analyses from Earthchem webportal (www.earthchem.org) were used. The rock names within GEOROCK database were matched to the rocks within the lithological class description in the Hartmann and Moosdorf (2012) work. The used lithological classes were: Unconsolidated sediments (SU), siliciclastic sedimentary rocks (SS), mixed sedimentary rocks (SM), basic volcanic rocks (VB), acid volcanic rocks (VA), basic plutonic rocks (PB), acid plutonic rocks (PA), metamorphic rocks (MT), carbonate sedimentary rocks (SC), pyroclastic rocks (PY), intermediate plutonic rocks (PI) and intermediate volcanic rocks (VI). Results containing the used sample number (n) and concentration ranges are provided in Table S 4. 25th and 75th percentiles ranges were used as lower and upper limit for the discussion, together with the calculated weathering rates (WR_{calc}) from the previous section, for obtaining the nutrient fluxes Nf_{calc} (Eq. (8)).

C4) Nutrient supply by weathering

In this section is presented the steps for calculating the spatially explicit nutrient supply and for calculating the averaged weathering nutrient supply. Averaged nutrient supply by weathering is used for a generalized discussion as the values consider spatially explicit nutrient fluxes of timberland areas with low or elevated weathering rates. Area specific information from the GLIM database (Hartmann and Moosdorf, 2012), timberland area and weathering rates from Hartmann et al. (2014b) were used to quantify the spatially explicit weathering nutrient supply (Eq. (8)). The minimal and maximal spatially explicit nutrient supply by weathering for timberland areas

is between $8.5 \times 10^{-3} - 0.2 \times 10^5$, $4.3 \times 10^{-3} - 1.63 \times 10^5$, $5.7 \times 10^{-3} - 0.2 \times 10^5$, and $0.3 \times 10^{-3} - 1.2 \times 10^3$ $\text{kg km}^{-2} \text{a}^{-1}$ for Mg, Ca, K, and P respectively.

To allow a general discussion Fig. 1, the spatially explicit values were grouped following the twelve lithological classes. The grouped values considered regions with higher and lower weathering rates for 25th and 75th quartiles of geochemical composition. For each of the twelve lithological classes, the lower weathering nutrient supply boundary was represented by the 25th quartiles of nutrient fluxes. The same was done for obtaining the weathering nutrient supply upper boundary, which considered the 75th quartiles. By this approach, it was possible to predict the nutrient fluxes from areas placed in regions with higher or lower weathering rates.

C5) Geogenic nutrient supply

Geogenic nutrient supply account for the atmospheric and weathering nutrient fluxes together. It was given by the respective sum considering spatially explicit: a) median atmospheric nutrient deposition values (section C1) to the b) nutrient supply by weathering (section C4), both in $\text{kg km}^{-2} \text{a}^{-1}$.

To identify the U.S. areas in which atmospheric or weathering nutrient contribution was higher, maps in which the weathering supply was subtracted from the atmospheric precipitation rates are presented for continental U.S. (Fig. S 9a to Fig. S 16a). Generally, atmospheric contribution is an important source of nutrients for continental U.S.

Looking within timberland areas, nutrient supply by weathering can be more important for forest nutrition than atmospheric nutrient deposition rates (Fig. S 9b to Fig. S 16b). The predominance of weathering supply over the atmospheric precipitation depends on weathering rates and chemical lithology composition. For minima (25th quartile) lithology chemical compositions (Table S 4) atmospheric precipitation is an important timberland nutrient source (Fig. S 10b, Fig. S 12b, Fig. S 14b and Fig. S 16b). If the lithology chemistry changes to the maxima (75th quartile; Table S 4), nutrient supply by weathering is the main nutrient source to timberlands (Fig. S 9, Fig. S 11b, Fig. S 13b and Fig. S 15b).

For the diagram presented Fig. 2, the same steps described in section C4 second paragraph were applied. The difference is that spatially explicit geogenic information was used for obtaining the 25th and 75th quartiles, respectively representing upper and lower boundaries. The twelve lithological class's geogenic nutrient supply 25th and 75th quartiles and median were compared to measured 25th and 75th quartiles and median nutrient fluxes within 115 U.S. catchments (Hartmann et al., 2014a). Only catchments composed by at least 95% forest covered area were considered. Due to the monitored catchment's lithological diversity, attributing simple way fluxes to certain lithological classes was not possible. Observed overestimation is attributed to the assumption of complete fresh lithology dissolution assumption and no sink (reactions with and within soil porosity, and erosion). Overestimation occurs for all the lithology classes for geogenic nutrient fluxes when compared to the analyzed watersheds (Fig. 9).

$$Nf_{catch} = \text{perct}\left(\frac{Q_{riv} * C_e}{A_{catch}}\right), \quad (\text{S } 2)$$

Where Nf_{catch} represents the measured nutrient flux [$\text{kg km}^{-2} \text{a}^{-1}$], C_e is the measured aqueous concentration of interest element 'e' (Mg, Ca, K or P) [kg km^{-3}], Q_{riv} is the measured river discharge [$\text{km}^3 \text{a}^{-1}$] and A_{catch} is the catchment area [km^2]. *perct* is the calculated 25th and 75th percentiles and median.

Table S 4: Chemical composition considering 25th, 75th quartiles and median for each lithological class and the sample number used to calculate the statistics (n values). Abbreviations: cf., subsection C3.

Lithological Class	Ca ⁹				K ⁹				Mg ⁹				P ⁹			
	[WT%]															
	25 th	75 th	Med	n	25 th	75 th	Med	n	25 th	75 th	Med	n	25 th	75 th	Med	n
SU	0.1	0.4	0.2	34	0.4	2.4	1.3	36	0.2	0.7	0.3	37	0.02	0.03	0.02	28
SS	0.3	4.5	1.1	7509	0.8	2.5	1.6	7672	0.4	1.5	0.9	7389	0.02	0.08	0.04	7191
SM	0.6	18.9	4.1	8571	0.5	1.9	1.1	8280	0.4	2.4	1.0	8474	0.02	0.06	0.03	7737
SC	0.6	23.7	7.8	5730	0.3	2.1	0.9	5412	0.5	2.7	1.0	5654	0.02	0.07	0.03	5013
VB	2.4	6.6	5.1	1973	0.8	3.1	1.6	2029	0.8	4.2	2.6	1953	0.04	0.12	0.08	1669
VI	2.7	4.8	3.8	1543	1.2	2.8	2.0	1563	0.8	2.2	1.5	1537	0.04	0.08	0.06	1334
VA	1.0	4.2	2.8	1177	1.6	3.7	2.6	1191	0.2	1.8	0.9	1157	0.02	0.07	0.04	932
PB	0.7	2.6	1.3	559	2.6	4.9	4.3	632	0.2	1.0	0.4	542	0.02	0.07	0.03	414
PI	0.7	5.0	2.1	98	0.9	2.5	1.6	245	0.5	3.0	1.1	114	0.02	0.19	0.03	22
PA	0.7	3.6	2.1	100	1.1	2.6	1.7	355	0.5	1.7	1.0	118	0.03	0.05	0.03	19
MT	0.2	7.8	1.7	739	0.2	2.4	1.2	901	0.4	7.5	2.0	696	0.01	0.04	0.02	487
PY	5.4	7.0	6.3	1629	0.6	1.7	1.0	1641	2.5	4.7	3.9	1629	0.05	0.16	0.10	1485

9 - (Sarbas, 2008).

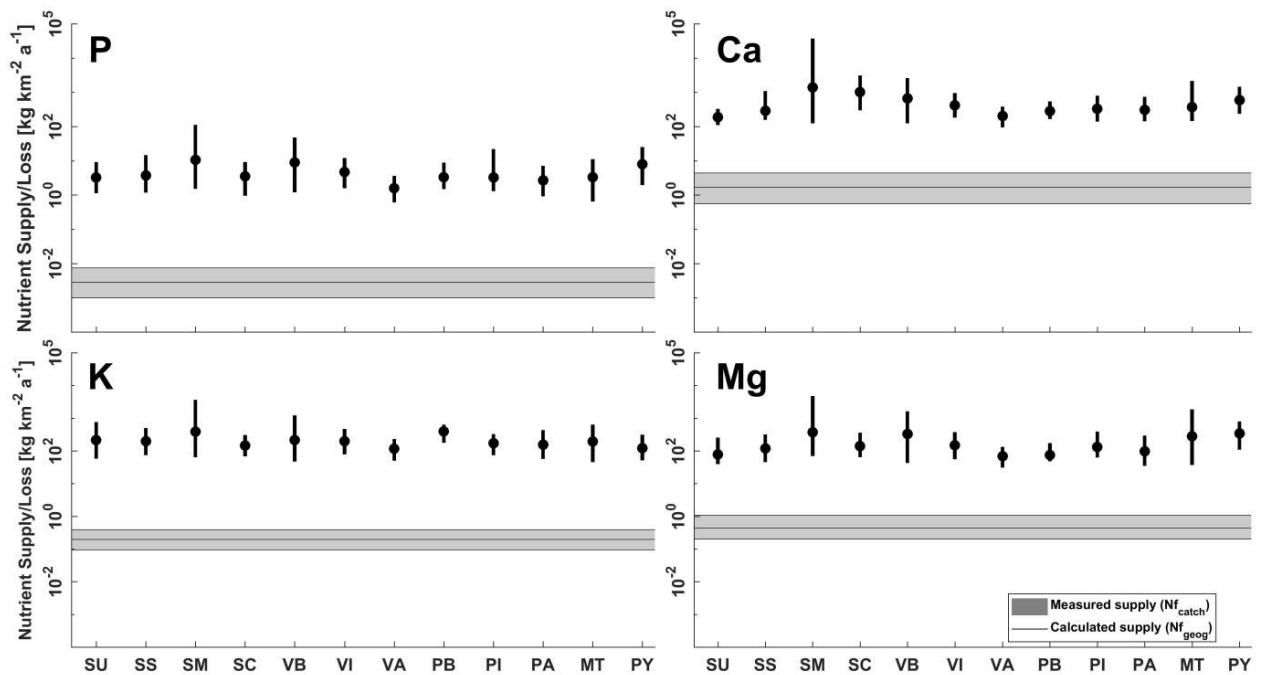


Fig. S 8: Comparison between measured and calculated nutrient fluxes. Horizontal lines represent averaged measured stream weathering rates (Nf_{catch}) for 115 U.S. catchments assuming that river fluxes represent on average long-term losses. Catchments consist of at least 95% of forest covered area (Hartmann et al., 2014a). Horizontal lines represent minimum median and maximum values. Vertical lines represent total weathering and atmospheric deposition supply (Nf_{geog}) following section's C5 steps. Note that the monitored catchment's lithological diversity did not allow for attributing fluxes to certain lithological classes in a simple way.

Spatial dependency between atmospheric deposition and weathering supply was investigated. Subtraction of weathering supply from the atmospheric deposition for each considered element was done. For the analysis, two distinct scenarios were investigated considering the median atmospheric deposition and 1) maximum scenario for weathering supply, or 2) minimum scenario for weathering supply (Fig. S 9a to Fig. S 16a). Within timberland

areas, the observed pattern occurring for continental U.S. is different. To elucidate this, frequency diagrams considering atmospheric and weathering nutrient supply within timberland areas are presented on the right side of the U.S. maps (Fig. S 9b to Fig. S 16b).

For the timberland areas, considering a maximum weathering supply scenario, the nutrient supply by weathering occurs for 88, 63, 69, and 73% of timberlands for Ca, K, Mg, and P respectively. Considering the minimum scenario for weathering supply, the weathering supply for timberland respectively decreases to 27, 36, 55, and 72% of timberlands for Ca, K, Mg, and P. The nutrient supply by weathering will be the main nutrient source within timberlands depending on factors like lithological element concentration and soil moisture.

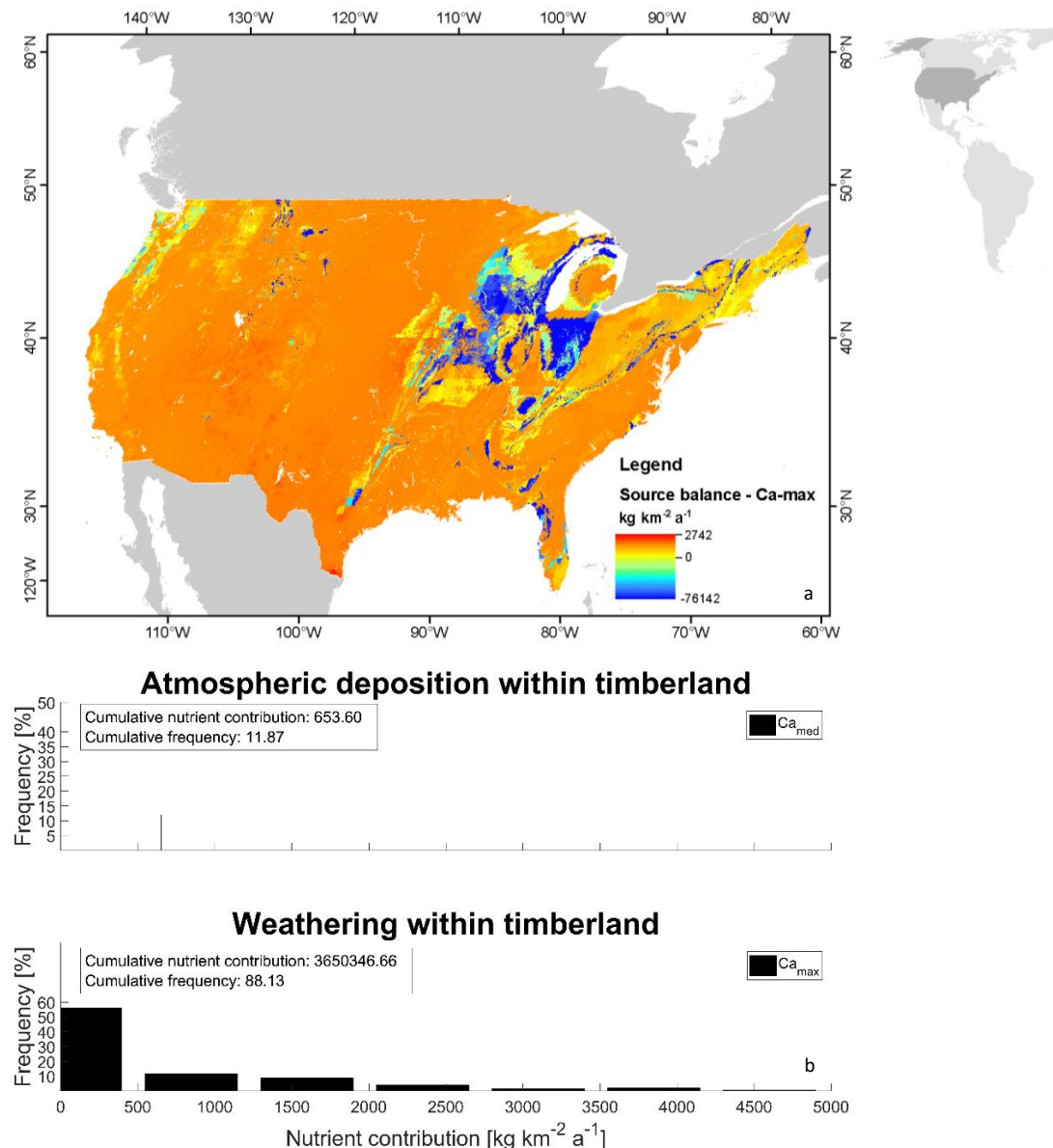


Fig. S 9: a) Map representing the result from median Ca atmospheric deposition minus the maximum Ca supply via weathering. Colder colors represent a higher nutrient supply by weathering than atmospheric deposition. Map generated with ESRI ArcGIS ver. 10.3.1 (<http://www.esri.com>). b) Frequency histograms for the Atmospheric and Weathering nutrient contribution influence within timberland areas considering U.S. difference map. For the weathering nutrient contribution, the values were multiplied by -1 to obtain positive values. Cumulative frequency shows the most contributing nutrient source to timberland nutrition. Weathering and atmospheric cumulative frequency sum up to 100%.

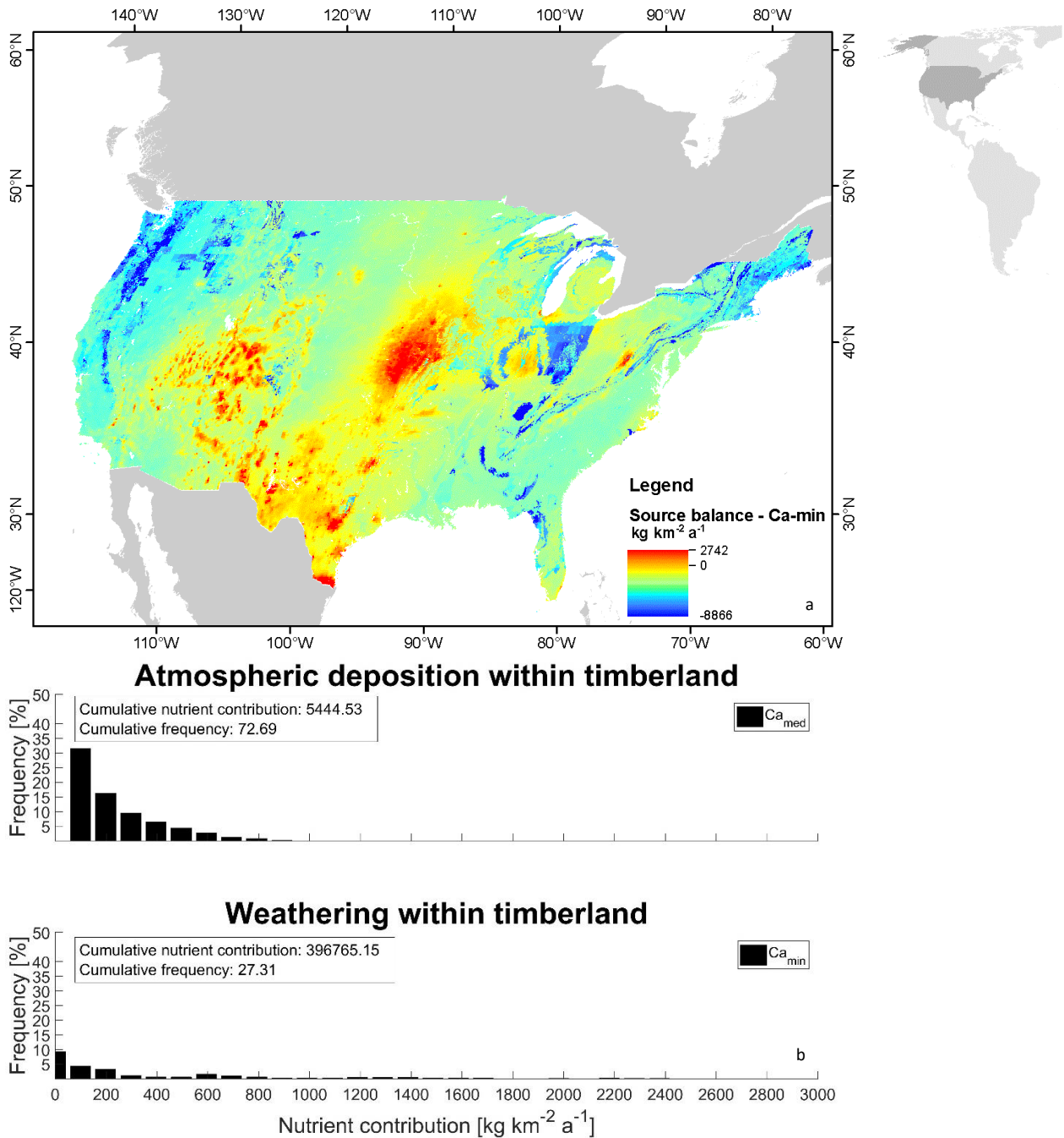


Fig. S 10: a) Map representing the result from median Ca atmospheric deposition minus the minimum Ca supply by weathering. Colder colors represent a higher nutrient supply by weathering than atmospheric deposition. Map generated with ESRI ArcGIS ver. 10.3.1 (<http://www.esri.com>). b) Frequency histograms for the Atmospheric and Weathering nutrient contribution influence within timberland areas considering U.S. difference map. For the weathering nutrient contribution the values were multiplied by -1 to obtain positive values. Cumulative frequency shows the most contributing nutrient source to timberland nutrition. Weathering and atmospheric cumulative frequency sum up to 100%.

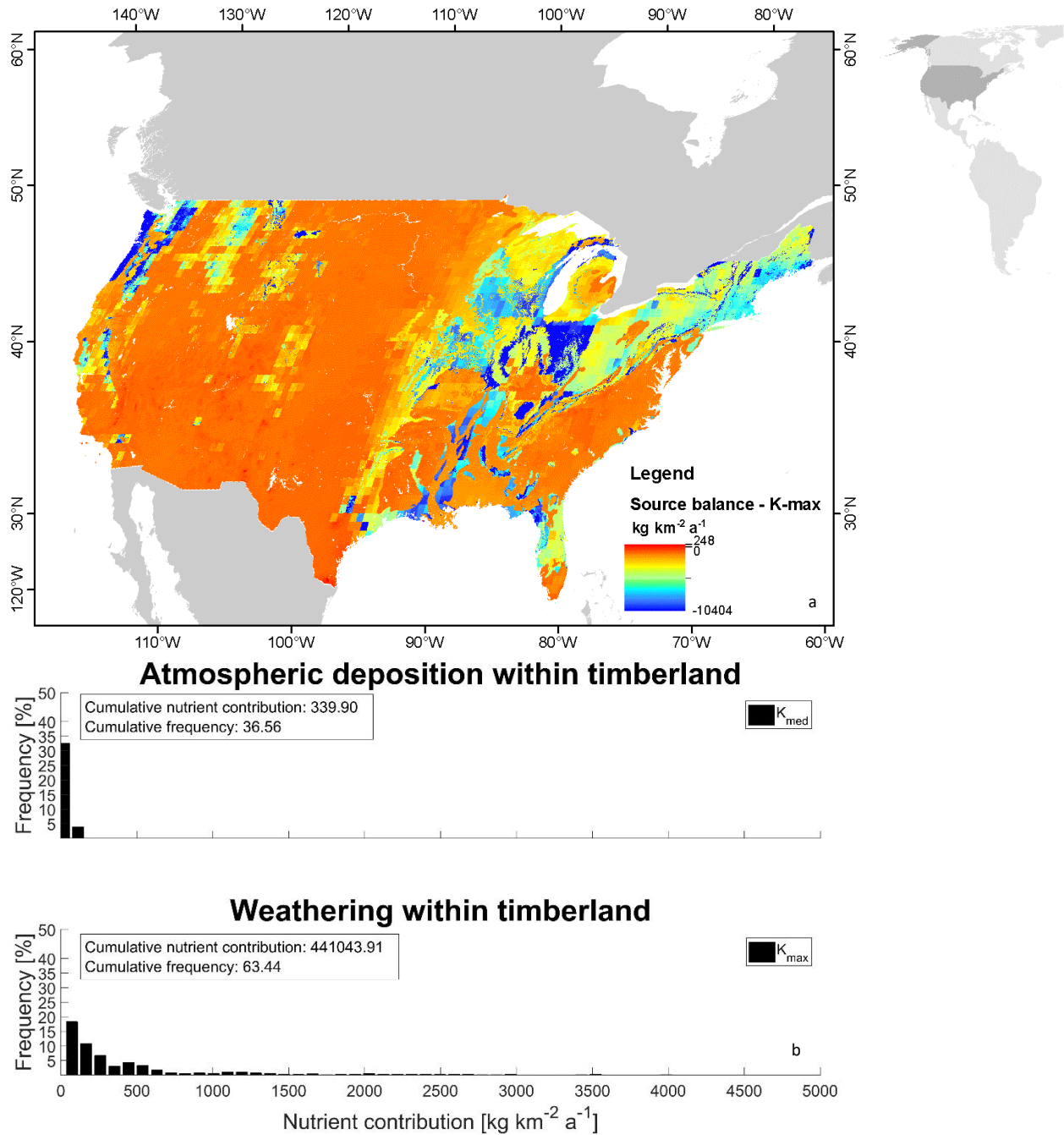
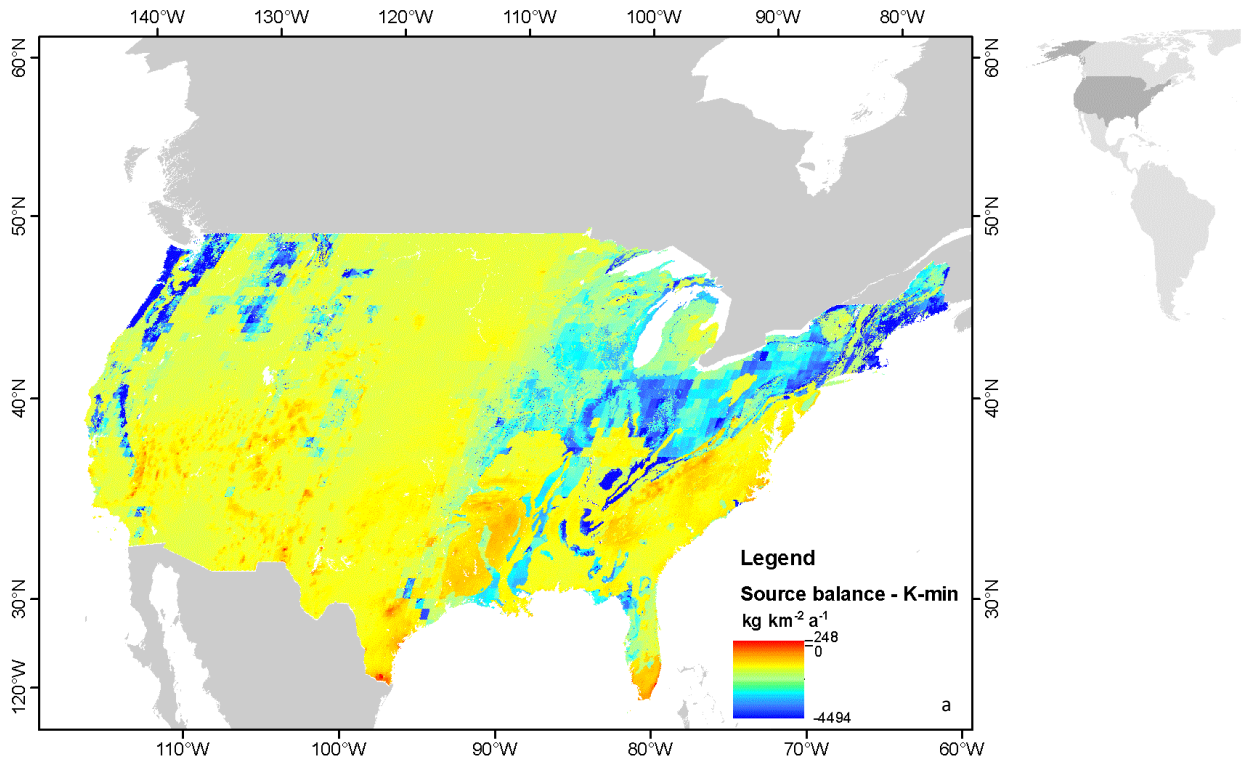
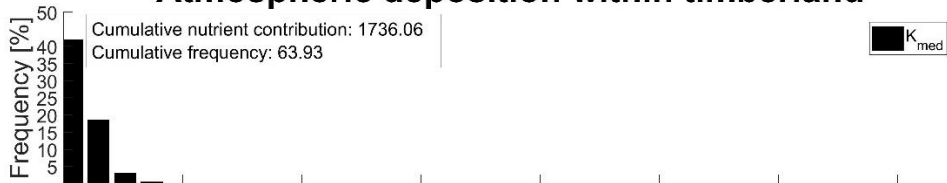


Fig. S 11: a) Map representing the result from median K atmospheric deposition minus the maximum K supply by weathering. Colder colors represent a higher nutrient supply by weathering than atmospheric deposition. Map generated with ESRI ArcGIS ver. 10.3.1 (<http://www.esri.com>). b) Frequency histograms for the Atmospheric and Weathering nutrient contribution influence within timberland areas considering U.S. difference map. For the weathering nutrient contribution the values were multiplied by -1 to obtain positive values. Cumulative frequency shows the most contributing nutrient source to timberland nutrition. Weathering and atmospheric cumulative frequency sum up to 100%.



Atmospheric deposition within timberland



Weathering within timberland

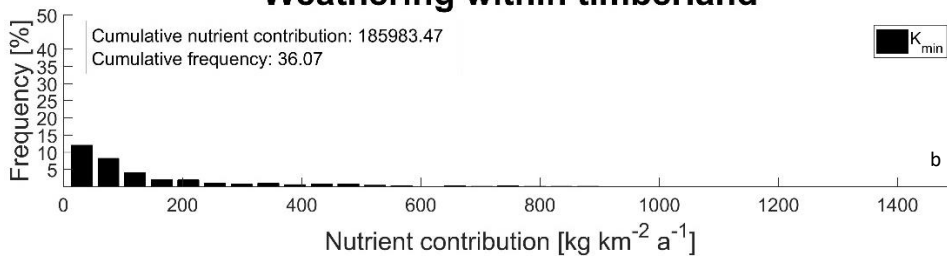


Fig. S 12: a) Map representing the result from median K atmospheric deposition minus the minimum K supply by weathering. Colder colors represent a higher nutrient supply by weathering than atmospheric deposition. Map generated with ESRI ArcGIS ver. 10.3.1 (<http://www.esri.com>). b) Frequency histograms for the Atmospheric and Weathering nutrient contribution influence within timberland areas considering U.S. difference map. For the weathering nutrient contribution the values were multiplied by -1 to obtain positive values. Cumulative frequency shows the most contributing nutrient source to timberland nutrition. Weathering and atmospheric cumulative frequency sum up to 100%.

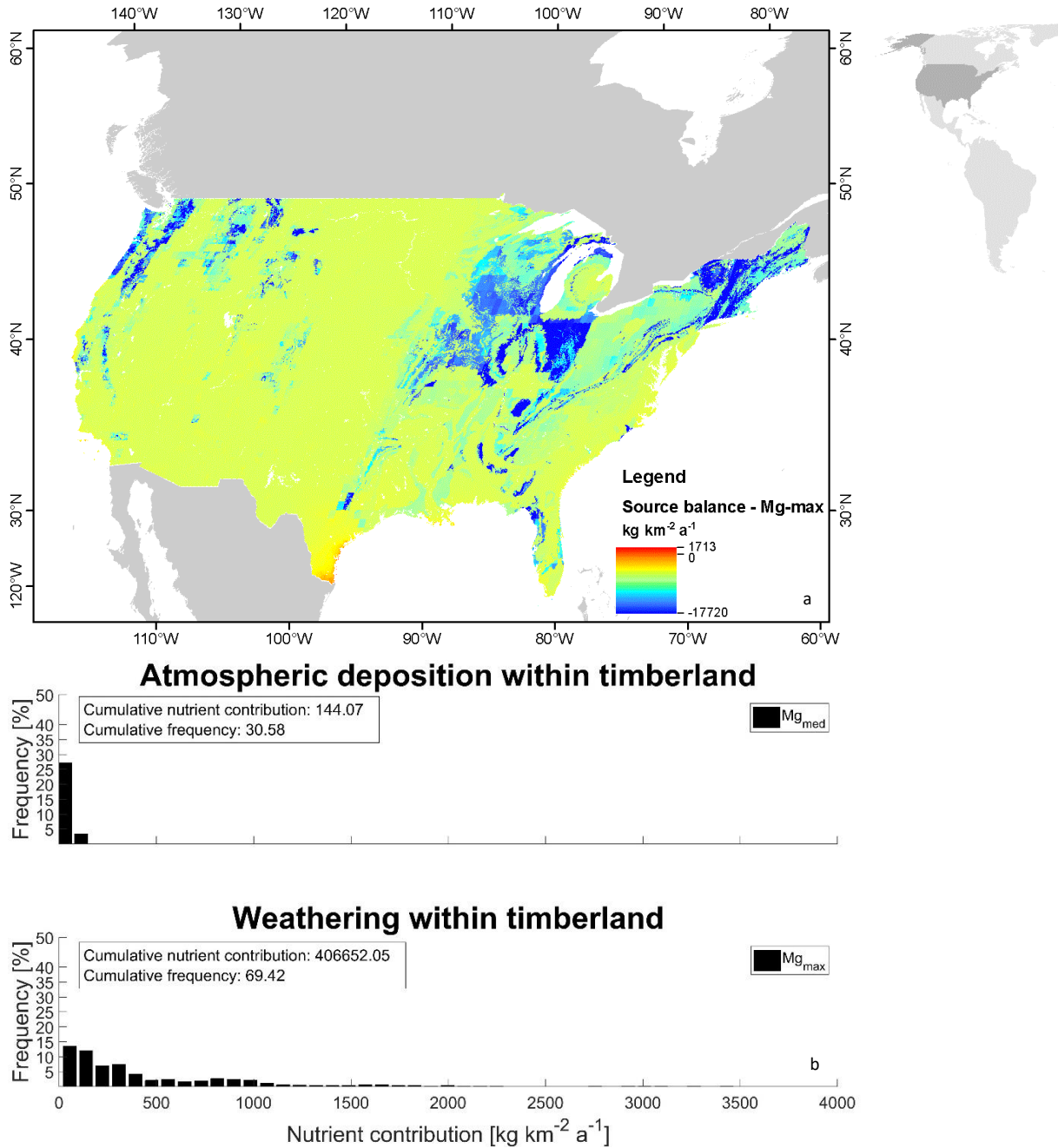


Fig. S 13: a) Map representing the result from median Mg atmospheric deposition minus the maximum Mg supply by weathering. Colder colors represent a higher nutrient supply by weathering than atmospheric deposition. Map generated with ESRI ArcGIS ver. 10.3.1 (<http://www.esri.com>). b) Frequency histograms for the Atmospheric and Weathering nutrient contribution influence within timberland areas considering U.S. difference map. For the weathering nutrient contribution the values were multiplied by -1 to obtain positive values. Cumulative frequency shows the most contributing nutrient source to timberland nutrition. Weathering and atmospheric cumulative frequency sum up to 100%.

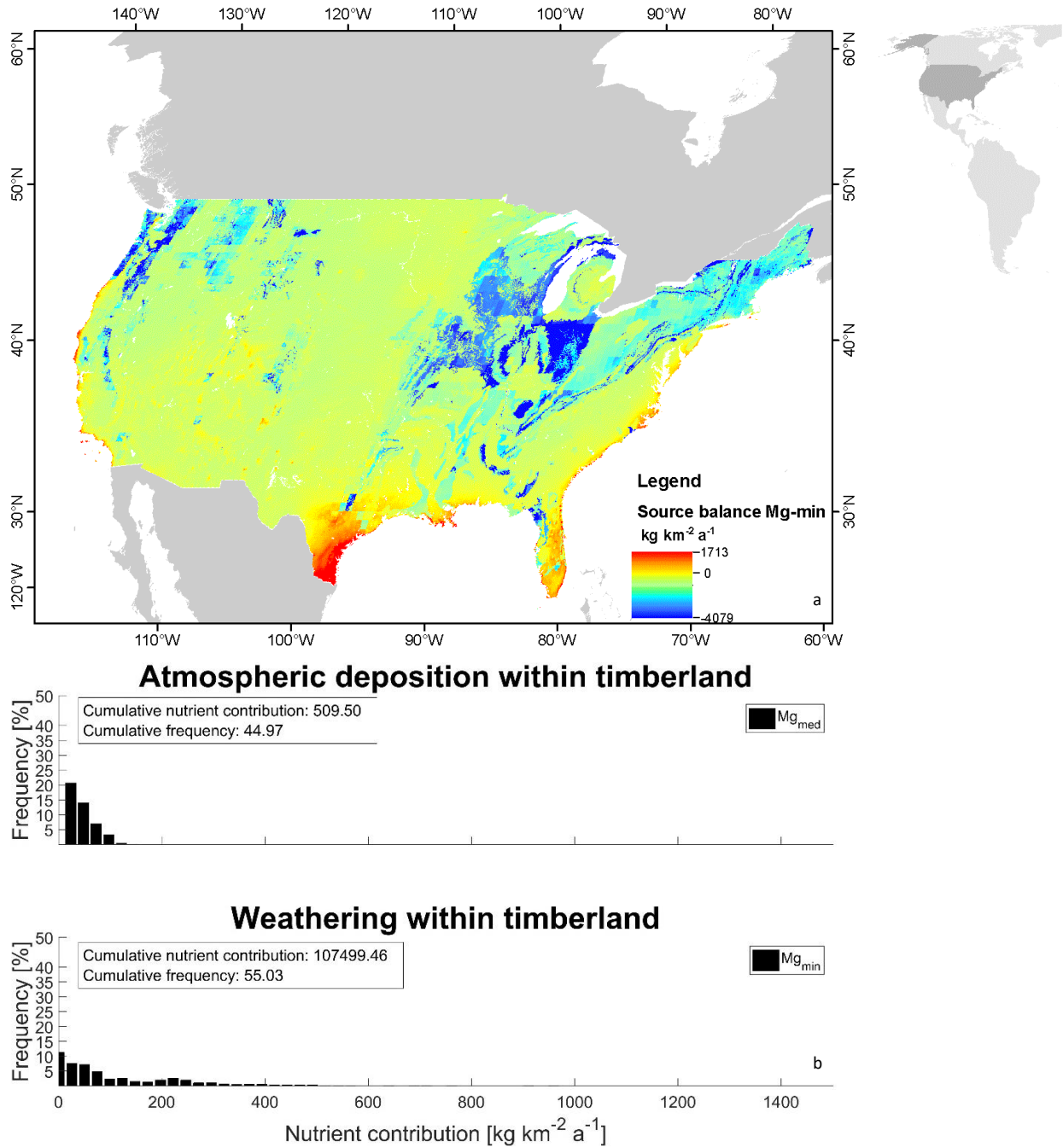


Fig. S 14: a) Map representing the result from median Mg atmospheric deposition minus the minimum Mg supply by weathering. Colder colors represent a higher nutrient supply by weathering than atmospheric deposition. Map generated with ESRI ArcGIS ver. 10.3.1 (<http://www.esri.com>). b) Frequency histograms for the Atmospheric and Weathering nutrient contribution influence within timberland areas considering U.S. difference map. For the weathering nutrient contribution the values were multiplied by -1 to obtain positive values. Cumulative frequency shows the most contributing nutrient source to timberland nutrition. Weathering and atmospheric cumulative frequency sum up to 100%.

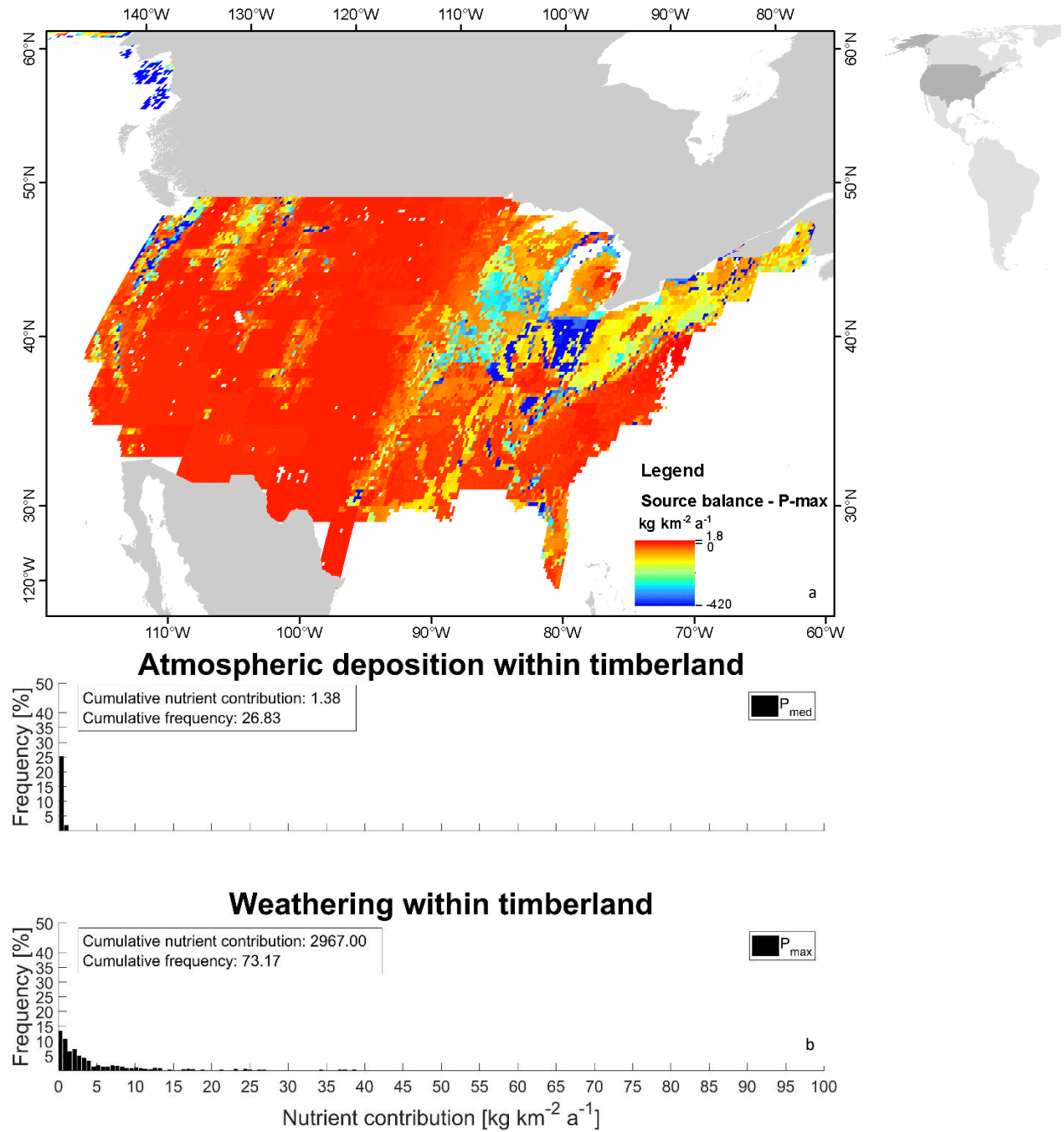
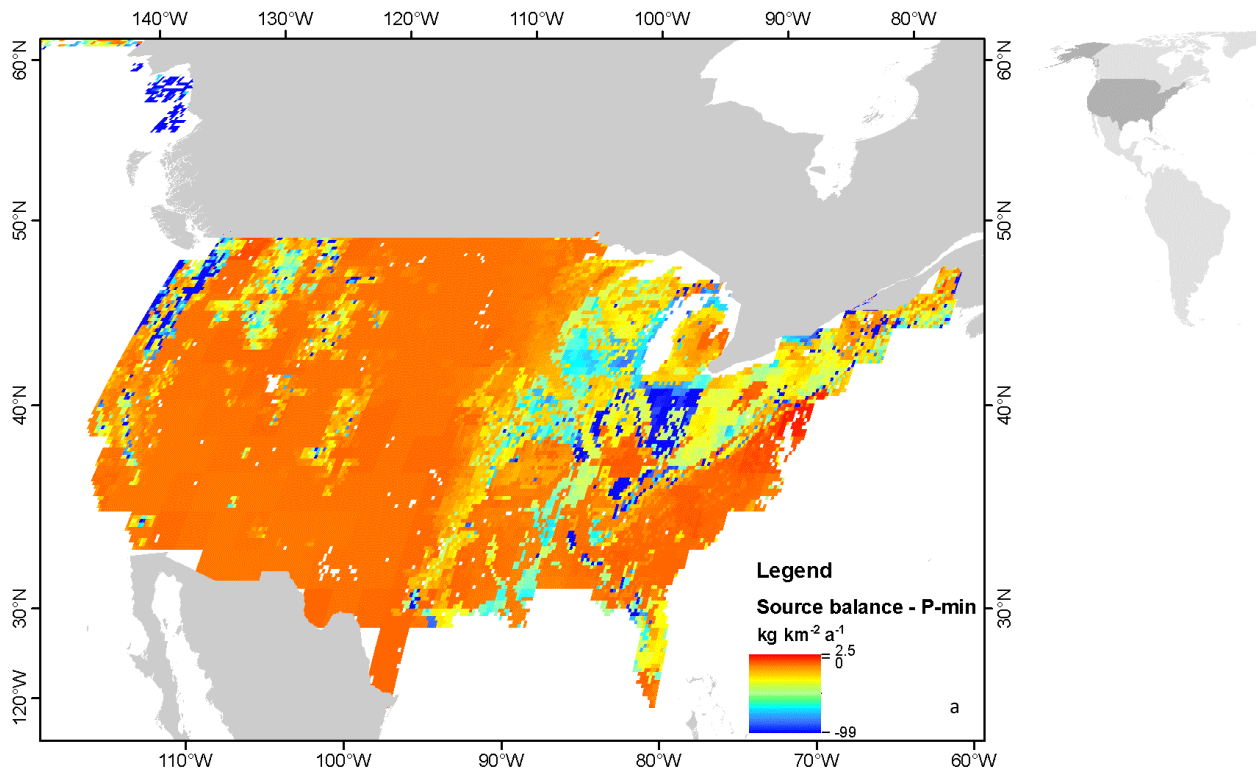
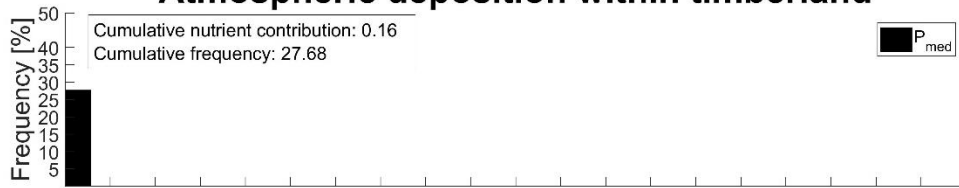


Fig. S 15: a) Map representing the result from P atmospheric deposition minus the maximum P supply by weathering. Colder colors represent a higher nutrient supply by weathering than atmospheric deposition. Map generated with ESRI ArcGIS ver. 10.3.1 (<http://www.esri.com>). b) Frequency histograms for the Atmospheric and Weathering nutrient contribution influence within timberland areas considering U.S. difference map. For the weathering nutrient contribution the values were multiplied by -1 to obtain positive values. Cumulative frequency shows the most contributing nutrient source to timberland nutrition. Weathering and atmospheric cumulative frequency sum up to 100%.



Atmospheric deposition within timberland



Weathering within timberland

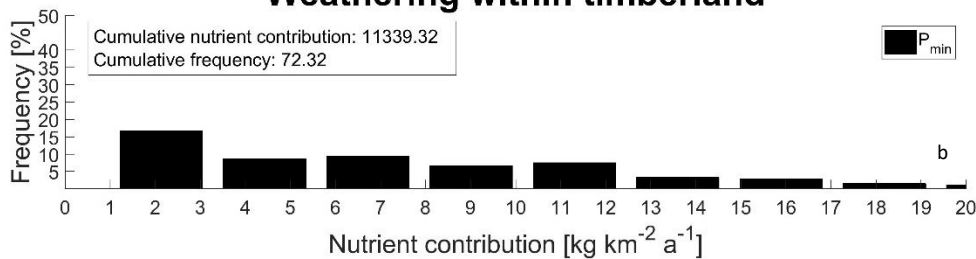


Fig. S 16: a) Map representing the result from P atmospheric deposition minus the minimum P supply by weathering. Colder colors represent a higher nutrient supply by weathering than atmospheric deposition. Map generated with ESRI ArcGIS ver. 10.3.1 (<http://www.esri.com>). b) Frequency histograms for the Atmospheric and Weathering nutrient contribution influence within timberland areas considering U.S. difference map. For the weathering nutrient contribution the values were multiplied by -1 to obtain positive values. Cumulative frequency shows the most contributing nutrient source to timberland nutrition. Weathering and atmospheric cumulative frequency sum up to 100%.

D. Nutrient budget

To assess the nutrient budget, the difference between geogenic nutrient input (weathering nutrient supply plus atmospheric deposition) and nutrient harvest loss was calculated. The nutrient budgets for minimum and maximum scenarios represent the spatially explicit nutrient losses and supply. The spatially explicit nutrient budget for Ca, P, Mg, and K (Fig. S 18 to Fig. S 25) reveals the actual nutrient gap for timberland areas considering the spatially explicit nutrient export based on harvest rates, tree-species and wood density and spatially explicit total nutrient supply.

To investigate lithological class efficiency in supply nutrients, diagrams considering 25th and 75th quartiles and median values for nutrient losses and supply are used. For the spatially averaged diagrams, special attention was given to the lower and upper boundaries of possible nutrient losses and supply. Lower and upper boundaries respectively correspond to scenarios 1 and 8 from Fig. S 17. For this calculation, quantified nutrient losses, as described on section B3, were used, being compared to the nutrient supply by weathering only (section C4 and Fig. 1) and geogenic nutrient supply (section C5 and Fig. 2).

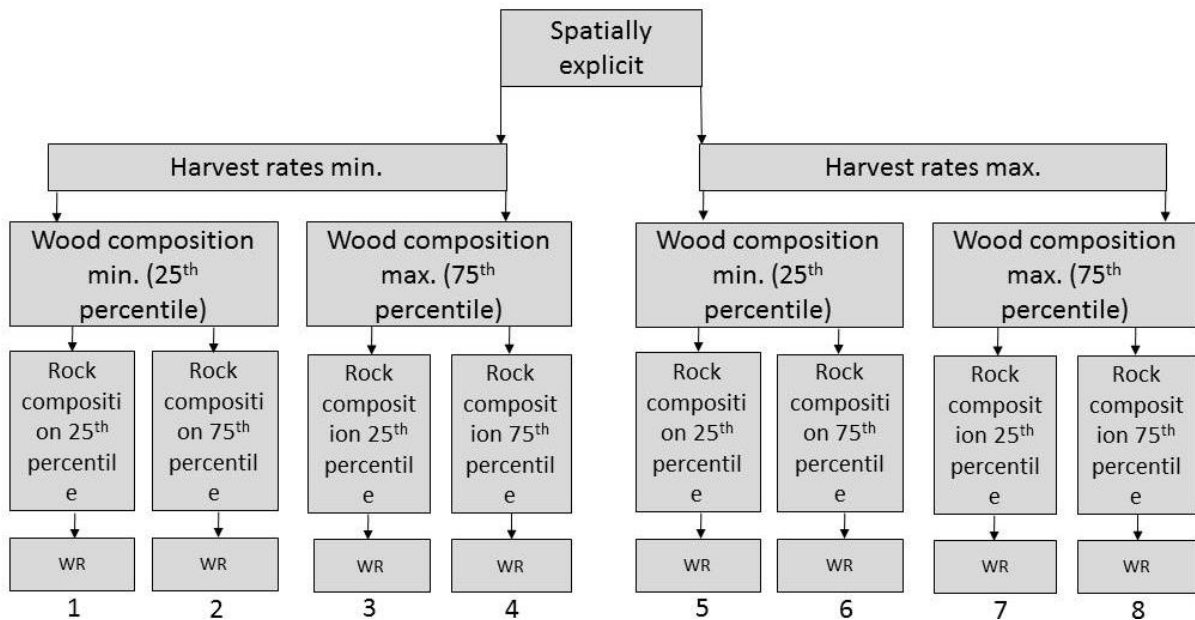


Fig. S 17: Nutrient budget scenarios and the respective scenario number. As threshold minimum and maximum, the overall 25th and 75th percentiles for nutrient supply rates based on rock content and for biomass content were chosen at fixed weathering and harvest rates corresponding to scenario 1 and 8 respectively. For $WR = WR_{calc}$ from (Hartmann et al., 2014b).

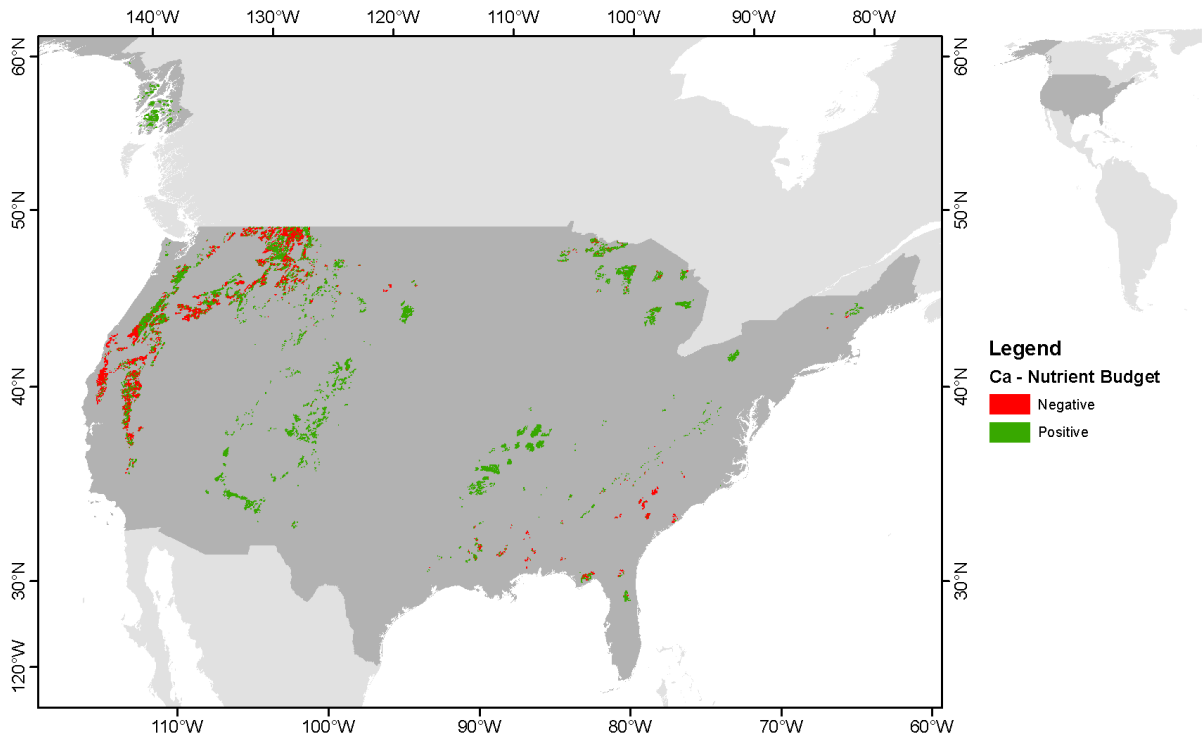


Fig. S 18: U.S. timberland spatially explicit nutrient budget for median atmospheric Ca deposition, and minimum (25th percentile) weathering nutrient supply and harvest loss. Red colors indicate areas with higher harvest nutrient loss than nutrient supply. Green colors represent the opposite. For the shown case, Ca nutrient deficiency occurs for 17% of timberland areas. Map generated with ESRI ArcGIS ver. 10.3.1 (<http://www.esri.com>).

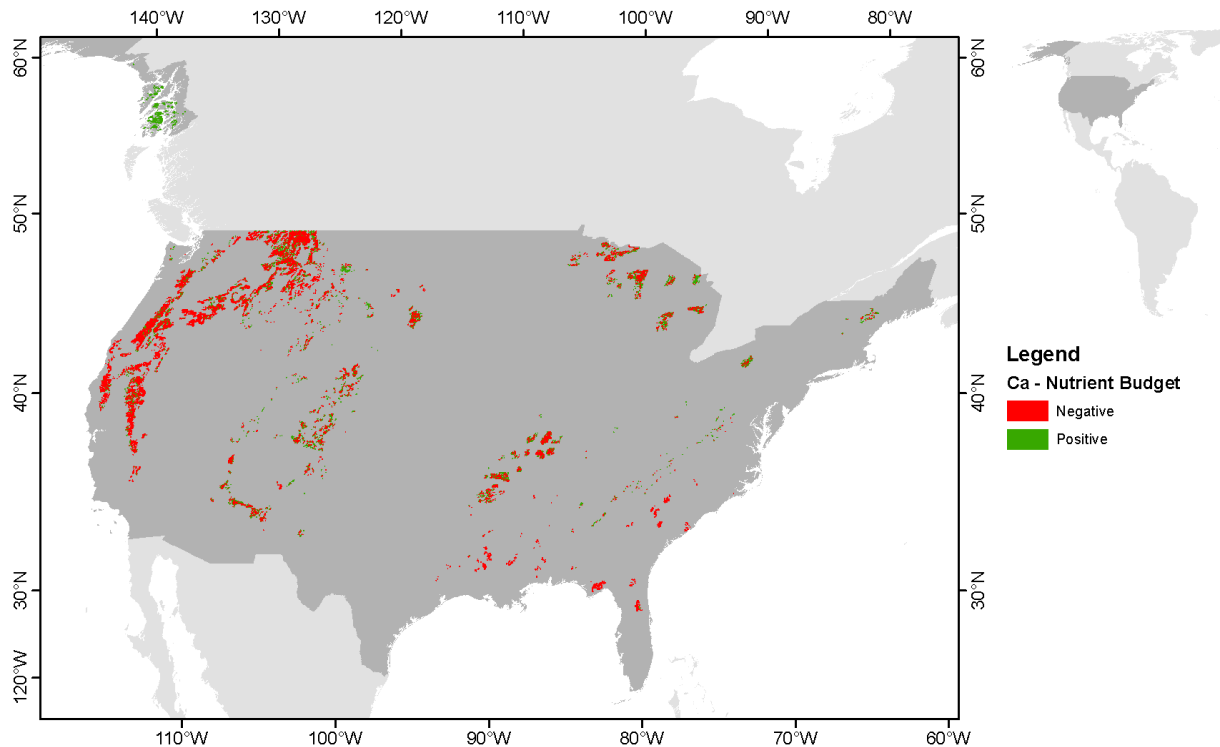


Fig. S 19: U.S. timberland spatially explicit nutrient budget for median atmospheric Ca deposition, and maximum (75th percentile) weathering nutrient supply and harvest loss. Red colors indicate areas with higher harvest nutrient loss than nutrient supply. Green colors represent the opposite. For shown case, Ca nutrient deficiency occurs for 50% of timberland areas. Map generated with ESRI ArcGIS ver. 10.3.1 (<http://www.esri.com>).

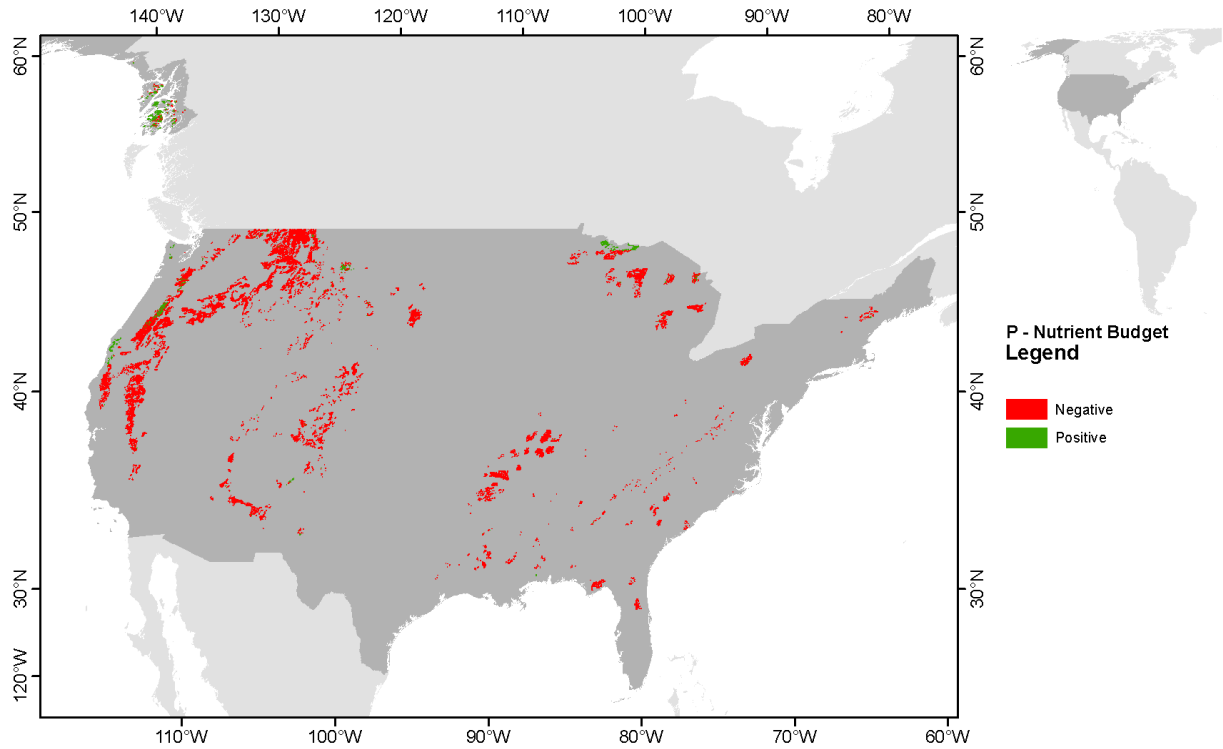


Fig. S 20: U.S. timberland spatially explicit nutrient budget for median atmospheric P deposition, and maximum (75th percentile) geogenic supply and harvest loss. Red colors indicate areas with higher harvest nutrient loss than nutrient supply. Green colors represent the opposite. For shown case, P nutrient deficiency occurs for 96% of timberland areas. Map generated with ESRI ArcGIS ver. 10.3.1 (<http://www.esri.com>).

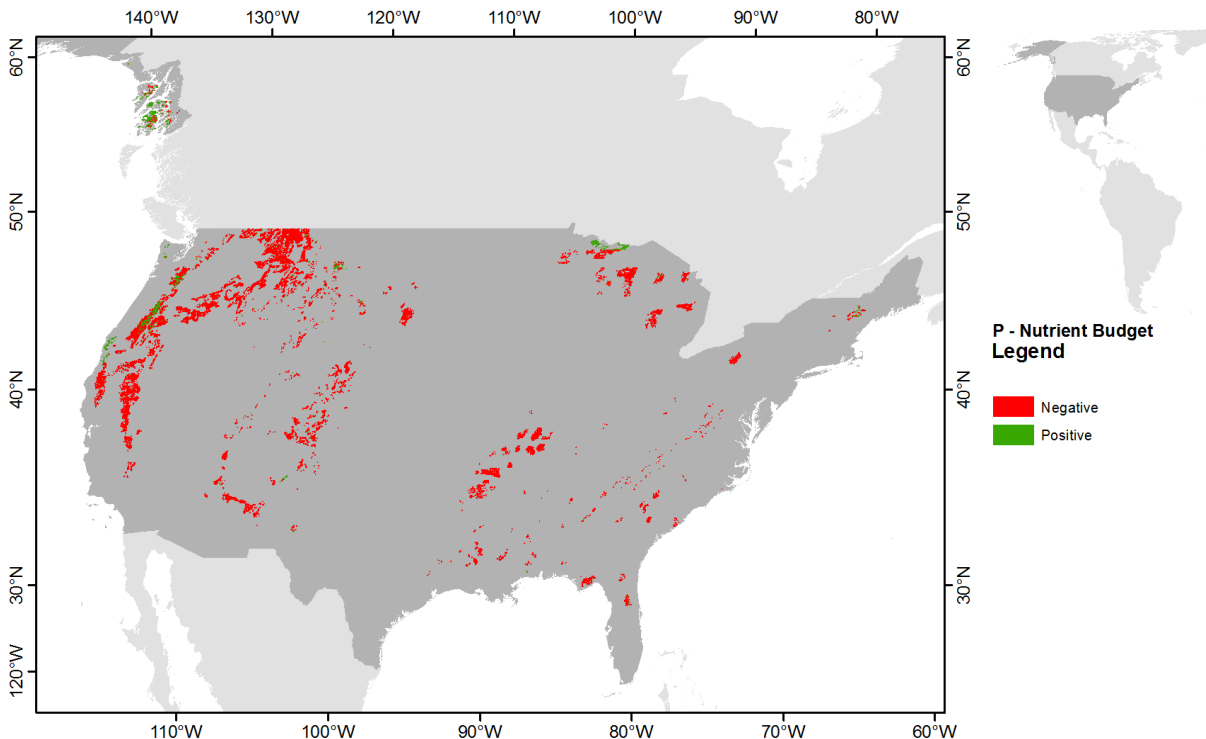


Fig. S 21: U.S. timberland spatially explicit nutrient budget for median atmospheric P deposition, and minimum (25th percentile) geogenic supply and harvest loss. Red colors indicate areas with higher harvest nutrient loss than nutrient supply. Green colors represent the opposite. For shown case, P nutrient deficiency occurs for 94% of timberland areas. Map generated with ESRI ArcGIS ver. 10.3.1 (<http://www.esri.com>).

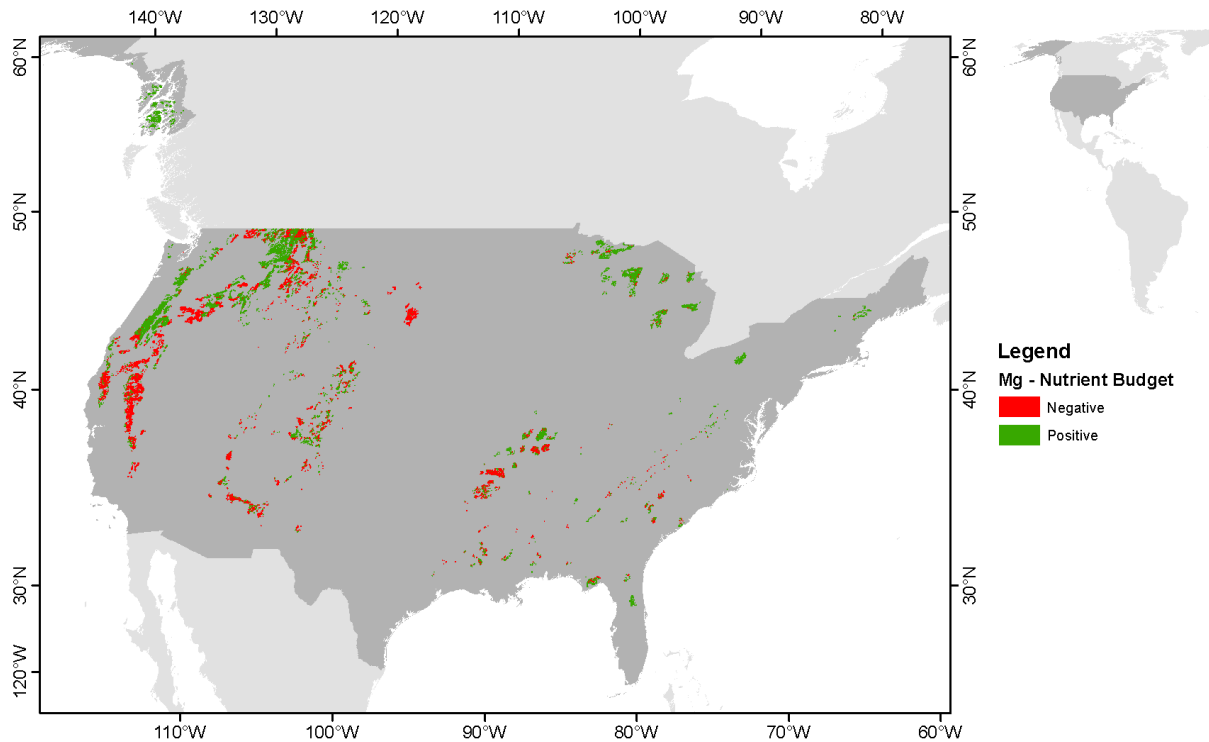


Fig. S 22: U.S. timberland spatially explicit nutrient budget for median atmospheric Mg deposition, and maximum (75th percentile) geogenic supply and harvest loss. Red colors indicate areas with higher harvest nutrient loss than nutrient supply. Green colors represent the opposite. For shown case, Mg nutrient deficiency occurs for 45% of timberland areas. Map generated with ESRI ArcGIS ver. 10.3.1 (<http://www.esri.com>).

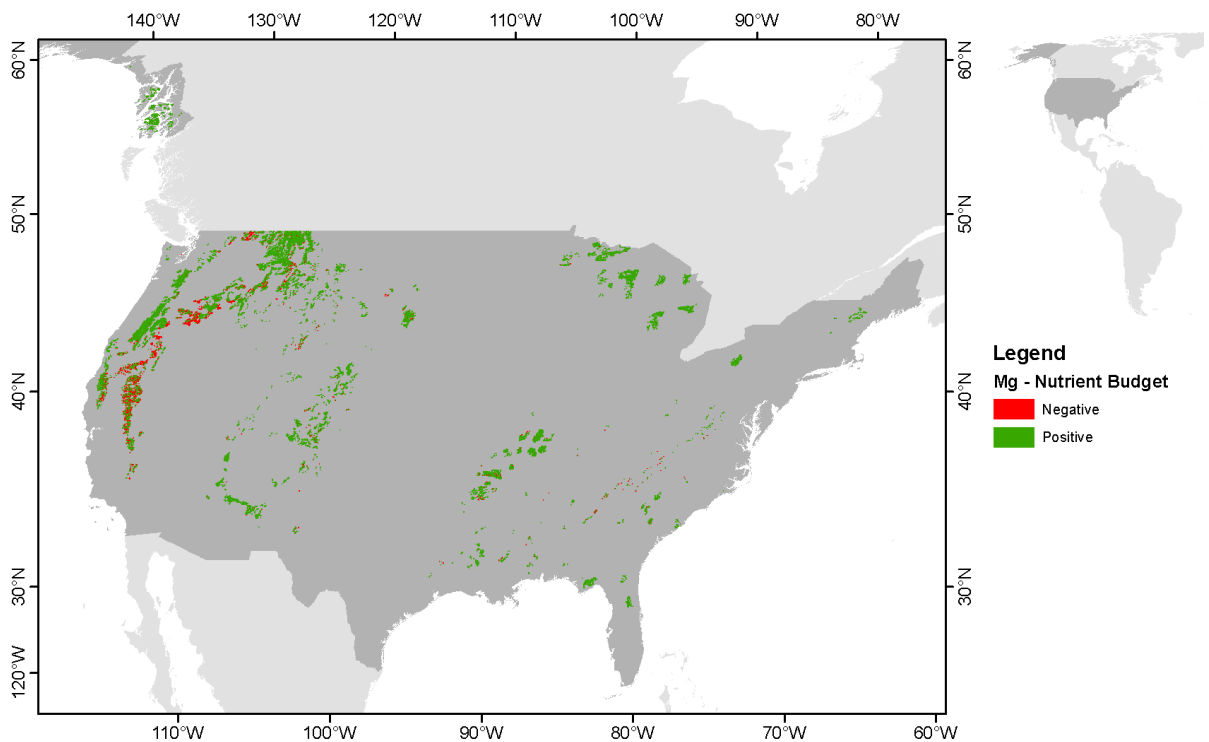


Fig. S 23: U.S. timberland spatially explicit nutrient budget for median atmospheric Mg deposition, and minimum (25th percentile) geogenic supply and harvest loss. Red colors indicate areas with higher harvest nutrient loss than nutrient supply. Green colors represent the opposite. For shown case, Mg nutrient deficiency occurs for 16% of timberland areas. Map generated with ESRI ArcGIS ver. 10.3.1 (<http://www.esri.com>).

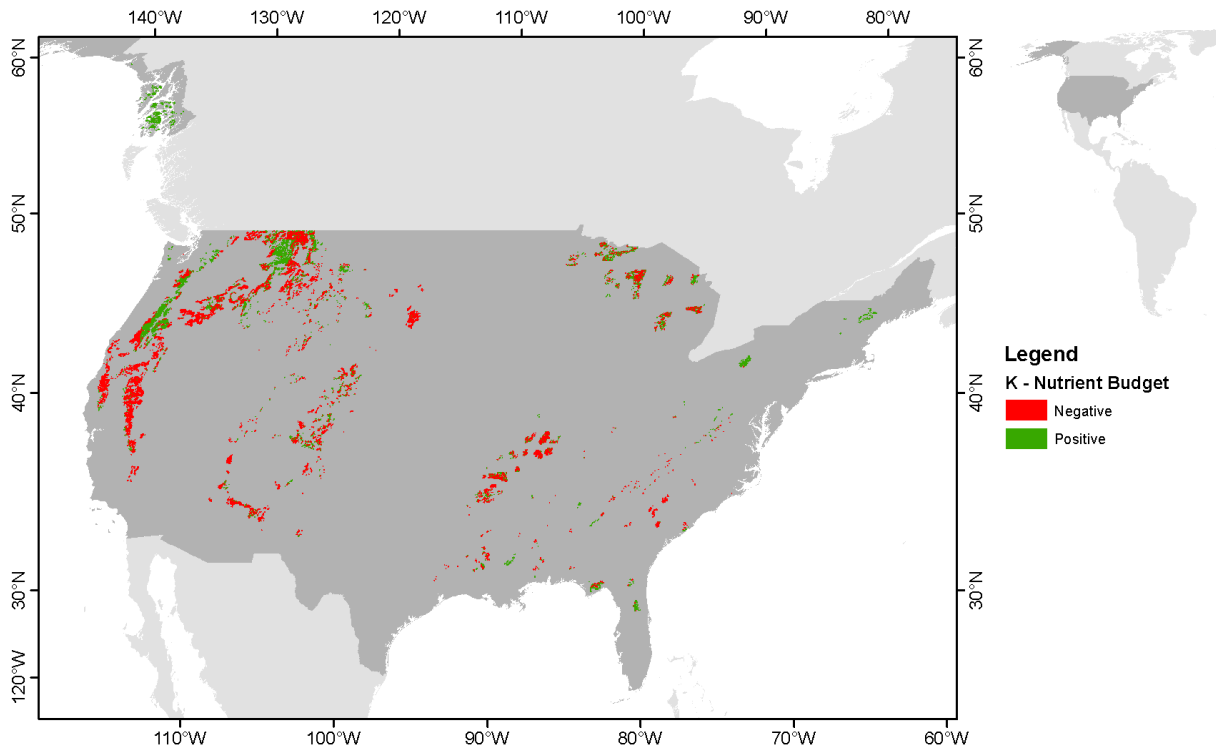


Fig. S 24: U.S. timberland spatially explicit nutrient budget for median atmospheric K deposition, and maximum (75th percentile) geogenic supply and harvest loss. Red colors indicate areas with higher harvest nutrient loss than nutrient supply. Green colors represent the opposite. For shown case, K nutrient deficiency occurs for 57% of timberland areas. Map generated with ESRI ArcGIS ver. 10.3.1 (<http://www.esri.com>).

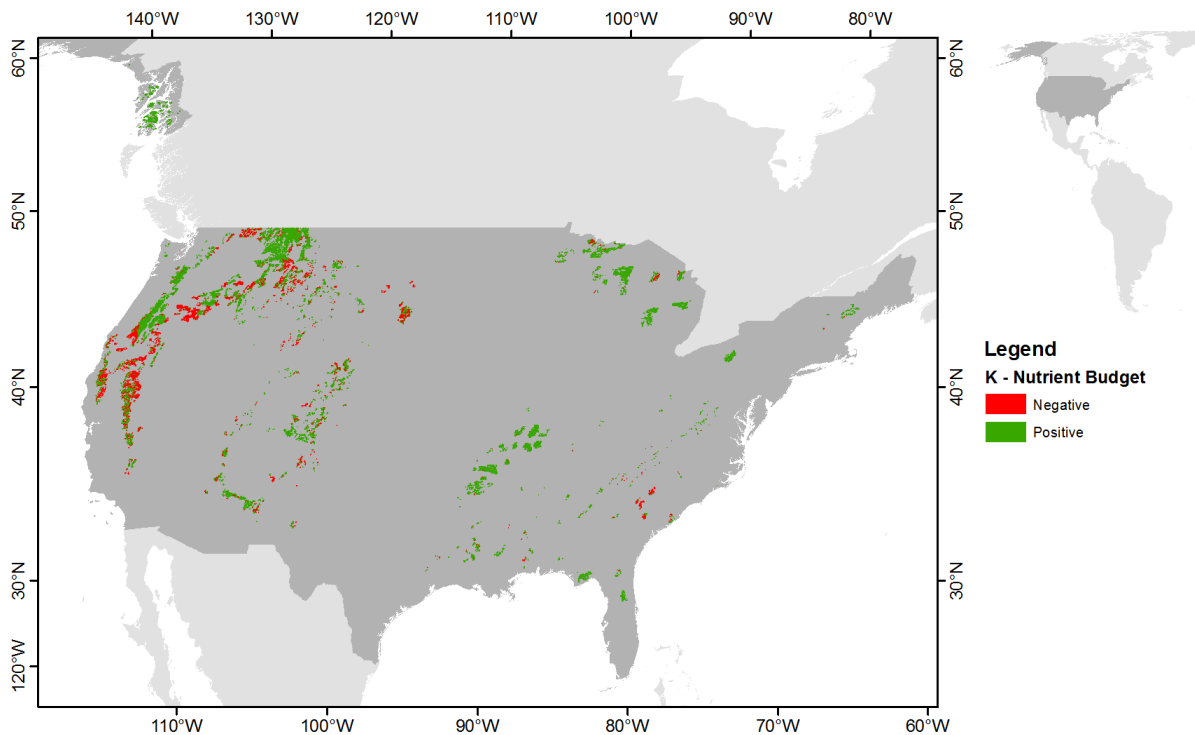


Fig. S 25: U.S. timberland spatially explicit nutrient budget for median atmospheric K deposition, and minimum (25th percentile) geogenic supply and harvest loss. Red colors indicate areas with higher harvest nutrient loss than nutrient supply. Green colors represent the opposite. For shown case, K nutrient deficiency occurs for 20% of timberland areas. Map generated with ESRI ArcGIS ver. 10.3.1 (<http://www.esri.com>).

The stoichiometric ratios used to estimate the median and ranges (5th and 95th percentiles) macronutrient demand by afforestation in the main text section “Nutrient demand Afforestation/Reforestation” are presented as an excel file “S2.xlsx”. In the chapter E, we present the results that were not presented in main text for EW coupled with AR that are: the potential P gaps and the necessary basalt powder deployment to bridge the estimated P gaps for an N-limited AR scenario and the related C-fixation reduction (Fig. S 26, Fig. S27, Fig. S 28, and Fig. S29) and the potential P gaps and the necessary basalt powder deployment to bridge the estimated P gaps for a N-unlimited AR scenario and the related C-fixation reduction (Fig. S 30, Fig. S31 , Fig. S 32, Fig. S33, Fig. S 34, and Fig. S35). In chapter F, we show the results for a hypothetical scenario assuming that the estimated maximum harvest rate by MAgPIE could be increased by one order of magnitude (Fig. S 36). The soil hydrology impacts for a coarse and for a fine rock powder texture is presented in chapter G for the P budget of geogenic P supply scenario two for the N-unlimited scenario, the impacts on soil hydraulic conductivity and plant-available water could be neglected (Fig. S 37). The results for impacts in soil hydrology are presented for the N-unlimited AR scenario, since the required amount of rock powder to bridge the projected P gaps will be higher than for an N-limited scenario. Consequently, the changes in soil hydraulic properties for the N-unlimited AR scenario will be more remarkable than for the N-limited AR-scenario.

E. EW coupled with AR

i. AR N-limited

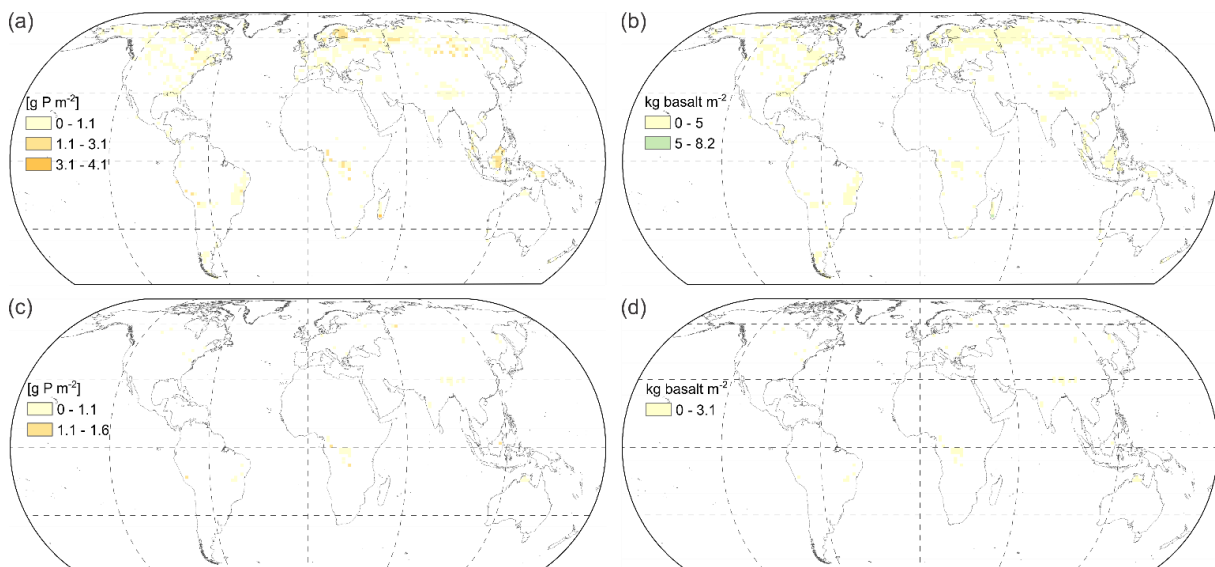


Fig. S 26: Areas with potential P gap for the nutrient budget of the N-limited AR scenario (after 94 years of simulation) assuming P concentrations within foliar and wood material corresponding to 5th percentile values (main text Table 1). a) Geogenic P supply scenario one (geogenic P from weathering plus atmospheric P deposition as source of P). b) Basalt deployment necessary to close P gaps from P budget scenario of Fig. S 26a. c) Geogenic P supply scenario two (geogenic P from soil inorganic labile P and organic P pools plus atmospheric P deposition and P from weathering as source of P). d) Basalt deployment necessary to close P gaps from P budget scenario of Fig. S 26c. Map generated with ESRI ArcGIS 10.7 (<http://www.esri.com>).

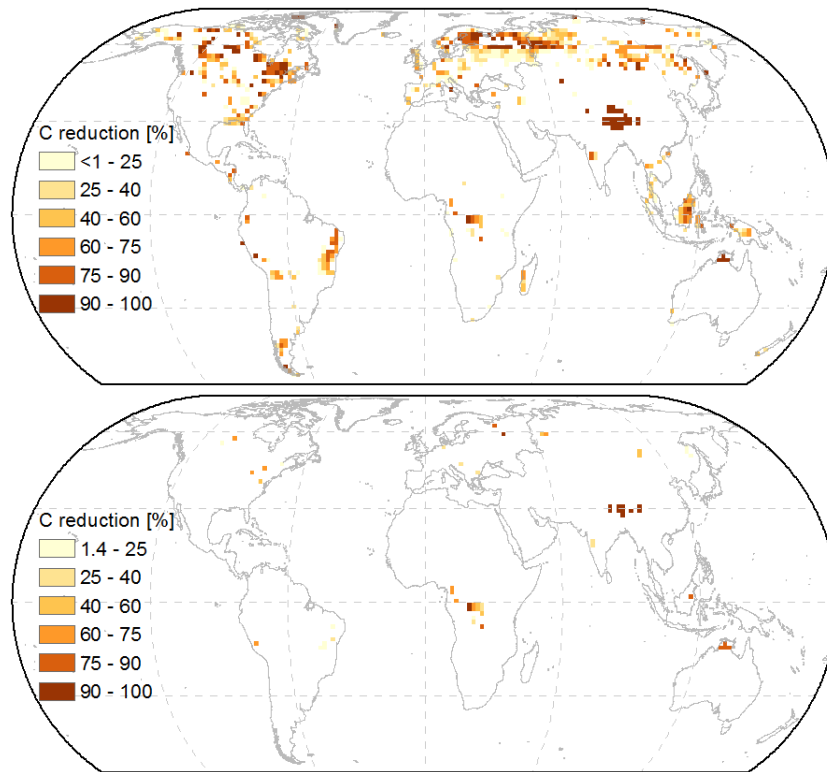


Fig. S27: Forest C sequestration reduction due to geogenic P limitation assuming P concentrations within foliar and wood material corresponding to 5th values (main text Table 1) estimated from stoichiometric C:P ratios. a) C-reduction based on P gaps of Fig. S 26a, obtained for geogenic P supply scenario one (geogenic P from weathering plus atmospheric P deposition as source of P). b) C-reduction based on P gaps of Fig. S 26c, obtained for geogenic P supply scenario two (geogenic P from soil inorganic labile P and organic P pools plus atmospheric P deposition and P from weathering as source of P). Map generated with ESRI ArcGIS 10.7 (<http://www.esri.com>).

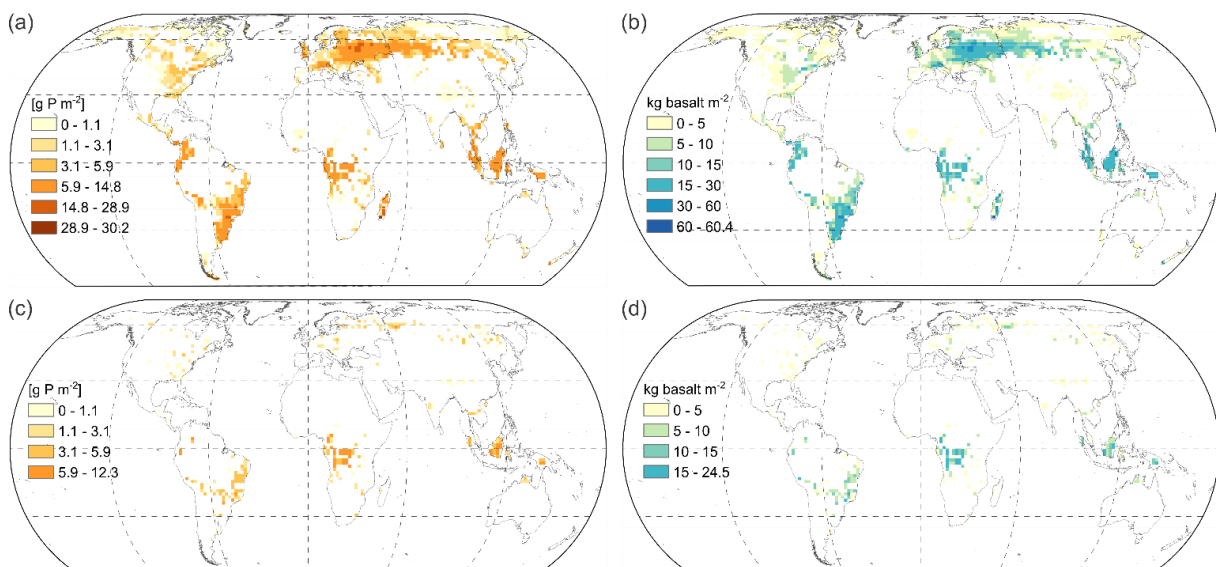


Fig. S 28: Areas with potential P gap for the nutrient budget of the N-limited AR scenario (after 94 years of simulation) assuming P concentrations within foliar and wood material corresponding to 95th percentile values (main text Table 1). a) Geogenic P supply scenario one (geogenic P from weathering plus atmospheric P deposition as source of P). b) Basalt deployment necessary to close P gaps from P budget scenario of Fig. S 28a. c) Geogenic P supply scenario two (geogenic P from soil inorganic labile P and organic P pools plus atmospheric P deposition and P from weathering as source of P). d) Basalt deployment necessary to close P gaps from P budget scenario of Fig. S 28c. Map generated with ESRI ArcGIS 10.7 (<http://www.esri.com>).

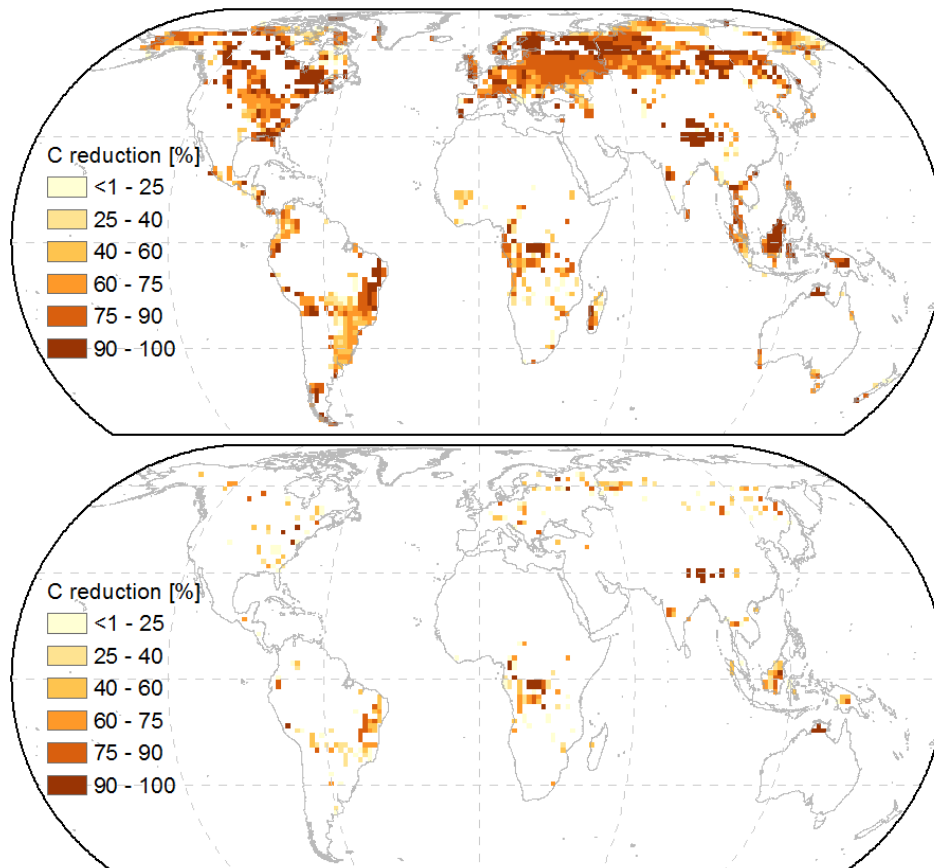


Fig. S29: Forest C sequestration reduction due to geogenic P limitation assuming P concentrations within foliar and wood material corresponding to 95th values (main text Table 1) estimated from stoichiometric C:P ratios. a) C-reduction based on P gaps of Fig. S 28a, obtained for geogenic P supply scenario one (geogenic P from weathering plus atmospheric P deposition as source of P). b) C-reduction based on P gaps of Fig. S 28c, obtained for geogenic P supply scenario two (geogenic P from soil inorganic labile P and organic P pools plus atmospheric P deposition and P from weathering as source of P). Map generated with ESRI ArcGIS 10.7 (<http://www.esri.com>).

ii. AR N-unlimited

The predicted C sequestration by N-unlimited AR scenario from Kracher (2017) is $\sim 2.4 \text{ Gt C a}^{-1}$. Different authors reported the potential C sequestration by afforestation or reforestation being of $0.3 - 3.3 \text{ Gt C a}^{-1}$ for the end of 2100 (National Research Council, 2015; Lenton, 2010; Lenton, 2014; Smith et al., 2015 apud Fuss et al., 2018). However, the predicted sequestration potential estimated by Kracher (2017) can fall to $\sim 1.4 \text{ Gt C a}^{-1}$ if geogenic P supply scenario one for mean P content within wood and leaves is selected. If geogenic P supply scenario two for mean P content within wood and leaves is selected, it fall to $\sim 2.2 \text{ Gt C a}^{-1}$.

The ideal P biomass additional demand (calculated from main text Eq. (1)), to sequester 224 Gt C (N-unlimited AR scenario) amounts to 244 Mt P on global scale for a mean wood and leaves P content; for 5th and 95th percentile, the estimated P demand would be 88 and 417 Mt P respectively. The potential C sequestration and the P demand of the N-unlimited AR scenario is higher than for the N-limited AR scenario.

The P budget for geogenic P supply scenario one, which considers P supply by weathering and atmospheric P deposition, for both N supply AR scenarios suggest that P deficiency areas are distributed along the world, but with higher occurrence within the northern hemisphere (Fig. S 32a). However, for geogenic P supply scenario two, which is the same as geogenic P supply scenario one plus geogenic P from soil inorganic labile P and organic P pools, the P deficiency areas are predominantly located at the southern hemisphere for both N supply AR scenarios (Fig. S 32c). If P is the only limiting nutrient, it is expected a C reduction of $1.8 - 52\%$ from the projected 224 Gt C ,

with mean C reduction of 39% for the geogenic P supply scenario one and 6% for the geogenic P supply scenario two (Table S6). If N and P are limiting nutrients, it is expected a C reduction of 16.5 – 59%, with mean C reduction of 47% for the geogenic P supply scenario one and 19% for the geogenic P supply scenario two. Accounting for N and P limitation on AR suggests that, on average; the biomass production will be affected, which decreases the C sequestration potential of AR strategies (Table S6). In some areas, the C sequestration reduction can reach up to 100% from predicted C sequestration of the AR models (Fig. S33).

Assuming a median P content of 500 ppm in basalt, the maximum mass applied in 94 years would be of 34 and 13 kg basalt m⁻² respectively for P gap from geogenic P supply scenarios one and two for the N-unlimited AR scenario and mean P concentrations within foliar and wood material (Fig. S 32). A total amount of 3.6 – 454 Gt basalt (N-unlimited AR scenario) applied by EW would be needed to cover the projected P gaps. To reach the maximum projected C sequestration potential of AR, covering the N and P biomass demand would be necessary. Basalt has a carbon capture potential of ~0.3 tCO₂ t⁻¹ basalt (Renforth, 2012), sequestering ~0.3 – ~37 Gt C (~1 – ~136.2 Gt CO₂) by the end of 2100 if basalt powder would be deployed to cover P gaps of the N-unlimited AR scenario.

The nutrient concentration of rocks will influence the necessary amounts to cover P gap of each P budget scenario for the AR scenarios. The cumulative applied rock powder mass will be different for each rock type (Table S5), with basalt being more effective to supply P for the estimated P gap areas due to relative high P content.

For a chemical composition corresponding to the 95th percentile, 10 kg basalt m⁻² would cover the maximum projected P gaps for all P supply scenarios. For a median chemical composition, deploying 34 kg basalt m⁻² would cover all the P gaps of the two geogenic P supply scenarios for the N-unlimited AR scenario and for the 5th percentile the necessary amount of rock would get even higher (Table S5).

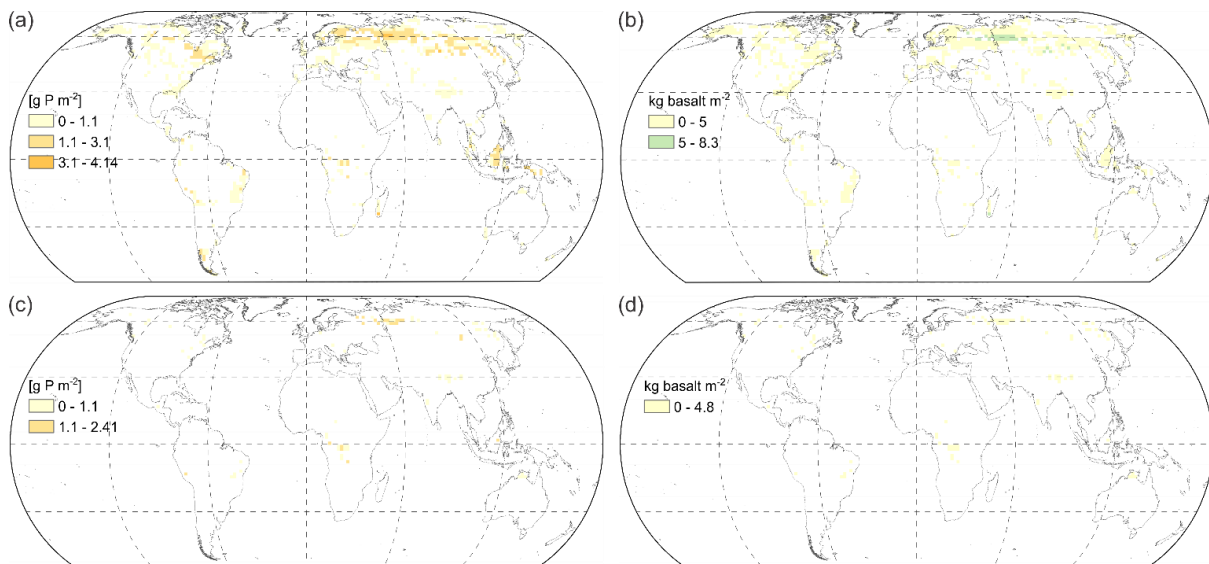


Fig. S 30: Areas with potential P gap for the nutrient budget of the N-unlimited AR scenario (after 94 years of simulation) assuming P concentrations within foliar and wood material corresponding to 5th percentile values (main text Table 1). a) Geogenic P supply scenario one (geogenic P from weathering plus atmospheric P deposition as source of P). b) Basalt deployment necessary to close P gaps from P budget scenario of Fig. S 30a. c) Geogenic P supply scenario two (geogenic P from soil inorganic labile P and organic P pools plus atmospheric P deposition and P from weathering as source of P). d) Basalt deployment necessary to close P gaps from P budget scenario of Fig. S 30c. Map generated with ESRI ArcGIS 10.7 (<http://www.esri.com>).

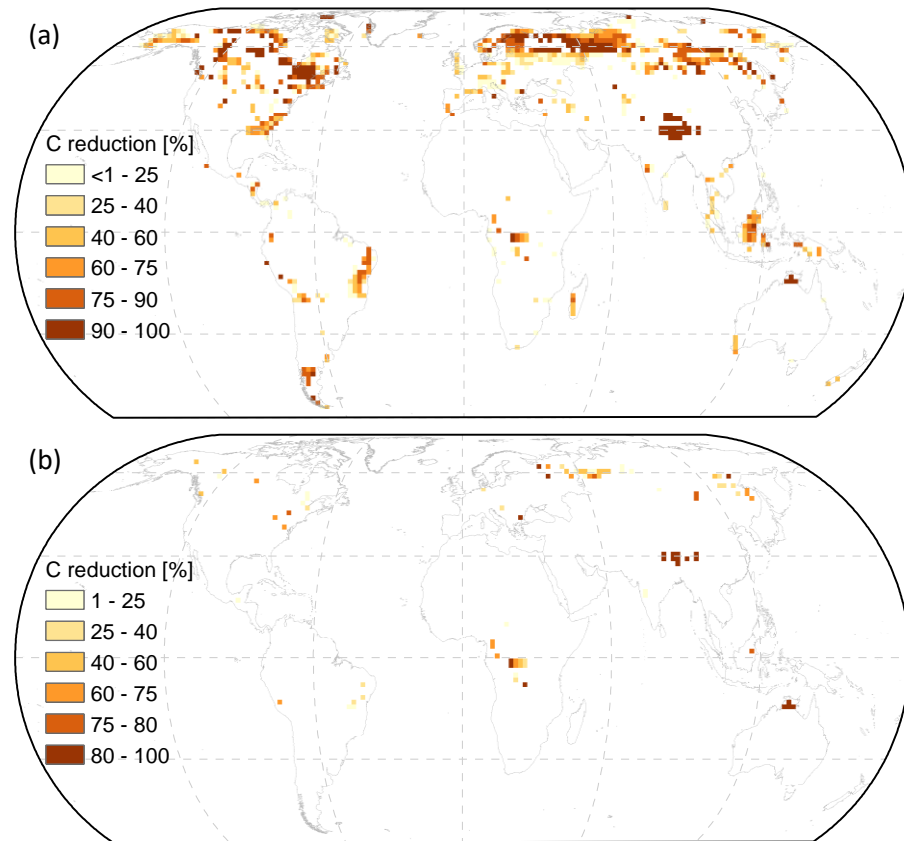


Fig. S31: Forest C sequestration reduction due to geogenic P limitation assuming P concentrations within foliar and wood material corresponding to 5th values (main text Table 1) estimated from stoichiometric C:P ratios. a) C-reduction based on P gaps of Fig. S 30a, obtained for geogenic P supply scenario one (geogenic P from weathering plus atmospheric P deposition as source of P). b) C-reduction based on P gaps of Fig. S 30c, obtained for geogenic P supply scenario two (geogenic P from soil inorganic labile P and organic P pools plus atmospheric P deposition and P from weathering as source of P). Map generated with ESRI ArcGIS 10.7 (<http://www.esri.com>).

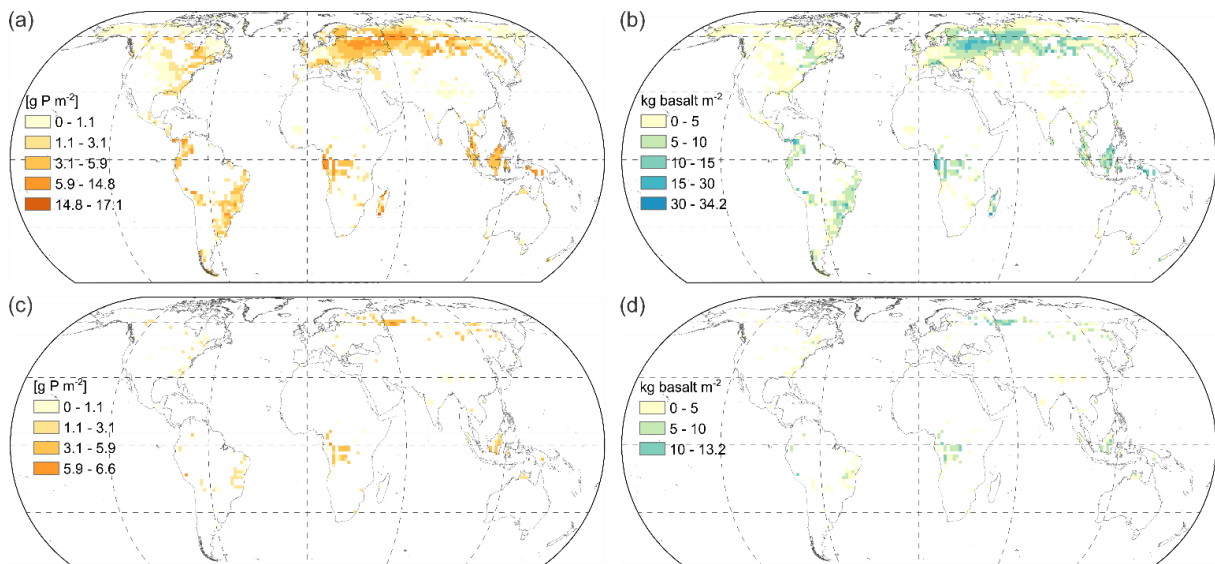


Fig. S 32: Areas with potential P gap for the nutrient budget of the N-unlimited AR scenario (after 94 years of simulation) assuming P concentrations within foliar and wood material corresponding to mean values (main text Table 1). a) Geogenic P supply scenario one (geogenic P from weathering plus atmospheric P deposition as source of P). b) Basalt deployment necessary to close P gaps from P budget scenario of Fig. S 32a. c) Geogenic P supply scenario two (geogenic P from soil inorganic labile P and organic P pools plus atmospheric P deposition and P from weathering as source of P). d) Basalt deployment necessary to close P gaps from P budget scenario of Fig. S 32c. Map generated with ESRI ArcGIS 10.7 (<http://www.esri.com>).

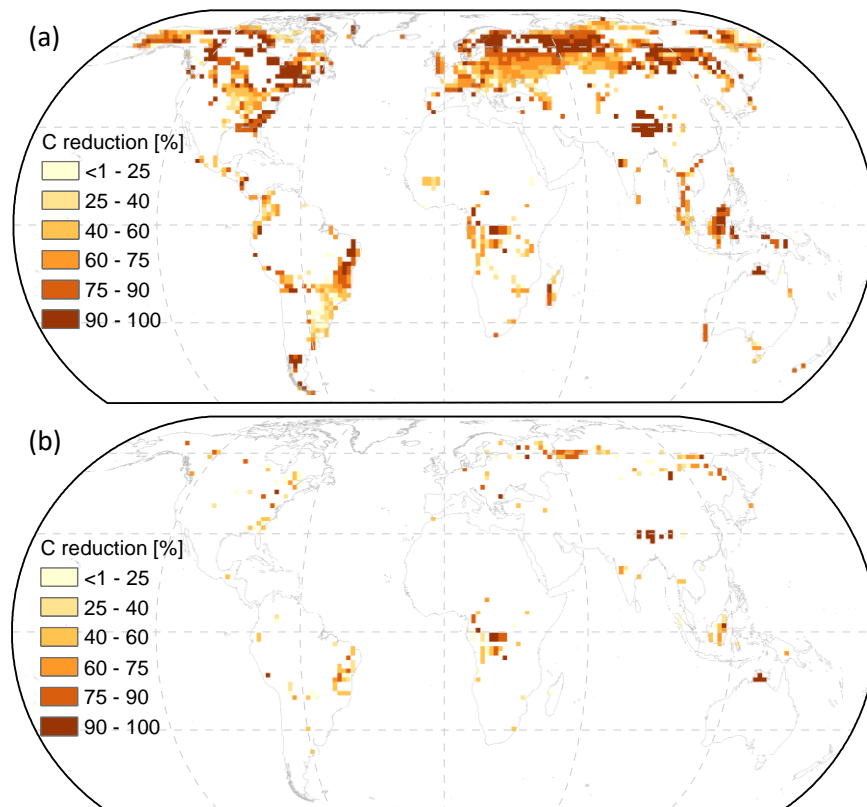


Fig. S33: Reduction on forest C sequestration due to geogenic P limitation. C-reduction estimated from stoichiometric C:P ratios for the N-unlimited AR scenario assuming P concentrations within foliar and wood material corresponding to mean values (Table 1 main text). a) C-reduction based on P gaps of Fig. S 32a, obtained for geogenic P supply scenario one (geogenic P from weathering plus atmospheric P deposition as source of P). b) C-reduction based on P gaps of Fig. S 32c, obtained for geogenic P supply scenario two (geogenic P from soil inorganic labile P and organic P pools plus atmospheric P deposition and P from weathering as source of P). For resulting global C reduction check Table S6. Map generated with ESRI ArcGIS 10.7 (<http://www.esri.com>).

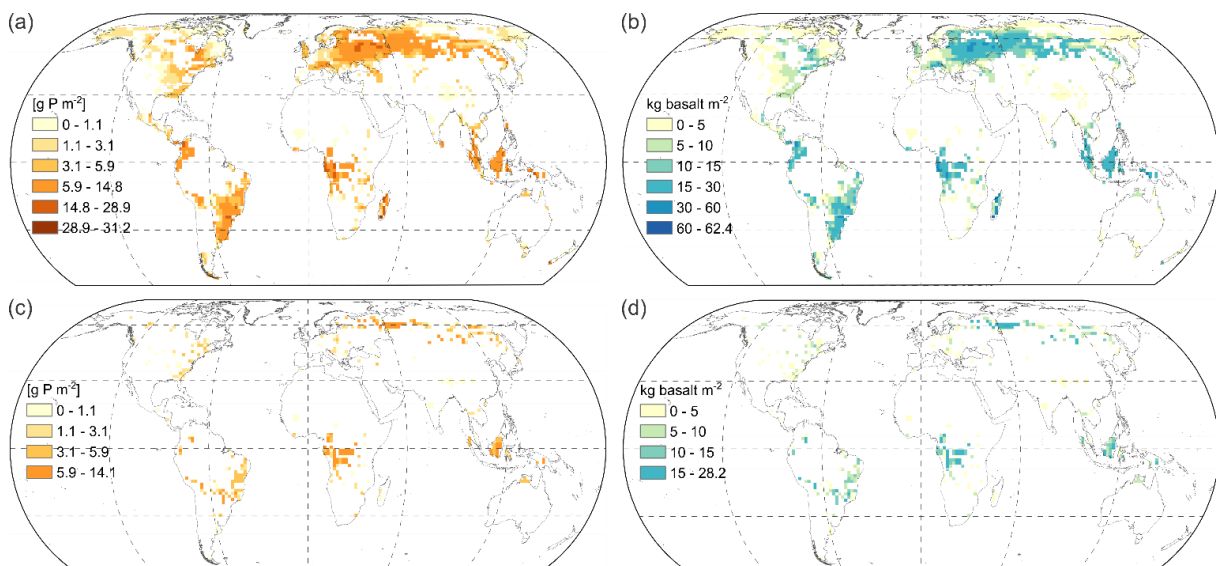


Fig. S 34: Areas with potential P gap for the nutrient budget of the N-unlimited AR scenario (after 94 years of simulation) assuming P concentrations within foliar and wood material corresponding to 95th percentile values (main text Table 1). a) Geogenic P supply scenario one (geogenic P from weathering plus atmospheric P deposition as source of P). b) Basalt deployment necessary to close P gaps from P budget scenario of Fig. S 34a. c) Geogenic P supply scenario two (geogenic P from soil inorganic labile P and organic P pools plus atmospheric P deposition and P from weathering as source of P). d) Basalt deployment necessary to close P gaps from P budget scenario of Fig. S 34c. Map generated with ESRI ArcGIS 10.7 (<http://www.esri.com>).

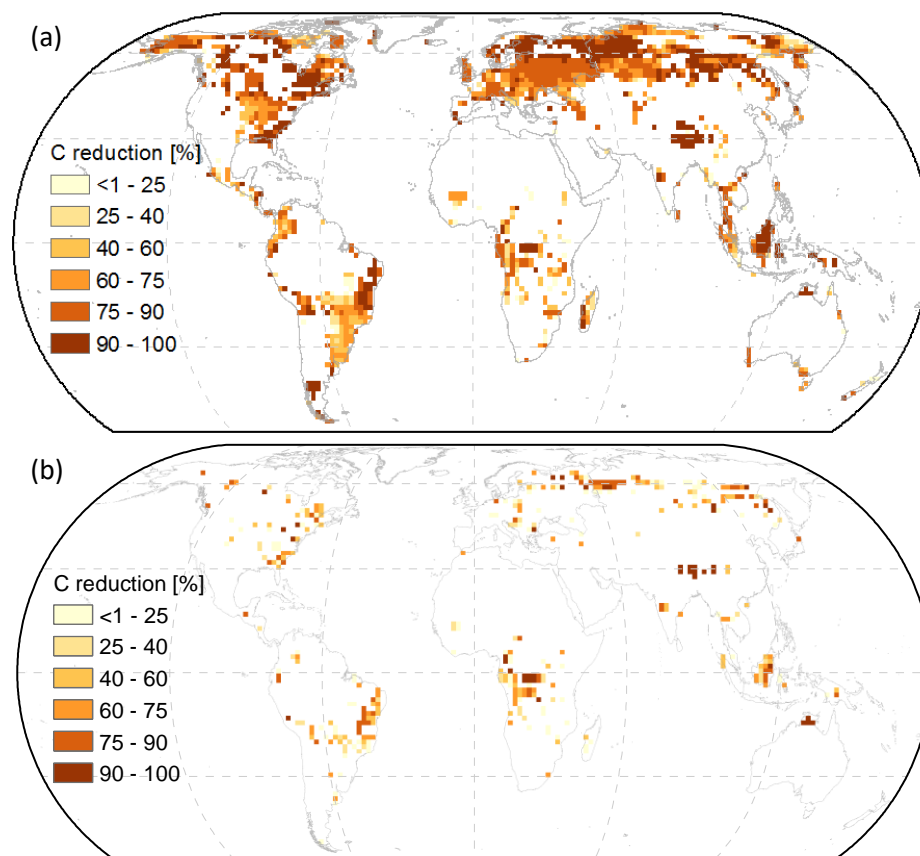


Fig. S35: Forest C sequestration reduction due to geogenic P limitation assuming P concentrations within foliar and wood material corresponding to 95th values (main text Table 1) estimated from stoichiometric C:P ratios. a) C-reduction based on P gaps of Fig. S 34a, obtained for geogenic P supply scenario one (geogenic P from weathering plus atmospheric P deposition as source of P). b) C-reduction based on P gaps of Fig. S 34c, obtained for geogenic P supply scenario two (geogenic P from soil inorganic labile P and organic P pools plus atmospheric P deposition and P from weathering as source of P). Map generated with ESRI ArcGIS 10.7 (<http://www.esri.com>).

Table S5: Rock powder application for a chemistry corresponding to the 5th percentile, assuming full rock dissolution, to cover maximum and median estimated P gaps for the N-unlimited AR scenario (minimum values can be neglected). For the potential macronutrient supply, see Fig. 7 main text and Fig. S 32.

	P gap [g P m ⁻²]	Rhyolite	Dacite	Andesite	Basalt
			[kg rock m ⁻²]		
Scenario one	17.1	783.4	156.7	120.5	112.0
	2.1	19.0	6.3	6.0	3.8
Scenario two	6.6	302.6	60.5	46.5	43.2
	1.8	17.0	5.7	5.3	3.4

Table S6: Global P gap, maximum estimated P gap, maximum C sequestration reduction, and global C reduction for the natural N supply (N-limited) AR scenario (projected C sequestration of 190 Gt C) and for the N fertilization (N-unlimited) AR scenario (projected C sequestration of 224 Gt C).

N supply	Geogenic P supply	Maximum estimated P gap [g P m ⁻²]			Global P gap [Mt P]			Maximum C sequestration reduction [kg C m ⁻²]			Global C reduction [Gt C]		
		Wood and leaves P content											
		5 th percentile	mean	95 th percentile	5 th percentile	mean	95 th percentile	5 th percentile	mean	95 th percentile	5 th percentile	mean	95 th percentile
Unlimited	Scenario one	4.1	17.1	31.2	16.0	100.0	227.0	10.0	15.0	16.0	34.0	88.0	117.0
	Scenario two	2.4	6.6	14.1	1.8	15.0	49.0	4.6	6.1	7.6	4.0	13.0	25.0

F. EW coupled to bioenergy grass production

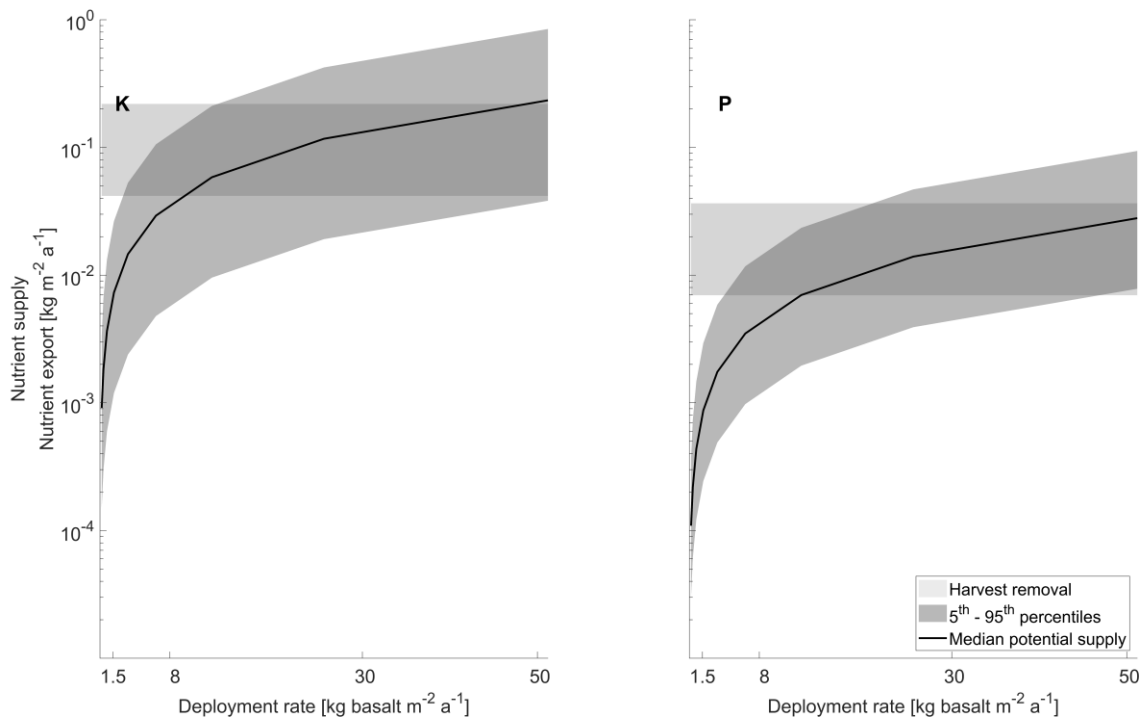


Fig. S 36: Projected K and P supply (logarithmic curve) by basalt complete dissolution given as median ranges (5th and 95th percentiles) for bioenergy grasses K and P demand (horizontal filled boxes) based on global minimum $0.7 \text{ kg m}^{-2} \text{ a}^{-1}$ and maximum $36 \text{ kg m}^{-2} \text{ a}^{-1}$ harvest rates.

G. Impacts on soil hydrology

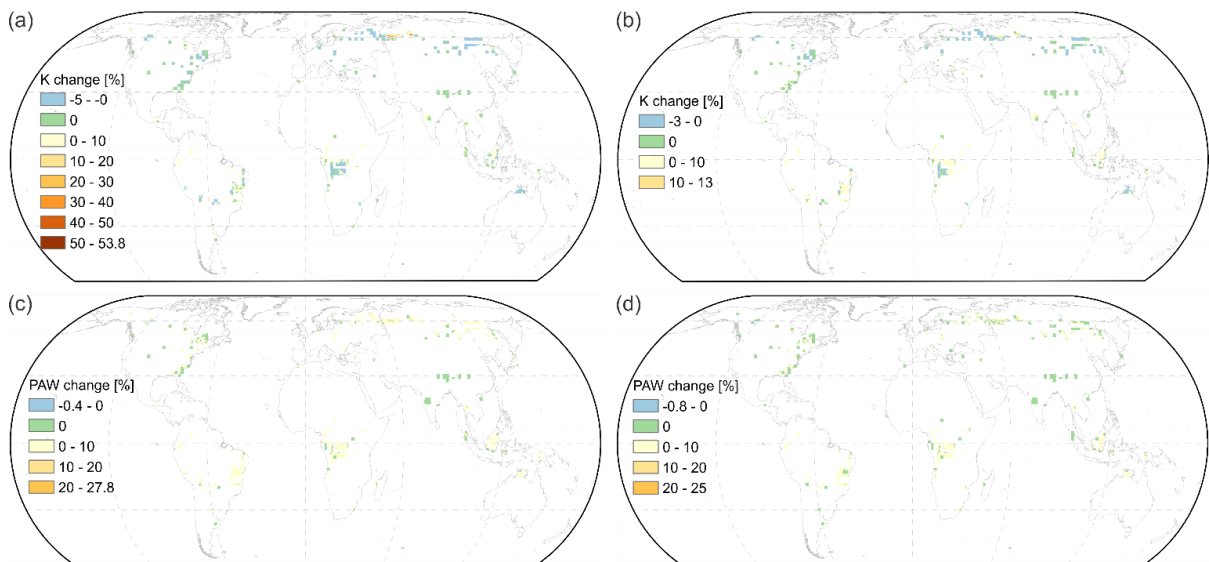


Fig. S 37: Impacts on soil hydrology estimated according to Saxton and Rawls (2006) equations for basalt deployment mass coincident to areas with potential P gap for the nutrient budget of the N-unlimited AR scenario assuming P concentrations within foliar and wood material corresponding to mean values (Fig. S 32c). a) Hydraulic conductivity (K) changes relative to initial soil values for a fine basalt texture (15.6% clay, 83.8% silt, and 0.6% sand) being deployed. b) Hydraulic conductivity (K) changes relative to initial soil values for a coarse basalt texture (15.6% clay, 53.8% silt, and 30.6% fine sand) being deployed. c) Plant available water (PAW) changes relative to initial soil values for a fine basalt texture being deployed. d) Plant available water (PAW) changes relative to initial soil values for a coarse basalt texture being deployed. Map generated with ESRI ArcGIS 10.7 (<http://www.esri.com>).

H. Systematic-review

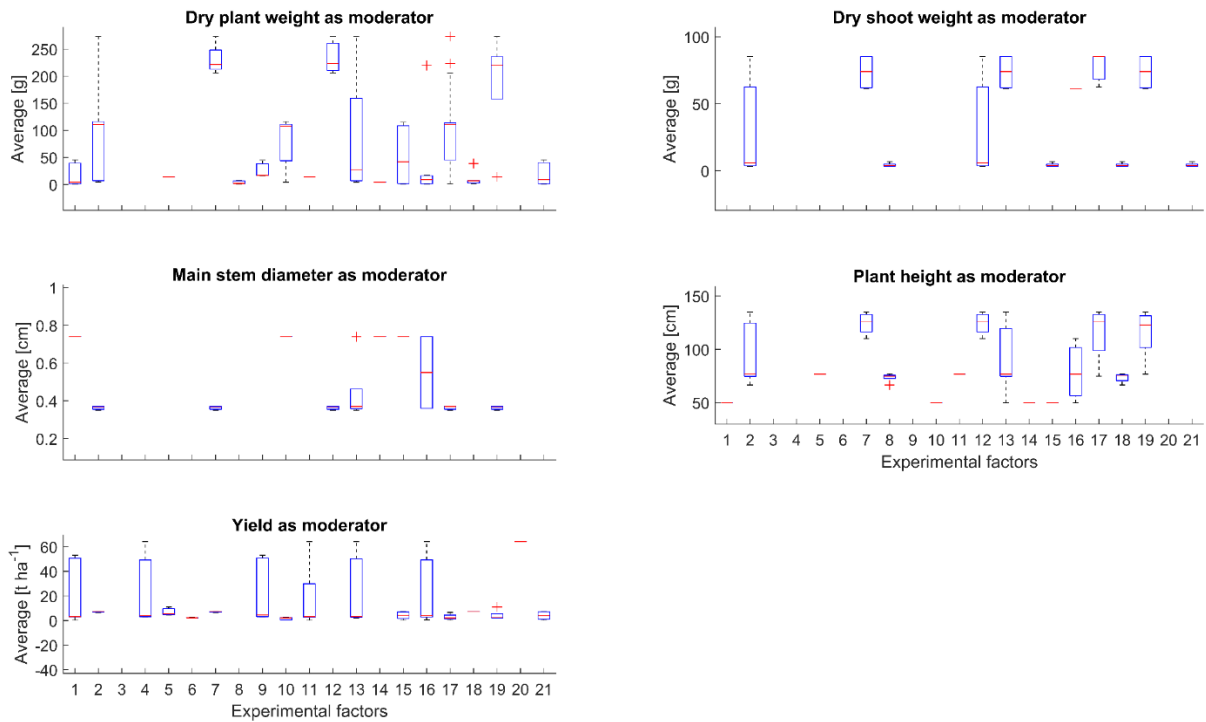


Fig. S 38: Descriptive statistics from the input EW data for the meta-analysis accounting only for the mean of experiments from selected papers. The numbers from x axis correspond to the following experimental factors (cf., section 2.1 from main text): 1) ≤ 3 months, 2) 3 – 6 months, 3) 6 – 9 months, 4) 9 – 12 months, 5) 12 – 24 months, 6) 24 – 40 months, 7) < 0.053 mm, 8) 0.053 – 0.1 mm, 9) 0.1 – 0.2 mm, 10) 0.2 – 2 mm 11) Field, 12) Lab, 13) Basic, 14) Intermediate, 15) Acid, 16) < 10 t ha⁻¹, 17) 10 – 40 t ha⁻¹, 18) ≥ 40 t ha⁻¹, 19) Fine, 20) Medium, and 21) Coarse.

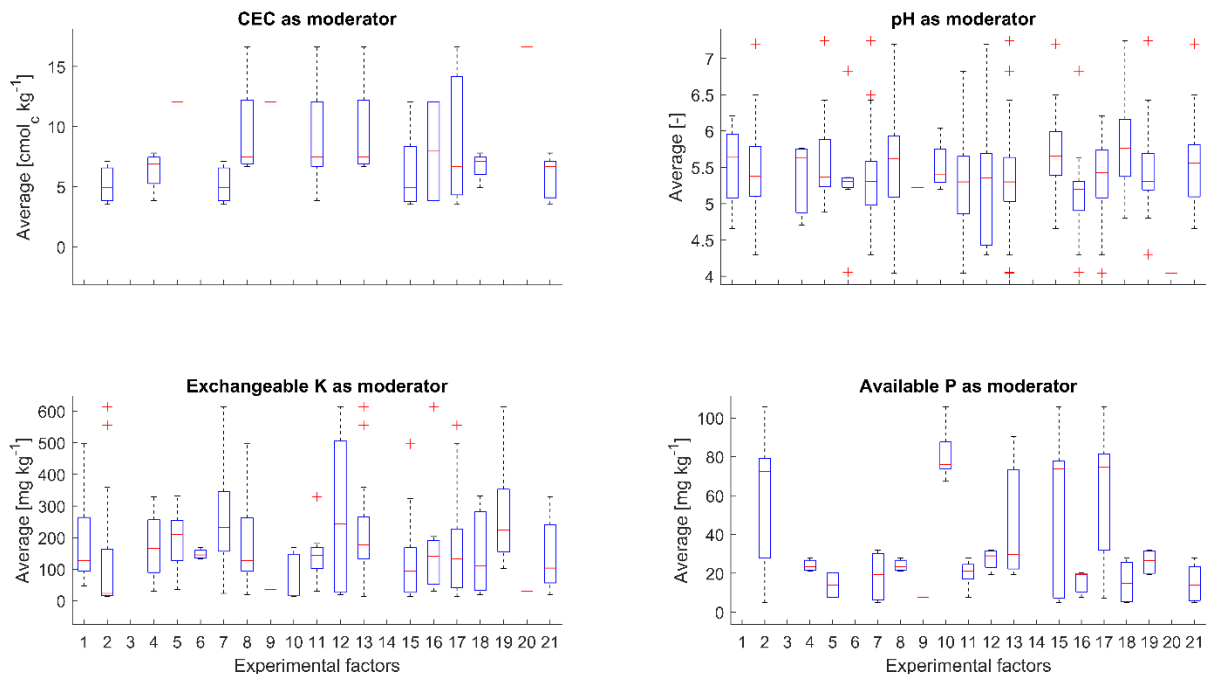


Fig. S 39: Descriptive statistics from the input EW data for the meta-analysis accounting only for the mean of experiments from selected papers. The numbers from x axis correspond to the following experimental factors (cf., section 2.1 from main text): 1) ≤ 3 months, 2) 3 – 6 months, 3) 6 – 9 months, 4) 9 – 12 months, 5) 12 – 24 months, 6) 24 – 40 months, 7) < 0.053 mm, 8) 0.053 – 0.1 mm, 9) 0.1 – 0.2 mm, 10) 0.2 – 2 mm 11) Field, 12) Lab, 13) Basic, 14) Intermediate, 15) Acid, 16) < 10 t ha⁻¹, 17) 10 – 40 t ha⁻¹, 18) ≥ 40 t ha⁻¹, 19) Fine, 20) Medium, and 21) Coarse.

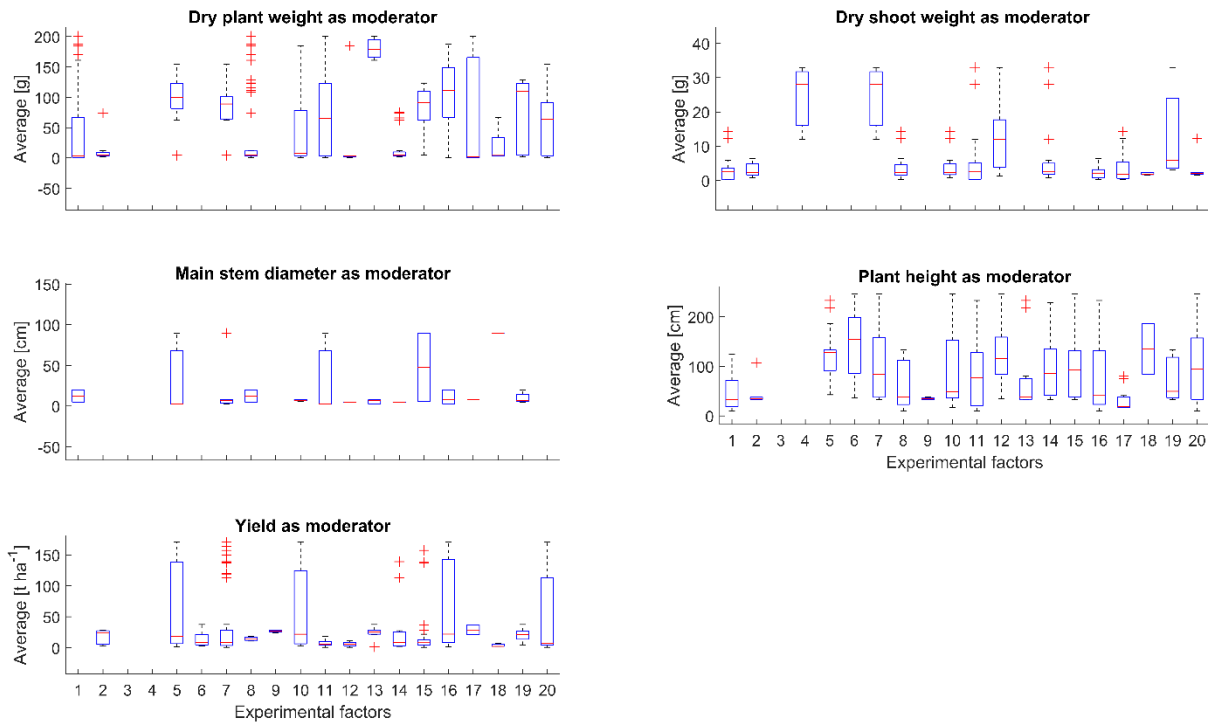


Fig. S 40: Descriptive statistics from the input Biochar data for the meta-analysis accounting only for the mean of experiments from selected papers. The numbers from x axis correspond to the following experimental factors (cf., section 2.1 from main text): 1) ≤ 3 months, 2) 3 – 6 months, 3) 6 – 9 months, 4) 9 – 12 months, 5) 12 – 24 months, 6) 24 – 40 months, 7) Field, 8) Lab, 9) Field, 10) Lab, 11) $\leq 350^\circ\text{C}$, 12) 350 – 500 $^\circ\text{C}$, 13) $> 500^\circ\text{C}$, 14) $< 10 \text{ t ha}^{-1}$, 15) 10 – 30 t ha^{-1} , 16) 30 – 80 t ha^{-1} , 17) $\geq 80 \text{ t ha}^{-1}$, 18) Fine, 19) Medium, and 20) Coarse.

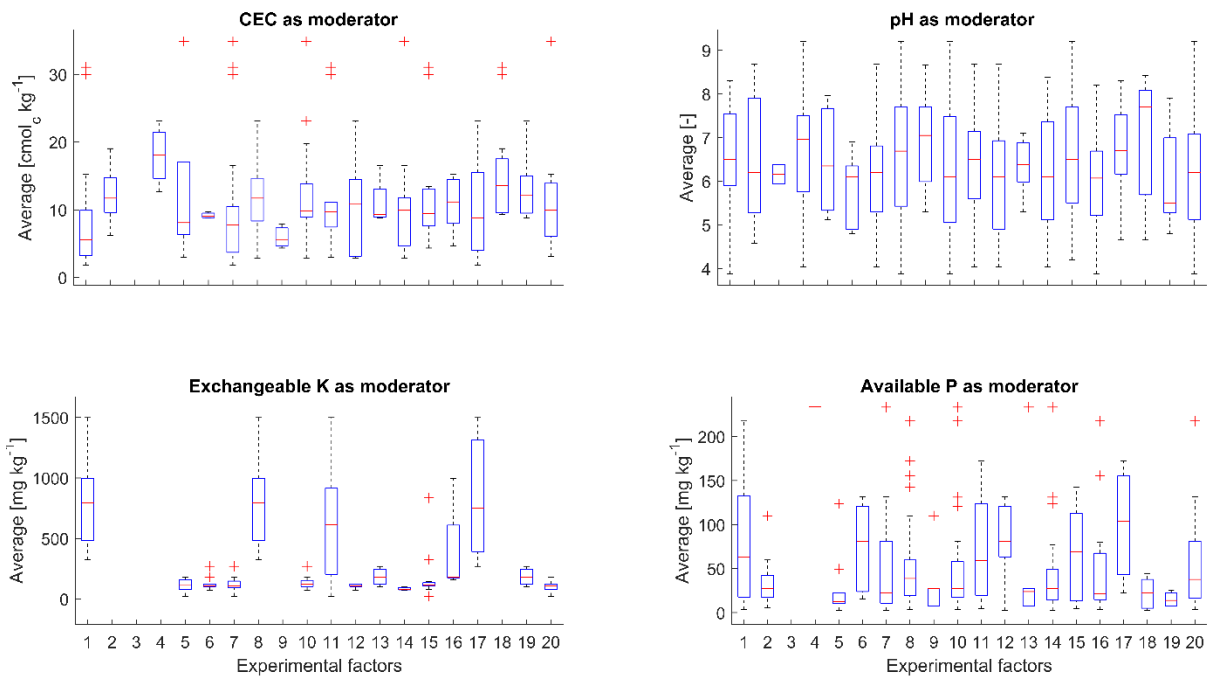


Fig. S 41: Descriptive statistics from the input Biochar data for the meta-analysis accounting only for the mean of experiments from selected papers. The numbers from x axis correspond to the following experimental factors (cf., section 2.1 from main text): 1) ≤ 3 months, 2) 3 – 6 months, 3) 6 – 9 months, 4) 9 – 12 months, 5) 12 – 24 months, 6) 24 – 40 months, 7) Field, 8) Lab, 9) Field, 10) Lab, 11) $\leq 350^\circ\text{C}$, 12) 350 – 500 $^\circ\text{C}$, 13) $> 500^\circ\text{C}$, 14) $< 10 \text{ t ha}^{-1}$, 15) 10 – 30 t ha^{-1} , 16) 30 – 80 t ha^{-1} , 17) $\geq 80 \text{ t ha}^{-1}$, 18) Fine, 19) Medium, and 20) Coarse.

Table S7: Used references within enhanced silicate rock weathering (EW) database and investigated properties.

Paper	Soil texture	Location	Crop	Rock powder treatment	Running time (months)	Property investigated								
						CEC	pH	Exchangeable K	Available P	Dry total plant mass	Dry shoot mass	Main stem diameter	Plant height	Yield
(Anda et al., 2009)	Clay	Malaysia	-	No fertilizer	15		X							
(Anda et al., 2015)	Clay	Malaysia	-	No fertilizer	24		X	X						
(Bakri et al., 2017)	Clay	Malaysia	Hevea brasiliensis	Fertilizer	6		X	X	X	X	X	X	X	
(Bamberg et al., 2013)	Sand	Brazil	Maize	P and compost	12	X	X							X
(Bolland and Baker, 2000)	Sand	Australia	Wheat	No fertilizer	1									X
(Carvalho, 2012)	-	Brazil	Bean	Compost	15	X	X	X	X					X
(Carvalho, 2012)	-	Brazil	Maize	Compost N,P,Ca,Mg,Cu,Zn,Mn,Co, and Mo	4			X	X	X				
(Coroneos et al., 1996)	Sand	Australia	Ryegrass	Mo	5		X	X			X			
(da Silva et al., 2012)	Clay	Brazil	Bean	K,P	36		X	X						X
(de Souza et al., 2013a)	Clay	Brazil	Grass	P	14					X				
(de Souza et al., 2013b)	Sand	Brazil	Maize	No fertilizer	2.4					X				
(Dietzen et al., 2018)	Sand	Denmark	-	No fertilizer	3		X							
(Erhart, 2009)	Sandy Clay	Brazil	Wine tree	No fertilizer	12		X							
(Feiden, 1991)	-	Brazil	Wheat	No fertilizer	4		X			X			X	
(Grecco et al., 2013)	Sand	Brazil	Maize	P	1.5					X				
(Hinsinger et al., 1996)	Sand	Australia	-	No fertilizer	3		X	X						
(Li and Dong, 2013)	-	China	Tomato	Rice straw	1					X		X	X	
(Luz et al., 2013)	Median	Brazil Czech	Sugarcane	No fertilizer	12			X						X
(Madaras et al., 2013)	Sand	Republic	Barley	NP	1.5					X				
(Melo et al., 2012)	Sandy Clay Loam	Brazil	-	Compost	6		X							
(Mersi et al., 1992)	-	Austria	-	No fertilizer	36		X							
(Noordin et al., 2017)	Sandy Clay	Malaysia	Hevea brasiliensis	No fertilizer	12	X	X	X	X					
(Panhwar et al., 2016)	Fine	Malaysia	Rice grain	NPK	18		X	X	X				X	X
(Sachse, 1927)	-	Germany	Turnip	No fertilizer	3									X

Table S7: Used references within enhanced silicate rock weathering (EW) database and investigated properties.

Paper	Soil texture	Location	Crop	Rock powder treatment	Running time (months)	Property investigated									
						CEC	pH	Exchangeable K	Available P	Dry total plant mass	Dry shoot mass	Main stem diameter	Plant height	Yield	
(Silva et al., 2013)	Loamy Sand	Spain	Ryegrass	No fertilizer	3.5	X	X	X	X						X
(Von Wilpert and Lukes, 2003)	Loam	Germany	Spruce Stand	No fertilizer	60	X	X								

Table S8: Used references within Biochar database and investigated properties.

Paper	Soil texture	Location	Crop	Biochar treatment	Running time (months)	Property investigated									
						CEC	pH	Available K	Available P	Dry total plant mass	Dry shoot mass	Main stem diameter	Plant height	Yield	
(Agbna et al., 2017)	Loam	China	Tomato	NPK	16					X				X	X
(Agegnehu et al., 2015a)	Sandy Clay Loam	Australia	Peanut	Compost, chicken manure, green waste	5	X	X		X						X
(Agegnehu et al., 2015b)	Clay	Australia	Maize	NPK, Compost	2	X								X	
(Agegnehu et al., 2016a)	Clay	Australia	Maize	Compost, chicken manure, green waste	4.8	X	X		X						X
(Agegnehu et al., 2016b)	Clay	Ethiopia	Barley	triple superphosphate, Urea (N)	6										X
(Amendola et al., 2017)	Clay	Italy	Grapevine	-	12	X	X		X						
(Amoakwah et al., 2017)	Sandy Loam	Ghana	-	P addition Poultry or farmyard manure, diammonium phosphate	6		X								
(Arif et al., 2017)	Silty Clay Loam	Pakistan	Maize		24		X		X					X	X
(Backer et al., 2016)	Loamy Sand	Canada	Switchgrass	N fertilizer	36		X	X	X					X	X
(Bamminger et al., 2016)	Silt Loam	Germany	Winter rapeseed	-	12		X								
(Bandara et al., 2017)	-	Sri Lanka	Tomato	No treatment	2	X	X								
(Bass et al., 2016)	Clay	Australia	Banana	NPK	13	X	X		X						
(Boersma et al., 2017)	Loam	Australia	Cauliflower	NPK	12								X		X
(Bruun et al., 2014)	Sand	Denmark	Barley	NPK	3					X					
(Castaldi et al., 2011)	Silty Loam	Italy	Wheat	-	14		X								

Table S8: Used references within Biochar database and investigated properties.

Paper	Soil texture	Location	Crop	Biochar treatment	Running time (months)	Property investigated									
						CEC	pH	Available K	Available P	Dry total plant mass	Dry shoot mass	Main stem diameter	Plant height	Yield	
(Changxun et al., 2016)	Clay	China	Poncirus trifoliata	-	7		X								
(Chen et al., 2010)	Clay	Japan	Sugarcane	NPK	15							X	X	X	
(Chen et al., 2016)	Sandy Loam	China	Oryza sativa L. (Rice)	-	18		X								
(Chintala et al., 2014)	Clay Loam	USA	-	-	5.5	X	X								
(Curaqueo et al., 2014)	Silt Loam	Chile	Barley	-	6		X		X				X	X	
(De Tender et al., 2016)	Sandy Loam	Belgium	Lettuce	Fertilizer	2-3					X					
(Dong et al., 2013)	Sandy Loam	China	Rice	NPK	24	X	X	X	X				X		
(Dong et al., 2015)	Clay Loam	China	Rice	NPK	24		X					X		X	
(Drake et al., 2016)	Loam	Australia	Acacia mearnsii	-	3							X	X		
(El-Naggar et al., 2018)	Loamy Sand	China	-	-	24	X	X								
(Foster et al., 2016)	Sandy Clay Loam	USA	Maize	NPK	4		X								
(Guo et al., 2017)	-	China	M. pauh oi	Seawage	4		X					X			
(Haider et al., 2017)	Silty Sand	Germany	Maize	PKS	40										X
(Hossain et al., 2015)	-	Australia	Tomato	-	4					X			X		
(Hu et al., 2014)	Silty Clay Loam	Canada	Barley	No Fertilization	15		X								
(Inal et al., 2015)	Clay Loam	Turkey	Bean	Ammonium Nitrate	1.5		X								
(Jien and Wang, 2013)	Silty Clay	Taiwan	Pineapple	-	3.5	X	X								
(Jones et al., 2012)	Sandy Clay Loam	Wales	Dactylis glomerata	NPK	36		X		X				X	X	
(Jones et al., 2016)	Sandy Loam	France	Sunflower	Compost	1.5								X		
(Keith et al., 2015)	Loamy Fine Sand	Australia	Soybean	-	1							X			
(Kelly et al., 2015)	Clay	USA	-	NPK	2		X	X	X						
(Laghari et al., 2015)	Sand	China	Sorghum	NPK	2								X		
(Laghari et al., 2016)	Sand	China	Sorghum	-	2					X			X		
(Lee et al., 2015)	Loam	Korea	Soybean	-	1.5					X		X	X		
(Li et al., 2018)	Sandy Loam	China	Tomato	Fertilizer	24			X	X	X					X

Table S8: Used references within Biochar database and investigated properties.

Paper	Soil texture	Location	Crop	Biochar treatment	Running time (months)	Property investigated									
						CEC	pH	Available K	Available P	Dry total plant mass	Dry shoot mass	Main stem diameter	Plant height	Yield	
(Liang et al., 2014)	Silt Loam	China	Wheat	NPK	36	X		X	X						X
(Lin et al., 2015)	Loamy Sand	China	Soybean	NPK	12		X								
(Macdonald et al., 2014)	Sand	Australia	-	Ruakura nutrient solution	4.5		X		X	X	X				
(Martinsen et al., 2014)	Sand	Zambia	-	NPK and Urea	1	X	X								
(Mete et al., 2015)	Sand	Bangladesh	Soybean	NPK	4		X		X						
(Mickan et al., 2016)	Sandy Loam	Australia	Clover	-	2		X				X				
(Nguyen et al., 2018)	-	Australia	-	Fertilizer	12		X								
(Park et al., 2011)	-	Australia	Indian mustard	-	2		X				X				
(Pfister and Saha, 2017)	Sandy loam	USA	Sunflower	NPK	3		X								X
(Pratiwi and Shinogi, 2016)	Loam	Japan	Rice	NPK	3										X
(Robertson et al., 2012)	Silt Loam	Canada	Pine	Urea	12	X	X								
(Rousk et al., 2013)	-	Canada	-	NPK	36		X								
(Rutigliano et al., 2014)	Silty Loam	Italy	Wheat	NP	14		X								
(Saxena et al., 2013)	Loam	India	French beans	Di-ammonium phosphate, Biofertilizer	2						X	X			
(Upadhyay et al., 2014)	Sand	Australia	Lettuce	-	2					X	X				
(Vaccari et al., 2011)	Sandy Loam	Italy	Durum Wheat	NP	24		X								X
(Vaccari et al., 2015)	Silty Clay	Italy	Tomato	NPK	2	X			X	X					
(Wang et al., 2016b)	Loam	China	Soybean	NPK	-							X	X		
(Xu et al., 2016)	-	China	-	Urea	5		X								
(Zhao et al., 2014)	Silt Loam	China	Wheat	NPK	6	X	X								
(Zhou et al., 2018)	-	China	Wheat	Inorganic fertilizer NPK	24		X								
(Zhu et al., 2014)	Sandy Loam	China	Maize	NPK	1	X	X		X						
(Zhu et al., 2017)	Silt Loam	China	Maize	NPK	24		X			X					X

Table S9: Percentage changes on plant properties after biochar deployment for different experimental factors.

Moderators Experimental factor	Dry total plant mass			Dry shoot mass			Main stem diameter			Plant height			Yield		
	CL [%]	Mean [%]	CU [%]	CL [%]	Mean [%]	CU [%]	CL [%]	Mean [%]	CU [%]	CL [%]	Mean [%]	CU [%]	CL [%]	Mean [%]	CU [%]
0 – 3 months ^a	-37	17	117	-61	100	918	-21	15	66	-17	24	88	-	-	-
3 – 6 months ^a	-46	29	210	-23	32	127	-	-	-	-18	10	48	-13	25	81
6 – 9 months ^a	-	-	-	-	-	-	-	-	-	-	-	-	-	-	-
9 – 12 months ^a	-	-	-	-72	6	301	-	-	-	-	-	-	-	-	-
12 – 24 months ^a	20	35	53	-	-	-	-74	4	323	-1	8	17	-3	33	83
24 – 40 months ^a	-	-	-	-	-	-	-	-	-	-13	1	19	1	5	8
Field ^b	-39	42	227	-72	6	301	-27	18	89	-24	7	53	-24	13	68
Lab ^b	6	18	31	-21	53	195	-21	15	66	-16	19	69	7	23	42
≤350°C ^c	-	-	-	-	-	-	-	-	-	-26	9	61	-8	18	51
350°C – 500°C ^c	-36	35	182	-54	22	223	-44	26	183	-28	9	64	-19	23	87
>500°C ^c	2	13	27	-62	106	1033	-74	4	323	-11	20	62	-26	3	43
Woody biochar ^d	-71	17	380	-26	5	49	-	5	-	-24	5	44	-20	-4	16
Crop residues biochar ^d	-46	0.5	87	-	-	-	-27	20	99	-27	13	75	-8	12	35
≤10 t ha ^{-1e}	-32	27	137	-53	22	216	-	5	-	-25	7	54	-17	17	65
10 t ha ⁻¹ – 30 t ha ^{-1e}	9	24	40	-	-	-	-	6	-	-9	8	27	-27	5	52
30 t ha ⁻¹ – 80 t ha ^{-1e}	24	45	70	-32	86	407	-29	20	104	-32	26	130	-16	35	117
>80 t ha ^{-1e}	-51	15	171	-23	74	294	-	-	-	-16	31	103	-	4	-
Fine ^f	-12	15	50	-70	46	598	-	-	-	-	4	-	-83	8	594
Medium ^f	0	13	29	-47	18	161	-21	20	82	-24	10	60	-8	14	43
Coarse ^f	-40	43	242	-28	19	97	-	-	-	-18	17	66	-30	12	79
Summary	15	29	44	-23	49	186	-21	16	71	-18	13	56	-22	14	67

The uppercase letters indicate the different groups of experimental factors: a- ; b- experimental type; c- biochar pyrolysis temperature; d- used feedstock for biochar production; e- deployment rate of biochar; and f- soil texture.

Table S10: Percentage changes on soil properties after biochar deployment for different experimental factors.

Moderators	CEC			pH			Exchangeable K			Available P		
	Experimental factor	CL [%]	Mean [%]	CU [%]	CL [%]	Mean [%]	CU [%]	CL [%]	Mean [%]	CU [%]	CL [%]	Mean [%]
0 – 3 months ^a	-28	36	155	-20	11	54	-55	93	738	-17	19	71
3 – 6 months ^a	-14	35	110	-8	7	24	-	-	-	-6	4	15
6 – 9 months ^a	-	-	-	-	-	35	-	-	-	-	-	-
9 – 12 months ^a	-38	6	82	-8	4	18	-	-	-	-	-	-
12 – 24 months ^a	-59	21	262	-6	5	17	-63	103	998	-48	58	376
24 – 40 months ^a	-35	1	55	-2	5	13	-65	22	319	-21	-6	12
Field ^b	-22	28	108	-21	8	48	-54	41	333	-10	1	13
Lab ^b	-15	31	103	-6	8	23	-55	93	738	-15	21	71
≤350°C ^c	-100	55	49684	-3	-0.2	3	-	-	-	-3	0.01	3
350°C – 500°C ^c	-13	11	42	-9	5	20	-57	35	326	-21	16	70
>500°C ^c	-30	32	149	-15	9	39	-45	96	600	-27	25	113
Woody biochar ^d	-18	24	86	-10	5	24	-51	9	140	-33	3	58
Crop residues biochar ^d	-14	0.3	17	-12	8	32	-100	63	356247	-3	0.1	3
≤10 t ha ^{-1e}	-9	9	32	-2	3	7	-79	-13	264	-6	9	26
10 t ha ⁻¹ – 30 t ha ^{-1e}	-11	15	50	-6	3	13	-35	28	153	-20	1	28
30 t ha ⁻¹ – 80 t ha ^{-1e}	-39	23	146	-12	8	32	12	86	211	-16	18	66
>80 t ha ^{-1e}	-38	55	284	-14	20	67	-74	175	2793	-71	35	519
Fine ^f	-16	52	175	-9	5	21	-	-	-	-39	18	129
Medium ^f	-11	7	29	-11	4	21	-100	63	356247	-5	0.05	6
Coarse ^f	-18	7	41	-22	8	50	-40	31	183	-24	11	60
Summary	-14	29	95	-20	8	46	-46	54	338	-8	10	32

The uppercase letters indicate the different groups of experimental factors: a- ; b- experimental type; c- biochar pyrolysis temperature; d- used feedstock for biochar production; e- deployment rate of biochar; and f- soil texture. CL – Lower confidence interval, CU – Upper confidence interval.

Table S11: Percentage changes on plant properties after EW deployment for different experimental factors.

Moderators	Dry total plant mass			Dry shoot mass			Main stem diameter			Plant height			Yield			
	Experimental factor	CL [%]	Mean [%]	CU [%]	CL [%]	Mean [%]	CU [%]	CL [%]	Mean [%]	CU [%]	CL [%]	Mean [%]	CU [%]	CL [%]	Mean [%]	CU [%]
0 – 3 months ^a	-42	61	346	-	-	-	-	-	-	-	-	-	-	-7	6	22
3 – 6 months ^a	-29	-10	14	-55	27	256	-34	-19	-1	-39	-17	14	-48	69	448	
6 – 9 months ^a	-	-	-	-	-	-	-	-	-	-	-	-	-	-	-	-
9 – 12 months ^a	-	-	-	-	-	-	-	-	-	-	-	-	-	-98	-1	5389
12 – 24 months ^a	-	5	-	-	-	-	-	-	-	-	-	-	-	-65	76	803
24 – 40 months ^a	-	-	-	-	-	-	-	-	-	-	-	-	-	-	-4	-
<0.053 mm ^b	-57	-15	66	-71	-7	197	-34	-19	-1	-57	-24	34	-48	69	448	
0.053 mm – 0.1 mm ^b	-62	30	341	-47	56	364	-	-	-	-32	-11	16	-	-	-	-
0.1 mm – 0.2 mm ^b	-25	14	74	-	-	-	-	-	-	-	-	-	-	-6	8	23
0.2 mm – 2 mm ^b	-16	-1	18	-	-	-	-	-	-	-	-	-	-	-85	-22	313
Field ^c	-	5	-	-	-	-	-	-	-	-	-	-	-	-45	10	121
Lab ^c	-57	-15	66	-55	27	256	-34	-19	-1	-57	-24	34	-	-	-	-
Basic ^d	-41	-11	35	-71	-7	197	-54	-12	69	-46	-12	43	-42	17	139	
Intermediate ^d	-	-	-	-	-	-	-	-	-	-	-	-	-	-	-	-
Acid ^d	-48	40	275	-47	56	364	-	-	-	-	-	-	8	35	69	
<10 t ha ^{-1e}	-37	36	195	-	-	-	-	4	-	-99	-6	14481	-43	15	132	
10 t ha ⁻¹ – 40 t ha ^{-1e}	-25	-1	29	-97	-2	3094	-51	-19	34	-48	-18	30	-100	-13	21244	
≥40 t ha ^{-1e}	-86	9	772	-47	56	364	-	-	-	-42	-11	36	-	75	-	
Fine ^f	-48	-14	44	-71	-7	197	-34	-19	-1	-74	-18	154	19	71	144	
Medium ^f	-	-	-	-	-	-	-	-	-	-	-	-	-	-	-	-
Coarse ^f	-44	58	350	-47	56	364	-	-	-	-	-	-	6	34	69	
Summary	-47	11	134	-55	27	256	-54	-12	69	-46	-12	43	-0.4	23	52	

The uppercase letters indicate the different groups of experimental factors: a- ; b- grain size of used rock powder; c- experimental type; d- rock type chemistry; e- deployment rate of rock powder; and f- soil texture. CL – Lower confidence interval, CU – Upper confidence interval.

Table S12: Percentage changes on soil properties after EW deployment for different experimental factors.

Moderators	CEC			pH			Exchangeable K			Available P		
	CL [%]	Mean [%]	CU [%]	CL [%]	Mean [%]	CU [%]	CL [%]	Mean [%]	CU [%]	CL [%]	Mean [%]	CU [%]
0 – 3 months ^a	-	-	-	-5	10	27	-37	19	122	-	-	-
3 – 6 months ^a	-100	63	138717	-5	13	35	-79	16	539	-58	-1	131
6 – 9 months ^a	-	-	-	-	-	-	-	-	-	-	-	-
9 – 12 months ^a	-27	25	115	-7	10	30	-99	231	156212	-88	212	8198
12 – 24 months ^a	-	-	-	-5	7	20	-29	47	204	-	4	-
24 – 40 months ^a	-	-	-	-	-	-3	-36	26	149	-	-	-
<0.053 mm ^b	-100	63	138717	-8	18	50	-79	31	716	-67	6	233
0.053 mm – 0.1 mm ^b	-23	30	118	-5	9	24	-37	43	228	-88	212	8198
0.1 mm – 0.2 mm ^b	-	-	-	-	-	-	-	-	-	-	-	-
0.2 mm – 2 mm ^b	-	-	-	-21	7	44	-18	13	57	-45	-5	64
Field ^c	-16	20	71	-5	9	24	4	81	214	-55	111	887
Lab ^c	-	-	-	-25	11	64	-89	-36	280	-80	48	1014
Basic ^d	-23	30	118	1	14	27	-75	21	471	-53	50	381
Intermediate ^d	-	-	-	-	-	-	-	-	-	-	-	-
Acid ^d	-57	32	308	-6	8	23	-57	37	341	-57	-12	79
<10 t ha ^{-1e}	-	3	-	-4	6	17	-82	10	573	-	11	-
10 t ha ⁻¹ – 40 t ha ^{-1e}	-22	23	94	-3	9	22	-82	10	571	-50	11	143
≥40 t ha ^{-1e}	-12	48	149	5	18	34	76	232	526	-99	43	15549
Fine ^f	-	-	-	-9	12	37	-82	-5	405	-67	39	486
Medium ^f	-	-	-	-	-	-	-	-	-	-	-	-
Coarse ^f	-4	33	84	-3	11	26	-69	72	844	-83	44	1150
Summary	-7	26	72	-3	11	26	-67	30	421	-59	15	224

The uppercase letters indicate the different groups of experimental factors: a- ; b- grain size of used rock powder; c- experimental type; d- rock type chemistry; e- deployment rate of rock powder; and f- soil texture. CL – Lower confidence interval, CU – Upper confidence interval.

Acknowledgements

First, I would like to thank my family and my friends for the constant support and motivation. Prof. Dr. Jens Hartmann, thank you for the support. Dr. Thorben Amann, thank you for the supervision and scientific discussions. Prof. Dr. Jörn Peckmann, thank you for being the second reviewer of this thesis. I would also like to thank Prof. Dr. Jens Hartmann, Prof. Dr. Victor Brovkin, Prof. Dr. Jörn Peckmann, Prof. Dr. Lars Kutzbach, and Dr. Thorben Amann, for being part of my doctoral committee and for their critics to this thesis, which will be considered to improve this work, and in my scientific career. Prof. Dr. Lars Kutzbach, thank you for being part of my advisory panel.

SICSS is thanked for financial support, for promoting events in which PhD students can get in touch and share their experiences in science.

For the financial support, I would also like to thank the German Research Foundation's (Deutsche Forschungsgemeinschaft – DFG) priority program DFG SPP 1689 “Climate Engineering: Risks, Challenges, Opportunities?” and specifically the CEMICS2 project DFG-project HA4472/10-2 and the support of the DFG under Germany's Excellence Strategy – EXC 2037 “Climate, Climatic Change, and Society” project no. 390683824, and contributes to the Center for Earth System Research and Sustainability (CEN) of Universität Hamburg.

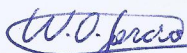
Finally, I would like to thank all the people who have contributed to my professional and personal development. There would not be enough pages to name all of you.

*“Valeu a pena? Tudo vale a pena
Se a alma não é pequena.
Quem quere passar além do Bojador
Tem que passar além da dor.
Deus ao mar o perigo e o abysmo deu,
Mas nelle é que espelhou o céu.”
Mar Portuguese, Fernando Pessoa*

Eidesstattliche Versicherung

Hiermit versichere ich an Eides statt, dass ich die vorliegende Dissertation mit dem Titel: „Assessment of enhanced silicate rock weathering feasibility as a soil ameliorant and its influence on other terrestrial negative emission technologies“ selbstständig verfasst und keine anderen als die angegebenen Hilfsmittel – insbesondere keine im Quellenverzeichnis nicht benannten Internet-Quellen – benutzt habe. Alle Stellen, die wörtlich oder sinngemäß aus Veröffentlichungen entnommen wurden, sind als solche kenntlich gemacht. Ich versichere weiterhin, dass ich die Dissertation oder Teile davon vorher weder im In- noch im Ausland in einem anderen Prüfungsverfahren eingereicht habe und die eingereichte schriftliche Fassung der auf dem elektronischen Speichermedium entspricht.

Hamburg, 18.09.2020


Wagner de Oliveira Garcia